Fibre Bragg Grating Strain Sensors

RICHARD WILLIAM FALLON

Doctor of Philosophy

Aston University

February 2000

Abstract

The fabrication of in-fibre Bragg gratings (FBGs) and their application as sensors is reported. The strain and temperature characteristic results for a number of chirped and uniform gratings written into three different host fibres are presented. The static and dynamic temperature response of a commercially available temperature compensated grating is reported. A five sensor wavelength division multiplexed fibre Bragg grating strain measurement system with an interrogation rate of 25 Hz and resolution of ± 10 με was constructed. The results from this system are presented.

A novel chirped FBG interrogation method was implemented in both the 1.3 and 1.5 μm telecommunication windows. Several single and dual strain sensor systems, employing this method, were constructed and the results obtained from each are reported and discussed. These systems are particularly suitable for the measurement of large strain. The results from a system measuring up to 12 mε and with a potential measurement range of 30 mε are reported. This technique is also shown to give an obtainable resolution of 20 με over a measurement range of 5 000 με for a dual sensor system. These systems are simple, robust, passive and easy to implement. They offer low cost, high speed and, in the case of multiple sensors, truly simultaneous interrogation. These advantages make this technique ideal for strain sensing in SMART structures. Systems based on this method have been installed in the masts of four superyachts. A system, based on this technique, is currently being developed for the measurement of acoustic waves in carbon composite panels. The results from an alternative method for interrogating uniform FBG sensors are also discussed. Interrogation of the gratings was facilitated by a specifically written asymmetric grating which had a 15 nm long linearly sloped spectral edge. This technique was employed to interrogate a single sensor over a measurement range of 6 mε and two sensors over a range of 4.5 mε. The results obtained indicated achievable resolutions of 47 με and 38 με respectively.

The fabrication and applications of long period gratings are also discussed. A novel long period structure fabrication technique is reported. Original temperature and strain characterisation results for a number of different period structures are presented and discussed. A number of results obtained from a novel FBG strain sensor interrogation technique which utilises a long period device as an edge filter are presented. A modulated single sensor system employing this method is demonstrated to give a resolution of 32 με and 0.5 με over measurement ranges of 5 mε and 110 με respectively. An un-modulated version of this system is shown to give a resolution of 50 με over a measurement range of 7.5 mε.

Key words: optical fibre, in-fibre Bragg gratings, strain sensors, SMART structures, interrogation techniques, long period gratings.

This one is for my family, though I don't know what they are going to do with it. It may come in useful for stunning a would-be burglar I suppose.

ACKNOWLEDGEMENTS:

I would like to thank the following for their help, advice and encouragement that kept me going even on days when the experiment blew up or the computers went down. Big thanks to Ian Bennion, who was an excellent supervisor, for his support throughout this work and his excellent grasp of the English language. Thanks to the MAST consortium, in particular Peter Foote and Frank Haran, for their help and advice. I would also like to acknowledge those nice people at Melles Griot for supporting my work and for supplying a temperature compensated grating for me to torture. Thanks to Steve Kidd for being an excellent external supervisor who was interested, supportive and bought the drinks in (what more can you ask for). Thanks also to Bert Biggs who is a fantastic lab technician who can knock together just about anything you need and has an uncanny knack of knowing where things are and remaining calm in a crisis. Also to John Williams who offered a number of useful comments and was very helpful during the re-write.

Major thanks to the following who made this thesis possible and my time at Aston enjoyable. Firstly, to Lin Zhang, who is undoubtably the finest research associate this side of the known universe, for her patience, help, support and understanding even when things went wrong. Secondly, to Andy Gloag, who supplied ideas, help, advice, beer and friendship (Baltimore sucks, but Bertha's mussels rocks!). Thirdly to Fluffy, who is just plain brilliant, thanks for the help, support, friendship and laughs and a great time in the States.

Lastly, I'd like to thank everyone in the Photonics research group for their support and help from lab work to thesis writing, from wine tasting to Fridays in the Sacks. It was fun.

Table of figures

1. Introduction

1.1 Bragg gratings

Fibre Bragg gratings (FBGs) have been much studied[1,2] since the development of the holographic writing technique by Meltz *et al.*[3] in 1989. They offer a wide range of applications in a number of fields[4] which include fibre sensors[5,6], fibre lasers[7], optical amplifiers[8] and microwave photonics[9]. FBGs also find a number of applications in telecommunication networks[10] such as in dispersion compensation[11], filtering[12], wavelength division multiplexing[13], optical switching[14] and pulse generation[15] systems. They have also found application in optical phase fibre conjucators[16] and as time delay elements for phased array antennas[17].

An in-fibre Bragg grating is a photoinduced spatial modulation of the refractive index in the core of an optical fibre. The core refractive index is altered by exposure to ultraviolet (UV) light. The desired modulation period/pattern may be obtained by suitably interfering two coherent beams of UV light from the same laser. The period of the interference fringes determines the period of the refractive index modulation.

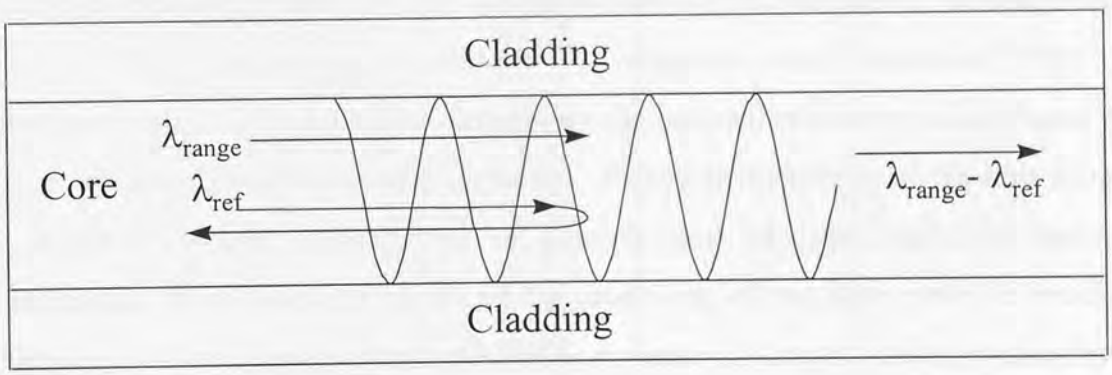

Figure 1.1: Refractive index modulation for an in-fibre uniform grating, where λ_{range} is a range of wavelengths incident on the structure and λ_{ref} is the reflected wavelength.

A FBG can be considered to be a wavelength selective mirror. Light travelling down the fibre is incident on the refractive index perturbation and is partially reflected. However, the majority of the reflected waves destructively interfere with each other. If the period of the refractive index modulation is equal to an integer number of half

wavelengths then the Bragg resonance condition is satisfied and those waves interfere constructively. In this case, the reflected light adds constructively in the backward direction to form a back-reflected peak with a central wavelength defined by the grating parameters.

It is possible to vary the period of the perturbation along the length of the grating. Such a structure is capable of reflecting a range of wavelengths. This gives rise to two types of gratings: (i) uniform, where the period is constant, (ii) chirped where it varies.

A uniform or chirped FBG may be described in terms of transmittance, reflectance and bandwidth. Transmittance is the minimum amount of light transmitted by the grating at the Bragg wavelength of the structure. This is usually expressed as a percentage of the total amount of light incident on the structure at that wavelength. If a grating is considered to be a lossless reflector (transmission losses are typically around 0.05%) then its reflectance is the complement of its transmittance. The bandwidth of a grating is defined to be its full width half maximum (FWHM). A uniform fibre grating typically has a bandwidth of no more than 1 nm. A chirped grating reflects a larger range of wavelengths and thus has a FWHM greater than 1 nm.

Grating formation is dependent on the photosensitivity of the fibre it is being inscribed into. The irradiation wavelength[18,19], intensity and exposure time[20] and photosensitivity of the host fibre determines the induced refractive index change[21] and, hence, the strength of the written structure. The photosensitivity of the host fibre may be increased by the introduction of dopants into its core, typically boron and germanium. It may also be increased by processing of the fibre prior to irradiation. There are two such processing methods: (i) pressure hydrogen loading which involves soaking the fibre in pressurised ($\sim$150 atmospheres) H_2 at room temperature for several days[22]; and (ii) "flame" brushing which involves heating the fibre up to 1 700°C, with a hydrogen-oxygen burner[23]. Both of these methods increase the obtainable refractive index change by over an order of magnitude.

A FBG can persist for decades (lifetimes in excess of 25 years are predicted) if it is properly annealed[24]. The first detailed study of grating stability[25] proposed that the UV decay of the UV-induced index change could be described by a power law function of

time with a small exponent ($<<1$). The authors described the observed slowing in the decay following the initial rapid decay. This indicates that the gating may be stabilised by isothermal annealing. This involves elevating the temperature of the grating to a high temperature (300-600°C) for a short time. During this period, the initial rapid decay of the UV-induced index change is exhausted, hence stabilising the grating. Isothermal annealing results in a slight reduction (a few percent) in the reflectivity and a shift in the Bragg wavelength of the structure[26]. However, once annealed a structure held at 80°C for 25 years will only lose a further 0.02% of its reflectivity. This level of thermal and temporal stability is more than sufficient for most applications.

Both uniform and chirped gratings may be written in a number of ways. The two main techniques are the two beam holographic interferometric[3] and phase mask technique[27]. Each of these methods has advantages and disadvantages. The holographic technique is flexible, but only permits the inscription of short (~ 5 mm) gratings. The phase mask technique is less flexible but it permits the manufacture of both long[28] and novel structures[29,30]. It also offers excellent reproducibility making it more suitable than the holographic technique for bulk grating fabrication. Both techniques yield high performance gratings which are suitable for application in the sensor field.

1.2 Fibre Bragg grating sensors

Single mode fibre sensors have displayed the potential to acts as temperature, strain and pressure[31] as well as acoustic vibration[32] and magnetic field[33] sensors since the 1960s. However, multiplexing of such sensors has been difficult and needed improvement to become commercially viable.

Fibre Bragg gratings, which are inherently sensitive to temperature, strain and pressure, represent a potentially attractive solution to this problem while demonstrating a number of other advantages. The response of a Bragg grating to one of these external parameters at its location is a shift in peak reflected wavelength by a proportional amount. This shift gives a Bragg sensor several advantages in addition to those normally associated with fibre optic sensors, i.e. small, light weight, immune to electromagnetic interference and ability to operate over a wide range of environmental conditions. These extra advantages include the output of the system being independent

of total light levels permitting the sensor to be easily operated intermittently without the need for recalibration or reinitialising of the system. The wavelength encoded nature of the information also facilitates WDM, achieved by assigning individual sensors to a different slice of the available source spectrum[34].

There are numerous methods for interrogating Bragg grating sensors. The majority of interrogation systems have been based on either in-line tuneable filters (i.e. Fabry-Perot[35] and acousto-optic[36]) or interferometry[37]. Tuneable filters offer moderate resolution and a large working range, which is a necessity for WDM arrays, at a moderate cost. They are good for measuring static and quasi-static strains only. The scanning speed of the filter, typically 500 Hz, precludes them from measuring dynamic strains. Interferometric techniques offer excellent resolution and are ideal for measuring dynamic strains. However, they are expensive, require complex electronics and offer only a limited working range.

One of the main drawbacks to the application of FBGs as sensors is their inherent dual sensitivity to temperature and strain. Hence, strain measurements are affected erroneously by temperature and vice-versa. A number of solutions to this cross-sensitivity problem have been reported. These include the writing of two gratings with different wavelengths at the same location[38] and the comparison of the output of a FBG sensor to that of another device[39]. The application of either of these methods enables the separation of the two measurands with reasonable resolution.

Fibre Bragg gratings have a number of advantages over other sensors and have found many applications. One of their main applications is in the structural and health monitoring in SMART structures. FBG sensors are capable of measuring strains in concrete and composite materials and they have been proved reliable in a number of different structures[40]. Other uses of FBGs include operating as load transducers[41] and temperature and ultra-sonic sensors in medical applications[42]. This list is expected to expand rapidly as FBG technology becomes more readily available at a reduced cost.

1.3 Thesis Summary

Chapters two and three are concerned with Bragg gratings and their application as sensors as discussed above. The remainder of this thesis is concerned primarily with the application of fibre Bragg gratings as strain sensors and novel methods for their interrogation. The suitability of fibre Bragg gratings as strain sensors has been demonstrated by a number of groups[43,44,45,46].

The fourth chapter presents the strain and temperature characterisation results for a number of gratings which may be employed in sensor networks. These include uniform and chirped structures which were inscribed into three commonly used host fibres, i.e. standard telecommunications, high germanium and boron-germania co-doped fibre. The effects of hydrogenation and the bandwidth of the grating are also examined. The temperature and strain characteristics of a bandpass structure inscribed into boron-germania co-doped fibre are also presented and discussed.

The effect of temperature on the central wavelength of a Bragg grating is not always desirable. This is especially true in systems were a constant Bragg wavelength is required regardless of the temperature of the environment, e.g. WDM and filter applications. A number of manufacturers have appropriately packaged FBGs so as to greatly reduce their temperature sensitivity. The temperature compensating properties of one such package produced by Melles Griot are presented and discussed in the second part of the fourth chapter.

The final part of the fourth chapter involves the implementation of a wavelength division multiplexed strain measurement system that has five sensors. The five gratings were wavelength division multiplexed onto a single line; an important advantage in the application of FBG sensors. Each sensor had a measurement range of 5 mε which is sufficient for the majority of SMART structure applications. The sensors were interrogated by a tuneable Fabry-Perot filter and the entire system was computer controlled. Results obtained from and the limits of this system are presented and discussed.

Chapter five concentrates on the interrogation of FBG strain sensors. Two novel interrogation methods will be presented and discussed. The first of these is the Identical Broadband Chirped Interrogation (IBCI) technique. The majority of current FBG strain sensor systems are interrogated by a tuneable filter, which has a limited speed, moderate cost and requires some control electronics, or an interferometer, which is expensive, fragile and needs complex control devices. The tuneable filter is the preferred method for SMART structures as it provides adequate resolution for moderate cost and complexity. The advent of on-line formation and the development of the phase mask technique means that the cost of FBG fabrication is set to fall drastically. Therefore, the cost of the sensor elements will fall, while the cost of tuneable filters remains static. The result could well be that the interrogation and de-multiplexing units account for a large proportion of the cost of a complete system. Bragg grating based sensor systems would be considerably more attractive if the cost of the interrogation unit was reduced. The IBCI technique was developed and implemented with the aim of reducing the cost and complexity of the interrogation system while maintaining high speed and adequate resolution. This system is based on the overlapping of a chirped sensor grating with an identical reference device. Strain applied to the sensor results in a linear shift in the spectral profile of the grating. The reference device is not strained, hence the respective spectral profiles no longer completely overlap. This results in light, which is proportional in intensity to the shift in the spectral profile of the grating, being transmitted by the reference structure. Hence, the IBCI system permits a linear relationship between strain and resultant optical power. The maximum sensing range of the system is determined by the bandwidths of the gratings employed, e.g. a 5 nm chirped grating facilitates a sensing range up to 5 mε. A number of systems employing the IBCI technique are presented and discussed. These include systems operating the 1.3 μm and 1.5 μm window which interrogate single and dual sensors. All of these systems are less expensive, required less electronics, were more robust and offered higher achievable interrogation rates than other interrogation techniques at the time. It is currently being developed in collaboration with British Aerospace for acoustic wave measurement in carbon composite panels.

The IBCI method has been so successful it has been adopted by the LINK sponsored MAST project. The MAST project was a collaboration between British Aerospace, Pendennis Shipyard, Carbospars and Aston University. The aim of the project was to develop and construct a composite superyacht mast which had the capability of real time strain monitoring. The IBCI technique was employed, as part of a complete strain sensor system[47], to interrogate four high strain (~ 15 mε) sensors. This monitoring system has been installed in the masts of four superyachts to date. Indeed these exciting, new developments in the ever-expanding SMART structure field have formed the basis of a trade magazine article[48] and an Open University electrical materials technology television programme.

The second half of the chapter examines a novel interrogation technique for uniform FBG strain sensors. The interrogation element in this system is a specially written Bragg grating that has an asymmetric spectral profile. The grating acts as an edge filter thus converting the strain dependent reflected wavelength into intensity. The writing of such a grating and the results obtained from a single and a dual sensor system are presented and discussed.

The final experimental chapter examines long period gratings and their application as interrogation elements. The first part of the chapter gives an overview of long period gratings and their applications. The second part of the chapter presents the temperature and strain characterisation results for a number of different period structures written into the same type of fibre. The final part of this chapter is concerned with the development and implementation of an interrogation system which employs one edge of a long period grating as an edge filter. The results obtained from a modulated and an un-modulated version of this system are presented and discussed.

Chapter 7 summaries the work presented in this thesis and outlines possible future work. Chapter 8 documents the publications associated with this body of work.

---

[1] I. Bennion, J.A.R. Williams, L. Zhang, K. Sugden and N.J. Doran "UV- written in-fibre Bragg gratings", *Optical and Quantum Electronics*, **28**, 1996, pp 93-13

[2] K.O. Hill and G. Meltz "Fiber Bragg grating technology fundamentals and overview", *J. Lightwave Tech.*, **15**, 1997, pp 1263-1276.

[3] G. Meltz, W.W. Morey and W.H. Glen, "Formation of Bragg gratings in optical fibres by a transverse holographic method," *Opt. Lett.*, **14**, 1989, pp 823-825.

[4] C.R. Giles "Lightwave applications of fiber Bragg gratings", *J. Lightwave Tech.*, **15**, 1997, pp 1391-1404.

[5] J. Dakin and B. Culshaw (Editors), "Optical fiber sensors: Applications, analysis and future trends", *Vol. 4*, Artech House, 1997.

[6] A.D. Kersey, M.A. Davis, H.J. Patrick, M. LeBlanc, K.P. Koo, C.G. Askins, M.A. Putnam and E.J. Friebele, "Fibre grating sensors", *J. Lightwave Tech.*, **15**, 1997, pp 1442-1463.

[7] J. Archambault and S. G. Grubb "Fiber gratings in lasers and amplifiers", *J. Lightwave Tech.*, **15**, 1997, pp 1378-1390

[8] J.F. Massicott, S.D. Willson, R. Wyatt, J.R. Armitage, R. Kashyap, D. Williams and R.A. Lobett, "1480 nm pumped erbium doped fibre amplifier with all optical automatic gain control", *Electron. Lett.*, **30**, 1994, pp 962-964.

[9] A. Molony, C. Edge and I. Bennion, "Fibre grating delay element for phased array antennas", *Electron. Lett.*, **31**, 1995, pp 1485-1486.

[10] P. Sansonetti, "Fibre grating devices for telecommunications applications", *Conf.: Bragg gratings, photosensitivity and poling in glass fibres and waveguides,* Williamsburg, U.S., Tech. Dig, 1997, JSuA3-1

[11] R. I. Laming, M. Ibsen, M. Durkin, M.J. Cole, M.N. Zervas, K.E. Ennser and V. Gusmeroli, "Dispersion compensation grattings", *Conf.: Bragg gratings, photosensitivity and poling in glass fibres and waveguides,* Williamsburg, U.S., Tech. Dig., 1997, BTuA7-1

[12] G.E. Town, K. Sugden, J.A.R. Williams, I. Bennion and S. Poole, "Wide-band Fabry-Perot-like filters in optical fiber", *IEEE Photon. Technol. Lett.*, **7**, 1995, pp 78-80.

[13] T.A. Strasser "Fibre grating devices for WDM communication systems", *Conf.: Bragg gratings, photosensitivity and poling in glass fibres and waveguides,* Williamsburg, U.S., Tech. Dig., 1997, BTuA1-1

[14] D. Taverner, N.G.R. Broderick, D.J. Richardson, R.I. Laming and M. Ibsen, "Nonlinear self-switching and multiple gap-soliton formation in a fibre Bragg grating", *Opt. Lett.*, **23**, 1998, pp 328-330.

[15] B.J. Eggelton, C.M. deSterke, R.E. Slusher and J.E. Sipe, "Distributed feedback pulse generator based on nonlinear fibre grating", *Electron. Lett.*, **32**, 1996, pp 2341-2342.

[16]C.R. Giles, V, Mizrahi and T. Erdogan, "Polarisation-independent phase conjucation in a relective optical mixer", *IEEE Photon. Technol. Lett.*, **7**, 1995, pp 126-128.

[17] A. Molony, C.Edge and I. Bennion, "Fibre grating time delay element for phased array antennas," *Electron. Lett.*, **31**, 1995, pp 1485-1486.

[18] I Bennion, D.C.J. Reid, C.J. Rowe and W.J. Stewart "High-reflectivity monomode-fibre grating filters", *Electron. Lett.*, **22**, 1986, pp 341-343.

[19] D.S. Starodubov, V. Grubsky, J. Feinberg, B. Kobrin and S. Juma "Bragg grating fabrication in germanosilicate fibers by use of near-UV light: a new pathway for refractive index changes" *Opt. Lett.*, **22**, 1997, pp 1086-1088.

[20] P. Niay, P. Bernage, S. Legoubin, M. Douay, W,X, Xie, J.F. Bayon, T. Georges, M. Monerie and B. Poumellec, "Behaviour of spectral transmissions of Bragg gratings written in germania-doped fibres: writing and erasing experiments using pulsed or cw uv exposure", *Optics Comms.*, **113**, 1994, pp 176-192.

[21] H.G. Limberger, P.Y. Fonjallaz and R.P. Salathe, "Spectral characterisation of photoinduced high efficient Bragg gratings in standard telecommunications fibres", *Electron. Lett.,,* **29**, 1993, pp 47-48.

[22] P.J. Lemaire, R.M. Atkins, V. Mizrahi and W.A. Reed, "High pressure H_2 loading as a technique for achieveing ultrahigh UV photosensivity and thermal sensitivity in GeO2 doped optical fibres", *Electron. Lett.,* **29**, 1993, pp 1191-1193.

[23] F. Bilodeau, B. Malo, J. Albert, D.C. Johnson, K.O. Hill, Y. Hibino, Y. Abe, M. Kawachi, "Photosensitisation of optical fibre and silca-on-silicon/silica waveguides", *Opt. Lett.*, **18**, 1993, pp 953-955.

[24] D.L. Williams and R.P. Smith "Accelerated lifetime tests on UV written intra-core gratings in boron germania co-doped silica fibre", *Electron. Lett.,* **31**, 1995, pp 2120-2121.

[25] T. Erdogan V. Mizrahi, P.J. Lemaire and D. Monroe "Decay of ultraviolet-induced fiber Bragg gratings" *J. Appl. Phys.*, **76**, 1994, pp 73-80.

[26] K..E. Chisholm, K. Sugden and I. Bennion, "Effects of thermal annealing on Bragg fibre gratings in boron/germania co-doped fibre", J. *Phys. D: Appl Phys.*, **31**, 1998, pp 61-64.

[27] K.O. Hill, B. Malo, F. Bilodeau, D.C. Johnson and J. Albert, "Bragg gratings fabricated in monomode photosensitive optical fibre by UV exposure through a phase mask", *Appl. Phys. Lett.*, **62**, 1993, pp 1035-1037.

[28] M.J. Cole, W.H. Loh, R.I. Laming, M.N. Zervaz and S. Barcelos, "Moving fibre/phase mask-scanning beam technique for enhanced flexibility in producing fibre gratings with a uniform phase mask", *Electron. Lett.*, **31**, 1995, pp 92-94.

[29] B. Malo, S. Theriault, D.C. Johnson, F. Bilodeau, J. Albert and K.O. Hill, "Apodised in-fibre Bragg grating reflectors photoimprinted using a phase mask", *Electron. Lett.*, **31**, 1995, pp 223-225.

[30] L.A. Everall, K.E. Chisholm, J.A.R. Williams, X. Liu, R.M. De La Rue and J.S. Aitchison, "Optimisation of length-constrained apodised in-fibre Bragg grating filters," *Submitted to Opt. Comms.*, Sept 98.

[31] G.B. Hocker, "Fiber-optic sensing of pressure and temperature", *Appl. Opt.*, **18**, 1979, pp 1445.

[32] N. Lagakos and J.A. Bucaro, "Linearly configured embedded fiber-optic acoustic sensor", *J. Lightwave Technol.*, **11**, 1993, pp 639-642.

[33] A. Dandridge, A.B. Tveten, G.H. Siegel, E.J. West and T.G. Giallo-Renzi, "Optical fibre magnetic field sensors", *Electron. Lett.*, **16**, 1980, pp 408-409.

[34] L.E. Giesler, J.R. Dunphy, W.W. Morey, G. Melzt and W. Glenn, "Instrumentation concepts for multiplexed Bragg grating sensors", *SPIE Sensors and Sensor Interrogation*, **1480**, 1991, pp 138-141.

[35] A.D. Kersy, T.A. Berkoff and W.W. Morey, "Multiplexed fibre Bragg grating strain-sensor system with a fibre Fabry-Perot wavelength filter", *Opt. Lett.*, **18**, 1993, pp 1370-1372.

[36] M.G. Xu, H. Geiger, J.L. Archambault, L. Reekie and J.P. Dakin"Novel interrogation system for fibre Bragg grating sensors using an acousto-optic tunable filter", *Electron. Lett.*, **29**, 1993, pp 1510-1511.

[37] A.D. Kersey, T.A. Berkoff and W.W. Morey, "High-resolution fibre-grating based strain sensor with interferometric wavelength-shift detection", *Electron. Lett.*, **28**, 1992, pp 236-238.

[38] M.G. Xu, J.L. Archambault, L. Reekie and J.P. Dakin, "Discrimination between strain and temperature effects using dual-wavelength fibre grating sensors", *Electron. Lett.*, **30**, 1994, pp 1085-1087.

[39] T. Liu, G.F. Fernando, L. Zhang, I. Bennion, Y.J. Rao and D.A. Jackson, "Simultaneous strain and temperature measurement using a combined fibre Bragg grating/extrinsic Fabry-Perot sensor", *Conf. Optical Fibre Sensors (OFS '97)*, Williamsburg, Virginia, Tech. Dig, 1997, OTuC-1.

[40] P. Ferdinand, S. Magne, V. Dewynter-Marty, C. Martinez, S. Rougeault and M. Bugaud, "Applications of Bragg grating sensors in Europe", *Conf. Optical Fibre Sensors (OFS '97)*, Williamsburg, Virginia, Tech. Dig, 1997, OTuB-1.

[41] C. Chang and A. Kersey, "Development of fiber Bragg grating sensor based load transducers", *Conf. Optical Fibre Sensors (OFS '97)*, Williamsburg, Virginia, Tech. Dig, 1997, OWC8-1.

[42] N.E. Fisher, J. Surowiec, D.J. Webb, D.A. Jackson, L.R. Gavrilov, J.W. Hand, L. Zhang and I. Bennion, "In-fibre Bragg gratings for ultrasonic medical applications", *Meas. Sci. Technol.*, **8**, 1997, pp 1050-1054.

[43] Y. Rao, "In-fibre Bragg grating sensors", *Meas. Sci. Technol.*, **8**, 1997, pp 355-375

[44] A.D. Kersey, M.A. Davis, H.J. Patrick, M. LeBlanc, K.P. Koo, C.G. Askins, M.A. Putnam and E.J. Friebele, "Fibre grating sensors", *J. Lightwave Tech.*, **15**, 1997, pp 1442-1463.

[45] W.W. Morey, G. Meltz and W.H. Glenn, "Fibre optic Bragg grating sensors", *SPIE Fibre optic and laser sensors VII*, **1169**, 1989, pp 98-107.

[46] S.M. Melle, A.T. Alavie, S. Karr, T. Coroy, K. Liu and R.M. Measures, "Strain sensing using a fibre optic Bragg grating", *SPIE Fiber Optic SMART Structures and Skins IV*, **1588**, 1991, pp 255-263.

[47] D. Roberts and P. Foote, "Carbon spars for superyachts and SMART mast technology", *International Conference on The Modern Yacht*, Portsmouth, 1998, paper 13.

[48] John Bell, "Smart masts chart novel design rules for polymers", *Opto and Laser Europe*, Issue 55, 1998, pp 30-34.

Chapter Two: In Fibre Bragg Gratings

2.1 Chapter Overview

The purpose of this chapter is to provide an overview of the in-fibre Bragg grating field including definitions, theory, photosensitivity, historical background, writing techniques and applications. This review is not intended to be exhaustive of this large and ever-expanding field. There exist a number of excellent review papers which provide more in-depth detail in technology[1,2], applications[3,4,5] and associated physical mechanisms[6].

2.2 Grating Theory

A fibre grating is a spatial modulation of the refractive index in the core of a fibre. In the first case to be considered this modulation is periodic, see figure 2.1 (a).

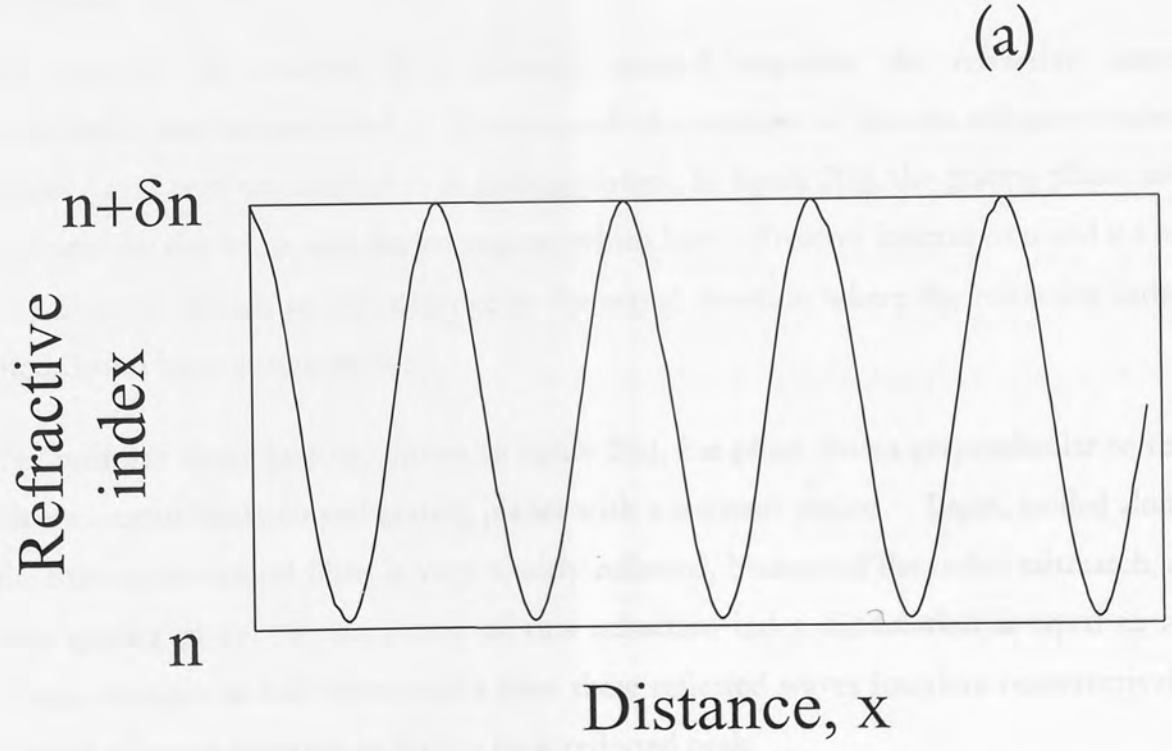

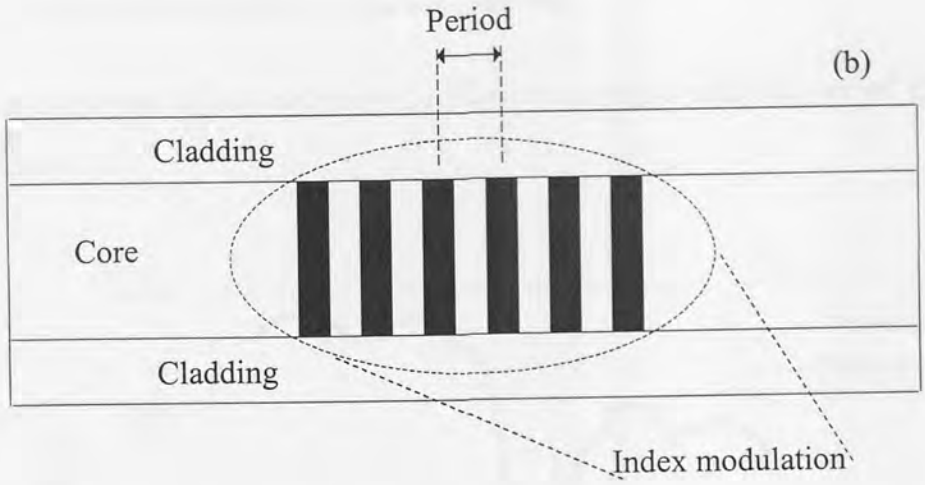

Figure 2.1(a) Refractive index perturbation against distance in the core of an optical fibre; (b) Illustration of the grating planes in a uniform Bragg grating with constant modulation amplitude.

(To simplify the analysis of a grating's spectral response, the refractive index modulation can be considered to be composed of a number of discrete refractive index planes (from here on referred to as grating planes). In figure 2(b), the grating planes are indicated by the white and shaded regions which have refractive indexes of n and $n+\delta n$ respectively. This is an approximate to the actual situation where the refractive index modulation has a cosine profile.)

The uniform Bragg grating, shown in figure 2(b), has phase fronts perpendicular to the fibre's longitudinal axis and grating planes with a constant period. Light, guided along the core of the optical fibre, is very weakly reflected, because of the index mismatch, at each grating plane. If the period of this refractive index modulation is equal to an integer number of half wavelengths then these reflected waves interfere constructively in the backward direction to form a back-reflected peak.

All of the other wavelengths scattered by the grating planes destructively interfere with each other. The reflection from each plane for these off-resonance wavelengths is very small. As an example a 1 mm long grating written at 1.5 μm with a strong Δn of 10^{-3}

will reflect ~0.05% of the off-resonance incident light. Therefore, a Bragg grating is a very good approximate to a loss-less reflector.

The transmission and reflection profiles of a typical uniform period grating are shown in figure 2.2.

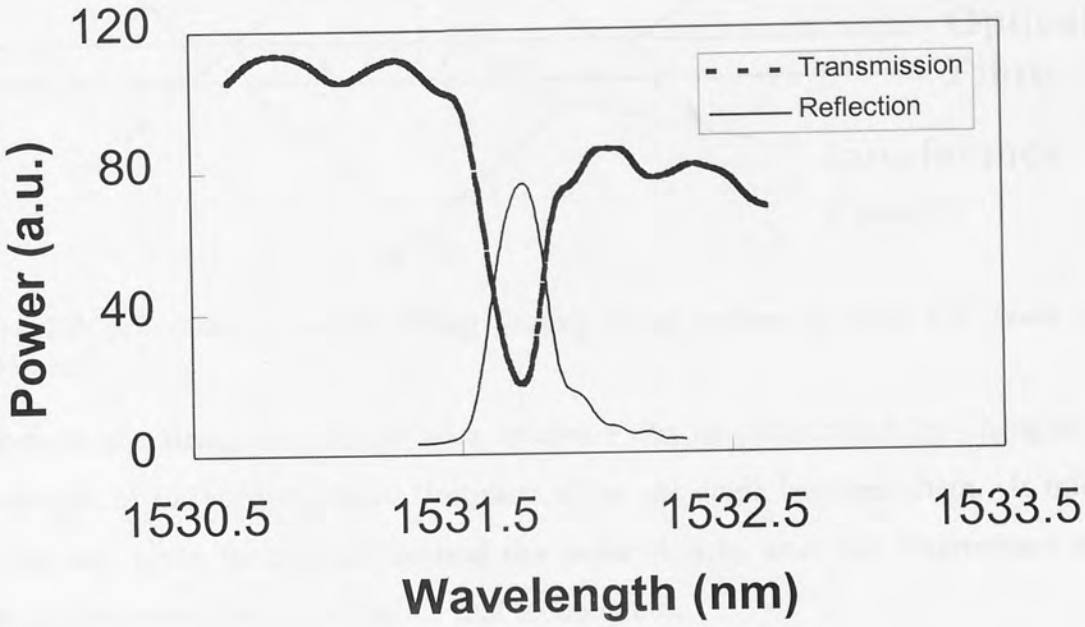

Figure 2.2: The spectral profile of a typical uniform grating in transmission and reflection.

The wavelength at which the light is reflected, i.e. the central wavelength of the grating, is determined by the period of the structure. The period of the device is dependent on the UV writing wavelength (λ_{UV}) and the angle between the two interfering beams (see figure 2.3). This relationship is expressed by:

$$\Lambda = \lambda_{UV} / 2 \sin(\theta/2) \qquad \textit{Equation 2.1}$$

where Λ is the period of the inscribed structure, λ_{UV} the writing wavelength and θ is the angle between the two interfering beams.

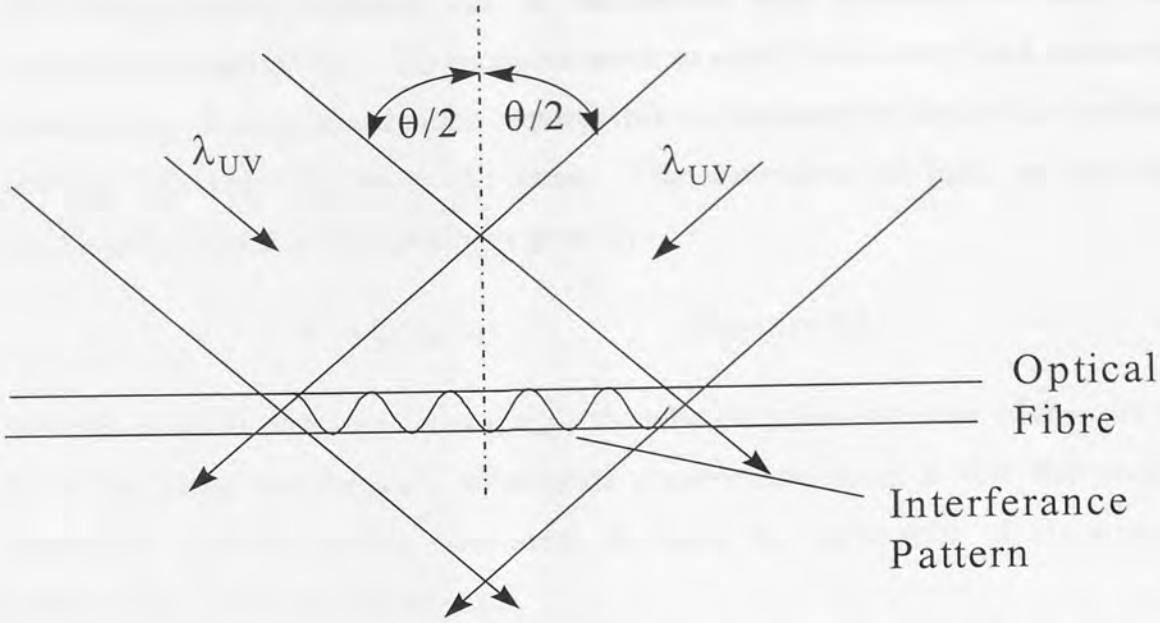

Figure 2.3: Schematic of a fibre Bragg grating being written by two UV beam (λ_{UV}) interference.

Therefore, the Bragg wavelength of a structure can be determined by changing the wavelength of the writing beams (impractical) or the angle between them. It follows that for any given inscription method the easier it is to alter the interference angle between the beams the more flexible that technique is.

A uniform fibre Bragg grating can be described, generally, by a phase and amplitude modulated sinusoidal perturbation of the core refractive index[2],

$$\delta n(z) = \delta n_0(z)[1 + m \cos(\frac{2\pi z}{\Lambda} + \phi)] \qquad \textit{Equation 2.2}$$

where $\delta n_0(z)$ is the amplitude of the refractive index modulation, m is the contrast (determined by the visibility of the UV fringe pattern) and ϕ is a phase factor.

There are a number of methods for modelling and understanding grating filtering characteristics[7,8] from this simple equation. One of these methods employs coupled mode theory to describe the interaction between guided waves and the periodic structure of the grating. In this treatment, the grating provides a mechanism by which energy can be transferred between the forward and backward travelling modes. A detailed description of this can be found in ref. 9.

The Bragg grating condition can be understood with reference to energy and momentum conservation. This condition needs to satisfy both energy and momentum conservation. Energy conservation requires that the frequency of the incident radiation and the reflected radiation is the same. The wavevector of light, at the Bragg wavelength, incident on the grating is given by:

$$\mathbf{k}_i = 2\pi n_{eff}/\lambda_b \qquad \textit{Equation 2.3}$$

where $\mathbf{k}_i$ is the incident wavevector, n_{eff} is the effective refractive index of the core and λ_b is the Bragg wavelength. Momentum conservation requires that the incident wavevector plus the grating wavevector, **K**, equal the wavevector of the scattered radiation $\mathbf{k}_f$. This is simply stated as:

$$\mathbf{k}_i + \mathbf{K} = \mathbf{k}_f \qquad \textit{Equation 2.4}$$

where the grating wavevector, **K**, has a direction normal to the grating planes with a magnitude $2\pi/\Lambda$. The diffracted wavevector is equal in magnitude, but opposite in direction, to the incident wavevector. Hence, equation 2.4 becomes:

$$2(2\pi n_{eff}/\lambda_b) = 2\pi/\Lambda \qquad \textit{Equation 2.5}$$

which simplifies to the Bragg condition:

$$p\lambda_b = 2n_{eff}\Lambda \qquad \textit{Equation 2.6}$$

where p is an integer. The strongest interaction is the fundamental Bragg order, i.e. $p=1$, and is the one usually considered.

The reflectivity of such a grating with constant modulation amplitude and period can be determined using coupled mode theory[10], and is given by:

$$R(L,\lambda) = \frac{\Omega^2 \sinh^2(sl)}{\Delta k^2 \sinh^2(sl) + s^2 \cosh^2(sl)} \qquad \textit{Equation 2.7}$$

where $R(L,\lambda)$ is the reflectivity that is a function of the grating length L and wavelength λ. Ω is the coupling co-efficient, Δk ($= k - \pi/\lambda$) is the de-tuning wavevector, $k = 2\pi n_0/\lambda$ is the propagation constant, where n_0 is the average refractive index of the fibre

core, and $s^2 = \Omega^2 - \Delta k^2$. The coupling coefficient, Ω, for sinusoidal variation of index perturbation along the fibre axis is given by:

$$\Omega = \frac{\pi \Delta n M_p}{\lambda} \qquad \textit{Equation 2.8}$$

where M_p is the fraction of the fibre mode power contained in the core. M_p can be approximated by $1 - V^{-2}$, assuming the grating is uniformly written through the core. V is the normalised frequency of the fibre and is given by:

$$V = (\frac{2\pi}{\lambda}) a (n_{co}^2 - n_{cl}^2)^{1/2} \qquad \textit{Equation 2.9}$$

where a is the core radius, n_{co} and n_{cl} are the core and cladding indices, respectively.

At the Bragg grating centre wavelength there is no wavelength detuning, i.e. $\Delta k = 0$; therefore the expression for reflectivity becomes:

$$R(L,\lambda) = \tanh^2(\Omega L) \qquad \textit{Equation 2.10}$$

Hence, the reflectivity of a grating may be increased by increasing the coupling co-efficient or by writing a longer structure. This relationship can be explained by considering a grating as a series of discrete refractive index planes, see figure 2(b). As mentioned earlier, light travelling down the core is weakly reflected at each of these planes. Light reflected at the Bragg wavelength of the grating constructively interferes. Therefore, the total reflection from a uniform grating, at this wavelength, is the sum of these reflections. The longer the device, the more grating planes there are for incident light to be reflected from, hence the higher the grating's reflectivity.

The coupling co-efficient determines the proportion of light reflected at each of the grating planes. The greater the coupling co-efficient, the higher the reflectivity at each grating plane and, hence, the higher the structure's overall reflectivity.

Equation 2.10 also indicates that for increasing ΩL the peak reflectivity of the grating rises to unity, accompanied by an increase in the amplitude of the side lobes. These side lobes are due to multiple reflections to and from opposite ends of the grating region.

The sine spectrum arises mathematically through the Fourier transform of a harmonic signal having a finite extent; an infinitely long grating would transform to an ideal delta function response in the wavelength domain.

A number of calculated reflection spectrum are shown in figure 2.4, where $\beta = 2n_{eff}/\lambda$;

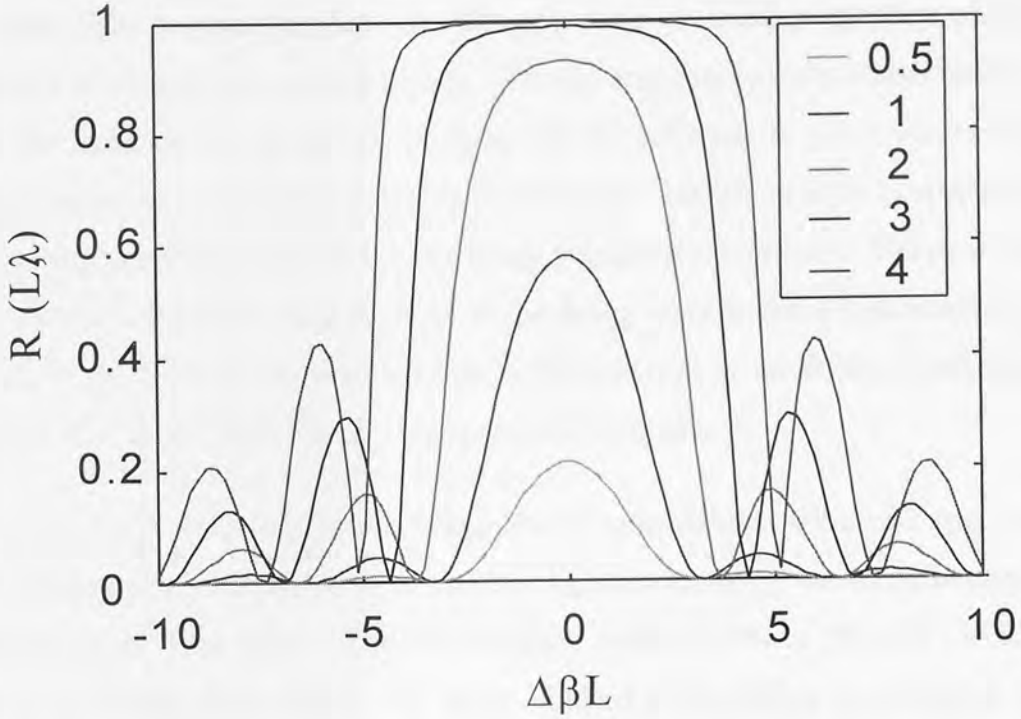

Figure 2.4: Reflectance R(L,λ) plotted against ΔBL for a periodic grating with values of ΩL = 0.5, 1, 2, 3, 4.

The bandwidth of a grating's spectral response is determined by both the coupling co-efficient and the length of the structure. Strong gratings (~100%) have a full width half maximum (FWHM) mainly determined by the coupling co-efficient. A large Ω gives a broader bandwidth, while increasing the length sharpens the reflection response. In the case of weak gratings the FWHM is inversely proportional to the length of the grating.

These relationships can again be explained by considering a uniform grating as a series of refractive index planes. At each grating plane a small fraction of the incident light is reflected. The more grating planes there are (i.e. the longer the grating) the more constructive interference will occur at the Bragg wavelength and the more destructive interference will occur for all other reflected wavelengths. Hence, the longer the grating, the sharper the spectral response.

In contrast, a high coupling co-efficient increases the proportion of light reflected from each plane. Therefore, less grating planes are required to obtain the same overall reflectivity. However, there are fewer grating planes for wavefronts to be reflected from. Therefore, there is less destructive interference between the off-resonance wavelengths which leads to a broader spectral response.

Consider light propagating through a Bragg grating. A small proportion of this light is reflected at each of the grating planes. Energy and momentum conservation requires that the light, at the Bragg wavelength, will be reflected at these planes to a much greater extent than the other incident wavelengths. Hence, as light propagates through the grating the proportion of it at the Bragg wavelength decreases. Indeed if the grating has $\sim$100% reflectivity then no light at the Bragg wavelength is transmitted. In other words, at the front of the grating there is 100% energy at the Bragg wavelength and at the end of it, zero. This "decay" is exponential in nature.

Consider 1 nW of power at the Bragg wavelength incident on a uniform grating. If each grating plane reflects 0.1% of incident light at the Bragg wavelength, then 1 pW is reflected at the first plane. The second plane reflects 0.1% of 999 pW i.e. 0.9999 pW and so on leading to an exponential decay. Indeed if the grating is strong, i.e. has a high value of Δn (typically 10^{-3}), then all of the light at the Bragg wavelength may be reflected before the end of the grating. In this case, the effective length of the grating has been reduced. Such a grating has a broad bandwidth for the reasons discussed previously. On the other hand, if the grating has a low value of Δn (typically 10^{-5}) then the grating will have a lower reflectivity and not all light at the Bragg wavelength may be reflected. The reflectivity may be increased by writing a longer structure (i.e. have more grating planes). Such a grating will have a sharper spectral response, for the reasons discussed earlier.

Gratings may be deliberately written to have large bandwidths. These structures are referred to as chirped gratings. Chirped gratings may be realised by varying (i) the period, see figure 2.5, along the length of the grating, or (ii) the core refractive index or (iii) both, along the length of the grating. From equation 2.6:

$$\lambda_b(z) = 2n_{eff}(z)\lambda(z) \qquad \textit{Equation 2.11}$$

where z is the distance along the grating.

The simplest type of chirped grating structure is one where the variation in the grating period is linear:

$$\Lambda(z) = \Lambda_0 + \Lambda_1 z \qquad \textit{Equation 2.12}$$

where Λ_0 is the starting period and Λ_1 is the linear change (slope) along the length of the grating.

Such a structure reflects a range of wavelengths. For example, consider a chirped grating 2 cm in length with have a starting wavelength at 1550 nm and a chirped value of 1 nm/cm. Such a grating will have an end wavelength of 1552 nm and, therefore, a central wavelength of 1551 nm. In figure 2.5 (a), the shorter wavelength λ_1 (e.g. 1550 nm) is reflected by the leading edge of the grating, whereas λ_2 (e.g. 1552 nm) traverses the structure until being reflected at the far end.

(a)

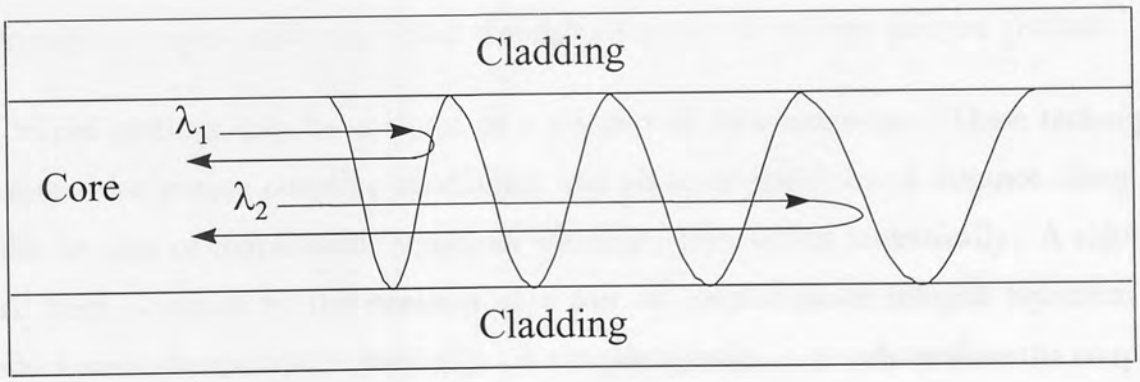

(b)

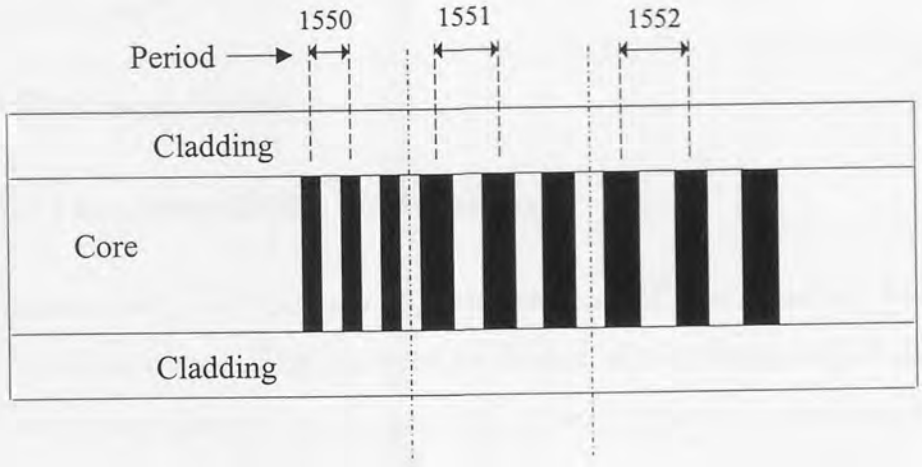

Figure 2.5: (a) Refractive index modulation for an in-fibre chirped Bragg grating. (b) A schematic diagram of a cascade of several gratings with increasing period that are used to simulate chirped gratings.

Chirped gratings may be considered as consisting of smaller length uniform Bragg gratings that have increasing period. Consider the previous example. Such a grating could simply be considered to consist of 3 uniform gratings with central wavelengths of 1550, 1551 and 1552 nm respectively, see figure 2.5 (b). Therefore light propagates through a chirped grating as it does through a number of uniform chirped gratings.

Chirped gratings may be analysed in a number of different ways. These techniques express the grating coupling co-efficient and phase as functions of distance along the fibre in a set of couple-mode equations which are then solved numerically. A solution has been obtained by the iteration of a pair of coupled-mode integral equations[11,12], which were then solved numerically. A simpler solution is to reformulate the coupled-mode equations into a second order equation, i.e. a Riccatti equation, and solve this numerically[13]. This method is much simpler as it can be treated as an initial value problem, permitting standard ordinary differential equation techniques to be easily used. An alternative approach involves considering the non-uniform grating as a series of short periodic structures[14]. These smaller devices can then be characterised by

different transfer matrices and the overall response is obtained by numerical matrix multiplication[15].

2.3 Photosensitivity

2.3.1 Photosensitivity Mechanisms

Photosensitivity is the mechanism responsible for grating formation. Fibre photosensitivity was first observed by Hill *et al.*[16] in Ge-O_2 doped silica optical fibres. These gratings (known as Hill gratings) were written by a wavelength of 488 nm from an Argon ion laser. At the time detailed studies[17] were undertaken into this phenomena and it was found that the grating strength, i.e. the magnitude of the photoinduced refractive index change, increased as the square of the light intensity, thus suggesting a two photon process. In 1989, Meltz *et al.*[18] demonstrated that gratings could be inscribed more efficiently at 244 nm. This subsequently led to the advancement of two main theories on fibre photosensitivity; the colour-centre[19] and glass densification models[20]. Both models were based on the photoionisation of GeO defects, which most likely lies at the origin of photosensitivity.

The former model is based on the trapping of the released electron resulting in the formation of a Ge E' colour centre. It can then be derived from the Kramers-Kronig[19] relationship that the refractive index of the fibre will be altered by this colour centre. There is a substantial body of evidence for this theory[21,22,23] which also further confirms that the mechanism responsible for Hill gratings was a two photon absorption into the 240 nm band. However, there are a number of experimental observations which the colour-centre model does not completely explain[24,25]. This led to the advancement of the latter model in which the photoionisation of GeO defects leads to glass densification[20]. There is also experimental evidence to support this theory[26].

The processes involved in the refractive index change are still not clearly understood, however, it is likely that more than one mechanism is responsible. This phenomena is not restricted to GeO_2 silica materials. Other materials which have had gratings inscribed in them including As_2S_3, Ce^{3+} and Eu^{2+}:Al_2O_3 which are discussed in references 27, 28 and 29 respectively.

In practice, the induced refractive index change (Δn) in GeO_2 fibres is positive. Its magnitude and hence the strength of the grating is determined by several parameters. These include irradiation conditions (wavelength, intensity, exposure time), dopants introduced into the fibre core and any processing of the fibre prior to irradiation. Gratings were written initially around 488 nm[16,30] then at 240 nm[18], 190 nm[31] and recently at 330 nm[32]. The authors of this final result postulate that the refractive index change in gratings written at this wavelength is due to a metamorphosis of the GeO_2 defect rather than by photoionisation.

The radiation intensity the fibre has to be exposed to for grating inscription is dependent on whether the UV source is pulsed[33] or cw[34]; typical values are between 100 - 1 000 mJ/cm^2 for the former and 50-300 mW for the latter. The higher the UV energy, the shorter the exposure time required to write a grating. Exposure time is the key factor in determining the reflectivity of the inscribed grating. The associated refractive index changes are strongly non-linear as a function of exposure time[35]. Also the greater the photosensitivity of the fibre the more rapidly the grating is inscribed e.g. seconds of exposure for boron-germania co-doped fibre compared with a few minutes for standard telecommunications fibre. It is also noted here that prolonged exposure may reduce the reflectivity of the grating. Indeed, if the grating is subject to fringeless UV illumination the refractive index along the exposed length saturates and the structure is erased.

The addition of dopants into germanium fibre can greatly increase the maximum obtainable Δn, i.e. the photosensitivity of the fibre is increased. Typical saturated values of Δn are 3.4×10^{-5} for standard low-loss fibre ($\sim$4mol% germania), 2.5×10^{-4} for high index fibre ($\sim$20mol% germania) and 7×10^{-4} for boron co-doped fibre ($\sim$15mol% germania)[36].

It is also possible to increase the maximum obtainable Δn by treating the fibre prior to exposure. The first of the two methods to be discussed is pressure hydrogen loading[37,38]. This typically involves soaking fibres in pressurised ($\sim$150 atmospheres) H_2 at room temperature for several days. This process is widely used for fibres containing GeO_2 and can increase Δn typically by two orders of magnitude to easily exceed 0.01. This

increase is thought to come from UV-initiated reactions of the H_2 with the doped glass matrix forming Si-OH groups and oxygen deficient Ge defects which are not dependent on the initial presence of defects. It has also been observed that any unreacted hydrogen will slowly diffuse out of the fibre which results in a shift in the wavelength of the grating[39]. The grating can be stabilised in terms of both wavelength and reflection, if it is post-annealed[40].

The second method, "flame brushing" is less common and involves heating the fibre, up to 1 700°C, with a hydrogen-oxygen burner[41]. This technique increases Δn by an order of magnitude and a value greater than 10^{-3} has been achieved in standard telecommunications fibre[41].

There has also been some investigation on other effects caused by UV exposure. Fonjallaz *et al.*[42] have shown that the tensile stress in the core of Ge doped fibres exposed to UV light is increased. They have further concluded that the photoinduced index change in these fibres is linearly related to this stress change with a proportionality factor of around 0.8×10^{-4} mm^2/kg.

An optical fibre also suffers mechanical degradation resulting from defects created during the fabrication process[43]. These defects, called flaws, act as stress intensifiers and may lead to the formation of fractures in the fibre. Exposure to UV irradiation generates further flaws in the fibre surface. These flaws, in the case of pulsed inscribing, increase with both writing power, total dose and possibly the writing wavelength.

Several studies were conducted into the effect irradiation parameters and fibre handling would have on the performance of the grating. These studies tended to concentrate on gratings photoinscribed with a single pulse of UV fluence. The first study conducted by Feced *et al.*[44] concluded that gratings written with a single pulse of fluence 1 J/cm^2 appreciably degrade the strength of stripped fibre. It further indicated that gratings written at 248 nm were more mechanically degraded than those inscribed at 193 nm. However, Askins *et al.*[45] later inscribed a number of gratings using a single pulse at 248 nm. These fibres suffered no degradation of strength due to the UV exposure. It was therefore concluded that while UV exposure may inflict some damage it is the handling and the stripping of the fibre which contributes mainly to the fail strength of the fibre.

A more recent study by Varelas *et al.*[46] proposed that flaws generated by UV exposure would be countered, to a certain extent, as prolonged exposure would increase the surface temperature of the fibre, hence thermally annealing some of the them. They reported that even with this compensation, the breaking stress of a treated fibre is reduced to 2.5 GPa as compared to 4.7 GPa for a non-irradiated fibre. While results differ from report to report they are all united in that both fibre preparation and irradiation parameters are important to the performance of any inscribed Bragg grating. Careful handling before and after exposure is also important.

2.3.2 Permanence of the inscribed structure

The refractive index change induced by UV light is not permanent. The first detailed study of grating stability[47] proposed a model to explain the thermal decay of fibre Bragg gratings inscribed in germanium co-doped silica fibre. The model showed that the decay of the UV-induced index change could be described by a power law function of time with a small exponent ($< < 1$). The authors described the observed slowing in the decay following the rapid initial decay through a mechanism in which carriers initially excited during writing are trapped in a broad energy distribution of trap states. Each of these states has an associated activation energy barrier that must be overcome in order for the carrier to escape and, hence, cause the index decay. These trapped states can decay with discrete time constants; low activation energy sites decay quickly, while high activation energy sites have a longer life time. The low energy sites will decay during an isothermal annealing process (see next paragraph), thus leaving the longer life, high energy activation states only. This process results in a slight reduction (a few percent) in the reflectivity of the grating, due to the decay of the low activation energy states. The remaining refractive index change can persist for decades (lifetimes in excess of 25 years are predicted[48]). If it is not annealed the reflectivity of the grating will decay rapidly at first, with this rate decreasing substantially with time[49].

Hence, annealing accelerates this initial rapid decay to its conclusion, thus stabilising the grating. Isothermal annealing involves heating the grating to temperatures of between 175-450°C for 6 hours or longer. This treatment also results in a shift in the Bragg wavelength of the structure. This shift is due to two processes; the thermal decay

of the inscribed refractive index change, as outlined above, and the annealing of any dopant-induced refractive index[50]. It is therefore important that any probable shift in wavelength and change in reflectivity caused by annealing is taken into account when writing the grating. It should also be noted that a grating, whether it is pre-annealed or not, can be erased thermally by heating it to around 900°C[51].

In conclusion, without annealing only a few percent of the refractive index will decay over decades at room temperature[49]. However, post-annealing greatly improves the stability of the device over a long period of time. For example, a grating annealed at 300°C for 10 minutes will have its reflectivity reduced from 99% to 90%. However, it is predicted that if this structure is then held at 80°C for 25 years it will only lose a further 0.02% of its reflectivity[48]. This level of thermal and temporal stability is more than sufficient for most applications.

2.4 Fabrication Techniques

2.4.1 Historical

The first grating was written in 1978, at the Canadian Communications Research Centre (CRC) by Hill *et al*[16]. The grating was formed when Argon-ion (488nm) laser radiation was launched into a momomode germania-doped fibre. This result was completely unexpected. In fact, the team was unaware of the growth of the grating until after several minutes when the reflected light intensity increased to a point were almost all the light was reflected from the fibre. Spectral measurements taken after this unexpected observation confirmed that a 1 metre Bragg grating with 90% reflectivity had been inscribed in the core. This was the first demonstration of photosensitivity and was due to the small amount of light reflected back from the end of the fibre interfering with the forward propagating light thus setting up the required standing wave pattern. Hill gratings attracted considerable attention, but as it was only possible to inscribe gratings close to the writing wavelength their application was severely limited.

The inscribed Bragg wavelength problem was alleviated, to a certain extent, by the direct writing method[52]. This involved cementing a single-mode fibre into a grooved

curve in a silica substrate. The fibre was then lapped and polished tangentially to the fibre down to a few tenths of a micron from the core. A thin layer of photoresist would be spun onto the polished surface and exposed to a two beam interference pattern from an argon-ion laser. This led to the formation of a Bragg grating by the interference process already covered. However, this technique was inefficient, limited and awkward. It was not until the advent of the UV holographic technique that Bragg gratings became commercially viable.

2.4.2 Holographic Technique

The first demonstration of this technique was by Meltz *et al.* in 1989[18]. The gratings initially fabricated, using this method, were written into germanosilicate fibre by a frequency doubled tuneable excimer-pumped dye laser operating at 244 nm. These initial structures had reflectivities of 50-55% and were about 4.4 mm in length. While, these gratings were not particularly strong the technique offered a way of writing a grating at any given wavelength by exposing the side of the fibre to the required UV interference pattern. It was also found that this technique was several orders of magnitude more efficient than those outlined by Hill *et al.*[16]. A schematic of the holographic set-up is shown in figure 2.6:

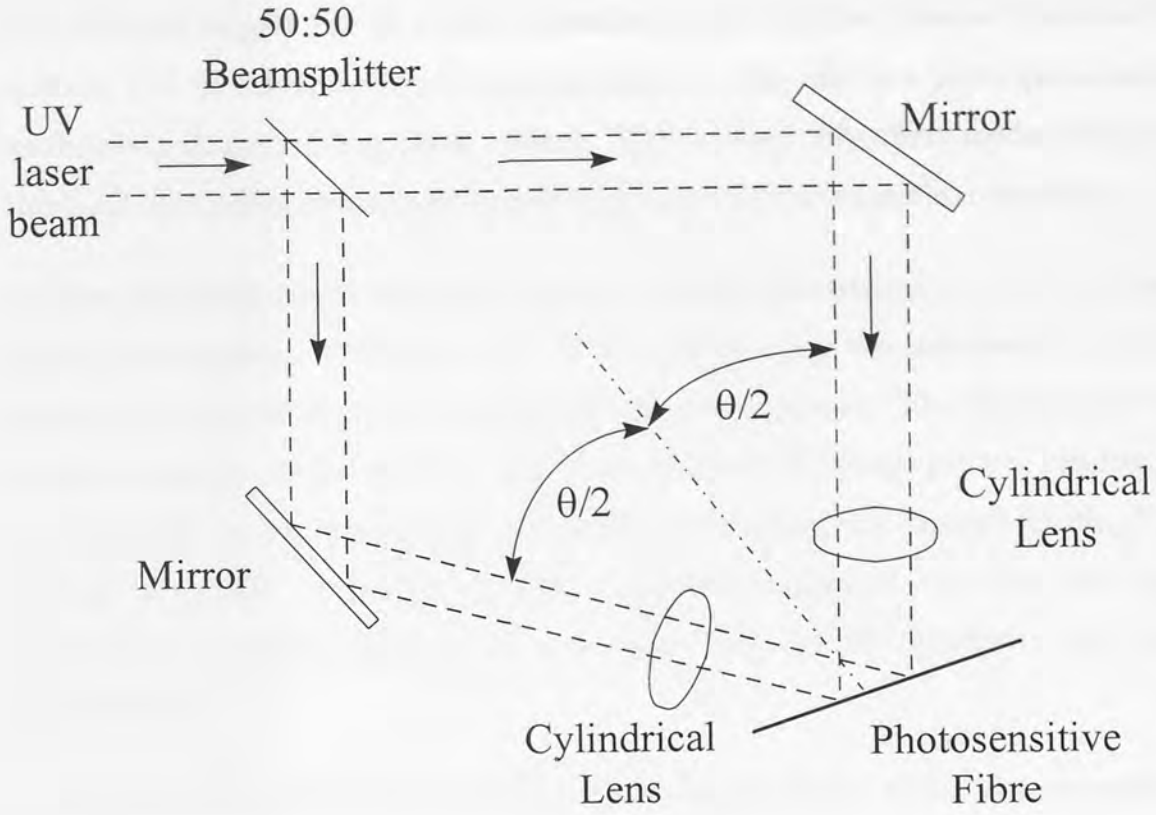

Figure 2.6: Schematic of the transverse holographic method for inscribing uniform FBGs.

In this experimental arrangement the output from a UV laser source is split by a 50:50 beamsplitter. These beams are then incident on two mirrors that are angled such that the laser light will converge at the fibre. Two lenses are employed to focus the beams onto the fibre while an aperture is used to select the central portion of the profile of the beam.

The interference angle and, hence, the Bragg wavelength of the inscribed device can be altered in one of two ways. Small changes may be accomplished by moving the fibre forwards or backwards with respect to the convergence point and then rotating the mirrors to maximise the overlap area on the fibre. Larger changes are brought about by varying the distance between the mirrors and the beamsplitter, hence varying the interference angle. This latter technique is both stable and simple. It offers excellent flexibility for writing gratings of the highest performance at any given wavelengths.

One of first reports of chirped grating fabrication employed the two beam holographic technique. This was communicated by Byron *et al.*[53] and involved exposing a tapered length of photosensitive fibre to a uniform period pattern. The taper was sufficient

(150→50 μm) to give rise to a linear variation in the effective index of the core. A uniform UV interference pattern superimposed on this effective index perturbation resulted in a chirped grating being formed. This method only offers modest chirp (< 3nm) and the small resultant core diameters leave the fibre susceptible to bend loss.

Another technique, which also used a uniform interference pattern to create a chirped grating, was suggested by Sugden *et al.*[54]. This time the chirp was introduced by simple mechanical deformation of an untapered fibre during exposure. The fibre is curved in an approximately circular arc with respect to a uniform UV fringe pattern, resulting in an effective fringe separation that varies continuously along the exposed length. This method is capable of producing both a reasonable amount of chirp and high reflectivities; a grating with a 7.5 nm chirp and >99% reflectivity has been demonstrated.

However, a much more flexible and controllable approach than either of these methods is available. The two beam interferometric holographic technique itself may be modified to write chirped gratings with bandwidths in excess of 50 nm[55]. High reflectivities (~100%), which are dependent on both fibre photosensitivity and exposure time, can be achieved with this method. Chirped gratings are realised by a method of dissimilar curvatures in the interfering wavefronts, which can be brought about by one of three different lens arrangements. The first involves placing a single cylindrical lens in one arm of the interferometer and none in the other[56]. The second involves placing lenses, of differing focal lengths, in both arms[57]. An alternative method is to place a two-lens telescope arrangement in one arm and no lens in the other[58] (see figure 2.7).

In this latter method of inscription two cylindrical lenses with the same focal length, f, are mounted a distance, d, apart; thus forming a telescope. The distance, d, is initially set to be twice the focal length of the lenses and they are arranged, in such a way, so as to produce a collimated beam. This results in the formation of an approximately uniform fringe interference pattern at the fibre as in the case of writing uniform gratings. The telescope is then slightly de-tuned by moving one of the lenses a small distance (Δd) along the path of the UV beam. This has the effect of slightly diverging

or converging the beam; depending on whether the lenses are moved closer or further apart. The more d departs from its original length the greater the period variation of the interference pattern. Therefore, an approximately uniform chirp is introduced into the resultant interference pattern the magnitude of which is dependant on Δd. It is also possible using this method to inscribe a grating with a quadratic chirp. This is achieved by inserting a telescope into each arm of the interferometer and de-focusing both of them by the required amount[58].

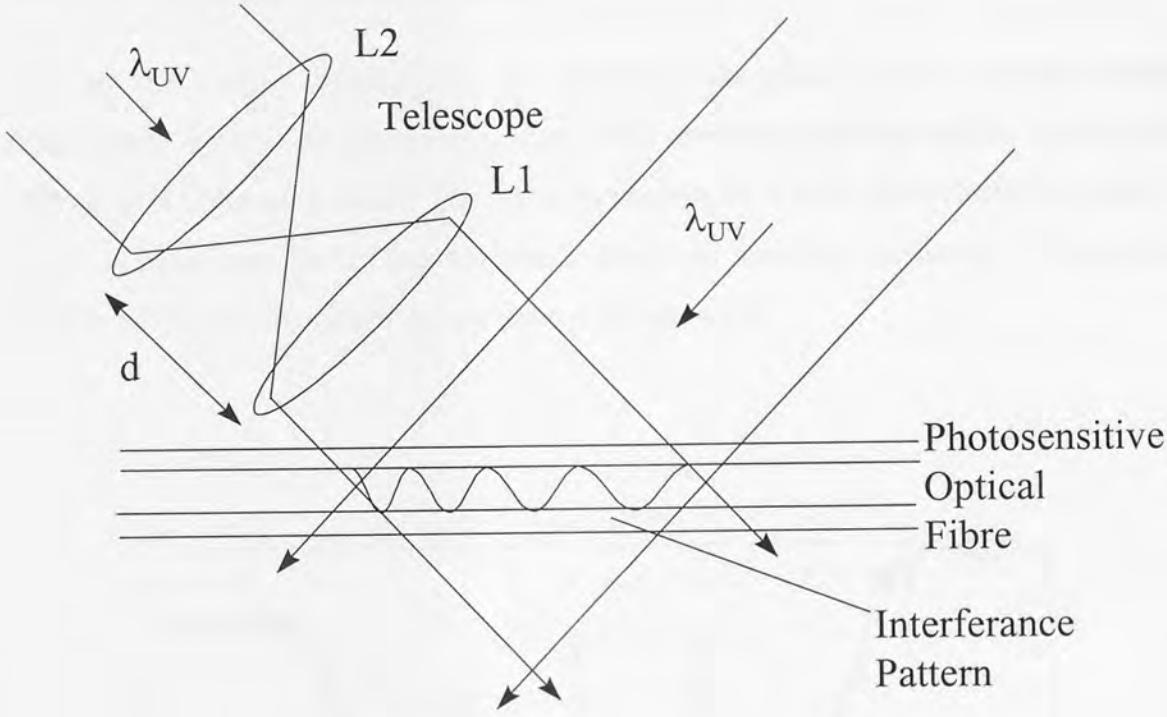

Figure 2.7: Telescopic lens interferometeric arrangement for chirped grating fabrication.

The holographic technique is also capable of writing Moiré gratings. A Moiré resonant structure basically consists of two Bragg gratings separated by an optical phase shift. This superposition of the two gratings produces a "beating" where the slowly varying grating envelope contains a rapidly varying component. Each null in the grating envelope gives rise to a passband in the resulting grating response. Such a structure may be realised by superimposing two gratings with equal amplitude, but slightly different periods (Λ_1,Λ_2). This superimposition results in a Moiré photorefractive grating with a rapidly varying component given by Λ_s:

$$\Lambda_s = 2\Lambda_1\Lambda_2/(\Lambda_1+\Lambda_2) \qquad \textit{Equation 2.12}$$

and a slowly varying envelope given by Λ_c:

$$\Lambda_c = 2\Lambda_1\Lambda_2/(\Lambda_1-\Lambda_2) \qquad \textit{Equation 2.13}$$

This results in a structure with an index modulation ($\Lambda n(z)$) which can be expressed as:

$$\Lambda n(z) = \Lambda n(2 + 2(\cos(\frac{2\pi z}{\Lambda_c}).\cos(\frac{2\pi z}{\Lambda_s})) \qquad \textit{Equation 2.14}$$

where z is the distance along the grating.

Due to the cosine variation of the envelope, the phase of the grating changes intrinsically by π at the crossover points. This produces a corresponding optical phase change of $\pi/2$ hence a Moiré grating is equivalent to a $\lambda/4$ phase-shifted grating. A Moiré grating may be written to have a single or multiple passbands. The spectral profiles of two Moiré structures are shown in figure 2.8:

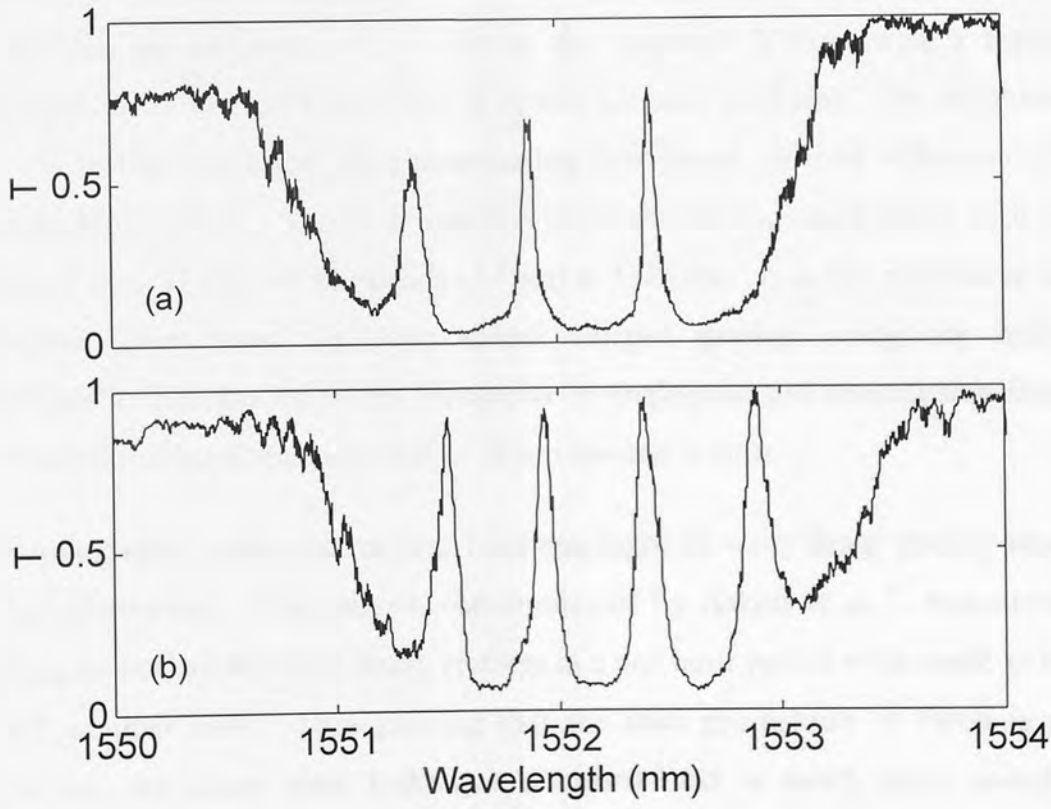

Figure 2.8: The transmission profiles of two Moiré gratings (a) a three passband structure, (b) a four passband structure.

The fabrication of in-fibre Moiré gratings was first reported by Reid *et al.*[59]. The Moiré grating was formed by a double exposure of two interference patterns of slightly different periods. The different periods were obtained by moving the device a precise amount perpendicular to the plane of the grating, thus changing the angle between the interfering beams. These gratings had a single passband and were written by the direct writing method[52] with an argon ion laser.

The first reported production of these gratings employing the holographic technique was by Legoubin *et al.*[60]. In this instance the small change in period between the two gratings was achieved by changing the writing wavelengths (from 243.09 to 243.15 nm) between exposures. A filter with a bandwidth of 0.2 nm centred at 1 200 nm and with a finesse, i.e. the ratio of the width of the resonance dip to the width of the Bragg reflection, of 6 was achieved using this method.

Another way of obtaining the required small change in period between the two structures is by altering the angle between the writing beams. This method was first reported by Zhang *et al.*[61] who, in the same communication, demonstrated that the Moiré concept can be extended to chirped gratings. The employment of chirped devices has the advantage of broadening the stopband; a filter with a transmission linewidth of 0.7 nm and a stopband of 12 nm has been produced. The stopband width can be further increased by concatenating broadband chirped reflectors with the chirped Moiré filter[62]. This technique has led to the fabrication of filters with rejection bands of over 25 nm and passbands of 1 nm at 1549 nm. It is also possible to fabricate bandpass filters based on concatenated chirped gratings using the holographic technique[63]. This has led to the formation of single-passband transmission filters with >30 dB out-of-band rejection over ~ 25 nm spectral widths.

The holographic technique has also been employed to write Bragg grating arrays with in-line fabrication. This process, communicated by Askins *et al.* [64], was successful in writing more than 450 fibre Bragg gratings in a one hour period with single pulses from a KrF excimer laser. Thus proving that the mass production of FBGs is possible. However, the phase mask technique discussed next is much more suited to the manufacture of a large number of identical gratings.

2.4.3 The Phase Mask Technique:

For a number of reasons this technique has now largely supplanted the holographic method, particularly in bulk grating fabrication were reproducibility is a key factor. This method was first applied by Hill *et al.*[65] in 1993. It involves UV exposure through a near-fibre contact phase mask, see fig. 1.7. A phase mask is a length of fused silica which has had a one-dimensional periodic (Λ_{PM}) surface-relief pattern, etched onto it, typically by electron beam lithography[66]. The depth of the corrugations (d) are determined by:

$$d = \lambda_{UV}/2(n_{s(UV)} - 1) \qquad \textit{Equation 2.15}$$

where λ_{UV} is the writing wavelength and $n_{s(UV)}$ is the refractive index of the silica at that wavelength.

UV light, which is incident normally on the phase mask, passes through it and is diffracted by the periodic corrugations. If d is written to have an amplitude determined by equation 2.15 then the UV beam normally incident on the phase mask will be entirely diffracted and no light will be transmitted into the zero order as required. In practice, light is transmitted into the zero order, typically less than 5%, with approximately 40% of the light being diffracted into the ±1 orders The light from these diffracted orders then interfere to inscribe a grating at a wavelength of:

$$\Lambda = \Lambda_{PM}/2 \qquad \textit{Equation 2.16}$$

Therefore the period is independent of, but the corrugation depth depends upon, the writing wavelength.

A variation of this technique which interferes the zero and -1 order by off normal incident has been demonstrated by Anderson *et al*[67].

The phase mask writing technique has a number of advantages:

(i) It yields high performance gratings *,

(ii) It simplifies the manufacturing process,

(iii) It gives high reproducibility,

(iv) It offers easier fibre alignment;

(v) It places lower coherence demands on the UV source;

(vi) It requires less stability of the inscribing apparatus than the holographic technique.

(*Note: A grating produced by this technique is only as good as the phase mask used. Lithographically induced phase masks are usually generated by stitching together small sub-sections (0.4 by 0.4 mm) of periodic corrugations on the mask substrate, in order to fabricate large phase structures. An error in the precise positioning of the various subsections will result in what is commonly referred to as a stitching error[68]. Large stitching errors in a phase mask result in a Bragg grating that is characterised by ghost peaks on both sides of the main reflection peak. This situation does not occur for gratings written using the holographic technique.)

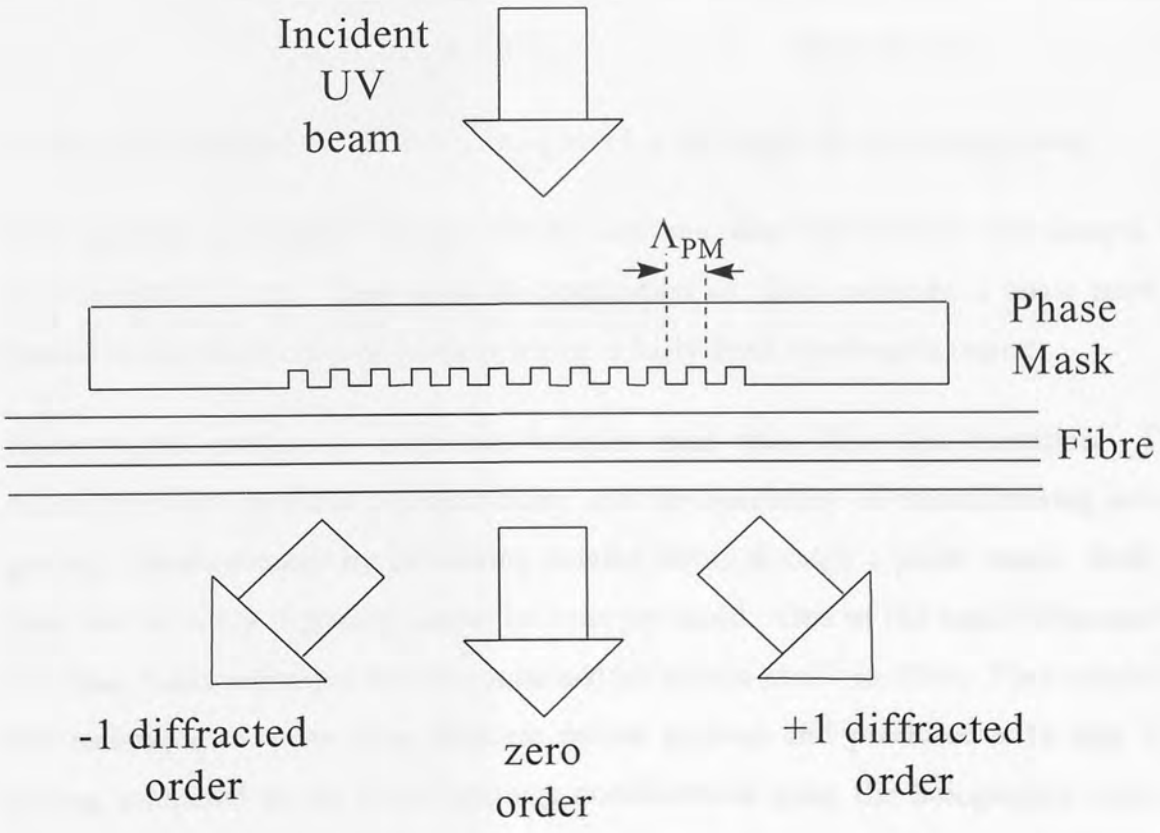

Figure 2.9: Schematic of the phase mask technique for the fabrication of Bragg gratings.

The obvious disadvantage to this technique is its written wavelength inflexibility, i.e. a separate phase mask is required for each different Bragg wavelength. This limitation can be overcome in several ways. The first was suggested by Prohaska *et al.*[69] and involves placing a magnifying lens before the phase mask, which can produce a shift in the Bragg wavelength of 2 nm. The second method is more common and involves stretching the fibre prior to and during exposure[70]. After the photoimprinting process, the fibre is relaxed resulting in a shift of ~2.5 nm in Bragg wavelength. Yet another technique was demonstrated by Othonos *et al.*[71]. In this instance, the spatial coherence of the UV source was a factor and the writing laser had to be modified accordingly. This modification led to the production of dramatically improved gratings and the ability to write structures with the fibre at an angle to the phase mask. In previously mentioned techniques, the fibre lies parallel to the phase mask. However, if the UV source has sufficient spatial coherence it is possible to place one end of the fibre against the mask and the other end at some distance, r, away. The inscribed Bragg wavelength is then given by:

$$\lambda_b = 2n\Lambda\,(1 + r^2/l^2)^{1/2} \qquad \textit{Equation 2.17}$$

where Λ is the period of the fibre grating and l is the length of the phase grating.

This method is suitable for fine tuning and can alter the written wavelength by approximately 2 nm. Even with the application of these methods, a phase mask is limited to the production of gratings within a fairly fixed wavelength region.

However, the previously mentioned benefits more than offset this limitation. This technique offers excellent reproducibility and the possibility of manufacturing several gratings simultaneously by irradiating parallel fibres through a phase mask. Both of these are necessary if gratings are to be mass produced. One of the main advantages of the phase mask technique was demonstrated by Martin *et al.*[72] in 1994. They employed this technique to write long, uniform period gratings and produced a 15 mm long grating compared to the 5 mm gratings manufactured using the holographic method. This was achieved by translating both the fibre and phase mask through the fixed, normally incident UV beam. Another method reported by Rourke *et al.*[73] involved moving the UV beam along the length of the phase mask while keeping it and the fibre

static. This produced a 50 mm long grating. A similar method allows the fibre to move relative to the phase mask while the UV beam is scanning[74]. This method produced gratings about 16 mm long but the main advantage of this technique lies in its flexibility so wavelength shifts, apodisation (discussed next) and phase-shifted gratings can be achieved. This technique was further developed to compensate for imperfections in the phase mask[75]. Thus, a 10 cm long "uniform" phase mask which normally produced gratings with an uncontrolled bandwidth of 0.23 nm was corrected to manufacture gratings with a bandwidth of 0.1 nm.

The phase mask technique can also be used to fabricate gratings with very controlled spectral characteristics. As discussed earlier, the main peak in the reflection spectrum of a finite length Bragg grating, with uniform modulation of the refractive index, is accompanied by a series of side lobes at adjacent wavelengths. This response is undesirable in certain applications such as wavelength division multiplexing and, to a certain extent, sensing. As mentioned earlier, these side lobes are due to multiple reflections to and from opposite ends of the grating region. Therefore, if the refractive index change is modulated, so that it is small at either end of the grating, then these reflections, and hence side lobes, will be reduced. If the amplitude of the index modulation along the length of the fibre is given a bell-like functional shape, rather than just being constant, then these secondary maxima are suppressed[12].

This procedure of adjusting the amplitude profile of the index modulation is called apodisation. There are several methods for writing apodised gratings with a phase mask. These have included exposing the fibre to UV light through a phase mask with a locally varying diffraction efficiency[76]; by symmetrically stretching the fibre by exactly half a period at the ends of the grating during writing[77] and by double exposure of the fibre through a "normal" phase mask[78]. The latter technique allowed the writing of a uniform grating, which, 0.4 nm from its central wavelength, had a reflectivity of 40 dB down on its peak reflectivity. This is an improvement of over 20 dB on an un-apodised structure with similar bandwidth and peak reflectivity.

It is also possible to write chirped gratings with the advantages afforded by the phase mask technique. These gratings can be obtained from the application of uniform or

chirped phase masks. The first category offers a modest amount of chirp, but permits tunability of the spectral properties of the structure. Such structures can be manufactured in a number of ways. The first of these was suggested by Hill *et al.*[79] and uses a double exposure method. The first exposure photoinduces a linear variation of $n_{eff}(z)$ along the section of irradiated fibre. This is achieved by positioning an opaque mask between the fibre and the UV beam, see figure 2.10. The mask is then translated at a constant velocity allowing the fibre to be exposed to the light; the initial section being exposed for more time than the final section, hence inducing different refractive index changes.

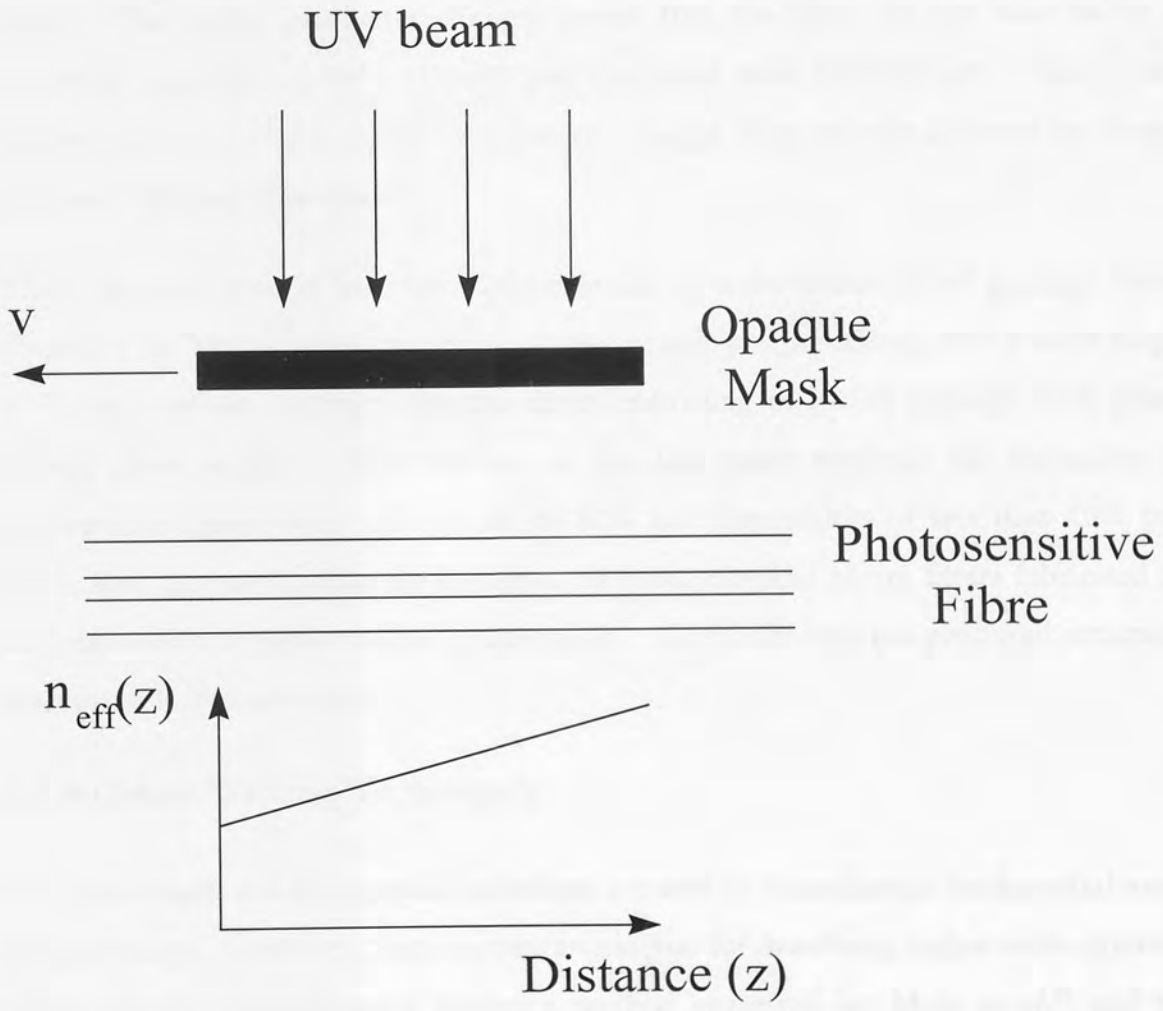

Figure 2.10: Initial UV exposure to photoinduce a linear variation of $n_{eff}(z)$ controlled by a moving opaque phase mask.

The second exposure is then done through a standard, uniform period phase mask onto the same section of fibre. Although the resulting structure has a linear period the photoinduced "background" variation of $n_{eff}(z)$ introduces the required chirp.

A phase mask equivalent of the chirping technique, reported by Byron *et al.*[53], was demonstrated by Putnam *et al.*[80] in 1995. Once again a tapered fibre was used, but in this case it was the strain gradient that resulted from the fibre being under tension that permitted the chirp. The tapered part of the fibre would be strained while being exposed to a uniform UV interference pattern. After exposure the fibre would be relaxed and, due to the strain gradient applied while writing, a chirped grating would result. This strain gradient technique meant that the fibre did not have to be as extremely tapered, i.e. only 115→85 μm compared with 125→50 μm. Again, only modest chirp is available (a few nanometers). Larger chirp may be achieved by using a dedicated chirped phase mask[81].

There are several ways to employ phase masks to write phase-shifted gratings, hence obtaining the Moiré grating response. These include postprocessing over a short length of a long uniform grating[82] and the direct inscribing of Moiré gratings with phase-shifted phase masks[83]. The authors of this last paper reported the formation of transmission peaks with reflectivities of 80% and bandwidths of less than 0.01 nm. There has also been recent developments in multipassband Moiré filters fabricated by dual exposure through a chirped phase mask[84]. This technique has produced structures with up to four passbands.

2.4.4 Other Writing Techniques

The phase mask and holographic technique are used to manufacture fundamental order Bragg gratings. However, there are two techniques for inscribing higher order gratings. These are the point-by-point exposure method suggested by Malo *et al.*[85] and the application of an amplitude mask[86]. The first of these involves photoinducing one period of refractive index change at a time. An excimer laser, operating in pulsed mode, was employed as the UV source. The fibre was exposed to the UV light through a slit, whose image then determined the length of each refractive index change. In between pulses the fibre was translated by the required amount before being exposed again. The

size of the slit image is too large to allow gratings to be written at the fundamental mode, however second order structures with reflectivities of up to 70% were obtained.

The second method employed an amplitude mask, which is considerably coarser and cheaper than a phase mask[86]. In the initial experiment, a lens was used to image the amplitude mask onto the fibre. The source employed was a pulsed KrF laser and moderate strength 6th order gratings were fabricated. However, the maximum strength was limited to 5.5 dB and significant loss due to fibre damage was observed.

This technique was utilised by Wagener *et al.*[87] to fabricate 4th and 5th order gratings with a frequency doubled Argon-ion laser. The UV output was focused to a broad line using a 10X beam expander and a 15 cm cylindrical lens before being incident on the amplitude mask located immediately in front of the fibre. The gratings fabricated were 5 mm and typically had transmission peaks of 22 dB around 1560 nm. These techniques have several advantages as they do not require laser coherence, alignment stability or mask precision. However, they will not replace the phase mask technique due to long exposure times and the high background DC change. Instead, they are likely to find application in the manufacture of low reflectivity gratings where precision and narrow linewidth is not required.

2.5 Applications

Bragg gratings have a large number of applications. The subject of this thesis is their application as sensing elements. However, a brief review of their other uses is presented here.

2.5.1 Fibre Lasers and Amplifiers

The wavelength selective nature of an FBG makes it ideal as a "mirror" for a fibre laser. Two gratings with high reflectivities of around 90% can be written into a fibre a few centimetres apart, thus defining a cavity length. A suitable dopant has to be added to this length of fibre to introduce a gain medium. Dopants introduced to date have included erbium[88,89] neodymium[90], praseodynium[91], erbium-yetterbium[92] and thulium[93].

A simple cavity arrangement is shown in figure 2.11. The length of doped fibre required for lasing in such an arrangement may be as small as a few centimetres[94]. It should be noted that the gratings may be formed either in the doped or normal fibre. If the gratings are written into standard fibre then they are spliced onto the ends of the doped fibre.

One of the advantages of this simple structure is that a shift in the spectral profile of a grating may be achieved by applying strain to it; this is covered thoroughly in the next chapter. The strain induced shift in Bragg wavelength of the two gratings that form the cavity permits the laser to be continuously tuned. This ability has been demonstrated for a single mode fibre laser by Ball *et al*[95]. The authors of this paper conclude that a tuning range of 21 nm for such a laser is obtainable.

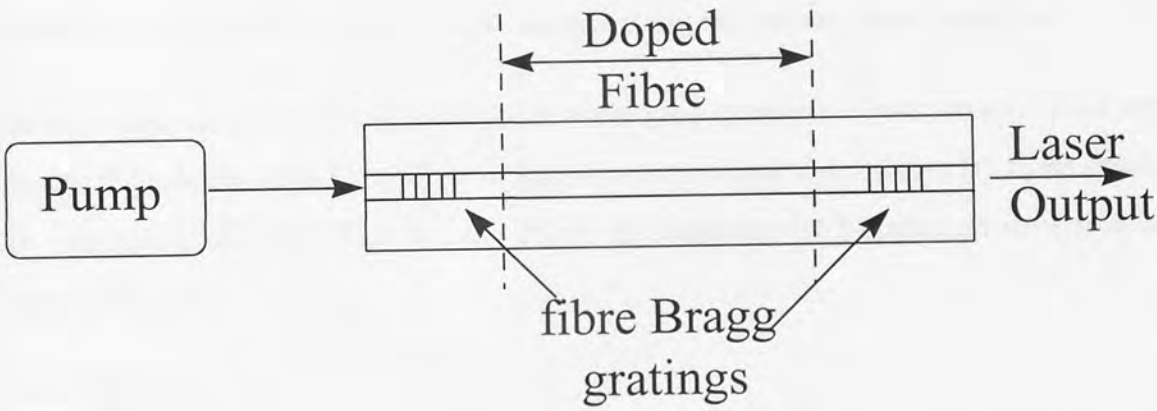

Figure 2.11: Configuration of a simple doped fibre laser with a lasing cavity formed by two FBGs.

It has also been demonstrated that, by using a more complex arrangement, pulses may be generated in fibre lasers employing FBGs[96]. Gratings in this area have also found application in the wavelength stabilisation of semiconductor lasers. This has occurred to the extent were wavelength-stabilised 980 nm pump lasers[97] are now commonly deployed to increase amplifier reliability. The judicious employment of gratings may also enhance amplifier performance by:

(i) the reflection of unused pump light back into the gain medium[98];

(ii) the discrimination of pump and signal light;

(iii) the flattening of the spectral profile of the amplifier gain[99];

(iv) the facilitating of gain control[100];

An arrangement for achieving all optical automatic gain control, reported by Massicott *et al.*[101], is show in figure 2.12.

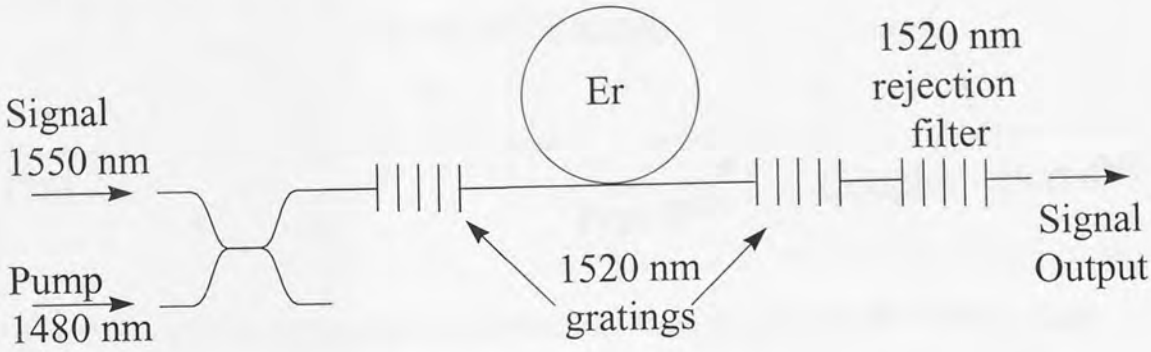

Figure 2.12: Schematic of an all optical automatic control erbium doped amplifier.

In this technique, two Bragg gratings are employed to define a laser cavity. This cavity forces the erbium doped amplifier to lase at a wavelength determined by these gratings; in this case 1520 nm. This has the effect of clamping the population inversion and, hence, the gain.

2.5.2 Filters

Moiré gratings, covered earlier on, are simpler to implement and do not require carefully controlled balanced arms, identical gratings or 3 dB couplers as in the systems to be discussed here. They make ideal filters for any fibre system that requires a narrowpass band within a reasonable stopband.

A range of other and similar filters may be realised by the use of chirped and uniform gratings. These include in fibre Fabry-Perot-like filters[102] and other types of comb devices[103]. One, similar in function to the Moiré filter, employs the Michelson approach. Figure 2.11 shows the all fibre arrangement for both a Michelson and a Mach-Zender interferometer implemented with 3 dB couplers and two identical FBGs.

Both interferometers share the same input port, with the Michelson arrangement terminating at the output ports marked Mi.

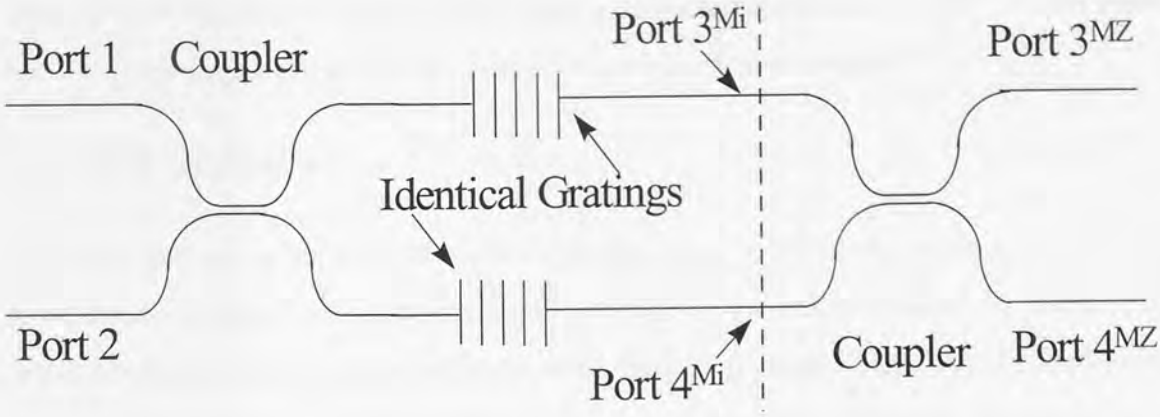

Figure 2.13:All-fibre grating-based Michelson and Mach-Zender interferometeric filters.

The Michelson interferometer is employed as a filter to pick out one wavelength from a multiwavelength signal. The chosen wavelength is determined by the Bragg wavelength of the identical gratings. For example a signal consisting of wavelengths $\lambda_1,\lambda_2,\lambda_B..\lambda_n$, where λ_B is the Bragg wavelength, is incident at port 1. The signal is split in two by the coupler with the two halves then being incident on the identical gratings. The structures reflect λ_B with the remaining wavelengths being transmitted, in equal portions, to ports 3 and 4. The reflected light is again incident on the coupler, but with a π phase difference between the two halves. This results in the emergence of the whole of the signal at λ_B from port 2. These devices have exhibited a 0.25 nm bandwidth passband, an excess loss of 1.2 dB and excellent temperature stabilisation[104].

The second type of interferometric filter shown in figure 2.13 is the Mach-Zender. Here a second 3 dB coupler is added to the Michelson arrangement; hence forming a Mach-Zender interferometer with outputs at ports 3^{MZ} and 4^{MZ}. This addition converts the bandpass to a wavelength add/drop filter[105]. In this arrangement, the wavelengths transmitted by the identical structures are incident on the second coupler. This recombining results in all their power emerging from port 4^{MZ} with, ideally, no power being transmitted from port 3^{MZ}. Thus the wavelength λ_B is dropped from the original signal, with the new signal being transmitted from port 3^{MZ}.

A wavelength λ_B to be added to a signal is incident on port 1, while the signal itself is placed on port 3[MZ]. This results in the new combined signal being emergent from port 2. One report of this type of all fibre filter has been produced which can multiplex/demultiplex a signal centred on 1558.7 nm with any other wavelength in the 1550 nm transmission window with a maximum insertion loss if 1.0 dB[106]. This type of filter is a key requirement for future telecommunication networks[107].

2.5.3 Other applications

There are several other uses of fibre Bragg gratings. One of the main ones yet to be mentioned is dispersion compensation[108], which is an entire subject in itself[3]. The desired compensation may be achieved with chirped gratings[109] and, to a limited extent, uniform structures[110]. This method utilises the fact that different wavelengths are reflected at different points along a grating; this effect is more pronounced in chirped gratings. Longer wavelengths travel further through the grating before being reflected. This allows the shorter wavelengths to "catch up" with the faster long wavelengths thus compressing the widened pulse. The more compensation required, which is determined by the distance the pulse has travelled in dispersive fibre, the longer the grating has to be. Experimental demonstrations have shown considerable pulse compression is achievable with such structures[111].

Bragg gratings are also now finding application in a number of telecommunication systems[112]. In addition to their dispersion compensation, filtering and WDM applications they have also been employed in optical switching[113] and pulse generation[114]. A recent communication by Broderick *et al.*[115] investigated non-linear pulse interactions in Bragg grating structures. The authors demonstrated the optical pushbroom in action, i.e. the continuous wave switching of a weak probe by a strong pump beam. This effect will find application in all optical networks.

One of their emerging applications is in the field of microwave photonics[116,117,118]. A recent communication by Zhang *et al.*[119] reported the demonstration of a tuneable optical radio frequency notch filter using a linearly chirped Bragg grating. This simple tuneable notch filter realised by the application of a linearly chirped grating can provide time delay linearly or continuously either by changing the wavelength of the optical

carrier or by tuning the grating. This technique offered a low cost, compact and flexible real signal processing technique for radio frequency systems.

Fibre Bragg gratings are compact, robust, light weight, immune to electromagnetic interference and can operate in a wide range of environmental conditions. The origins of the fibre photosensitivity and the processes involved in writing are still not fully understood. However, several methods for writing a range of such structures have been developed and a number of devices with complex responses have been realised. They have a number of applications and will play a prime role in fibre telecommunication and sensor systems of the future. It is highly likely that due to their robustness, flexibility and potential for mass production this field is likely to continue expanding for a number of years to come.

---

[1] I. Bennion, J.A.R. Williams, L. Zhang, K. Sugden and N.J. Doran "UV- written in-fibre Bragg gratings", *Optical and Quantum Electronics*, **28**, 1996, pp 93-13

[2] K.O. Hill and G. Meltz "Fiber Bragg grating technology fundamentals and overview", *J. Lightwave Tech.*, **15**, 1997, pp 1263-1276.

[3] C.R. Giles "Lightwave applications of fiber Bragg gratings", *J. Lightwave Tech.*, **15**, 1997, pp 1391-1404.

[4] J. Archambault and S. G. Grubb "Fiber gratings in lasers and amplifiers", *J. Lightwave Tech.*, **15**, 1997, pp 1378-1390.

[5] Y. Rao, "In-fibre Bragg grating sensors", *Meas. Sci. Technol.*, **8**, 1997, pp 355-375

[6] K.O. Hill, B. Malo, F. Bilodeau and D.C. Johnson "Photosensitivity in optical fibres", *Ann. Rev. Mat. Sci.*, **23**, 1993, pp 125-127.

[7] J. Bures, S. Lacroix and J. Lapierre, "Bragg reflector induced by photosensitivty in an optical fibre: model of growth and frequency response", *Appl.. Opt.*, **21**, 1982, pp 3502-3505.

[8] Y. Zhao and J.C. Palais, "Fiber Bragg grtaing coherence spectrum modelling, simulation and characteristics", J. Lightwave Tech., 15, 1997 pp 154-160.

[9] G.P. Agrawal, "Nonlinear fibre optics", *2nd ed, Academic Press*, San Diego, 1995, pp 451-456.

[10] D.K.W. Lam and B.K. Garside, "Characterisation of single-mode optical fibre filters," *Applied Optics*, **20**, 1981, pp 440-445.

[11] M. Matsuhara and K.O. Hill, "Optical-waveguide band rejection filters: design", *Appl. Opt.*, 13, 1974, pp 2886-2888.

[12] K.O. Hill, "Aperiodic distributed-parameter waveguides for integrated optics", *Appl Opt.*, 13, 1974, pp 1853-1856.

[13] H. Kogelnik, "Filter response of nonuniform almost-periodic structures", *Bell Syst Techn J.*, 55, 1976, pp109-1126.

[14] B-G. Kim and E. Garmire, "Comparison between the matrix method and the coupled-wave in the analysis of Bragg reflector structures", *J. Opt. Soc. Amer. A*, 9, 1992, pp132-136.

[15] J. Hong, W. Huang and T. Makino, "On the transfer matrix method for distributed feedback waveguide devices", *J. Lightwave Tech.*, 10, 1992, pp 1960-1968.

[16] K.O. Hill, Y. Fujii, D.C. Johnson and B.S. Kawasaki, "Photosensitivity in optical waveguides: Application to rejection filter fabrication," *Appl. Phys. Lett.*, 32, 1978, pp 647.

[17] D.K.W. Lam and B.K. Garside, "Characterisation of single-mode optical fibre filters," *Appl. Opt.*, 20, 1981, pp 440-445.

[18] G. Meltz, W.W. Morey and W.H. Glen, "Formation of Bragg gratings in optical fibres by a transverse holographic method," *Opt. Lett.*, 14, 1989, pp 823-825.

[19] D.P. Hand and P. St J Russell, "Photoinduced refractive-index changes in germanosilicate fibres", *Opt. Lett.*, 15, 1990 pp 102-104.

[20] J.P Bernardin and N.M. Lawandy "Dynamics of the formation of Bragg gratings in germanosilicate optical fibres", *Opt. Commun.*, 79, 1990, pp 194-199.

[21] K.D. Simmons, S LaRochelle, V. Mizrahi, G.I. Stegeman and D.L. Griscom, "Correlation of defect centres witha wavelength-dependent photosensitive response in germania-doped silica optical fibres", *Opt. Lett.*, 16, 1991, pp 141-143.

[22] T.E. Tsai, C.G. Askins and E.J. Friebele, "Photoinduced grating and intensity dependence of defect generation in Ge-doped silica optical fibre", *Appl. Phys Lett.*, 61, 1992, pp 390-392.

[23] R.M. Atkins, V. Mizrahi and T. Erdogan, "248 nm induced vacuum UV spectral changes in optical fibre preform cores: Support for a colour centre model of photosensitivity", *Electron. Lett.*, 29, 1993, pp 385-387.

[24] W.X. Xie, P. Niay, P. Bernage, M. Douay, J.F. Bayon, T. Georges, M. Monerie and B. Poumelle, "Experimental evidence of two types of photorefractive effects occuring during photoinscriptions of Bragg gratings within germanosilicate fibres", *Opt. Commun.*, 104, 1993, pp 185-195.

[25] P. Cordier, J C Doukhan, E Fertein, P Bernage, P Niay, J.F. Bayon and T. Georges, "TEM characterisation of structural changes in glass associated to Bragg grating inscription in a germanosilicate optical fibre preform", *Opt. Commun.*, 111, 1994, pp 269-275.

[26] K.S. Chiang, M G Sceats and D. Wong, "Ultraviolet photolytic-induced changes in optical fibres: the thermal expansion coefficient", *Opt. Lett.*, 18, 1993, pp 965-967.

[27] K. Tanaka, N. Toyosawa and H. Hisakuni "Photoinduced Bragg gratings in As2S3 optical fibres", *Opt. Lett.*, 20, 1995, pp 1976-1978.

[28] M.M. Broer, R.L Cone and J.R. Simpson "Ultraviolet-induced distributed feedback gratings in Ce3+-doped silica optical fibres", *Opt. Lett.*, **16**, 1991, pp 1391-1393.

[29] K.O. Hill, B. Malo, F. Bilodeau, D.V. Johnson, T.F. Morse, A. Kiliam, L.Reinhart and O. Kyunghwan "Photosensitivty in Eu^{2+}:Al_2O_3-doped-core fibre: preliminary results and application to mode converters", *Conf. On Optical Fibre Comm. (OFC '91)*, San Diego, California, Post-Deadline Papers, Feb 1991, PD3.

[30] I Bennion, D.C.J. Reid, C.J. Rowe and W.J. Stewart "High-reflectivity monomode-fibre grating filters", *Electron. Lett.*, **22**, 1986, pp 341-343.

[31] J. Albert, B. Malo, F. Bilodeau, D.C. Johnson, K.O. Hill, Y. Hibino and M. Kawachi, "Photosensitivity in germanium-doped silica optical waveguide and fibres using 193 nm light from an ArF excimer laser", *Opt. Lett.*, **19**, 1994, pp 387-389.

[32] D.S. Starodubov, V. Grubsky, J. Feinberg, B. Kobrin and S. Juma "Bragg grating fabrication in germanosilicate fibers by use of near-UV light: a new pathway for refractive index changes" *Opt. Lett.*, **22**, 1997, pp 1086-1088.

[33] J.L. Archambault, L. Reekie and P. St.J, Russell, "High reflectivity and narrow bandwidth fibre gratings written by single excimer pulse", *Electron. Lett.*, **29**, 1993, pp 28-29.

[34] R. Kashyap, J.R. Armitage, R. Wyatt, S.T. Davey and D.L. Williams, "All-fibre narrowband reflection gratings at 1500 nm", *Electron. Lett.*, **26**, 1990, pp 730-732.

[35] P. Niay, P. Bernage, S. Legoubin, M. Douay, W,X, Xie, J.F. Bayon, T. Georges, M. Monerie and B. Poumellec, "Behaviour of spectral transmissions of Bragg gratings written in germania-doped fibres: writing and erasing experiments using pulsed or cw uv exposure", *Optics Comms.*, **113**, 1994, pp 176-192.

[36] H.G. Limberger, P.Y. Fonjallaz and R.P. Salathe, "Spectral characterisation of photoinduced high efficient Bragg gratings in standard telecommunications fibres", *Electron. Lett.*,, **29**, 1993, pp 47-48.

[37] P.J. Lemaire, R.M. Atkins, V. Mizrahi and W.A. Reed, "High pressure H_2 loading as a technique for achieveing ultrahigh UV photosensivity and thermal sensitivity in GeO2 doped optical fibres", *Electron. Lett.*, **29**, 1993, pp 1191-1193.

[38] R.M. Atkins, P.J. Lemaire, T. Erdogan and V. Mizrahi, "Mechanisms of enhanced UV photosensitivity via hydrogen loading in germanosilicate glasses", *Electron. Lett.*, **29**, 1993, pp 1234-1235.

[39] B. Malo, J. Albert, K.O. Hill, F. Bilodeau and D.C. Johnson, "Effective index drift from molecular hydrogen diffusion in hydrogen-loaded optical fibres and its effect on Bragg grating fabrication", *Electron. Lett.*, 30, 1994, pp 442-444.

[40] P.J. Lemaire "Enhanced UV photosensitivity in fibres and waveguides by high pressure hydrogen loading", *Conf. On Optical Fibre Communication (OFC '95)*, San Diego, California, 1995, Tech. Dig., pp 162-163.

[41] F. Bilodeau, B. Malo, J. Albert, D.C. Johnson, K.O. Hill, Y. Hibino, Y. Abe, M. Kawachi, "Photosensitisation of optical fibre and silca-on-silicon/silica waveguides", *Opt. Lett.*, **18**, 1993, pp 953-955.

[42] P.Y. Fonjallaz, H.G. Limberger, R.P. Salathe, F. Cochet and B. Leuenberger, "Tension increase correlated to refractive-index change in fibres containing UV-written Bragg gratings", *Opt. Lett.*, 20, 1995, pp 1346-1348.

[43] R. Olshansky and D.R. Maurer, "Tensile strength and fatigue of optical fibres", *J. Appl. Phys.*, **47**, 1976, pp 4497-4499.

[44] R. Feced, M.P. Roe-Edwards, S.E. Kanellopolous, N.H. Taylor and V.A. Hendrick, "Mechanical strength degradation of UV exposed optical fibres", *Electron. Lett.*, **33**, 1997, pp 157-159.

[45] C.G. Askins, M.A. Putnam, H.J. Patrick and E.J. Friebele, "Fibre strength unaffected by on-line writing of single-pulse Bragg gratings", *Electron. Lett.*, **33**, 1997, pp 1333-1334.

[46] D. Varelas, H.G. Limberger, R.P Salathe and C. Kotrotsios, "UV-induced mechanical degradation of optical fibres", *Electron. Lett.*, **33**, 1997, pp 804-806.

[47] T. Erdogan V. Mizrahi, P.J. Lemaire and D. Monroe "Decay of ultraviolet-induced fiber Bragg gratings" *J. Appl. Phys.*, **76**, 1994, pp 73-80.

[48] D.L. Williams and R.P. Smith "Accelerated lifetime tests on UV written intra-core gratings in boron germania co-doped silica fibre", *Electron. Lett.*, **31**, 1995, pp 2120-2121.

[49] T. Erdogan V. Mizrahi, P.J. Lemaire and D. Monroe "Decay of ultraviolet-induced fiber Bragg gratings" *J. Appl. Phys.*, **76**, 1994, pp 73-80.

[50] K..E. Chisholm, K. Sugden and I. Bennion, "Effects of thermal annealing on Bragg fibre gratings in boron/germania co-doped fibre", J. *Phys. D: Appl Phys.*, **31**, 1998, pp 61-64.

[51] R.M. Atkins and V. Mizrahi "Observation of changes in UV absorption bands of single-mode germanosilicate core optical fibres on writing and thermally erasing refractive index gratings", *Electron. Lett.*, **28**, 1992, pp 1743-1744.

[52] I. Bennion, D.C.J. Reid, C.J. Rowe and W.J. Stewart, "High reflectivity monomode-fibre grating filters", *Electron. Lett.*, **22**, 1986, pp 341-343.

[53] K.C. Byron, K. Sugden, T. Bricheno and I. Bennion, "Fabrication of chirped Bragg gratings in photosensitive fibre", *Electron. Lett.*, **29**, 1993, pp 1659-1660.

[54] K. Sugden, I. Bennion, A. Molony and N.J. Copner, "Chirped gratings produced in photosensitive optical fibres by fibre deformation during exposure", *Electron. Lett.*, **30**, 1994, pp 440-442

[55] K. Sugden, I. Bennion, A. Molony M.C. Farries, D.C.J. Reid and M.J. Goodwin, "Fabrication and properties of chirped fibre gratings with reflection bandwidths exceeding 50 nm and narrow bandpass fibre grating filters", *CLEO Europe*, Amsterdam, Netherlands, Tech. Dig., 1994, CWF57.

[56] A. Katazir, A.C. Livanos, J.B. Shellan and A. Yariv, "Chirped gratings in integrated optics", *IEEE J. Quantum. Electron.*, **12**, 1977, pp 296-304.

[57] M.C. Farries, K. Sugden, D.C.J. Reid, I. Bennion, A. Molony and M.J. Goodwin, "Very broad reflection bandwidth (44 nm) chirped fibre gratings and narrow bandpass filters produced by the use of an amplitude mask", *Electron. Lett.*, **30**, 1994, pp 891-892.

[58] K. Sugden, L. Zhang, J.A.R. Williams and I. Bennion, "Dissimilar wavefront technique for linear and quadratic chirps", *Photosensitivity and quadratic non-linearity in glass waveguides: Fundamentals and applications*, U.S., 1995, Tech. Dig., pp. 136-139

[59] D.C.J. Reid, C.M. Ragdale, I. Bennion, D.J. Robbins, J. Buus and W.J. Stewart, "Phase-shifted Moiré gratin fibre resonators", *Electron. Lett.*, **26**, 1990, pp 10-12.

[60] S. Legoubin, E. Fertein, M. Douay, P. Bernage, P. Niay, F. Bayon and T. Georges, "Formation of Moiré grating in core of germanosilicate fibre by transverse holographic double exposure method", *Electron. Lett.*, **27**, 1991, pp 1945-1947.

[61] L. Zhang, K. Sugden, I. Bennion and A. Molony, "Wide-stopband chirped fibre Moiré grating transmission filters", *Electron. Lett.*, **31**, 1995, pp 477-279.

[62] K. Sugden, L. Zhang, J.A.R. Williams, R.W. Fallon, L.A. Everall, K.E. Chisholm and I. Bennion, "Fabrication and characterisation of bandpass filters based on concatenated chirped fibre gratings", *J. Lightwave. Technol.*, **15**, 1997, pp 1424-1432.

[63] K. Sugden, L. Zhang, J.A.R. Williams, R.W. Fallon, L.A. Everall, K.E. Chisholm and I. Bennion, "Fabrication and characterization of bandpass filters based on concatenated chirped fiber gratings", *J. Lightwave. Technol.*, **15**, 1997, pp 1424-1432.

[64] C.G. Askins, M.A. Putnam, G.M. Williams and E.J. Friebele, "Stepped-wavelength optical-fibre Bragg grating arrays fabricated in line on a draw tower", *Opt. Lett.*, **19**, 1994, pp 147-149.

[65] K.O. Hill, B. Malo, F. Bilodeau, D.C. Johnson and J. Albert, "Bragg gratings fabricated in monomode photosensitive optical fibre by UV exposure through a phase mask", *Appl. Phys. Lett.*, **62**, 1993, pp 1035-1037.

[66] X. Liu, R.M. De La Rue, T.F. Krauss, S. Thoms, S.E. Hicks, J.S. Aitchinson, L. Zhang, J.A.R. Williams and I. Bennion, "Electron beam production of phase masks for direct writing of photosensitive gratings", *CLEO Europe*, Germany, 1996, Tech. Dig., CThF3.

[67] D.Z. Anderson, V. Mizrahi, T. Erdogan and A.E. White, "Production of in-fibre gratings using a diffractive optical element", *Electron. Lett.*, **29**, 1993, pp 566-568.

[68] X. Lu et al. "The influence of phase mask stitch errors on the performance of UV-written Bragg gratings", *Conf.: Bragg gratings, photosensitivity and poling in glass fibres and waveguides*, Willaimsburg, U.S., Tech. Dig., 1997, BMG9-1.

[69] J.D. Prohaska, E. Snitzer, S. Rishton and V. Boegli, "Magnification of mask-fabricated fibre Bragg gratings", *Electron. Lett.*, **29**, 1993, pp 1614-1615.

[70] Q. Zhang, D.A. Brown, L. Reinhart, T.F. Morse, J.Q. Wang, G. Xiao, "Tuning Bragg wavelength by writing gratings on prestrained fibres", *Photon. Technol. Lett.*, **6**, 1994, pp 839-841.

[71] A. Othonos and X. Lee, "Novel and improved methods of writing Bragg gratings with phase masks," *Photon. Technol. Lett.*, **7**, 1995, pp1183-1185.

[72] J. Martin, and F. Ouellette, "Novel writing techniques of long and highly reflective in-fibre gratings", *Electron. Lett.*, **30**, 1994, pp 811-812.

[73] H.N. Rouke, S.R. Baker, K.C. Byron, R.S. Baulcomb, S.M. Ojha and S. Clements, "Fabrication and charcterisation of long, narrowband fibre gratings by phase mask scanning", *Electron. Lett.*, **30**, 1994, pp 1341-1342.

[74] M.J. Cole, W.H. Loh, R.I. Laming, M.N. Zervaz and S. Barcelos, "Moving fibre/phase mask-scanning beam technique for enhanced flexibility in producing fibre gratings with a uniform phase mask", *Electron. Lett.*, **31**, 1995, pp 92-94.

[75] W.H. Loh, M.J. Cole, M.N. Zervas and R.I. Laming, "Compensation of imperfect phase mask with moving fibre-scanning beam technique for production of fibre gratings", *Electron. Lett.*, **31**, 1995, pp 1483-1485.

[76] J. Albert, K.O. Hill, B. Malo, S. Theriault, F. Bilodeau, D.C. Johnson and L.E. Erikson, "Apodisation of the spectral of fibre Bragg gratings using a phase mask with variable diffraction efficiency", *Electron. Lett.*, **31**, 1995, pp 222-223.

[77] R. Kashyap, A. Swanton and D.J. Armes, "Simple technique for apodising chirped and unchirped fibre Bragg gratings", *Electron. Lett.*, **32**, pp 1226-1228.

[78] B. Malo, S. Theriault, D.C. Johnson, F. Bilodeau, J. Albert and K.O. Hill, "Apodised in-fibre Bragg grating reflectors photoimprinted using a phase mask", *Electron. Lett.*, **31**, 1995, pp 223-225.

[79] K.O. Hill, F. Bilodeau, B. Malo, T. Kitagawa, S. Theriault, D.C. Johnson, J. Albert and K. Takiguchi, "Chirped in-fibre Bragg gratings for compensation of optical fibre dispersion", *Opt. Lett.*, **19**, 1994, pp 1314-1316.

[80] M.A. Putnam, G.M. Williams and E.J. Friebele, "Fabrication of chirped fibre gratings", *Electron. Lett.*, **31**, 1995, pp 309-310.

[81] R. Kashyap, P.F. McKee, R.J. Campbell and D.L. Williams, "Novel method of producing all fibre photoinduced chirped gratings", *Electron. Lett.*, 30, pp 996-997.

[82] J. Canning and M.G. Skeats, "p phase-shifted periodic distributed structures in optical fibres by UV post-processing", *Electron. Lett.*, 30, pp 1244-1246.

[83] R. Kashyap, P.F. McKee and D. Armes, "UV written reflection grating structures in photosensitive optical fibres using phase-shifted phase masks", *Electron. Lett.*, 30, 1994, pp 1977-1978

[84] L.A. Everall, K. Sugden, J.A.R. Williams, I. Bennion, X. Liu, J.S. Aitchison, S. Thoms and R.M. De La Rue. "Fabrication of multipassband moire resonators in fibers by the dual-phase-mask exposure method", *Opt. Lett.*, **22**, pp 1473-1475.

[85] B. Malo, K.O. Hill, F. Bilodeau, D.C. Johnson and J. Albert, "Point-by-point fabrication of micro-Bragg gratings in photosensitive fibre using single excimer pulse refractive index modification techniques", *Electron. Lett.*, **29**, 1993, pp 1669-1669.

[86] S.J. Mihailov, and M.C. Gower, "Recording of efficient high-order Bragg reflectors in optical fibres by mask image projection and single pulse exposure with an excimer laser", *Electron. Lett.*, 30, 1994, pp 707-709

[87] J.L. Wagener, R.P. Espindola and A.M. Vengsarkar, "Strong higher-order fiber Bragg gratings written with an amplitude mask", *Conf.: Bragg gratings, photosensitivity and poling in glass fibres and waveguides*, Willaimsburg, U.S., Tech. Dig., 1997, BME-1.

[88] R.P Davey, R.P.E Felming, K. Smith, R, Kashyap and J.R. Armitage, "Mode-locked erbium fibre laser with wavelength selection by means of a fibre Bragg grating reflector", *Electron. Lett.*, **27**, 1991, pp 2087-2088.

[89] J.L. Zyskind, V. Mizrahim D.J. DiGiovanni and J.W. Sulhoff, "Short single frequency erbium-doped fibre laser", *Electron. Lett.*, **28**, 1992, pp 1385-1387.

[90] G.A. Ball, W.W. Morey and J.P. Waters, "Nd^{3+} fibre laser utilising intra-core Bragg reflectors", *Electron. Lett.*, **26**, 1990, pp 1829-1830.

[91] M. Douay, T. Feng, P. Bernage, P. Niay, E. Delevaque and T. Georges, "Birefringence effect of optical fibre laser with intracore fibre Bragg grating", *Photon. Technol. Lett.*, 4, 1992, pp 844-846.

[92] J.T. Kringlebotn, J.L. Archambault, L. Reekie, J.E. Townsend, G.G. Vienne and D.N. Payne, "Highly-efficient, low-noise grating-feedback Er3+:Yb3+ codoped fibre laser", *Electron. Lett.*, 30, 1994, pp 972-973.

[93] S. Boj, E. Delevaque, J.Y. Allain, J.F. Bayon, P. Niay, P. Bernage, "High efficiency diode pumped thulium-doped silica fibre lasers with intracore Bragg gratings in the 1.9-2.1 mm band", *Electron. Lett.*, 30, 1994, pp 1019-1020.

[94] G.A. Ball and W.H. Glenn, "Design of a single-mode linear-cavity erbium fiber laser utilising Bragg reflectors", *J. Lightwave. Technol.*, 10, 1992, pp 1338-1343.

[95] G.A. Ball and W.W. Morey, "Continuously tunable single-mode erbium fibre laser", *Opt. Lett.*, 17, 1992, pp 420-422.

[96] M.E. Fermann, K. Sugden and I. Bennion, "Generation of 10nJ picosecond pulses for a modelocked fibre laser", *Electron. Lett.*, 31, 1995, pp 194-195.

[97] B.F. Ventrudo, G.A. Rogers, G.S. Lick, D. Hargreaves and T.N. Demayo, "Wavelength and intensity stabilization of 980 nm diode lasers coupled to fibre Bragg gratings", *Electron. Lett.*, 30, 1994, pp 2147-2149.

[98] I. Riant, P. Bousselet, P. Sansonetti, P. Garabediam and J.L. Beylat, "20% pump power saving using photoinduced intracore fibre Bragg grating in erbium doped fibre amplifier", *Electron. Lett.*, 30, 1994, pp 221-223.

[99] R. Kashyap, R. Wyatt and R.J. Campbell, "Wideband gain flattened erbium fibre amplifier using a photosensitive fibre blazed grating", *Electron. Lett.*, 29, 1993, pp 154-156.

[100] E. Delevaque, T. Georges, J.F. Bayon, M. Monerie, P. Niay and P. Bernage, "Gain control in erbium-doped fibre amplifiers by lasing at 1480 nm with photoinduced Bragg gratings written on fibre ends", *Electron. Lett.*, 29, 1993, pp 1112-1114.

[101] J.F. Massicott, S.D. Willson, R. Wyatt, J.R. Armitage, R. Kashyap, D. Williams and R.A. Lobett, "1480 nm pumped erbium doped fibre amplifier with all optical automatic gain control", *Electron. Lett.*, 30, 1994, pp 962-964.

[102] G.E. Town, K. Sugden, J.A.R. Williams, I. Bennion and S. Poole, "Wide-band Fabry-Perot-like filters in optical fiber", *IEEE Photon. Technol. Lett.*, 7, 1995, pp 78-80.

[103] B.J. Eggleton, P.A. Krug, L. Poladian and F. Ouellette, "Long periodic superstructure Bragg gratings in optical fibres", *Electron. Lett.*, 30, 1994, pp 1620-1622.

[104] F. Bilodeau, K.O. Hill, B. Malo, D.C. Johnson and J. Albert, "High-return-loss narrowband all-fibre bandpass Bragg transmission filter", *Photon. Technol. Lett.*, 6, 1994, pp 80-82.

[105] D.C. Johnson, K.O. Hill, F. Bilodeau and S. Faucher, "New design concept for a narrowband wavelength-selective optical tap and combiner", *Electron. Lett.*, 23, 1987, pp 668-669.

[106] T.J. Cullen, H.N. Rourke, C.P. Chew, S.R. Baker, T. Bricheno, K.C. Byron and A. Fielding, "Compact all-fibre wavelength drop and insert filter", *Electron. Lett.*, 30, 1994, pp 2160-2162.

[107] T.A. Strasser "Fibre grating devices for WDM communication systems", *Conf.: Bragg gratings, photosensitivity and poling in glass fibres and waveguides,* Williamsburg, U.S., Tech. Dig., 1997, BTuA1-1

[108] R. I. Laming, M. Ibsen, M. Durkin, M.J. Cole, M.N. Zervas, K.E. Ennser and V. Gusmeroli, "Dispersion compensation grattings", *Conf.: Bragg gratings, photosensitivity and poling in glass fibres and waveguides,* Williamsburg, U.S., Tech. Dig., 1997, BTuA7-1

[109] J.A.R. Williams, I. Bennion, K. Sugden and N.J. Doran "Fibre dispersion compensation using a chirped in-fibre Bragg grating", *Electron. Lett.*, 30, 1994, pp 985-987.

[110] H.G. Winful, "Pulse compression in optical fibre filters", *Appl. Phys. Lett.*, **46**, 1985, pp 527-529.

[111] R. Kashyap, S.V. Chernikov, P.F. McKee and J.R. Taylor, "30 ps chromatic dispersion compensation of 400fs pulses at 100Gbits/s in optical fibres using an all fibre photoinduced chirped reflection grating", *Electron. Lett.*, 30, 1994, pp 1078-1080.

[112] P. Sansonetti, "Fibre grating devices for telecommunications applications", *Conf.: Bragg gratings, photosensitivity and poling in glass fibres and waveguides,* Williamsburg, U.S., Tech. Dig, 1997, JSuA3-1.

[113] D. Taverner, N.G.R. Broderick, D.J. Richardson, R.I. Laming and M. Ibsen, "Nonlinear self-switching and multiple gap-soliton formation in a fibre Bragg grating", *Opt. Lett.*, **23**, 1998, pp 328-330.

[114] B.J. Eggelton, C.M. deSterke, R.E. Slusher and J.E. Sipe, "Distributed feedback pulse generator based on nonlinear fibre grating", *Electron. Lett.*, **32**, 1996, pp 2341-2342.

[115] N.G.R. Broderick, D. Taverner, D.J. Richardson, M. Ibsen and R.I. Laming, "The optical pusbroom in action", *Conf.: Bragg gratings, photosensitivity and poling in glass fibres and waveguides,* Williamsburg, U.S., Tech. Dig, 1997, BMB4-1.

[116] D.B. Hunter and R.A. Minasian, "Microwave optical filters using in-fiber Bragg grating arrays", *IEEE Microwave and Guided Wave Lett.*, **6**, 1996, pp 103-105.

[117] A. Molony, C. Edge and I. Bennion, "Fibre grating delay element for phased array antennas", *Electron. Lett.*, **31**, 1995, pp 1485-1486.

[118] J.L. Cruz, B. Ortega, M.V. Andres, B. Gimeno, D. Pastor, J. Capmany and L. Dong, "Chirped fibre Bragg gratings for phased-array antennas", *Electron. Lett.*, 33, pp 545-546.

[119] W. Zhang, J.A.R. Williams, L.A. Everall and I. Bennion, "Tuneable radio frequency filtering using linearly chirped fibre grating", *European Conference on Optical Communications (ECOC '98)*, Madrid, Spain, Tech. Dig, 1998.

Chapter Three: Fibre Bragg Grating Sensors

3.1 Chapter Overview

The purpose of this chapter is to present the theory behind and the recent developments in FBG sensors[1,2]. This will include an examination of the temperature, pressure and strain sensitivities inherent to a Bragg grating. There is also a review of the capabilities of FBG sensors, compared to those offered by conventional optical fibre and electrical sensors. The bulk of this chapter is aimed at examining a number of FBG interrogation techniques. There is also an overview of methods employed to separate the effects of temperature and strain on the grating. The chapter concludes with an examination of the growing number of applications for FBG sensors.

3.2 Theory

In-fibre Bragg gratings are inherently sensitive to temperature, strain and pressure.

3.2.1 Temperature Sensitivity

A variation in temperature applied to a grating, results in a change in its periodic modulation, hence shifting its Bragg wavelength. This is brought about by both the thermal expansion of the fibre and the refractive index change which is attributed to the thermo-optic effect. This leads to a fractional change in the Bragg wavelength, λ_B, which is given by[3]:

$$\Delta\lambda_B/\lambda_B = (a + \xi)\Delta T \qquad \textit{Equation 3.1}$$

where $a = (1/\Lambda)(\delta\Lambda/\delta T)$ is the thermal expansion co-efficient of the fibre (0.55×10^{-6} for fused silica). The quantity $\xi = (1/n_{eff})(\delta n_{eff}/\delta T)$ represents the thermo-optic coefficient, which is about 8.3×10^{-6} for germania-doped silica-core fibre[4], and ΔT is the applied temperature change. It is clear from these figures that the thermo-optic induced refractive index change is the dominant effect. This results in not only different sensitivities for varying wavelengths, but also for different fibre dopants. Measurements with respect to the former have shown sensitivities of 6.8 pm/°C[5] and 13

pm/°C[6] for 580 and 1550 nm FBGs respectively. The effect of different fibre dopants on temperature sensitivity will be examined in the next chapter.

It is possible to mechanically improve the thermal sensitivities of such structures. One method suggested by Le Blanc *et al.*[7] involves gluing the fibre to a metallic substrate that has a large thermal expansion coefficient, e.g. aluminium, zinc etc. This technique resulted in an overall temperature sensitivity of 38 pm/°C. A much more elegant and effective approach involves using a polymer overlayer[8]. In this experiment, the authors used two polymer materials, Nylon-6 and PTFE, which both have large thermal expansion coefficients, as driving elements for the inscribed structure. The gratings employed were 5 mm in length and were written in germanium doped fibre. The more successful of the two polymers was the nylon, which gave an average thermal sensitivity of 150 pm/°C.

There is also interest in producing extremely high and low temperature Bragg grating sensors for use in extreme environments. This has led to a novel approach for fabricating high temperature resistant gratings[9] and there has been a recent report of an FBG sensor operating down at 10 K[10]. High temperature resistant gratings written using the method outlined by Fokine *et al.*[9] are stable at temperatures up to and greater than 800°C. For low temperature sensing, the FBGs employed were bonded to a PMMA substrate and a temperature sensitivity of 11pm/K near 10K was obtained. Such devices are expected to make ideal temperature sensors for superconducting devices as they are free from electromagnetic interference.

3.2.2 Strain sensitivity

A shift in Bragg wavelength may also be obtained by the application of an applied axial strain. This change is again due to two processes; a physical alteration in the period of the grating and the strain-optic induced change in the core refractive index. The corresponding change in wavelength, due to applied strain, is given by[5]:

$$\Delta\lambda_B = \lambda_B(1-p_e)\varepsilon \qquad \textit{Equation 3.2}$$

where ε is the applied axial strain and p_e is the effective strain-optic constant, which is given by:

$$p_e = (n_{eff}^2/2)\,[(p_{12} - \nu(p_{11} + p_{12})] \qquad \textit{Equation 3.3}$$

where p_{11} and p_{12} are components of the strain-optic tensor and ν is Poisson's ratio. For a typical germanosilicate optical fibre $p_{11} = 0.113$, $p_{12} = 0.252$, $\nu = 0.16$ and $n_{eff} = 1.482$. This gives a strain-optic constant of 0.22 for germanosilicate fibre[11].

Once again the response of the structure is dependent on both the interrogation wavelength and the fibre type which determines the effective strain-optic constant. The responses for a grating at 800 nm and 1550 nm were measured to be 0.52[5] and 1.2[12] pm/με respectively. These results are in good agreement with equation 3.2.

The maximum axial tensile strain that is measurable with a FBG sensor is limited only by the fibre strength. A typical fibre can withstand an applied tensile strain of about 1% before its strength begins to degrade. This corresponds to a wavelength shift of about 10 nm in the 1.3 μm window. However, silica is 23 times stronger under compression than tension. This property has been exploited to demonstrate a Bragg grating fibre laser that is continuously tuneable over 32 nm[13].

3.2.3 Other measurands

FBGs are also inherently sensitive to pressure. Pressure, applied to an optical fibre, results in a change in its physical length and refractive index. This manifests itself as a shift in the Bragg wavelength of the grating. The sensitivity of a FBG written at 1550 nm in germanosilcate fibre was determined to be -3 pm/MPa over a pressure range of 70 MPa[14]. The group who reported this went onto enhance this sensitivity by a factor of four by mounting the FBG sensor in a hollow glass bubble to achieve mechanical amplification[15].

It is also possible, by the application of specialised coatings, to convert the effects of other measurands into strain along the coated section of fibre. Thus, a grating written into a section of fibre, which is then appropriately coated, may be used to measure other physical parameters. For example, a nickel coating makes the fibre sensitive to magnetic fields[16] whereas PVF_2 permits the sensing of electric fields with a grating.

More recently it has been demonstrated that uncoated FBGs may be employed to measure dynamic magnetic fields. This is possible as the dynamic field induces a slight change in the refractive index of the fibre experienced by left and right-circularly polarised light in an FBG[17]. Thus, when a longitudinal magnetic field is applied to the grating two Bragg wavelengths, corresponding to the two different circular polarisations, are obtained. However, the sensitivity of this effect is weak and, consequently, the difference is very small. This effect is measurable though if an interferometric scheme, which offers very high sensitivity is used, to interrogate the sensor. It would also be possible to perform dynamic measurements of large values of current and voltage with such an arrangement.

3.3 Advantages of fibre Bragg grating sensors

Many optical fibre interferometric temperature and strain sensors have been reported since the late 1970s[18,19]. These have demonstrated the potential for very high resolution, the realisation of which is dependent on the capability of the system used to measure the wavelength/phase shift induced by the measurand. This led to both the development of the frequency-division, time-division and coherence multiplexing of such sensors[20], as well as intensity based systems[21]. More recently interferometric sensors, using optical fibres as transduction mediums, have been demonstrated that are capable of simultaneously measuring temperature and strain[22]. In one such case this has been achieved with resolutions of 5°C and 10 με respectively[23]. The high resolution of such schemes is inherently due to the fact that minute external perturbations may lead to measurable changes in phase, wavelength, intensity or polarisation of the wave propagating along the fibre. The list of detectable measurands by fibre optic sensors does not end with temperature and strain but includes pressure[19], acoustic vibrations[24] and electrical and magnetic fields[25].

In addition to these factors, fibre sensors have a number of advantages over their electrical counterparts, which include the facts that they are immune to EM interference, small size (about 5 mm long and 1 mm diameter) and low in weight. They also offer electrically passive operation in a wide range of environments and high sensitivity along with multiplexing capabilities. Such is the range of advantages

obtainable by employing optical fibre sensors, instead of electrical devices they have been put forward as candidates for SMART structure sensing[26]. However, they have had few real commercial successes, as many of these devices were developed to displace conventional electro-mechanical sensor systems that are well established and have proven reliability and manufacturing costs.

However, this trend has been reversed by those fibre sensors, which offer new capabilities in addition to the ones previously mentioned such as distributed sensing and inherent self referencing. Fibre Bragg grating devices provide this capability. In addition, the sensing information from a FBG sensor is inherently encoded into the Bragg wavelength, which is an absolute parameter[2]. Hence, the output of such a system is independent of total light levels so losses in connectors and couplers and fluctuations in the interrogating light source may be easily operated intermittently without the need for re-calibration or re-initialising the system. The wavelength encoded nature of the information also facilitates distributed sensing and wavelength division multiplexing (both discussed later) along a single fibre by assigning individual sensors to a different slice of the available source spectrum[27]. Bragg gratings can also be easily mass produced[28] and written into a fibre without altering its diameter.

All these advantages have given FBG sensors the edge over electrical sensors. They are ideal for structures that monitor their own internal strain, temperature and structural integrity in real time[29]. Such structures are known as SMART structures. This and other applications will be examined more closely later on.

3.4 Interrogation Methods

3.4.1 Basics

For the majority of this chapter methods of interrogation for strain sensors will be discussed although the wavelength shifts measured are applicable to all measurands a FBG sensor is capable of determining. As discussed in 3.2, the response of a Bragg grating to an external parameter at its location is a shift in its peak reflected wavelength by a proportional amount. Therefore, the simplest way to interrogate a FBG sensor is to measure its momentary Bragg wavelength and compare this to its original un-

strained wavelength. An optical spectrum analyser is capable of measuring the reflected wavelength with acceptable resolution. A diagram of a suitable set-up for the interrogation of a sensor array is shown in figure 3.1:

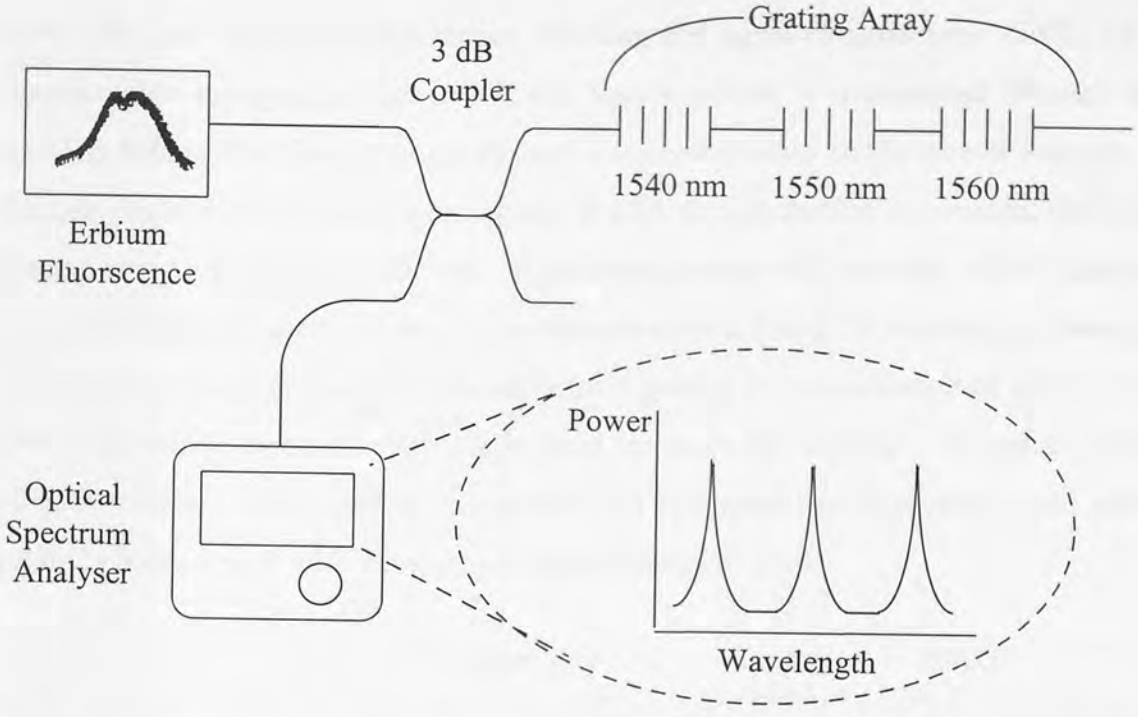

Figure 3.1: Diagram of a Bragg grating array optical spectrum analyser interrogation system.

FBGs written around 1550 nm are typically illuminated by an erbium fluorescence source, whereas 1300 and 800 nm structures are interrogated by SLEDs. The sources used for these shorter wavelengths are cheaper and require less control. However, the response of gratings, written at these shorter wavelengths, to a given measuand is lower (e.g. 0.52 pm/με at 800 nm[5] compared to 1.2 pm/με at 1550 nm[12]). The ideal source for illuminating FBG sensors would be high power, broadband and flat. To this end Dagenais *et al.*[30] have developed a source which consists of an ASE erbium source, a gain flattening device and a fibre amplifier. This device gives a total output power of 30 mW over a bandwidth of 32 nm with a fairly flat spectral top. Such a power source would permit the multiplexing of six sensors each with a sensing range of 5 mε. The maximum wavelength division multiplexing capability of a given uniform FBG sensor system is dependent on the bandwidth of the source (BWS), the number of sensors (n) and their maximum sensing range (MSR). This dependency can be expressed by:

$$BWS \geq n \times MSR \text{ nm} \qquad \textit{Equation 3.4}$$

It is also noted at this point that it is possible to spatially multiplex a number of sensing lines by the application of coupler trees, see figure 3.2. The limit on the number of sensor lines is determined by the source power. The light reaching the sensor array is halved for each coupler added, hence reducing the signal-to-noise ratio (SNR) of the system. For example, in figure 3.2, the source power is transmitted through four couplers before emerging from the system, i.e. one-sixteenth of the power emerges. In the case of the 30 mW source over 32 nm, if a linear distribution is assumed, the power density is approximately 1 mW/nm. A uniform grating will typically reflect light over a range of approximately 0.2 nm, i.e. in this example 0.2 mW. Assuming no losses, the total power emerging from the system from a grating is one sixteenth of this, i.e. 12.5 nW. This would be an acceptable light level for most photodiodes. Therefore, for the 30 mW source a system employing wavelength and spatial multiplexing could address up to 24 sensors each with a maximum sensing range of 5 mε.

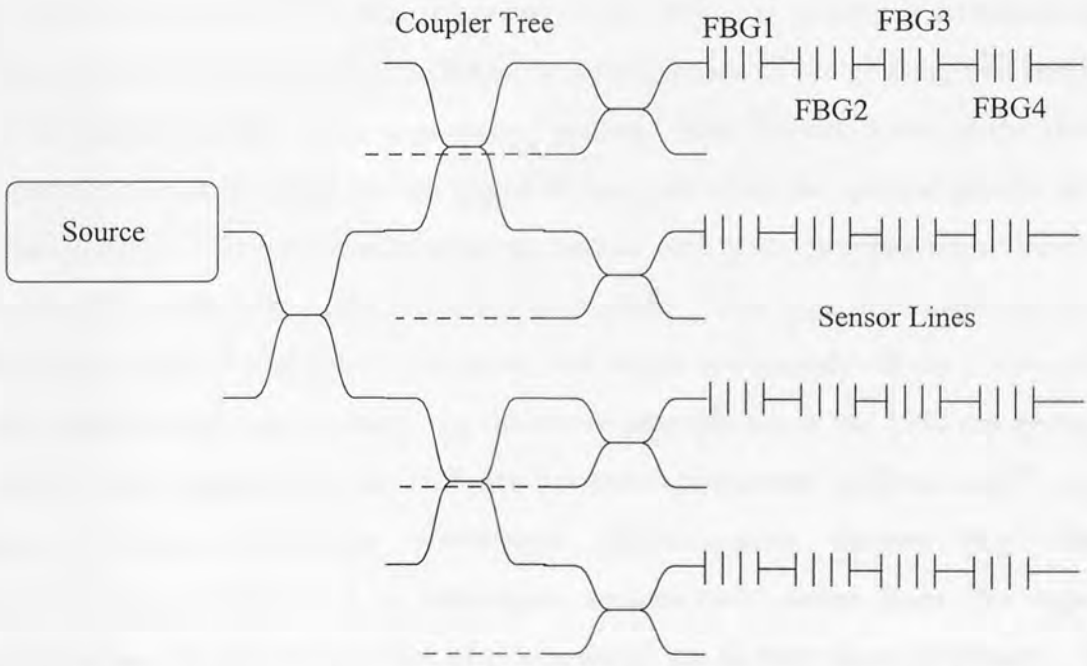

Figure 3.2: Wavelength and spatial division multiplexed FBG sensor network. The dotted lines indicate the system output ports.

The array shown in figure 3.1 is typical of a WDM sensor grating array. The OSA is able to scan a large range (>100 nm) at low resolution (0.1 nm) and a low speed (0.1 Hz). However, it is also able to examine the transmission spectra of gratings in a sensor

array. While the OSA interrogation technique is simple and reliable it is not practical. It has a low interrogation rate (0.1 Hz) and resolution (0.1 nm). They are also bulky and cost tens of thousands of pounds. Despite all this it is usually the first method applied to test the workability of a system in the laboratory, as everything that is occurring can be clearly seen. This method has also found application in a multiplexed FBG sensor system that monitors the load in power transmission lines[31].

It is noted here that an OSA can also observe the side lobes in the spectral response of the grating. As previously discussed, these secondary maxima exist at adjacent wavelengths of the main peak. These side lobes can be measured by the OSA and ignored. However, they can become problematic in a WDM array.

Consider two gratings wavelength division multiplexed on a single fibre, with central wavelengths of 1550 nm and 1555 nm respectively. Both gratings have a bandwidth of 0.2 nm. This gives each sensor a measurement range of 4.7 mε. If the 1550 nm grating is stretched any further than this then its main spectral profile peak will coincide with that of the unstrecthed 1555 nm. However, if the 1550 nm grating is stretched to its full limit then the side lobes, to the longer wavelength side of the grating, will interfere with the spectral profile of the unstretched grating. Also the side lobes to the shorter wavelength side of the 1555 nm grating will interfere with the spectral profile of the strained grating. This cross-interference can lead to both gratings appearing to have two main peaks, thus making strain extraction ambiguous. This type of interference is one form of cross-talk. Cross-talk occurs when one sensor erroneously effects the output of another/other sensors in a system. In the above example when the 1550 nm grating is stretched it may appear that the 1555 nm has been compressed while it is still at zero strain. Systems that use wavelength discrimination devices (e.g. filters, intereferometers, OSAs etc.) to interrogate sensors only suffer from this type of crosstalk when the spectral profiles of two gratings are in very close proximity. This cross-talk can be reduced by using apodised gratings (see chapter two). However, apodised grating are more complex to write than un-apodised gratings. Also side lobes cause little cross-talk (typically –70 dB) in such systems and this only occurs when the spectral profiles of the gratings are close together. Therefore most sensor systems employ un-apodised gratings.

3.4.2 Tuneable Filters

One of the two most successful techniques for interrogating FBG sensors utilises a tuneable passband filter to track the reflected signal or signals. The output of such a system is the convolution of the reflection spectrum of the FBG and transmission profile of the tuneable filter, see figure 3.3. When these two spectra match the output of the system is at a maximum. Hence, when this occurs, the central wavelength of the filter is equal to the peak wavelength of the sensor. The resolution of such a system is determined by the SNR of the returned FBG signal and the linewidths of both the filter and the sensor. This type of system is only good for measuring static and quasi-static strain; the limit placed on this ability is fixed by the scanning speed of the filter. However, such systems usually offer moderate resolution and a large working range, which is a necessity for WDM arrays.

A number of suitable filters have been suggested for this type of system, which include acousto-optic, FBG-based and Fabry-Perot (FP) filters, see figure 3.3. Each of these filter types offer different advantages and disadvantages. An acousto-optic filter has been used successfully in such an interrogation scheme[32,33] and a multiplexed system with a resolution of 0.4 με and a scanning rate of 10 Hz has been reported[34]. However, these systems require both feedback systems and complex components and are highly temperature sensitive[34].

The second type of filter involves the matching of two identical fibre Bragg gratings[35]. This technique involves using one of the structures as a sensor while the other acts as a tuneable filter. The narrowband reflection of an FBG acts as a "passband" which may be tuned over several nanometres by the application of strain. This structure is stretched until maximum reflection is obtained. This occurs when the strain on the FBG filter is identical to that on the sensor. This method has resulted in a system with a dynamic strain resolution of 0.01 με/√Hz for low frequency oscillations[36]. However, the filter FBG is tuned by an expensive piezoelectric actuator, which requires control electronics and can only stretch the grating by a small amount (typically 200-500 με). Hence, the measurement range of such a system is limited to about 500 με. The

multiplexing of sensors using such a technique is expensive as each structure requires its own piezoelectric actuator, which typically cost up to a thousand pounds each.

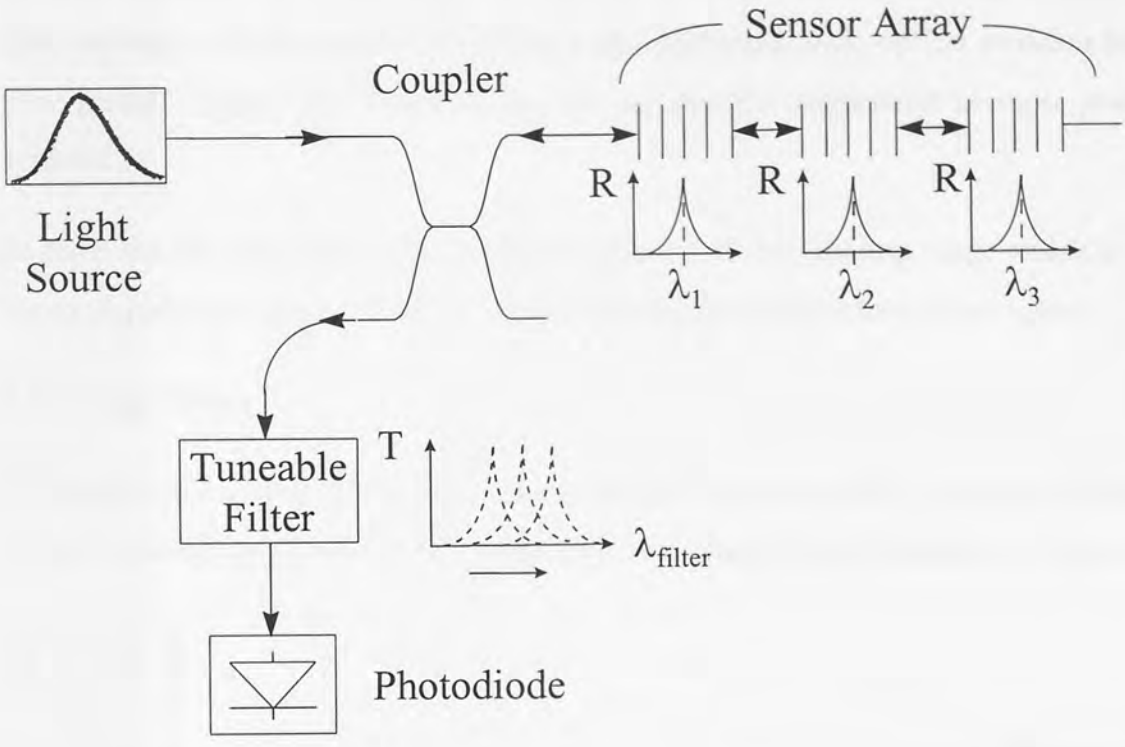

Figure 3.3: Tuneable filter FBG sensor interrogation technique.

The most popular filter for this type of system is the Fabry-Perot[37]. The fibre Fabry-Perot (FP) filter passes one narrowband wavelength component, which depends on the spacing between the mirrors in the device. The distance between the mirrors is controlled, via piezoelectric stacks, by an input voltage. This input voltage usually takes the form of a saw-tooth wave, which scans the filter across all the gratings in the range. Thus by calibrating the applied voltage against wavelength it is possible to determine the peak wavelength of each sensor. Typical FP filters are compact and have free spectral ranges, i.e. scanning ranges, of around 50 nm and bandwidths of about 0.3 nm. It follows from equation 3.4 that such a filter permits up to 16 sensors with a sensing range of 3 mε to be multiplexed on a single fibre line. The resolution of such a filter is about 0.8 pm corresponding to 0.8 με and they can be scanned at rates of up to 500 Hz. This has permitted the implementation of systems with a resolution of around 1 με.

A system that employed an electromagnetic optical switch to address a number of FBG sensor arrays and a FP filter as the interrogation element was recently developed[38]. This system typically scanned and averaged all 60 sensors in 2.5 seconds which is deemed adequate for static strain monitoring in most civil engineering applications. The resolution of this system was about 1 με. However, such optical switches have a very limited lifetime and therefore are not suitable for application in most practical systems.

In short the tuneable filter method offers a wide (>40 nm) sensing range which is ideal for multiplexing a large number of sensors, but has limited resolution and speed.

3.4.3 Edge Filters

Another device used in Bragg sensor interrogation is the edge filter. Instead of having a narrow tuneable passband, an edge filter has a broadband sloped response, see figure 3.4.

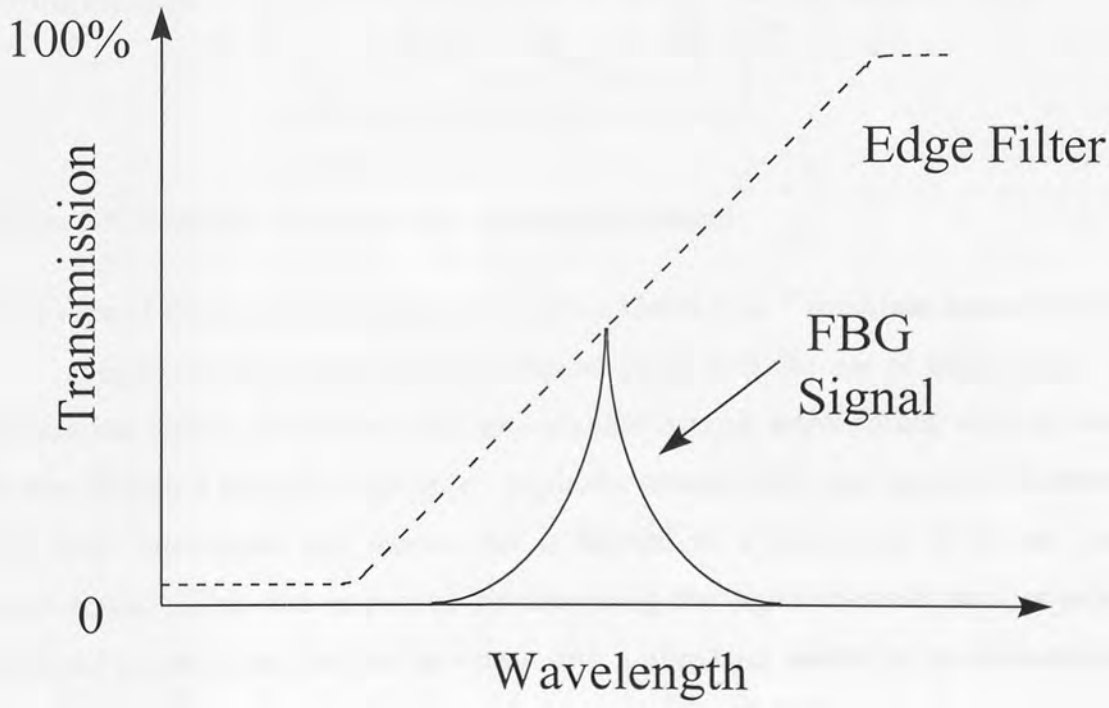

Figure 3.4: A typical wavelength response of an edge filter.

The sloped profile of an edge filter permits a linear relationship between the wavelength of the reflected signal and the output intensity of the system. It is clear from figure 3.4 that the longer the wavelength of the signal then the greater the transmission of the

filter. However, as this system is intensity based it requires a reference arm to normalise out fluctuations in the power source etc. A simple schematic of such a system is shown in figure 3.5:

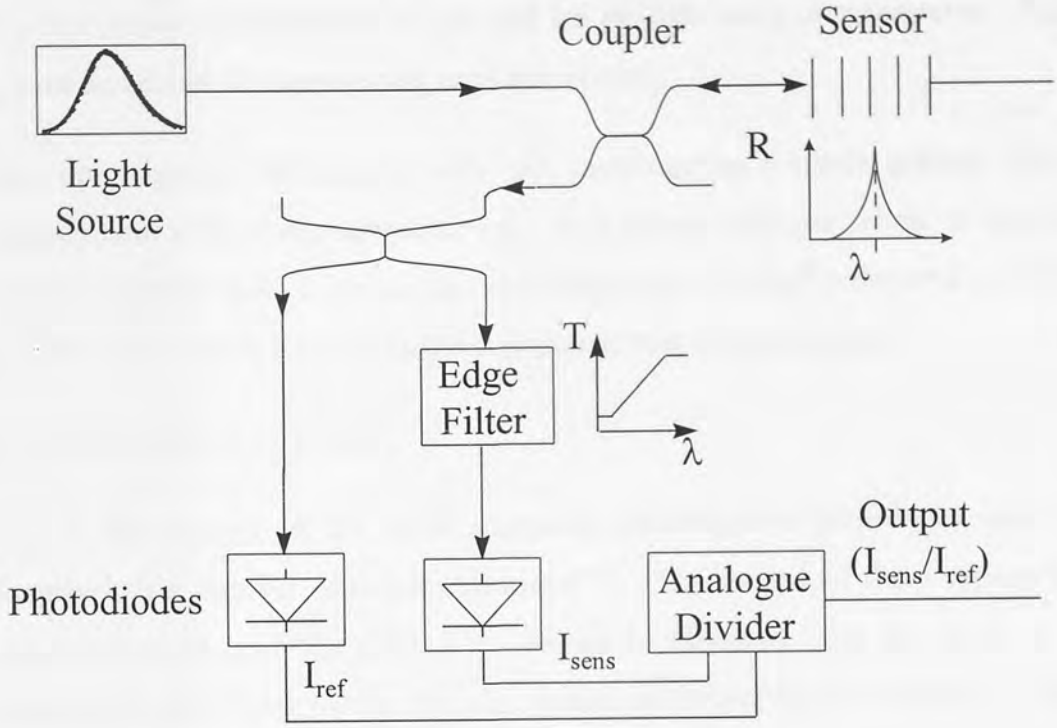

Figure 3.5: Schematic of an edge filter interrogation system.

This type of system was first demonstrated by Melles *et al.*[39] for strain measurement. In this example the edge filter response was achieved with the use of bulk optics. This system has several advantages over schemes that contain active filters; such as low cost (a few thousand pounds), high speed (typically several kHz) and passive. However, it can only interrogate one sensor and is limited to a resolution of a few tens of microstrain. This was improved by increasing the signal-to-noise ratio, which was achieved by replacing the grating sensor with a fibre laser sensor (to be discussed later). This modified system was shown to have a resolution of 5 με and a frequency response of 13 kHz[40].

Another system which works on the edge filter approach was demonstrated by Lobos Ribeiro *et al.*[41]. The required linear wavelength response was realised over the range 1520-1530 nm by a biconical fibre filter. This filter is basically a section of single-mode

tapered depressed-cladding fibre, which consists of a contracting tapered region of decreasing fibre diameter followed by an expanding taper of increasing fibre diameter. This system is all-fibre making it more compact and it avoids the problems of unwanted reflections and power loss usually associated with bulk optic systems. Static and dynamic strain resolutions of 3.5 με and 1.5 με/√Hz were demonstrated. Again, this system is capable of interrogating only one grating.

This interrogation technique is ideal for interrogating a single grating with a wide measurement range (tens of millistrain). It is cheap, with the whole system costing a few thousand pounds. It is also fast, operating up to 13 kHz[40] compared to 0.1 Hz with an OSA , however it has a limited resolution at tens of microstrain.

3.4.4 Interferometric sensors

This is the second of the most successful interrogation techniques and has been described in a number of communications[42,43]. The second of these reported a strain resolution of 0.6 nε/√Hz at 500 Hz. As can be observed from this early result these systems are ideal for detecting dynamic strains with very high resolution. The general principle of the interferometric technique is shown in figure 3.6:

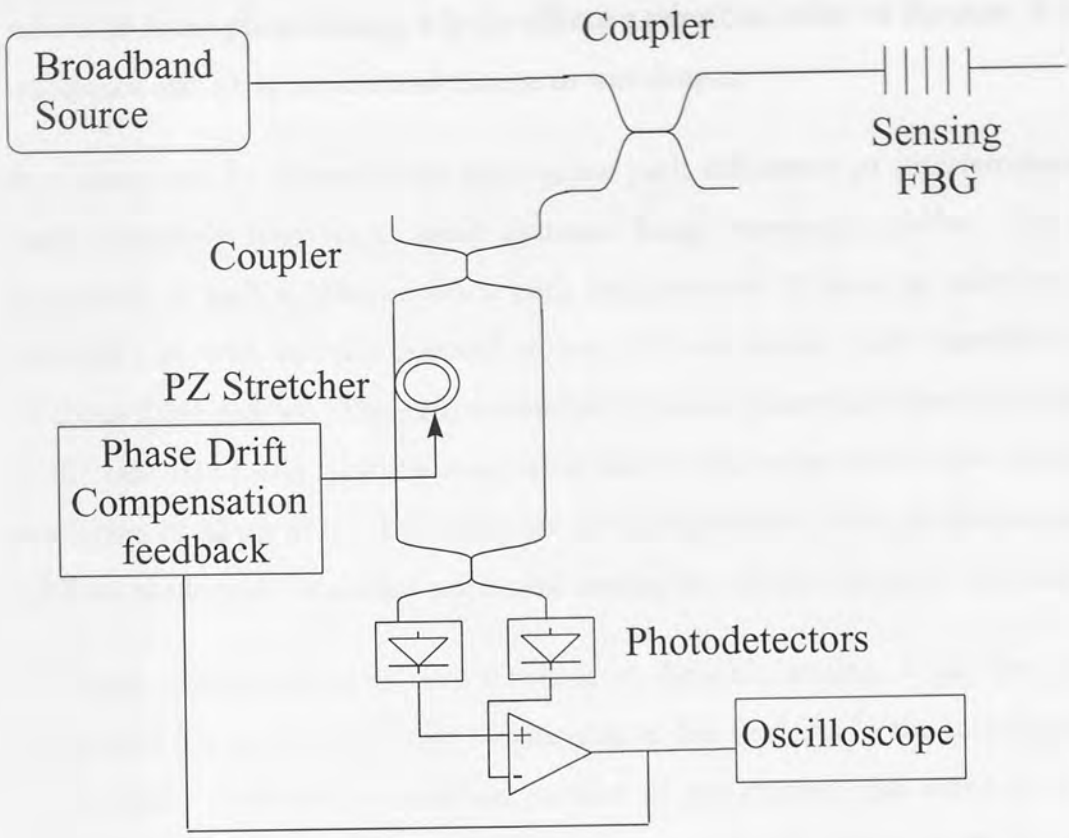

Figure 3.6: Diagram of a basic interferometric technique for the interrogation of FBG sensors.

The figure basically shows an unbalanced interferometer which is effectively an optical filter element with a transfer function of the form $(1 + \cos\phi)$ where ϕ is a phase term which is dependent on the input wavelength.

The light reflected from an FBG sensor is tapped off using a coupler, with each half travelling through unequal lengths of a Mach-Zender interferometer. The difference between these two paths must be kept less than the effective coherence length of the FBG signal (~ 1cm for a 1 cm grating illuminated at 1300 nm). These two signals are then recombined and interfere, giving rise to a raised cosine transfer function. The piezoelectric stretcher is adjusted as necessary to keep the interferometer in quadrature. As previously mentioned, the output phase is dependent on the input wavelength. Therefore as the sensor is stretched the reflected wavelength changes which alters the output phase. The relationship between these two parameters is given by:

$$\Delta\phi = 2\pi dn\Delta\lambda/\lambda^2 \qquad \textit{Equation 3.5}$$

where $\Delta\phi$ is the phase change, n is the effective refractive index of the core, d is the path imbalance and $\Delta\lambda$ is the induced change in wavelength.

It is clear that by choosing the appropriate path difference an interferometer can be made extremely sensitive to weak dynamic Bragg wavelength shifts. The predicted sensitivity of such a system with a path imbalance of 10 mm, an effective refractive index of 1.46 with an FBG centered around 1550 nm would yield a sensitivity ($\Delta\phi/\Delta\varepsilon$) of about 0.045 rad/$\mu\varepsilon$. The high resolution dynamic phase shift detection capability of $\sim 10^{-6}$ rad/$\sqrt{Hz}$ being typically achievable with such sensors would give rise to a strain resolution of 20 p$\varepsilon/\sqrt{Hz}$. This limit has yet to be obtained, though this method clearly achieves the highest attainable resolution among the current detection methods.

Although this technique is very sensitive to dynamic strains, it can be problematic when used for quasi-static strain measurements due to drifts in the interferometer bias phase itself. However, a modified version of the system that employs a reference wavelength to compensate for the thermal induced phase drift in a scanned interferometer has been developed[44]. This approach has been able to improve the ability of FBGs to monitor temperature and perform differential temperature measurements[45]. A strain resolution of 6 n$\varepsilon/\sqrt{Hz}$ at 1 Hz and a temperature resolution of 0.05°C with a range of 60°C and good thermal stability have been demonstrated.

The problem with such interferometric systems is that of sensing range. The measurement range of a FBG is determined by the free spectral range of the wavelength scanner, which is inversely proportional to the optical path difference (OPD) of the interferometer. However, the resolution is directly proportional to the OPD. Therefore, an interferometric interrogation technique has either excellent resolution or a wide sensing range. This situation was addressed recently by Rao *et al.*[46]. Their technique was based on the use of two sets of fringes obtained with a stepped bulk Michelson interferometric wavelength scanner with dual cavity lengths. The optical phase output from the cavity with the larger OPD gives a high resolution measurement, while the other phase output is used to determine the number of fringes obtained with the longer cavity. The authors anticipated an increase of 100 times in the unambiguous range to resolution with this technique.

A second, faster solution offering a wider scanning range was later reported by the same group[47]. This involves employing two scanning interferometers to interrogate one sensor. The first interferometer had a large scanning range, but poor resolution. The second interferometer had a limited unambiguous sensing range and excellent resolution. Hence, the first interferometer finds the signal to within the unambiguous sensing range of the second, which then determines its wavelength with high resolution.

There have been a number of communications with regards to the multiplexing of Bragg gratings and interrogating them with an interferometer. These have included interrogating an array with short scan interferometry[48] and a system employing an interferometric wavelength scanner and a low resolution spectrometer[49]. A novel method was reported by Berkoff *et al*[50]. that employed a bandpass wavelength division multiplexer to separate the reflected signals from a four sensor array. Each of these separated signals were then measured by an unbalanced Mach-Zender interferometer. This system offers high resolution, about 1.5 nε/√Hz for each sensor, and low cross-talk, typically -70 dB.

Yet another technique was demonstrated by Kersey *et al.*[51] which is based on the use of distributed Bragg gratings in an otherwise conventional interferometric sensor configurations. The gratings in this case did not act as the sensors, but defined the interferometeric paths for the Michelson and Mach-Zender interferometer sensors.

3.4.5 Other Interrogation Methods

There exist a number of other techniques for interrogating FBG sensors. These have included two techniques that require narrowband rather than broadband illumination. These involve grating interrogation by: (i) a tuneable laser[52] and (ii) a frequency modulated laser diode[53]. The former of these involved interrogating a single sensor but concluded that many could be interrogated in series. The grating was scanned over a range of 2.5 nm with a period of 10 ms. A strain resolution of 76 nε/√Hz over a range of 2 000 με was reported. The latter involves stimulating a sensor grating by a ramped modulated multimode laser diode light source, thus generating an electrical carrier at the detector output. The phase of the carrier is dependent on the difference between the Bragg wavelength and the laser mode wavelength. Hence, any change in Bragg

wavelength due to external influences (i.e. strain and temperature) modifies the output phase. This resulted in a system with a temperature and strain sensitivity of 0.05°C/√Hz and 0.7 με/√Hz respectively.

Further increases in the resolution of the systems already mentioned, can be obtained by employing active rather than passive FBG elements, i.e. laser sensors. Such sensors work on the same principle as the continuously tuneable laser sensor mentioned previously[54] and were later demonstrated by the same group[55]. In a communication by Koo *et al.*[56] laser sensors were interrogated by an interferometer in a WDM arrangement. This system showed strain resolutions of $7\times10^{-15}/\sqrt{Hz}$ and $5.6\times10^{-14}/\sqrt{Hz}$ for multimode and single mode laser sensors respectively.

Other novel interrogation techniques have involved the application of highly overcoupled couplers[57] and two-element quantum well waveguided photodiodes[58]. The first of these demonstrated a resolution of about 10 με. The latter system is based on the absorption edge of a two element quantum well detector, which permits a linear relationship between photocurrent and the incident wavelength. This method was demonstrated to have a precision of ±4 με over a range of 6 mε.

3.5 Temperature/Strain Discrimination

One of the main drawbacks to the application of FBGs as sensors is their inherent dual sensitivity. As discussed earlier, FBGs are inherently sensitive to temperature and strain with both manifesting themselves in a wavelength shift, which is directly proportional to the measurand. Hence, strain measurements are effected anomalously by temperature and vice-versa. A number of solutions to this cross-sensitivity problem have been reported.

3.5.1 Twin fibre Bragg gratings

One method suggested by Xu *et al.*[59], employs two FBGs written at different wavelengths into the same section of fibre. These superimposed gratings had central wavelengths of 850 and 1300 nm respectively and were interrogated by optical spectrum analysers, see figure 3.7:

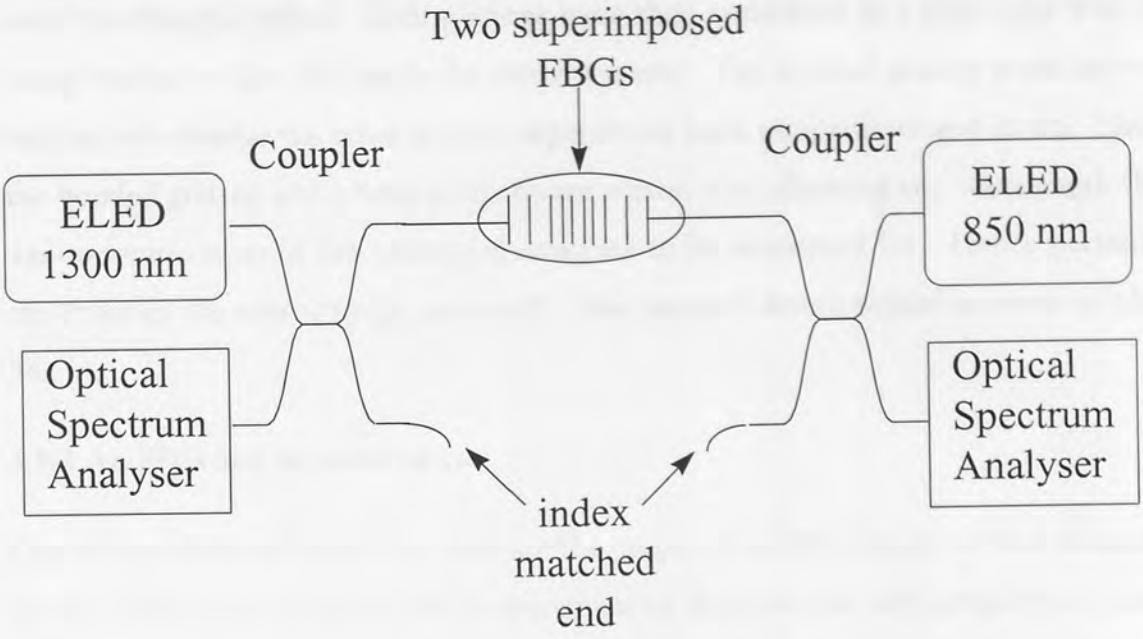

Figure 3.7: Diagram of interrogation system for strain/temperature discrimination by two superimposed FBGs.

This method utilises the fact, following from equations 3.1 and 3.2, that the superimposed gratings have different temperature and strain sensitivities. Therefore, by measuring the two different induced wavelength shifts it is possible to write two simultaneous equations in the form,

$$\Delta\lambda_{B(850)} = K_{\varepsilon(850)}\Delta\varepsilon + K_{T(850)}\Delta T \qquad \textit{Equation 3.6 (a)}$$

$$\Delta\lambda_{B(1300)} = K_{\varepsilon(1300)}\Delta\varepsilon + K_{T(1300)}\Delta T \qquad \textit{Equation 3.6 (b)}$$

where $\Delta\lambda_B$ is the total Bragg wavelength shift, K_ε and K_T are the respective temperature and strain sensitivities for the structures and the 1300 and 850 subscripts denote the gratings original wavelength.

Therefore, by initial calibration of the gratings to determine their sensitivities, i.e. K_ε and K_T, it is possible to solve the above equations with respect to $\Delta\varepsilon$ and ΔT. This system demonstrated errors of typically 10 με and 5°C over a measurement range of 600 με and 50°C.

Another twin grating technique was demonstrated by Song *et al.*[60]. Instead of setting up a set of simultaneous equations they inscribed two gratings one centimetre apart in the

same wavelength region. Both gratings were then embedded in a glass tube with one being bonded to the tube while the other was not. The bonded grating could now not be strained whereas the other grating experienced both temperature and strain. Hence, the bonded grating acts a basic temperature sensor, thus allowing any wavelength shifts due to temperature in the unbonded structure to be accounted for. Hence permitting the strain in the sensor to be calculated. This method demonstrated an error of about 5%.

3.5.2 An FBG and an other sensor

One of the other methods is to compare the output of an FBG sensor to that of another device. These have included the measurement of displacement and temperature using a low finesse cavity and a fibre Bragg grating[61]. A low finesse cavity is of simple design, small dimensions and is ideal for measuring displacement. It is also temperature sensitive. However, by designing an appropriate sensor head it is possible to employ an unstrained FBG as a temperature sensor. This system was interrogated by a Mach-Zender interferometer and gave errors of only 6% and 3% in temperature and displacement respectively.

A similar method suggested by Liu *et al.*[62] combines a FBG with an extrinsic Fabry-Perot sensor. A schematic of the complete sensor is shown in figure 3.8. This design effectively consists of two sensors in series; an unstrained FBG and an air cavity extrinsic Fabry Perot sensor. Here, the FBG element acts as a temperature sensor and the extrinsic Fabry Perot is a strain sensor. The total length of the sensor head is 20 mm. The sensor was interrogated by a CCD card and a computer. The resolution of this system was low; a few tens of microstrain and a few degrees for strain and temperature respectively.

An all fiber approach which does not involve encasing was reported by Kanellopoulos *et al.*[63]. This utilised the different changes in the resonant wavelengths of a rocking filter and a FBG. The two gratings were written 2 cm apart in elliptical-core D-type fibres and interrogated by an optical spectrum analyser. This limited the system to an accuracy of 165 $\mu\varepsilon$ and 1.5°C for temperature and strain respectively. However, the

authors concluded that novel ways of interrogating the grating spectra would improve the system.

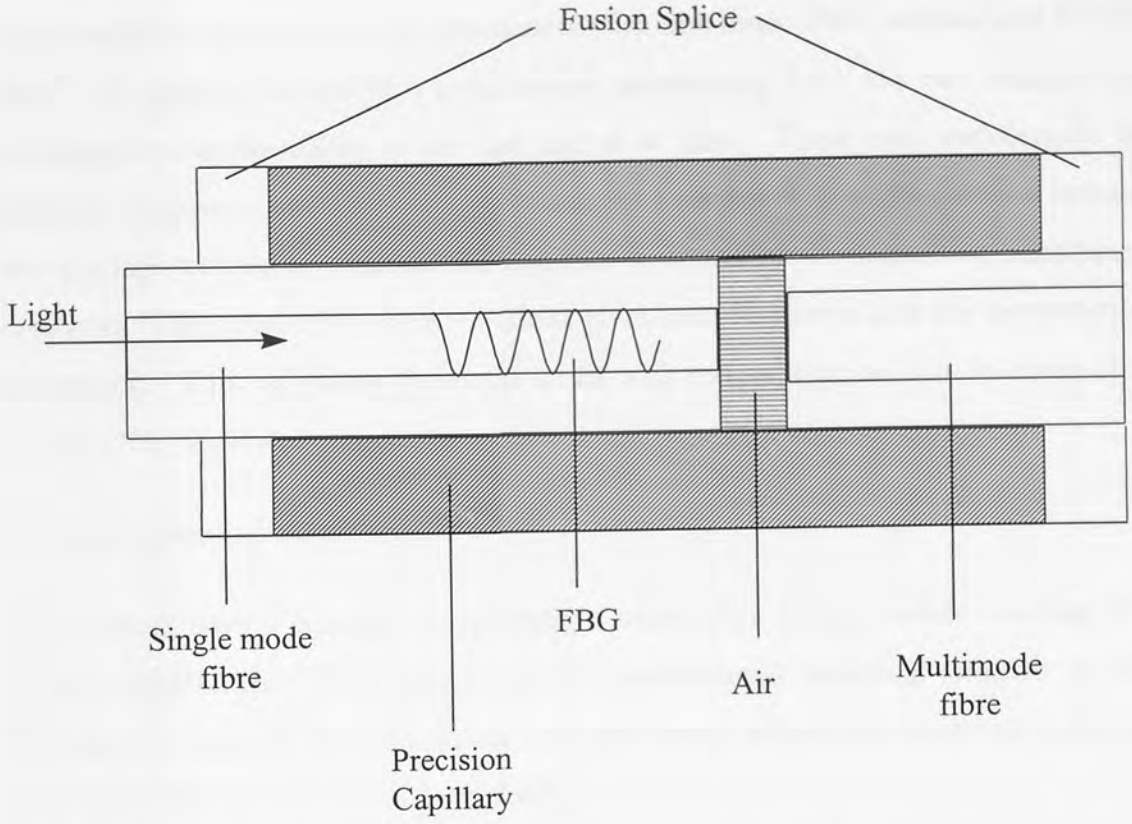

Figure 3.8: Cross-section of FBG/extrinsic Fabry-Perot sensor for distinguishing strain and temperature.

Another dual grating technique employs a FBG and a long period grating. These structures and this system will be discussed in chapter 6.

3.5.3 Other techniques

A temperature independent strain sensor was reported by Xu *et al.*[64]. This was achieved by inscribing a chirped grating in a tapered optical fibre. The taper has the effect of creating a strain gradient along the length of the structure when linear strain is applied to it. This strain gradient linearly chirps the grating, i.e. changes its bandwidth. While the Bragg wavelength of the device is still altered by strain and temperature, the bandwidth is only increased with strain. The larger the chirp of the grating the broader the range of reflected wavelengths and, hence, the greater the reflected intensity. Thus,

a linear relationship between strain and output intensity is resultant. Such a system has demonstrated a strain resolution of 4.4 με over a range of 4 mε.

It is possible to separate the two parameters with one linear FBG written into PANDA fibre[65]. A grating written into polarisation maintaining fibre has two distinct Bragg wavelengths corresponding to the fast and slow axes. These two wavelengths have different temperature and strain sensitivities. In a similar way to the method involving two gratings written at different wavelengths it is possible to write two simultaneous equations. The solution of these equations gives both the strain and the temperature at the grating. This technique measured strain and temperature within an error of ±20 με and ±2°C respectively.

3.6 Applications of FBG Sensors

FBG sensors have a number of advantages over other sensors while realising novel sensing possibilities. They have replaced conventional electrical sensors in some systems; for example SMART masts that previously employed them are now being fitted with FBG sensors (see chapter five).

Their main application is in SMART structures[26]. They have proved themselves useful and reliable in aerospace[66] and marine[67] structures, bridges[68] and even nuclear power plants[69]. In the majority of these applications FBGs are employed to measure strains in concrete structures[68] or composite materials[70]. Vohra *et al.*[67] reported the installation of an FBG sensor system into a composite panel that was then subjected to water wave slamming. This experiment provided the opportunity to measure the dynamics of a composite panel due to wave slamming. This information is important in the design of a ship and gives an indication of the survival potential of the hull in extreme conditions. FBGs are also used to detect cracks and monitor the integrity of the material in which they are embedded. A recent communication by Marty *et al.*[69] outlined an FBG sensor system that was employed to detect cracks, measure strain and monitor the integrity of the shield of nuclear power plants. Their system involved the application of both surface-mounted and embedded Bragg grating extensometers. They concluded that such devices are convenient for surface-strain measurements on buildings as well as for *in situ* measurements.

A whole host of other applications and the future potential of FBG sensors are discussed in ref. 71. One of the largest projects involving FBG sensors was STABILOS[72]. The main aim of this project was to implement an optical fibre sensing technology to monitor the load and displacement changes in underground excavations of mines, tunnels and storage caverns. It was also envisioned that such a system would have the potential to be extended to all civil engineering constructions. The authors demonstrated a new geo-technical FBG based instrumentation that employed a tuneable Fabry-Perot filter to interrogate the sensors and a computer to process the data. The complete sensing network was installed in a German mine in April 1997[71].

FBG sensors have also found use in devices outside of the SMART structure field such as in gyroscopes[73] and load transducers[74]. They have also found application in monitoring long electric power lines[31]. This application could not be performed by electrical sensors due to electromagnetic interference. FBG sensors are immune to electromagnetic interference and their light weight, small size and low transmission loss makes them ideal to monitor the physical loads on a long (30 km) electrical transmission system. Another application that can not be performed by conventional sensors is the monitoring of cryogenic temperatures in a strong magnetic field such as that emanated by a superconducting magnet. FBG sensors are ideal for this application and have been demonstrated to perform well in strong magnetic fields at temperatures near 10K[10].

They have also started to find application in the medical field[75]. In this example, an FBG makes an ideal temperature sensor for cardiac monitoring. Conventional thermistor and thermocouple devices have been fulfilling this role for many years and are still widely used. However, as they are electrically active they are not appropriate for use in a number of medical applications, such as NMR analysis. Bragg grating sensors have the advantage of being dielectric and hence are virtually immune to electric and magnetic fields. Initial experiments on this application indicate that FBG sensors are in good agreement with the electrical sensors already employed. FBG sensors offer the advantage of longer length hence a more accurate measurement could be achieved by the smoothing of temperature profiles. FBGs are also capable of measuring ultrasonic waves, which are employed in a number of medial applications, including

ultrasound surgery. Their small size, electromagnetic immunity and multiplexing capability makes them ideal for determining the strength of such fields[76] *in vivo* which is of great importance. An experimental arrangement for a homodyne scheme that demonstrates this capability is shown in figure 3.9.

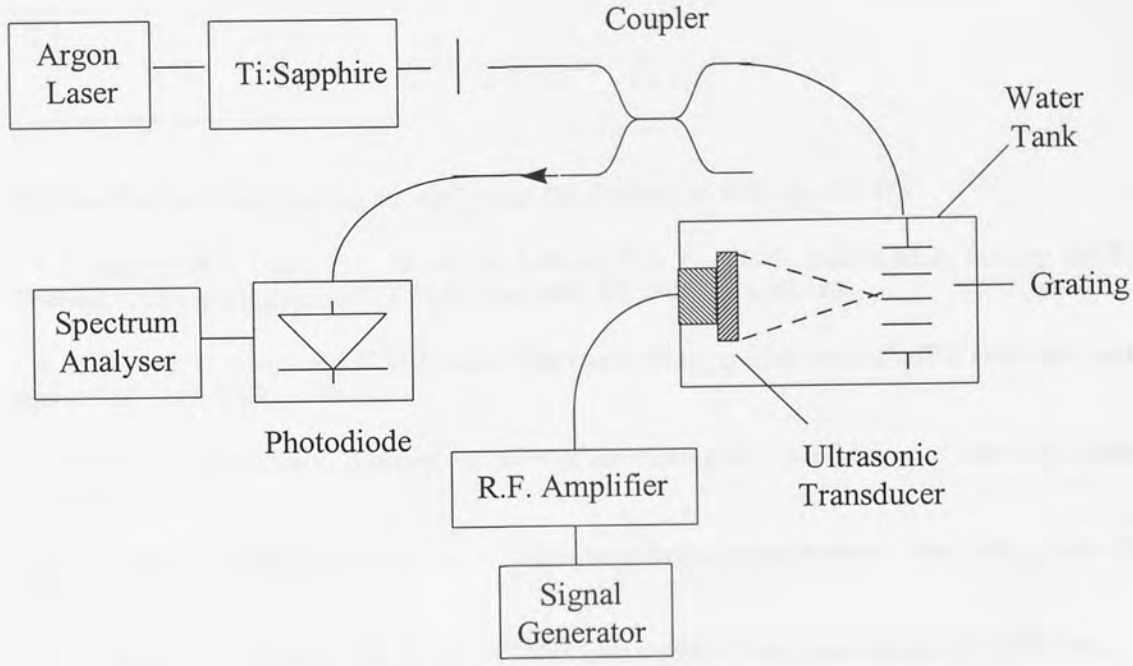

Figure 3.9: Experimental arrangement of a homodyne detection scheme for ultrasonic sensing with a FBG.

Both the FBG and the piezoelectric concave transducer were positioned within a tank of water. An argon-ion pumped Ti-Sapphire laser was used to illuminate the grating though the authors point out that it could be replaced with a laser diode. The grating had a Bragg wavelength of 815 nm, a peak reflectivity of 90% and a bandwidth of 0.2 nm. The system was biased, by tuning the emission wavelength of the Ti-Sapphire laser, so that any change in the reflected wavelength would result in a near maximum change in the power reflected by the grating. The reflected power was detected by a silicon photodiode connected to a spectrum analyser. The authors reported a resolution of 2.2×10^{-4} atm/$\sqrt{\text{Hz}}$ for this system.

These examples demonstrate the wide range of fields that Bragg grating sensors have penetrated. It is anticipated that, as the cost of FBGs come down, their application as sensors will increase significantly. Therefore, they are expected to increase their share in the sensor market as they move into new areas.

---

[1] Y. Rao, "In-fibre Bragg grating sensors", *Meas. Sci. Technol.*, **8**, 1997, pp 355-375

[2] A.D. Kersey, M.A. Davis, H.J. Patrick, M. LeBlanc, K.P. Koo, C.G. Askins, M.A. Putnam and E.J. Friebele, "Fibre grating sensors", *J. Lightwave Tech.*, **15**, 1997, pp 1442-1463.

[3] W.W. Morey, G. Meltz and W.H. Glenn, "Fibre optic Bragg grating sensors", *SPIE Fibre optic and laser sensors VII*, **1169**, 1989, pp 98-107.

[4] S. Takahasi and S. Shibata, "Thermal variation of attenuation for optical fibres", *J. Non-Crys. Solids*, 30, 1979, pp 359-370.

[5] W.W. Morey, G. Meltz and W.H. Glenn, "Fiber optic Bragg grating sensors", *Proc. SPIE*, **1169**, 1989, pp 98-107.

[6] W.W. Morey, J.R. Dunphy and G. Meltz, "Multiplexing fibre Bragg grating sensors", *SPIE Proc., Distributed and Multiplexed Fibre Optic Sensors*, **1586**, 1991, pp 216-224.

[7] M. Le Blanc, S.Y. Huang, M.M. Ohn and R.M. Measures, "Tunable chirping of a fibre Bragg grating using a tapered cantilever bed", *Electron. Lett.*, 30, 1994, pp 2163-2165.

[8] J.L. Cruz, L. Dong and L. Reekie, "Improved thermal sensitivity of fibre Bragg gratings using a polymer overlayer", *Electron. Lett.*, **32**, 1996, pp 385-387.

[9] M.A. Fokine, B.E. Sahlgren and R. Stubbe, "A novel approach to fabricate high temperature resistant fiber Bragg gratings," *Conf.: Bragg gratings, photosensitivity and poling in glass fibres and waveguides,* Williamsburg, U.S., Tech. Dig, 1997, BSuD5.

[10] T. Mizunami, S. Gupta and T. Shimomura," Fiber Bragg grating cryogenic temperature sensor down to 10K", *Optical Fibre Senors (OFS '97), Williamsburg, Viginia*, Tech. Dig., OThC36-1.

[11] S.M. Melle, A.T. Alavie, S. Karr, T. Coroy, K. Liu and R.M. Measures, "Strain sensing using a fibre optic Bragg grating", *SPIE Fiber Optic SMART Structures and Skins IV*, **1588**, 1991, pp 255-263.

[12] S.M. Melle, A.T. Alavie, S. Karr, T. Coroy, K. Liu and R.M. Measures, "A Bragg grating-tuned fibre laser strain sensor system", *IEE Photon. Technol. Lett.*, 5, 1993, pp 263-266.

[13] G.A. Ball and W.W. Morey, "Compression tuned single frequency Bragg grating fibre laser", *Opt. Lett.*, **19**, 1994, pp 1979-1981.

[14] G.M. Xu, H. Geiger and J.P. Dakin, "Optical in-fibre grating high pressure sensor", *Electron. Lett.*, **29**, 1993, pp 398-399.

[15] G.M. Xu, H. Geiger and J.P. Dakin, "Fibre grating pressure sensor with enhanced sensitivty using a glass-bubble housing", *Electron. Lett.*, **32**, 1996, pp 128-129.

[16] H. Okamura "Fibre-optic manetic sensor utilising metal-coated fibre", *Electron. Lett.*, **23**, 1987, pp 834-835.

[17] A.D. Kersey and M.J. Marron, "Fibre Bragg high-magnetic-field probe", *SPIE Proc. 10th International Conf. on Optical Fibre Sensors*, 1994, pp 53-56.

[18] C.D. Butter and G.B. Hocker, "Fiber optic strain gauge", *Appl. Phys.*, **17**, 1978 pp 2867.

[19] G.B. Hocker, "Fiber-optic sensing of pressure and temperature", *Appl. Opt.*, **18**, 1979, pp 1445.

[20] A. Dandridge and A.D. Kersey, "Multiplexed interferometric fiber sensor arrays", *SPIE Distributed and Multiplexed Fiber Optic Sensors*, **1586**, 1991, pp 176-180.

[21] G. Behiem and D.J. Anthan, "Fiber optic photoelastic pressure sensor with fiber-loss compensation", *Opt. Lett.*, **12**, 1987, pp 220-222.

[22] F. Farahi, D.J. Webb, J.D.C. Jones and D.A. Jackson, "Simultaneous measurement of temperature and strain: Cross-sensitivity considerations", *J. Lightwave Technol.*, **8**, 1990, pp 138-142.

[23] A.M. Vengsarkar, W. C. Michie, L. Jankovic, B. Culshaw and R.O. Claus, "Fiber-optic dual-technique sensor for simultaneous measurement of strain and temperature", J. *Lightwave Technol.*, **12**, pp 170-176.

[24] N. Lagakos and J.A. Bucaro, "Linearly configured embedded fiber-optic acoustic sensor", *J. Lightwave Technol.*, **11**, 1993, pp 639-642.

[25] A. Dandridge, A.B. Tveten, G.H. Siegel, E.J. West and T.G. Giallo-Renzi, "Optical fibre magnetic field sensors", *Electron. Lett.*, **16**, 1980, pp 408-409.

[26] B. Mason, D. Hogg and R.M. Measures, "Fiber optic strain sensing for smart adaptive structures", *1st European Conf. On Smart Structures and Materials*, Glasgow, Tech Dig., 1992, pp 135-138.

[27] L.E. Giesler, J.R. Dunphy, W.W. Morey, G. Melzt and W. Glenn, "Instrumentation concepts for multiplexed Bragg grating sensors", *SPIE Sensors and Sensor Interrogation*, **1480**, 1991, pp 138-141.

[28] C.G. Askins, M.A. Putnam, G.M. Williams and E.J. Friebele, "Stepped-wavelength optical-fiber Bragg grating arrays fabricated in line on a draw tower", *Opt. Lett.*, **19**, 1994, pp 147-149.

[29] R.M. Measures, S. Melle and K. Liu, "Wavelength demodulated Bragg grating fibre optic sensing systems for addressing smart structure critical issues", *J. Smart Material Structures*, **1**, 1992, pp 36-44.

[30] D.M. Dagenais, L. Goldberg, R.P. Moeller, H.J. Patrick and W.K. Burns, "High-Power broadband source at 1.5 mm for fiber sensor applications", *Conf. Optical Fibre Sensors (OFS '97)*, Williamsburg, Virginia, Tech. Dig, 1997, OWC22-1.

[31] Y. Ogawa, J. Iwasaki and K. Nakamura, "A multiplexing load monitoring system of power transmission lines using fibre Bragg gratings", *Conf. Optical Fibre Sensors (OFS '97)*, Williamsburg, Virginia, Tech. Dig, 1997, OThC16-1.

[32] M.G. Xu, H. Geiger, J.L. Archambault, L. Reekie and J.P. Dakin"Novel interrogation system for fibre Bragg grating sensors using an acousto-optic tunable filter", *Electron. Lett.*, **29**, 1993, pp 1510-1511.

[33] T. Coroy, P.J. Ellerbrock, R.M. Measures and J.H. Belk, "Active wavelength demodulation of Bragg fibre-optic strain sensor using acousto-optic tunable filter", *Electron. Lett.*, **31**, 1995, pp 1602-1603.

[34] H. Gieger, M.G. Xu, N.C. Eaton and J.P. Dakin, "Electronic tracking system for multiplexed fibre grating sensors", *Electron. Lett.*, **31**, 1995, pp 1006-1007.

[35] L.A. Ferreira, J.L Santos and F. Farahi, "Pseudoheterodyne demodulation technique for fibre Bragg grating sensors using two matched gratings", *Photon. Technol. Lett.*, **9**, 1997, pp 487-489.

[36] M.A. Davies and A.D. Kersey, "Matched-filter interrogation technique for fibre Bragg grating arrays", *Electron. Lett.*, **31**, 1995, pp 822-823.

[37] A.D. Kersy, T.A. Berkoff and W.W. Morey, "Multiplexed fibre Bragg grating strain-sensor system with a fibre Fabry-Perot wavelength filter", *Opt. Lett.*, **18**, 1993, pp 1370-1372.

[38] M.A. Davis, D.G. Bellemore, M.A. Putnam and A.D. Kersey, "Interrogation of 60 fibre Bragg grating sensors with microstrain resolution capability", *Electron. Lett.*, **32**, 1996, pp 1393-1394.

[39] S.M. Melle, K. Liu, and R.M. Measures, "A passive wavelength demodulation system for guided-wave Bragg grating sensors", *Photon. Technol. Lett.*, **4**, 1992, pp 515-518.

[40] S.M. Melle, T. Alavic, S. Karr, T. Coroy, K. Liu and R.M. Measures, "A Bragg-grating tuned fibre laser strain sensor system", *Photon. Technol. Lett.*, **5**, 1993, pp 263-266.

[41] A.B. Lobos Riberio, L.A. Ferreira, M. Tsvetkov and J.L. Santos, "All-fibre interrogation technique for fibre Bragg sensors using a biconical filter", *Electron. Lett.*, **32**, 1996, pp 382-383.

[42] A.D. Kersey, T.A. Berkoff and W.W. Morey, "Fibre-grating based strain sensor with phase sensitive detection", *1st European Conf. On Smart Structures and Materials*, Glasgow, Tech Dig., 1992, pp 61-67.

[43] A.D. Kersey, T.A. Berkoff and W.W. Morey, "High-resolution fibre-grating based strain sensor with interferometric wavelength-shift detection", *Electron. Lett.*, **28**, 1992, pp 236-238.

[44] A.D. Kersey, T.A. Berkoff and W.W. Morey, "Fiber optic Bragg grating sensor with drift-compensated high resolution interferometric wavelength shift detection", *Opt. Lett.*, **18**, 1993, pp 72-74.

[45] A.D. Kersey and T.A. Berkoff, "Fibre-optic Bragg grating differential-temperature sensor", *Photon. Technol. Lett.*, **4**, 1992, pp 1183-1185.

[46] Y.J. Rao, D.A. Jackson, L. Zhang and I. Bennion, "Dual-cavity interferometric wavelength-shift detection for in-fibre Bragg gratings sensors", *Opt. Lett.*, **21**, 1996, pp 1556-1558.

[47] Y.J. Rao, D.A. Jackson, L. Zhang and I. Bennion, "Dynamic range enhancement of in-fibre Bragg grating sensors with two cascaded scanning interferometers", *Conf. Optical Fibre Sensors (OFS '97)*, Williamsburg, Virginia, Tech. Dig, 1997, OThC27-1.

[48] D.A. Flavin, R. McBride and J.D.C. Jones, "Absolute measurement of wavelengths from a multiplexed in-fibre Bragg grating array by short-scna interferometry", *Conf. Optical Fibre Sensors (OFS '97)*, Williamsburg, Virginia, Tech. Dig, 1997, OTuB3-1.

[49] Y.J. Rao, D.J. Webb, D.A. Jackson, L. Zhang and I. Bennion, "High-resolution, wavelength-division-multiplexed in-fibre Bragg grating sensor system", *Electron. Lett.*, **32**, 1996, pp 924-926.

[50] T.A. Berkoff and A.D. Kersey, "Fiber Bragg grating array sensor system using a bandpass wavelength division multiplexer and interferometric detection", *Photon. Techno. Lett.*, **8**, 1996, pp 1522-1524.

[51] A.D. Kersey and M.J. Marrone, "Bragg grating based nested fibre interferometer", *Electron. Lett.*, 32, 1996, pp 1221-1223.

[52] T. Coroy, L.M. Chappell, N.J. Guillermo, S.Y. Huang, R.M. Measures and K.D. Chik, "Peak detection demodulation of a Bragg fiber optic sensor using a gain coupled distributed feedback tunable laser", *Conf. Optical Fibre Sensors (OFS '97)*, Williamsburg, Virginia, Tech. Dig, 1997, OWC17-1.

[53] L.A. Ferreira, J.L. Santos, E.V. Diatzikis and F. Farahi, "Fiber optic Bragg sensor demodulation using a frequency modulated laser diode", *Conf. Optical Fibre Sensors (OFS '97)*, Williamsburg, Virginia, Tech. Dig, 1997, OWC-1.

[54] G.A. Ball and W.W. Morey, "Continuously tunable single-mode erbium fibre laser", *Opt. Lett.*, 17, 1992, pp 420-422.

[55] G.A. Ball, G. Meltz and W.W. Morey, "Polarimetric heterodyning Bragg-grating fiber laser sensor", *Opt. Lett.*, **18**, 1993, pp 1976-1978.

[56] K.P. Koo and A.D. Kersey, "Bragg grating-based laser sensors systems with interferometric interrogation and wavelength division multiplexing", *J. Lightwave. Technol.*, **13**, 1995, pp 1243-1249.

[57] Q. Zhang, D.A. Brown, H. Kung, J.E. Townsend, M. Chen, L.J. Reinhart and T.F. Morse, "Use of highly overcoupled couplers to detect shifts in Bragg wavelength", *Electron. Lett.*, 31, 1995, pp 480-482.

[58] A. Densmore and P.E. Jessop, "Wavelength monitoring devices for use in optical fibre sensors", *Conf. on Lasers and Electro-optics (CLEO '98)*, San Francisco, California, Tech. Dig., 1998, CTuA5.

[59] M.G. Xu, J.L. Archambault, L. Reekie and J.P. Dakin, "Discrimination between strain and temperature effects using dual-wavelength fibre grating sensors", *Electron. Lett.*, 30, 1994, pp 1085-1087.

[60] M. Song, S.B. Lee, S.S. Choi and B. Lee, "Simultaneous strain and temperature sensing using two fiber Bragg gratings embedded in a glass tube", *Conf. on Lasers and Electro-optics (CLEO '97)*, Baltimore, Maryland, Tech. Dig., 1997, CThL59.

[61] L.A. Ferreira, A.B. Lobos Riberio, J.L. Santos and F. Farahi, "Simultaneous measurement of displacement and temperature using a low finesse cavity and a fiber Bragg grating", *Photon. Technol. Lett.*, **8**, 1996, pp 1519-1521.

[62] T. Liu, G.F. Fernando, L. Zhang, I. Bennion, Y.J. Rao and D.A. Jackson, "Simultaneous strain and temperature measurement using a combined fibre Bragg grating/extrinsic Fabry-Perot sensor", *Conf. Optical Fibre Sensors (OFS '97)*, Williamsburg, Virginia, Tech. Dig, 1997, OTuC-1.

[63] S.E. Kanellopoulos, V.A. Handerek and A.J. Rogers, "Simultaneous strain and temperature sensing with photogenerated in-fiber gratings", *Opt. Lett.*, 20, 1995, pp 333-335.

[64] M.G. Xu, L. Dong, L. Reekie, J.A. Tucknott and J.L. Cruz, "Temperature-independent strain sensor using a chirped Bragg grating in a tapered optical fibre", *Electron. Lett.*, 31, 1995, pp 823-825.

[65] M. Sudo, M. Nakai, K. Himeno, S. Suzaki, A. Wada and R. Yamacuhi, "Simultaneous measurement of temperature and strain using PANDA fiber grating", *Conf. Optical Fibre Sensors (OFS '97)*, Williamsburg, Virginia, Tech. Dig, 1997, OWC7-1.

[66] P.D. Foote "Fiber Bragg grating strain sensors for aerospace SMART structures", *2nd European Conf. SMART Structures and Materials*, Glasgow, Scotland, **2361**, 1994, p 162.

[67] S.T. Vohra, M.A. Davies, A. Dandridge, C.C. Chang, B. Althouse, H. Patrick, M. Putnam, T. Tsai, G. Wang, P.O. Baalerud, G.B. Haavsgard and K. Pran, "Sixteen channel WDM fiber Bragg grating dynamic strain sensing system for composite panel slamming tests", *Conf. Optical Fibre Sensors (OFS '97)*, Williamsburg, Virginia, Postdeadline Papers, 1997, PD3-1.

[68] R.M. Measures, T. Alavie, R. Masskant, S. Huang and M. LeBlanc, "Bragg grating fiber optic sensing for bridges and other structures", *2nd European Conf. SMART Structures and Materials*, Glasgow, Scotland, **2361**, 1994.

[69] V. Dewynter-Marty, S. Rougeault, P. Ferdinand, D. Chauvel, E. Toppani, M. Leygonie, B. Jarret and P. Fenaux, "Concrete strain measurements and crack detection with surface-mounted and embedded Bragg grating extensometers", *Conf. Optical Fibre Sensors (OFS '97)*, Williamsburg, Virginia, Tech. Dig, 1997, OFA2-1.

[70] Y.J. Rao, D.A. Jackson, L. Zhang and I. Bennion, "Strain sensing of modern composite materials with a spatial/wavelength multiplexed fibre grating network", *Opt. Lett.*, **21**, 1996, pp 683-685.

[71] P. Ferdinand, S. Magne, V. Dewynter-Marty, C. Martinez, S. Rougeault and M. Bugaud, "Applications of Bragg grating sensors in Europe", *Conf. Optical Fibre Sensors (OFS '97)*, Williamsburg, Virginia, Tech. Dig, 1997, OTuB-1.

[72] P. Ferdinand, O. Ferragu, J.L. Lechien, B. Lescop, S. Magne, V. Marty, S. Rougeault, G. Kotrotsios, V. Neuman, Y. Depeursinge, J.B. Michel, M. Van Uffelen, D. Varelas, H. Berthou, G. Pierre, C. Renouf, B. Jarret, Y. Verbandt, W. Stevens, M.R.H. Voet and D. Toscano, "Mine operating accurate STABILity control with Optical fiber Sensing and Bragg grating technology: The European BRITE/EURAM STABILOS project", *J. Lightwave Technol.*, **13**, 1995, p 1303-1313.

[73] N. Cerre, E. Taufflieb, T. Gaiffe, N. Faussot, P. Simonpietri and H.C. Lefvre, "Fiber Bragg grating for use within high-accuracy fiber optic gyroscope", *Conf. Optical Fibre Sensors (OFS '97)*, Williamsburg, Virginia, Tech. Dig, 1997, OWB7-1.

[74] C. Chang and A. Kersey, "Development of fiber Bragg grating sensor based load transducers", *Conf. Optical Fibre Sensors (OFS '97)*, Williamsburg, Virginia, Tech. Dig, 1997, OWC8-1.

[75] Y.J. Rao, D.A. Jackson, D.J. Webb, L. Zhang and I. Bennion, "In-fibre Bragg grating flow-directed thermodilution catheter for cardiac monitoring", *Conf. Optical Fibre Sensors (OFS '97)*, Williamsburg, Virginia, Tech. Dig, 1997, OThA2-1.

[76] N.E. Fisher, J. Surowiec, D.J. Webb, D.A. Jackson, L.R. Gavrilov, J.W. Hand, L. Zhang and I. Bennion, "In-fibre Bragg gratings for ultrasonic medical applications", *Meas. Sci. Technol.*, **8**, 1997, p 1050-1054.

Chapter Four: Temperature and Strain Characterisation of uniform, chirped and bandpass in-fibre Bragg gratings

4.1 Chapter Overview.

This chapter presents the strain and temperature characterisation results for a number of chirped and uniform gratings written into three different host fibres. The aim of this work is to highlight the effect of the host fibre, as well as any pre-processing of it, and the bandwidth of the inscribed structure may have on its response to the aforementioned parameters. The characteristics of a commercially available temperature compensated grating and its applications will be presented and discussed. The chapter concludes with the development, implementation and testing of a multiplexed strain sensor system. The interrogation of the sensor array is facilitated by an in-fibre Fabry-Perot filter.

4.2 The need for characterisation

It is necessary to calibrate the response of gratings if they are to be employed as sensors. In addition, any FBG system designer needs to know how a grating will respond to a change of temperature in its vicinity or to strain that is unintentionally applied to it, regardless of application. For example, a fibre laser, employing FBGs as mirrors[1], situated in a laboratory would drift due to thermal fluctuations unless it was either suitably isolated or kept at a controlled temperature. This required characterisation, at first glance, would appear to be fairly straightforward and indeed results for the sensitivities of uniform inscribed structures have been published[2,3]. However, these have been limited to uniform gratings in boron-germania co-doped fibre.

It is clear that any dopants in a fibre which alter the thermo-optic coefficient and/or photoelastic constant will effect temperature and strain sensitivities. There is also a need to assess the effect, if any, that the type of grating and fibre pre-processing treatment, i.e. hydrogenation, may have on sensitivity. There is also the possibility that strain and temperature may affect the spectral profile of the grating. To date there has been no published work that has addressed these issues. However, it is necessary for

any possible affects to be known if a system employing Bragg gratings is to be designed while taking into account possible induced changes in wavelength. The purpose of this chapter is to fill part of this gap in knowledge and examine possible ways to eliminate unwanted thermal fluctuations in the Bragg wavelength of the grating.

4.3 Characterisation

All the gratings characterised were in the 1.5 μm region and illuminated by erbium fluorescence. Table 4.1 gives the values of the peak reflections and bandwidths of the uniform and chirped gratings examined. All gratings were written to saturation by the transverse two beam interferometric holographic technique[4]. The structures were inscribed at a wavelength of 244 nm derived from a frequency doubled argon ion laser. They were all 5mm long.

The chirped gratings were realised by placing two cylindrical lenses with the same focal length, a distance apart, in one arm of the interferometer. The distance was set to be twice the focal length of the lenses and they were arranged to produce a collimated beam. This resulted in the formation of an approximately linear fringe interference pattern at the fibre as in the case of writing uniform gratings. The telescope was then slightly de-tuned by moving one of the lenses away from the other along the path of the UV beam. This had the effect of slightly diverging the beam. The lens was moved until the desired amount of divergence was realised to write chirped gratings with the required bandwidth.

No structures were inscribed in non-hydrogenated standard fibre due to the fact that it is not sufficiently photosensitive to permit writing. It is observed that there is a decrease in peak reflection with the increasing chirp rate of the inscribed structures. This is due to the depletion of the available photosensitivity.

The standard telecommunications (stand.) fibre, high germania (Ge) fibre and boron-germania (B/Ge) co-doped fibres had 4 mol%, 20 mol% and 15 mol% concentrations of germanium respectively.

Fibre	Linear	Chirp			Resonator
Stand./H_2	~0.5nm/90%	~6nm/100%	~12nm/80%	~20nm/70%	_
Ge/H_2	~0.6nm/99%	~6nm/100%	~12nm/95%	~20nm/85%	_
B/Ge/H_2	~1nm/99%	~6nm/100%	~12nm/100%	~25nm/99%	T ~ 90% R ~99% f ~ 30
Ge	~0.2nm/50%	_	_	_	_
B/Ge	~0.2nm/90%	_	_	_	_

Table 4.1 Fibre gratings for characterisation of temperature and strain response.

The bandwidths of the chirped gratings were selected to give a range of chirp to examine if it effects the grating's sensitivity or if its spectral profile is altered in anyway by the application of heat or strain.

Figure 4.1 shows the experimental arrangement used to examine the gratings. Both the transmission and reflection profiles of the test gratings were interrogated by a HP optical spectrum analyser (OSA). The spectral profile of the grating at each sample point was taken 10 times and averaged by the OSA, thus reducing random noise. This averaged data was collected by an in-house written computer program (JWScope) and analysed in Microsoft Excel. The central wavelength of the structure was determined by averaging the wavelengths corresponding to the upper and lower half width maxima. This central wavelength was the reference point monitored to determine the induced spectral shift.

Heat was applied to the structure by a 5 cm^2 18.8 W Peltier heat pump. The grating was positioned in the centre of the Peltier and a heat sink compound was used to ensure good thermal contact between the pump and the grating. The temperature of the pump was maintained by an ILX temperature controller and monitored by a standard thermistor. The thermistor was calibrated for use with the temperature controller. The thermistor and sensor were then placed on the Peltier and covered with heat sink compound to ensure good thermal contact. The thermistor was placed sufficiently

close to the sensing structure for it to be considered to be at the same temperature as the fibre.

This simple system had an achievable temperature range of 0°C to 90°C with a resolution of 0.1°C. The grating was initially cooled to 0°C and heated, in steps of 5°C, up to 80°C. The Peltier was given sufficient time to stabilise at each new temperature before data collection commenced.

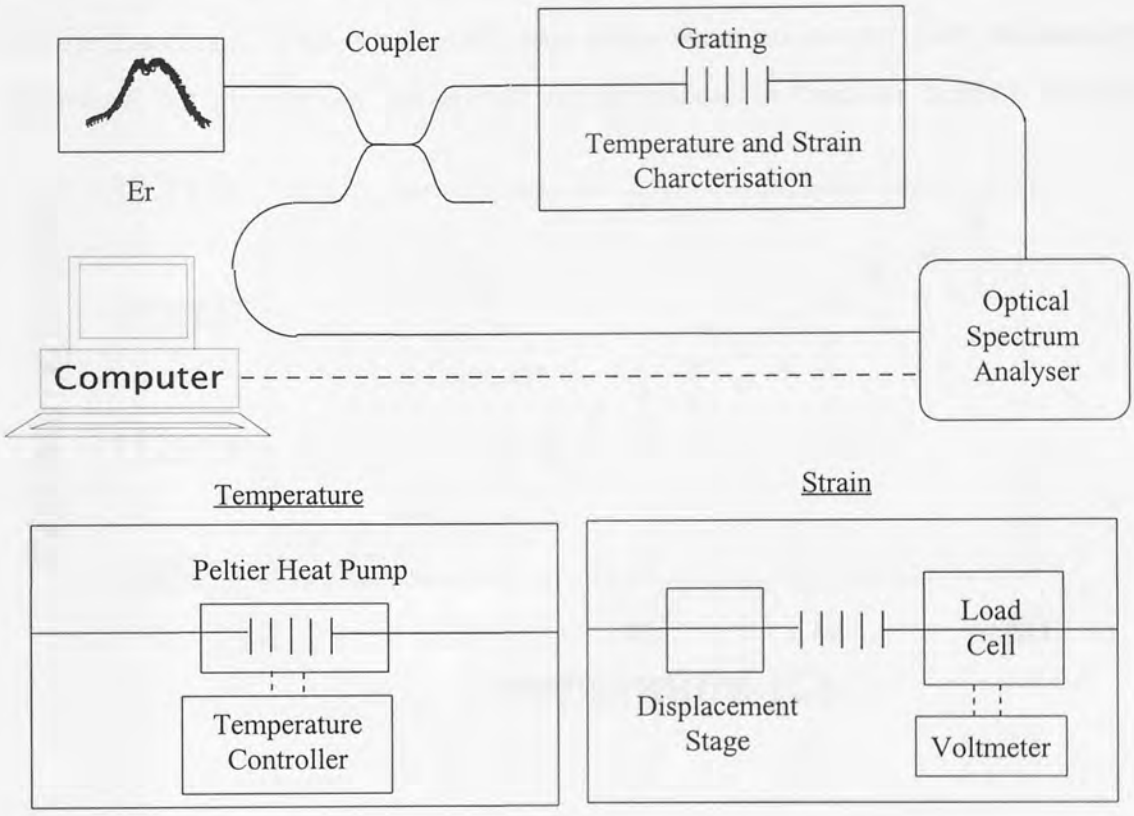

Figure 4.1: Experimental arrangement for temperature and strain characterisation.

For strain characterisation, the fibre jacket was stripped over a 5 mm length at two points 10 cm apart with the grating in between the two. The stripped fibre sections were then glued to two grooved steel blocks. This stripping ensured that the fibre instead of just the protective jacket was being stretched. The steel blocks were subsequently mounted onto a load cell and a mechanical displacement stage. The displacement stage had a resolution of 1 μm. The load cell was used to locate the "zero strain" point and ensure that there was no slippage between the blocks and the fibre. Any such slippage would manifest itself as a non-linear relationship between the output voltage of the load cell and the distance moved by the displacement stage. The grating

was stretched from 0 to 4 mε (0.4%), in steps of 250 με. At the completion of characterisation the grating was removed from the plates by the application of de-bonder. The plates were then cleaned with ethanol before gluing the next grating to be examined on to the plates.

The plots obtained for the temperature characterisation of the uniform structures and a list of all the temperature sensitivities are shown in figure 4.2 and table 4.2, respectively. Note: error bars are difficult to see on several of the graphs and figures contained within this thesis. This is especially true when there are several plots on one graph. Therefore, for consistency, all errors will be quoted in brackets beneath the figure.

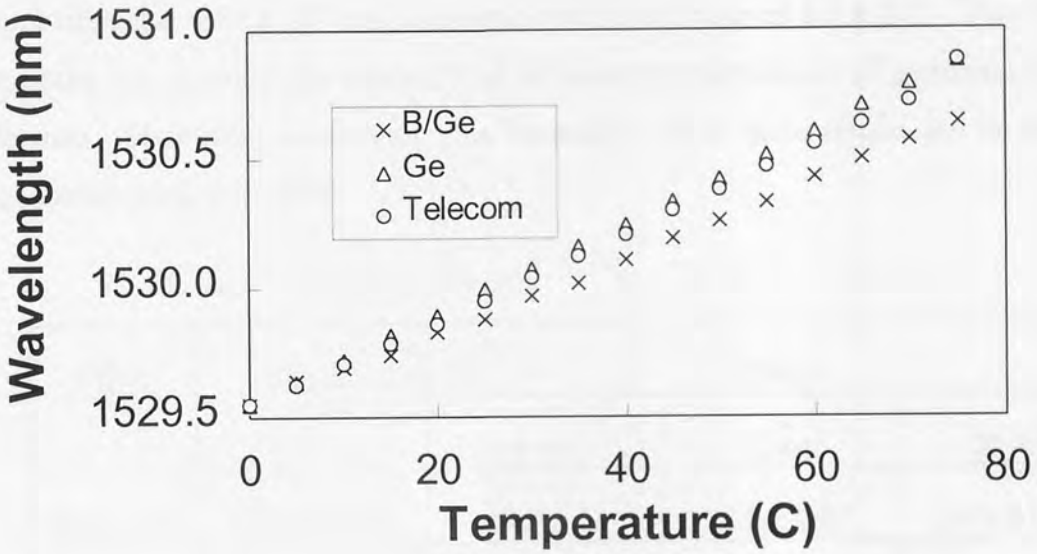

Figure 4.2: Graph of Bragg wavelength against temperature for uniform gratings in different host fibres.

(Errors in figure 4.2 are ± 0.2°C for temperature and ±0.06 nm for wavelength)

It is clear that hydrogenation does not affect the temperature sensitivities of the gratings. The differences between the readings for hydrogenated and non-hydrogenated are within experimental error. The standard telecommunications and high germanium doped fibres are highly sensitive to temperature. The fibre boron-germania co-doped is ~15 % less responsive than the other two. There is also a trend to decreasing sensitivity with increasing chirp size. This is possibly due to inaccuracies in calculating the central wavelength. These are due to the fact that the OSA has a fixed set of data

points obtainable in a single scan. Hence, a large scan range has low resolution and a small scan range has a high resolution. Therefore, to examine a large chirp the resolution of the scan is necessarily low which can lead to an increasing inaccuracy in the measurement of shift in the central wavelength. This idea is further supported by the result for the 20 nm chirp grating inscribed in standard telecommunications fibre. This result is greater than that of the corresponding 6 and 12 nm chirped structures. At this time no results for such structures have been communicated, hence it is not possible to draw a comparison. However, no change in sensitivity with varying chirp is predicted by equation 3.1. This equation predicts a sensitivity of 13.3 pm/°C for germania doped silica which is assumed to have the thermal expansion coefficient of pure silica, i.e. 0.55×10^{-5} and a thermo-optic coefficient of 8.3×10^{-6}. This value does not take into account the effect of the different concentrations of germanium or other dopants. However, considering this limitation all of these results are in fairly good agreement with this value.

Fibre	Linear	Chirp		
		6 nm	12 nm	20 nm
Stand./H_2	17.3 ± 0.05	13 ± 0.07	12.8 ± 0.07	14.6 ± 0.09
Ge/H_2	17.7 ± 0.05	12.5 ± 0.07	12.2 ± 0.07	10.6 ± 0.06
B/Ge/H_2	15.1 ± 0.04	11.2 ± 0.06	11.9 ± 0.07	9 ± 0.08
Ge	18.1± 0.05	-	-	-
B/Ge	14.8 ± 0.04	-	-	-

Table 4.2 Temperature sensitivities of chirped and linear Bragg gratings in different host fibres.

(All values are in pm/°C)

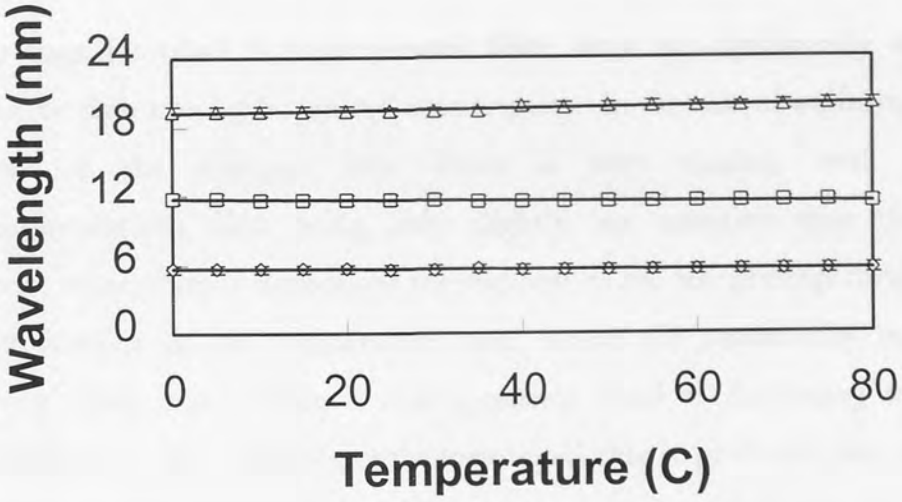

Figure 4.3: Bandwidth response to temperature for chirped gratings in germanium fibre.

(Errors in figure 4.3 are ±0.2°C for temperature and ± 0.1 nm for wavelength)

Figure 4.3 demonstrates the relationship between chirp size and temperature for the high doped germanium fibre. On all plots obtained the bandwidth remained constant within experimental error. Therefore, the spectral profile of the grating is linearly shifted with increasing temperature and, as such, is temperature insensitive.

The strain response for the uniform structures are shown in figure 4.4, with the results for all gratings being displayed in table 4.3.

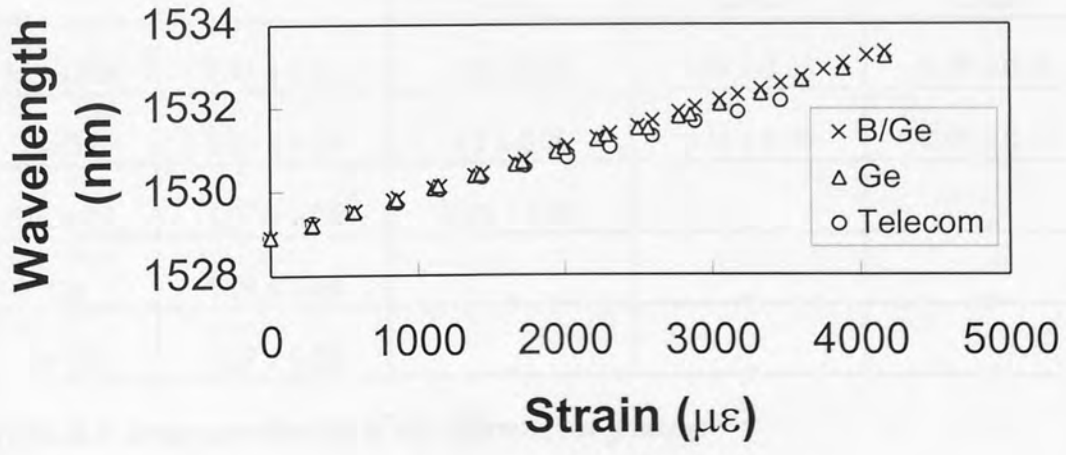

Figure 4.4: Strain response of uniform gratings inscribed in different hydrogenated fibres.

(Errors in figure 4.4: ± 15 με for strain and ± 0.06 nm for wavelength)

The gratings inscribed in hydrogenated fibre show no significantly different strain response to their non-hydrogenated counterparts. In the case of uniform structures the response of the different host fibres is very similar, with the standard telecommunications fibre being only slightly less sensitive than the other two. However, when chirp is introduced the response of the test gratings diverge. This is in marked contrast to the temperature case, where the sensitivities converged with increasing chirp size. There is also a general trend to decreasing sensitivity with increasing chirp size. As previously mentioned this is probably due to the lowered resolution of the OSA. Again, this variation is not predicted by equation 3.2. Assuming a value of 0.22 for the effective photosilicate constant the predicted sensitivity is 1.21 pm/με. Therefore, all the readings taken are in fairly good agreement considering that the calculation does not take into account different concentrations of germanium or other dopants.

The bandwidth was monitored with increasing strain and again the spectral profile of the grating was linearly shifted without change. Both these results suggest that the application of linear strain and temperature will shift the profile of the grating without altering it in anyway. This was cross-checked by examining the reaction of a more complex structure to strain and temperature.

Fibre	Linear	Chirp		
		6nm	12nm	20nm
Stand./H_2	0.93 ± 0.04	0.8 ± 0.05	0.96 ± 0.05	0.78 ± 0.06
Ge/H_2	1.03 ± 0.04	1.2 ± 0.06	1.13 ± 0.06	0.94 ± 0.05
B/Ge/H_2	1.07 ± 0.03	0.95 ± 0.05	_	_
Ge	1.04 ± 0.04	_	_	_
B/Ge	1.07 ± 0.05	_	_	_

Table 4.3: Strain sensitivities of the different test gratings

(All values are in pm/με).

A bandpass structure was inscribed into boron-germania co-doped fibre. This was realised by inscription of a Moiré grating. The required small change between the two superimposed gratings was achieved by altering the angle between the two writing beams[5]. The inscribed structure had three narrow passbands in a stopband approximately 10 nm wide. It had a peak transmission of 90% for the passbands and the stopband had a rejection of 99%. The finesse of a filter was defined as the ratio of the width of one of the transmission peaks to the width of the stopband and was determined to be 30 for this structure. Its complete spectral profile is shown in figure 4.5. The solid line indicates the measurement taken with the broadband source and the OSA. The broken line indicates the superior resolution scan performed by a combination of a tuneable laser and the OSA. A Hewlett Packard tuneable laser was employed. This system improves the resolution of the measurement from 0.1 nm for the OSA used in conjunction with erbium fluorescence illumination, to 0.01 nm.

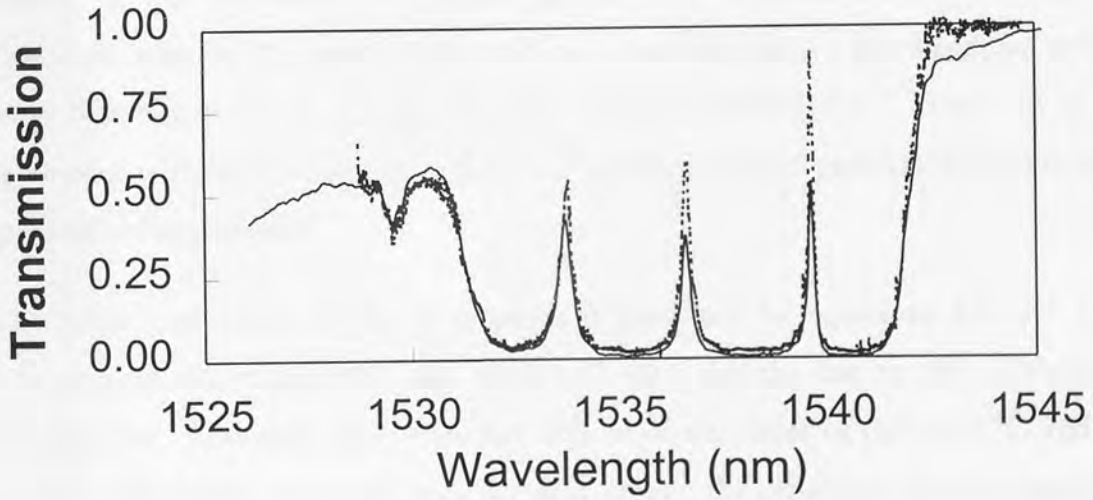

Figure 4.5: The spectral profile of the bandpass structure examined.

The central wavelength (as defined earlier) of each passband in transmission was calculated and monitored to check for any induced alterations in the gratings overall profile. The results for strain characterisation are shown in figure 4.6. The transmission points indicate the central wavelength of the three passbands while the reflection ones trace the movement of the upper and lower half width maxima.

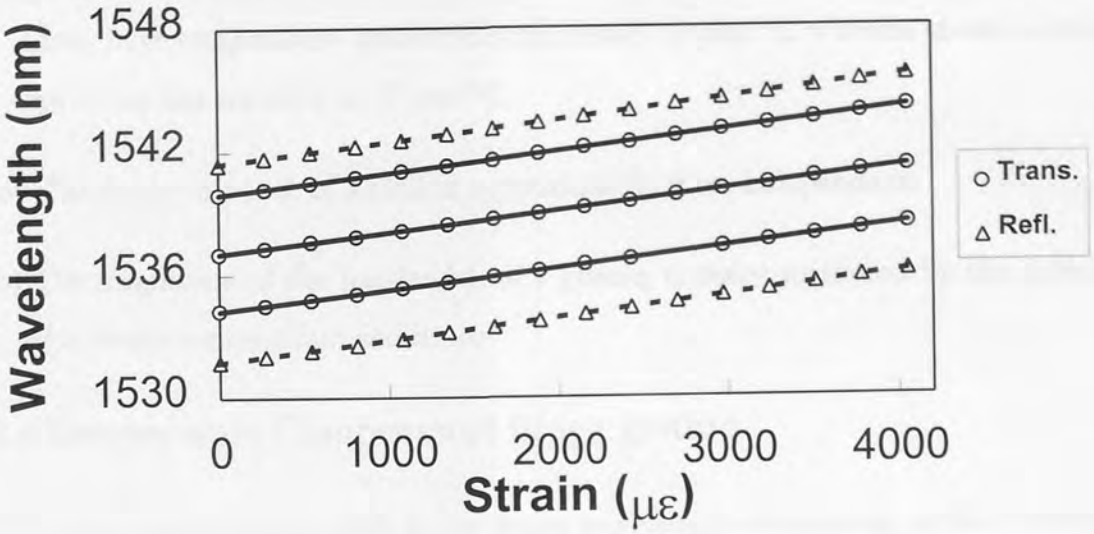

Figure 4.6: Results from the strain characterisation of the bandpass structure.

It is clear from the above graph that the entire structure moves linearly and the spectral profile is not effected. A similar graph was obtained for the temperature characterisation. The temperature and strain sensitivities of the bandpass structure were determined to be 13 pm/°C and 1 pm/με respectively. These are in good agreement with the results obtained for the standard chirped gratings written in boron-germania co-doped fibre.

The linear movement of the three peaks is predicted by equations 3.1 and 3.2. It follows that the response of each peak will vary slightly due to the different peak wavelengths. However, this difference will be of the order of 0.09 pm/°C and 0.007 pm/με. Therefore, over these measurement ranges, the difference in wavelength shifts will be 7.2 pm and 28 pm for temperature and strain respectively. These values are far below the resolution of the OSA and therefore not detectable.

It is possible to draw a number of conclusions from this data, which are as follows:

(i) Hydrogenation has a negligible effect on the temperature and strain characteristics of a grating.

(ii) Temperature and strain sensitivities are host fibre dependent.

(iii) Gratings inscribed in standard telecommunications and high doped germanium fibres have temperature sensitivities of around 17 pm/°C whereas those in co-doped boron are less sensitive at 13 pm/°C.

(iv) The strain response of a FBG is approximately fibre independent.

(v) The magnitude of the bandwidth of a grating remains unaltered by the application of constant temperature and strain.

4.4 Temperature Compensated Bragg grating

The temperature induced shift in the Bragg wavelength of a grating, while desirable and necessary for temperature sensing, is not suitable for other applications. For example if the grating is to be employed as a mirror to define a fibre laser cavity it needs to have a constant Bragg wavelength. However, the Bragg wavelength of the structure will be undesirably influenced by small temperature changes in the environment causing a corresponding shift in the output of the laser. This can be eliminated by actively controlling the temperature at the grating using a Peltier heat pump for example. This method is suitable for use in the laboratory but may not always be viable. Bragg gratings are now finding application in WDM devices[6] that will be placed in underground systems. Underground the temperature will only change by a few degrees Centigrade. However, this is sufficient to shift the multiplexing wavelengths of the WDM by 0.05 nm. This shift needs to be compensated for, but the active method is not appropriate in such an environment.

It is possible, to a certain extent, to eliminate temperature effects by appropriately straining and relaxing the fibre. The required temperature dependent strain can be achieved by appropriately packaging the structure. The grating is held under tension by two metal strips inside the package, see figure 4.7. When the temperature of the package is increased the metal strips thermally expand. Therefore, as the Bragg wavelength is red shifted by the increase in temperature the strain on the grating is relaxed. The appropriate choice of metal can result in the temperature effect being counteracted by decreasing strain. Melles Griot have designed, produced and marketed such a package, one of which they kindly supplied. In this case, the fibre is bonded to

metal strips rather than being clamped to metal blocks. The following is an investigation of its compensating properties.

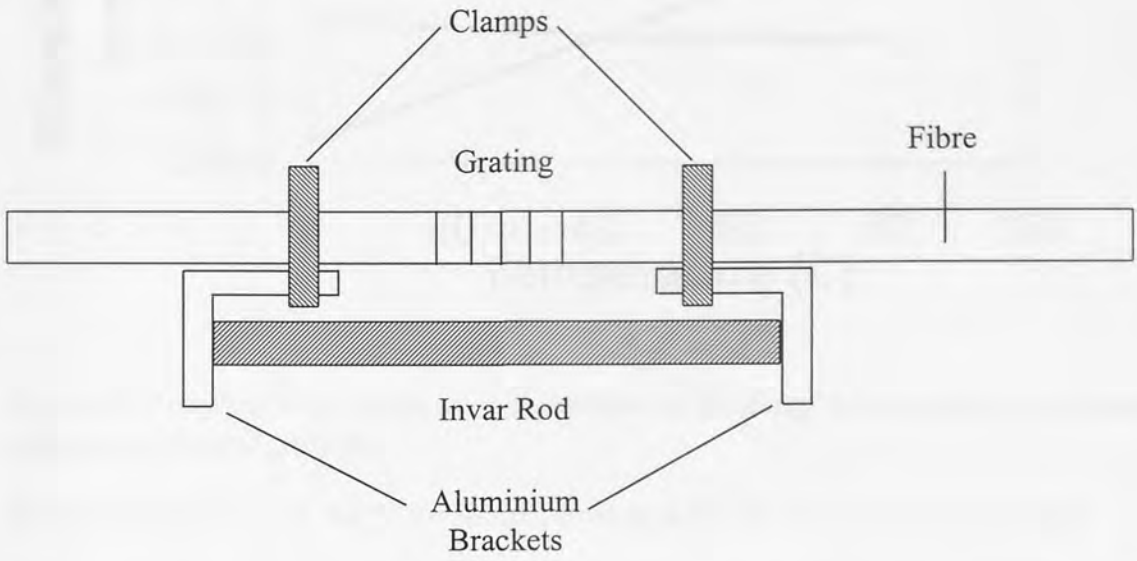

Figure 4.7: Schematic of an experimental table-top temperature-compensating mount.

The compensated grating was 5 mm long, had a bandwidth of 0.4 nm and a Bragg wavelength of 1538 nm. The complete package was 4 cm long. The central wavelength was again taken to be the average of the upper and lower width half maxima for the purposes of this experiment. The reflection of the grating was measured by the OSA and again the data was collected by JWScope and processed in Excel.

The complete package was mounted on the centre of the Peltier heat pump with good thermal contact being ensured by the application of heat sink compound. Once again the temperature of the Peltier was regulated by an ILX temperature controller. The complete package was cooled to 0°C, then heated, in steps of 5°C, up to 80°C. The Peltier was allowed to stabilise at the selected temperature before data was collected. Figure 4.8 displays the results obtained for the temperature compensated and an uncompensated grating. The shift in central wavelength over the temperature range for the uncompensated structure was 1 nm compared to 0.1 nm for the compensated one. Therefore, the compensation package makes the grating an order of magnitude less sensitive than an uncompensated structure.

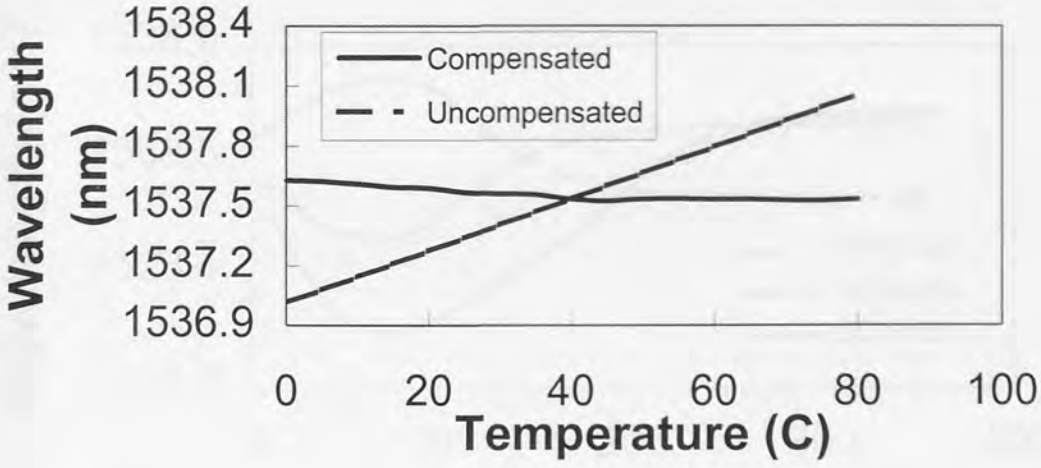

Figure 4.8: Graph to show temperature dependence of the Bragg wavelength for compensated and uncompensated gratings.

(Errors on figure 4.8: ± 0.2°C for temperature and ± 0.06 nm for the wavelength).

The results shown in figure 4.8 are for stable, static temperature values. The response of the device to a rapid change in temperature was also examined. There is a possibility that this would occur in the field, if there was an explosion or fire close to the device. The temperature stabilised grating was positioned and data was collected and processed as in the stable temperature case. The experiment was performed by heating and stabilising the grating to a temperature T_1. The temperature controller was then adjusted to give a lower temperature T_2. Results were taken every 5 seconds from the start of the cooling until the wavelength stabilisation of the grating was reached. The initial experiment involved cooling the grating from 90 to 25°C. The results of which are shown in figure 4.9. It is clear that the curve is composed of two parts; an initial rapid decrease in wavelength then a slower increase until the stable value, found in the initial part of this experiment, is reached. It was decided to investigate this phenomena further by taking a series of similar readings for cooling from 50 to 25°C and heating over the same range. The results are also shown in figure 4.9.

The 50 to 25°C cooling curve mirrors the respective heating curve. This indicates that the stabilisation times and temperature characteristics are identical whether the grating is heated or cooled at the same speed over an identical range.

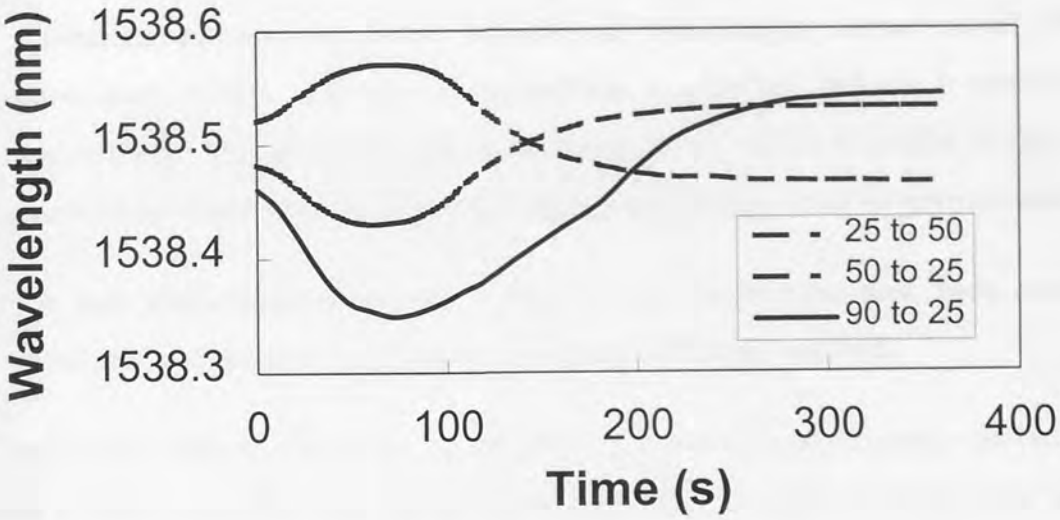

Figure 4.9: Bragg wavelength of temperature compensated grating during and after a rapid temperature change.

(Errors in figure 4.9: ± 0.5 s for time and ± 0.06 nm for wavelength).

It follows from the two cooling curves that the greater the temperature change the more the Bragg wavelength shifts in the opposite direction to its new equilibrium point. These two curves do however have a number of similar characteristics:

(i) For the initial 80 seconds the Bragg wavelength decreases rapidly. This corresponds to the time it takes for the device to be cooled to T_2. This indicates that the temperature shift induced in the fibre is more dominant than the compensating strain effect. This is probably due to the fact that the refractive index of the fibre core is able to change virtually instantaneously with temperature. As previously mentioned this is due to both the thermal-optic co-efficient, which is the dominant effect, and thermal expansion. Thus, the Bragg wavelength is shifted almost immediately by temperature, however the balancing effect, brought about by a change in applied tensile strain, takes longer. The thermal expansion/contraction of the metal strips takes longer to react fully to the change in temperature.

(ii) The temperature then reaches the new steady temperature, T_2, and the refractive index settles to its new value. Hence, the curve reaches a minimum.

(iii) The effect of cooling on the grating has now been exhausted and the compensation mechanism becomes dominant. Initially, the metal strips contract rapidly thus the curve rises rapidly. The rate of contraction, as expected, reduces as equilibrium is approached. This gives rise to a "contracting curve" which is similar to the cooling curve of an object that is initially at a higher temperature than its environment.

(iv) A new stable value is reached. Both of the effects have now been completely exhausted and the new equilibrium wavelength has been reached.

These results indicate that if the temperature of a grating is significantly altered rapidly then it takes some time for equilibrium to be reached. This "settling time" depends mainly on the magnitude of the temperature change. The amount of initial deviation from the final wavelength of the grating, i.e. in cooling how far it drops at the start, is dominated by the rate of temperature change.

It is therefore expected that there will be a maximum possible deviation from the initial wavelength that is equal to the temperature induced shift in uncompensated fibre. For example, the fibre is cooled sufficiently rapidly for the strip contracting effect to be ignored in regime (i) from 70 to 0°C. The maximum deviation would be 70 x 0.013 nm/C (the sensitivity of co-doped boron fibre), i.e. 0.91 nm. The maximum stabilisation time is governed by the response time of the compensating strips.

This type of compensation package would be ideal for application in both the field and the laboratory were a constant, unchanging wavelength is required. It is good in environments that have a slowly changing temperature in a range from 0 to 80°C. This would be the case for a large number of the environments in which gratings are employed.

4.5 Characterisation of multiplexing experiment

One of the more popular methods for addressing a sensor array involves the application of a fibre Fabry-Perot wavelength filter[7,8]. The sensor array contains a number of gratings that have their nominal Bragg wavelengths and operational domains chosen not to overlap and so that all fall within the spectrum of the source. The filter is then employed to scan through the source spectrum with the reflection from the array being

monitored. Peaks in the reflection output occur when the filter and grating wavelengths are equal.

A similar system to that discussed earlier was developed. The aim was to demonstrate a multiplexing system that could be entirely controlled by a computer. A schematic of the system developed is shown in figure 4.10.

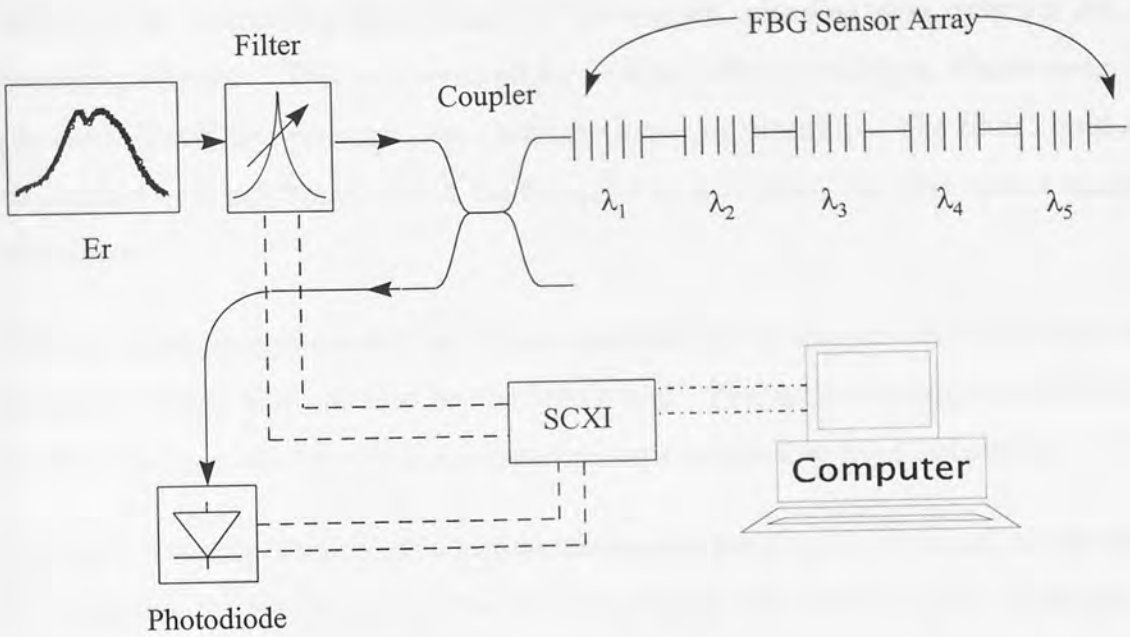

Figure 4.10: Multiplexed FBG five sensor array with a computer controlled in-fibre Fabry-Perot filter.

The complete system consists of a New Focus photodiode, a National Instruments (NI) SCXI system, a NI data acquisition (DAQ) card, a Queensgate in-fibre Fabry-Perot tuneable filter and an in-house constructed erbium fluorescence source. The SCXI system conditions signals, multiplexes up the input and output channels of the DAQ card and facilitates the connections between the apparatus and the computer.

The Fabry-Perot filter employed had a free spectral range, which defines the maximum spectrum that the array can utilise, of 40.3 nm. It had an insertion loss of 3.0 dB and a bandwidth of 0.31 nm. The piezoelectric stacks inside the filter were controlled by the Queensgate microfilter controller. The controller had an analogue and 14 bit digital input that could be used to select the required transmission wavelength or scan the filter. Initially, the digital interface was employed to scan the filter as this is inherently suffers from less electromagnetic interference and can scan in smaller steps than

analogue control. However, this method was too slow; a 25 nm scan took several seconds to complete. Therefore, the ± 10V analogue input was employed. The first step in controlling the device by the computer was to calibrate the output of filter with respect to the input voltage. This was achieved by connecting the output of the filter to the OSA. A voltage was then written to the filter controller and the central output wavelength of the device was calculated. The accuracy of this measurement was increased by centralising the transmitted wavelength, scanning over only 0.6 nm and averaging 50 scans. This was repeated for several different voltages, which were then plotted in Excel and produced the necessary linear relationship. The filter could now be scanned over any range within the its limits by generating the appropriate analogue waveform.

The low-noise photodiode had an in-built amplifier and its output was in the form of an analogue voltage that was read by the DAQ card. The entire system, except the light source, was controlled by the computer running a program written in LabView.

The LabView program permits a virtual instrument panel to be displayed on the screen and operated in a Windows environment. A program was written which permitted the user to scan the filter over any range between 1525 and 1565 nm at any scan rate, up to a maximum of 50 Hz. The required output analogue waveform was constructed by calculating the wavelengths required in the scan, converting these to the corresponding voltages and writing these values to an array. This array would then be continuously written to the analogue output buffer, hence scanning the filter. The program was written to scan the required wavelength range in steps of 40 pm, the smallest movement obtainable with this filter. The data was instantly collected from the photodiode after each new value had been written to the filter. This synchronisation is achieved by the DAQ card. The writing of an analogue value causes a pin to go high which permits the output voltage of the photodiode to be read. The program writes this voltage next to the corresponding wavelength in a two dimensional array which, when the scan had been completed, displayed this as a graph on the virtual instrument panel. The virtual instrument acts as an Optical Spectrum Analyser, though it has a much higher scanning rate and resolution over a limited range.

The LabView program is also capable of calculating the central wavelength of a number of gratings within its scanning range. The main data array corresponding to the entire scan is broken down into sub-arrays. Each of these sub-arrays covers the wavelength operating range of one sensor. The maximum photodiode voltage in one of these sub-arrays is then located, halved and the two wavelengths corresponding to this value, i.e. the upper and lower width half-maxima, are found. The average of these two values is then displayed on the screen as the central wavelength of that sensor. The program was written to scan and calculate the central wavelengths of five uniform FBG sensors at a rate of 25 Hz.

All the sensor gratings were written by the two beam interferometric holographic technique with the UV light derived from a frequency-doubled argon ion laser. They were 5 mm in length and had bandwidths of 0.5 nm. The inscribed structures had Bragg wavelengths of 1534, 1539, 1544, 1549 and 1554 nm respectively. This permits a tensile strain sensing range of 4 mε for each sensor. The gratings were spliced together in this order with the 1554 nm grating being closest to the source. It is important that the gratings are placed in this order. The spectral profile of the erbium source is such that the 1534 grating reflects far more power than the others. Therefore, by placing the 1554 grating, which is on the trailing edge of the fluorescence, nearest to, and the 1534 structure furthest away from the source the reflected light levels will be similar.

In the initial experiment the 1539 nm grating was glued to the two grooved blocks and mounted onto the strain arrangement discussed in section 4.2. The sensor was then stretched in steps of 500 με to 3 500 με. A figure displaying a number of plots taken from the virtual instrument panel on the computer are shown in figure 4.11. The large peak at 1534 nm corresponds to the peak in the erbium fluorescence.

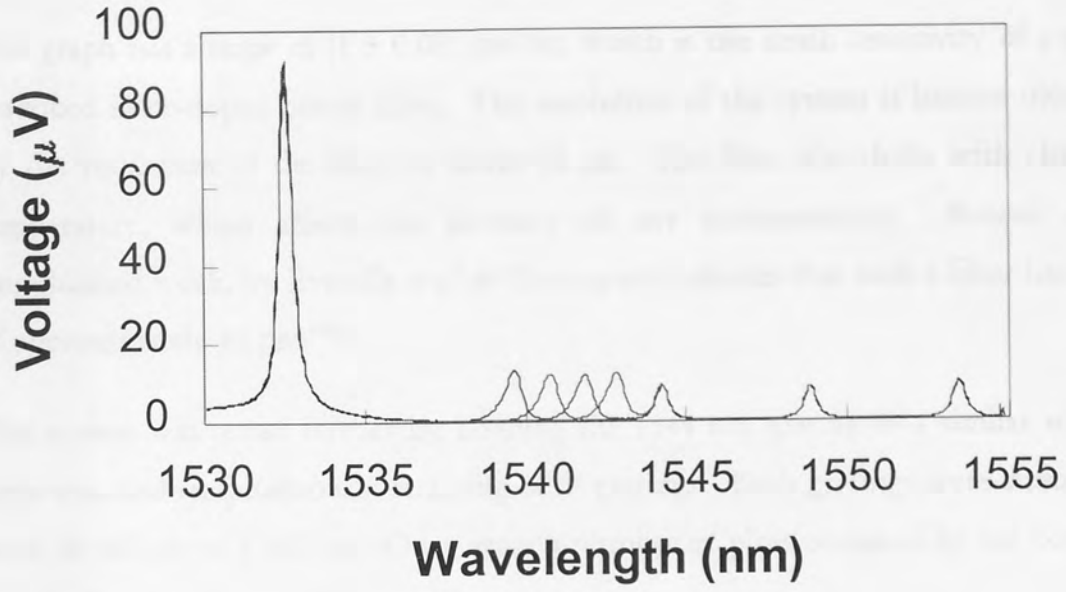

Figure 4.11: Traces of the complete sensing array with one element being placed under different strains

It is clear from the plot that the stretching of one grating does not effect the readings from the remainder of the array. The spectral profile of the stretched grating is linear, indicating that the interrogation system does operate properly. A graph to display the induced shift in Bragg wavelength against strain is shown in figure 4.12:

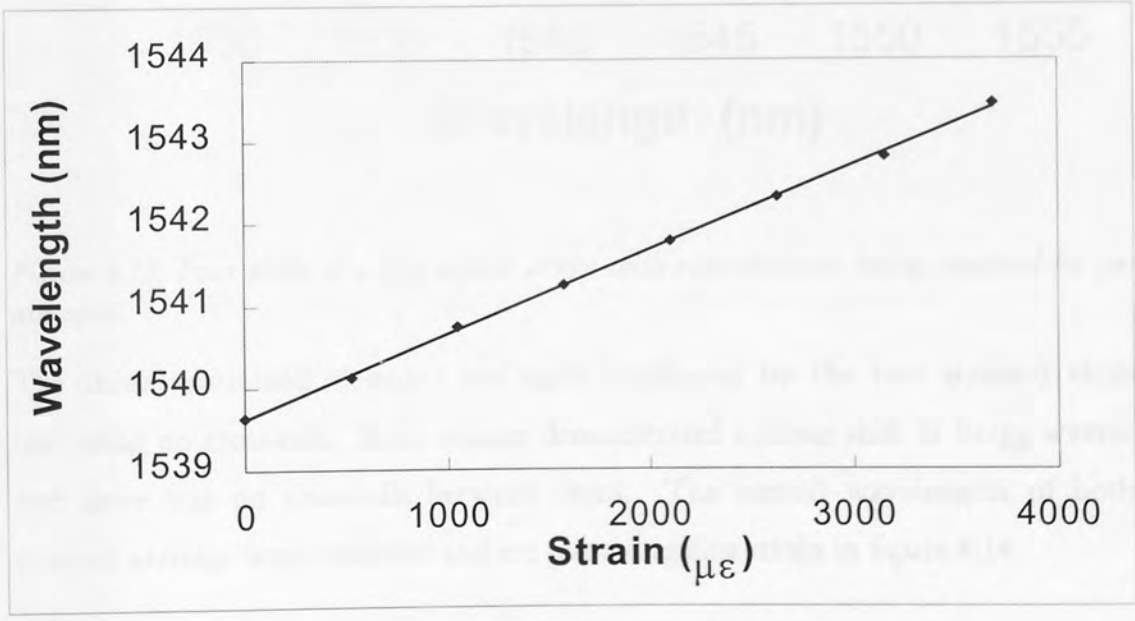

Figure 4.12: Graph to show the relationship between the induced Bragg wavelength shift and strain for one sensor in an array

(Errors on figure 4.12 are ± 10 με for strain and ± 0.06 nm for wavelength).

The graph has a slope of (1 ± 0.05) pm/με, which is the strain sensitivity of a grating inscribed in co-doped boron fibre. The resolution of the system is limited ultimately by the resolution of the filter to about 10 με. The filter also drifts with change in temperature, which affects the accuracy of any measurements. Recent, as yet unpublished work, by Everalla *et al* at Carbospars indicates that such a filter has a drift of approximately 10 pm/°C.

The system was tested further by bonding the 1544 nm grating to a similar straining apparatus and simultaneously straining both gratings. Both gratings were stretched in steps of 500 με to 3 500 με. Once again a number of plots obtained by the computer are displayed in figure 4.13.

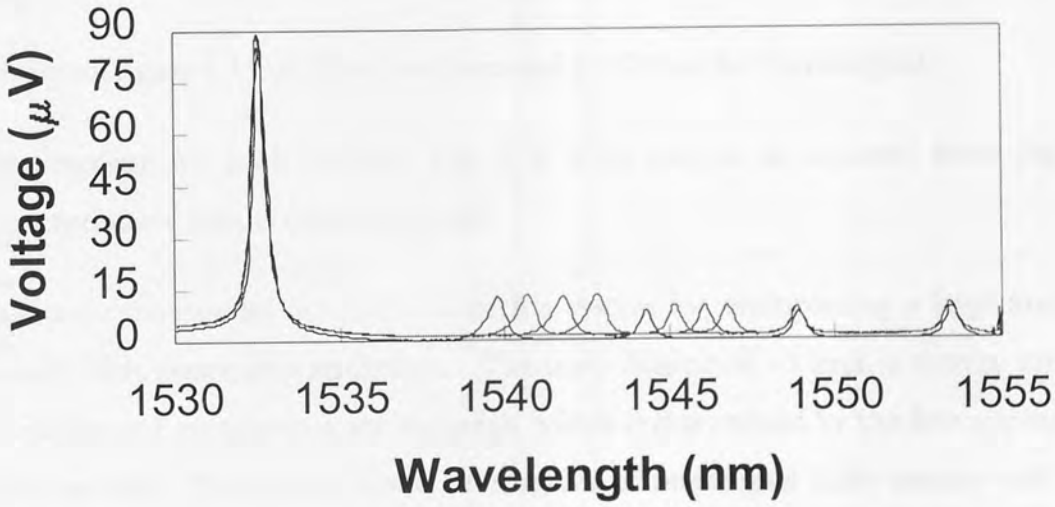

Figure 4.13: Four plots of a five sensor array with two elements being strained by various amounts.

The three unstrained elements are again unaffected by the two strained elements, indicating no cross-talk. Both sensors demonstrated a linear shift in Bragg wavelength and there was no cross-talk between them. The central wavelengths of both the strained gratings were recorded and are plotted against strain in figure 4.14.

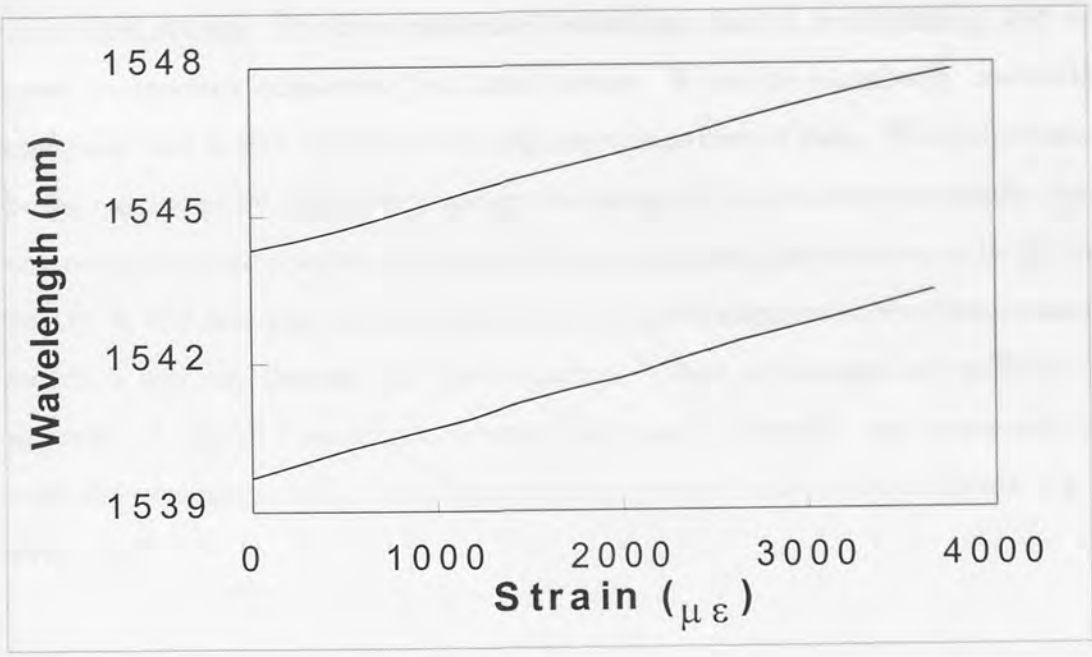

Figure 4.14: Graph to show induced strain shift in Bragg wavelength for two sensors in an array.

(Errors on figure 4.14: ± 10 με for strain and ± 0.06 nm for wavelength).

The response for both gratings was (1 ± 0.05) pm/με as expected from the strain characterisation results discussed earlier.

This demonstrates the suitability of such a system for multiplexing a large number of sensors with reasonable resolution. The main limitation of such a system are speed, resolution and maximum scanning range, which is determined by the free spectral range of the system. This system could be extended to interrogate eight sensors each with a tensile strain measurement range of 4 mε. The interrogation rate of the system is ultimately limited by the read/write speed (12.5×10^6 read/writes per second) of the DAQ card. The scanning speed can be increased at the expense of resolution, i.e. by reducing the number of data points acquired in the scan. For example, a scan of 20 nm with a step size of 4 pm has the same number of data points as one over 40 nm at 8 pm. Therefore, the maximum scanning speed for each of these would be the same. It is therefore important to know this trade-off and take it into account when designing a system.

In conclusion, the in-fibre Fabry-Perot filter method is a reasonable cost (a Fabry-Perot filter with controller typically costs six thousand pounds) and easily initiated and

controlled system. It offers moderate resolution, ease of multiplexing and sufficient speed to monitor quasi-static and static strain. It can be completely controlled by a computer that is also capable of storing large quantities of data. This information may be later analysed by a designer to adapt the design of the structure to match a variety of environmental and operating conditions (e.g. strengthen the structure at its greatest load point). It will also play a vital role in informing the engineer of the performance of the structure and any damage that has occurred. These advantages are sufficient for the majority of SMART sensing structures like mines[9], aircraft[10] and composite panels[11], with the exceptions being those that require dynamic strain measurements, e.g. marine structures[12].

---

[1] G.A. Ball and W.H. Glenn, "Design of a single-mode linear-cavity erbium fiber laser utilising Bragg reflectors", *J. Lightwave. Technol.*, **10**, 1992, pp 1338-1343.

[2] S.M. Melle, A.T. Alavie, S. Karr, T. Coroy, K. Liu and R.M. Measures, "A Bragg grating-tuned fibre laser strain sensor system", *IEE Photon. Technol. Lett.*, **5**, 1993, pp 263-266.

[3] W.W. Morey, J.R. Dunphy and G. Meltz, "Multiplexing fibre Bragg grating sensors", *SPIE Proc., Distributed and Multiplexed Fibre Optic Sensors*, **1586**, 1991, pp 216-224.

[4] G. Meltz, W.W. Morey and W.H. Glen, "Formation of Bragg gratings in optical fibres by a transverse holographic method," *Opt. Lett.*, **14**, 1989, pp 823-825.

[5] L. Zhang, K. Sugden, I. Bennion and A. Molony, "Wide-stopband chirped fibre moire grating transmission filters", *Electron. Lett.*, **31**, 1995, pp 477-279.

[6] T.A. Strasser "Fibre grating devices for WDM communication systems", *Conf.: Bragg gratings, photosensitivity and poling in glass fibres and waveguides,* Williamsburg, U.S., Tech. Dig, 1997, BTuA1-1.

[7] A.D. Kersy, T.A. Berkoff and W.W. Morey, "Multiplexed fibre Bragg grating strain-sensor system with a fibre Fabry-Perot wavelength filter", *Opt. Lett.*, **18**, 1993, pp 1370-1372.

[8] M.A. Davis, D.G. Bellemore, M.A. Putnam and A.D. Kersey, "Interrogation of 60 fibre Bragg grating sensors with microstrain resolution capability", *Electron. Lett.*, **32**, 1996, pp 1393-1394.

[9] P. Ferdinand, O. Ferragu, J.L. Lechien, B. Lescop, S. Magne, V. Marty, S. Rougeault, G. Kotrotsios, V. Neuman, Y. Depeursinge, J.B. Michel, M. Van Uffelen, D. Varelas, H. Berthou, G. Pierre, C. Renouf, B. Jarret, Y. Verbandt, W. Stevens, M.R.H. Voet and D. Toscano, "Mine operating accurate STABILity control with Optical fiber Sensing and Bragg grating technology: The European BRITE/EURAM STABILOS project", J. Lightwave Technol., 13, 1995, p 1303-1313.

[10] P.D. Foote "Fiber Bragg grating strain sensors for aerospace SMART structures", *2nd European Conf. SMART Structures and Materials*, Glasgow, Scotland, 2361, 1995, p 162.

[11] Y.J. Rao, D.A. Jackson, L. Zhang and I. Bennion, "Strain sensing of modern composite materials with a spatial/wavelength multiplexed fibre grating network", *Opt. Lett.*, 21, 1996, pp 683-685.

[12] S.T. Vohra, M.A. Davies, A. Dandridge, C.C. Chang, B. Althouse, H. Patrick, M. Putnam, T. Tsai, G. Wang, P.O. Baalerud, G.B. Haavsgard and K. Pran, "Sixteen channel WDM fiber Bragg grating dynamic strain sensing system for composite panel slamming tests", *Conf. Optical Fibre Sensors (OFS '97)*, Williamsburg, Virginia, Postdeadline Papers, 1997, PD3-1.

Chapter Five: Novel Strain Sensor Interrogation Techniques

5.1 Chapter Overview

This chapter looks at the conception, implementation and development of two novel FBG strain sensor interrogation techniques. The first of these was developed for the DTI funded MAST project. A brief overview of the MAST project and its aims will be given. Both of the systems to be discussed were developed for the interrogation of strain sensors in SMART structures. The first of these to be discussed is the Identical Broadband Chirped Interrogation (IBCI) technique. This has been demonstrated to offer simple, low cost, high speed interrogation for a number of chirped FBG strain sensors in both the 1.3 and 1.5 μm windows.

The second system is based on the edge filter response afforded by a grating with an asymmetric spectral response. This system offers similar advantages to the IBCI technique in the 1.5 μm window. However, this method interrogates uniform FBG sensors rather than chirped structures and thereby utilises less optical bandwidth. The main disadvantages are the complexities involved in the writing of a grating with an asymmetric spectral profile and the jagged response inherent in the sloping edge of the grating's response.

5.2 The MAST Project

The aim of the MAST research project was to develop and construct a composite super-yacht mast that had the capability of real time strain monitoring. The project ran for 2.5 years and was sponsored by the DTI. It was a collaboration between British Aerospace, Pendennis Shipyard, Carbospars and Aston University.

Carbon fibre and composite masts are now preferred for many racing and cruising yacht spars. They offer the combined benefits of high strength and light weight. They also offer a range of material structural properties achievable by using a combination of different fibres and different lay-up orientations. However, lack of information on the performance of these different combinations in sea-faring trials makes it impossible for

the designer to design the optimum mast for a given set of sailing conditions. The required information can only be gathered from strain sensors operating on or in the mast while the yacht is at sea. To date, this task has been performed by electrical sensors, which have been attached to the mast. Such systems have a very limited lifetime (approximately six months in the experience of Carbospars) due to the sensors either being ripped off the structure or rusted by salt water. Such sensor systems also suffer from the usual problems of electromagnetic interference and lack of multiplexing capability.

Fibre Bragg grating sensors offer several advantages including size (typically 5 mm long and around a mm in diameter), being immune to electromagnetic interference and the fact that they can be embedded into the mast and are, therefore, not effected by the extreme environment. Such sensors can be employed to provide valuable design feedback on actual loads, give overload warning signals, be used to accurately set-up the mast during the mast tuning operation and provide "a black box" history of the mast loading details. This type of structural health and usage monitoring is also of interest to a number of other fields including civil engineering[1] and aerospace[2]. Such capabilities could drastically reduce the cost of ownership by demonstrating the durability of the structure hence reducing both inspection overheads and insurance.

The envisioned mast would have the total capacity to interrogate 40 sensors along its structure, which would be up to 60 m in length. Five sensors were multiplexed on a single fibre with a system of 8 parallel fibres providing spatial multiplexing. The sensors were all in the 1.3 μm window and illuminated by a single SLED. They were all linked to a single remote instrument panel and interrogated by a tuneable Fabry Perot filter, as covered in the previous chapter, at a frequency of 500 Hz. Each sensor had a measurement range of ± 3 500 με. The measurement resolution for each sensor was determined to be ± 10 με. However, sea-faring strains may exceed this specified range in certain regions of extreme load. A second independent system comprising four gratings capable of measuring ± 15 mε was developed at Aston. This novel system was known as the Identical Broadband Chirped Interrogation (IBCI) technique and is the subject of the next section.

5.3. The Development of the IBCI system at 1.5 μm

5.3.1 Initial development

As discussed earlier, the MAST project required a number of FBG sensors that could measure large strains of up to 1.5%. These sensors were to be strategically placed near the base of the yacht mast where strains are at their greatest. While, it was possible to use uniform FBG sensors and interrogate them with a tuneable filter an alternative, superior solution might be sought and found within the constraints of the project. This solution needed to be cheaper, more robust, offer high speed interrogation and be easier to install and maintain. It was not required, however, to offer as high a resolution as the other sensors with 50 με being an acceptable value.

The first step in developing an appropriate interrogation system was to examine previous work. An interferometeric technique[3,4] would be expensive, fragile and the high resolution it offers unnecessary. An edge filter system while attractive was either achieved by unsuitable bulk optics[5] or specialist, difficult filter fabrication[6]. The Fabry-Perot filter method[7] was already being utilised. An acousto-optic filter[8] approach would have similar disadvantages to the Fabry-Perot approach and is highly temperature sensitive[9]. One of the remaining methods is to interrogate the grating with another grating as first suggested by Davies *et al.*[10]. This method, as previously discussed, interrogates uniform gratings by matching the wavelength of a sensor to that of the reference grating.

The use of an identical grating to interrogate an FBG sensor can be taken a step further. The main disadvantage of the matching technique is the fact that the reference grating has to be stretched and matched by an expensive piezoelectric system; a piezoelectric stack with controller costs in the region of a thousand pound. The solution to this is not to match the gratings and, therefore, not require a piezoelectric stretcher system. In this case, uniform gratings are not workable as such a system would only indicate that either the gratings were matched and, therefore, at the same strain or not. However, the work completed and discussed in the previous chapter concluded that the spectral profile of a chirped grating is linearly shifted, without change, to a longer wavelength

on the application of tensile strain. Hence, if the reference and sensor gratings were chirped then when the sensing structure is stretched the gratings would still overlap but not completely. The fraction of overlap would be proportional to the strain applied to the sensor, i.e. the larger the strain, the less the overlap.

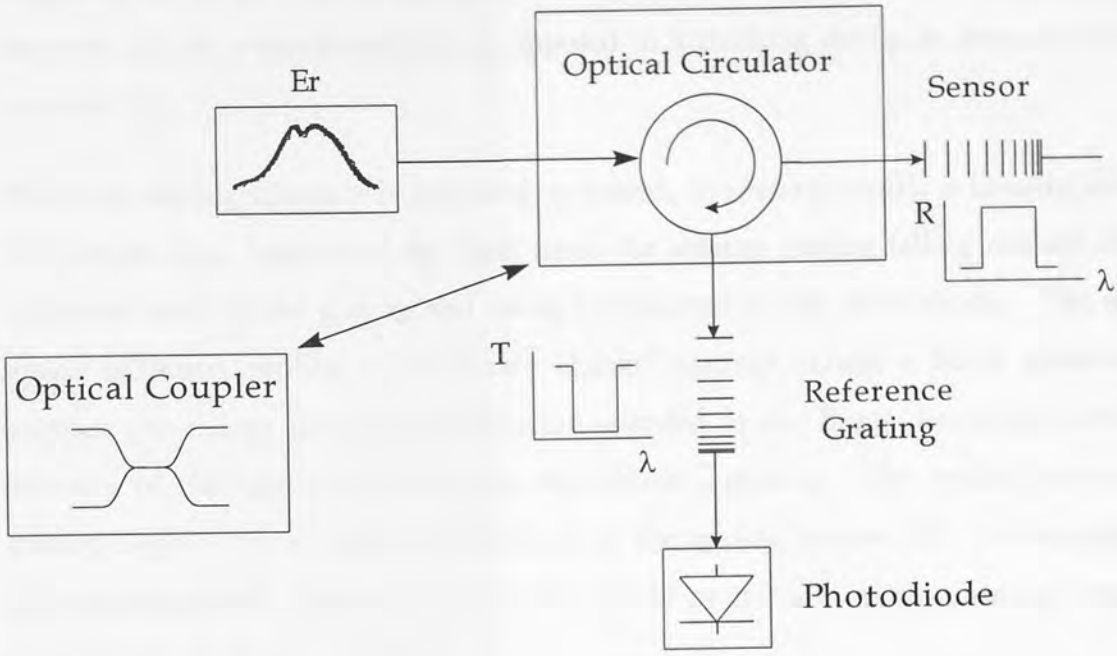

Figure 5.1: Schematic diagram of experimental set-up for IBCI system employing (a) a circulator and (b) a coupler.

This theory was tested using the experimental arrangement shown in figure 5.1. It consists of a broadband erbium fluorescence source, an optical circulator, two identical chirped gratings and an Anritsu photodetector. The broadband fluorescence was achieved by pumping a length of erbium doped fibre with a 980 nm pump diode. The Halo optical circulator had a total insertion loss of 2 dB and a peak isolation of 65 dB. Light injected into a port of the optical circulator is transmitted to the next port in succession or, in the case of the final port, lost. Thus, light from the erbium source is directed to the chirped grating sensor. The sensor reflected a range of wavelengths, with the remainder being transmitted. The fibre after the grating was curved tightly ensuring any transmitted light was lost from the system as opposed to being back reflected at the end of the fibre.

The light reflected from the sensor re-enters the circulator emerging at the reference grating port. The reference grating, which the reflected light is incident on, is kept

unstrained. If the sensor is also unstrained then its reflection profile is the complement of the transmission profile of the reference structure. Hence, the reference structure transmits minimal light. This transmitted light is measured by the photodiode. Light reflected/rejected by the reference grating is returned to and lost in the circulator. The important point to note is that this technique describes the fact that the reference structure acts as a rejection filter, as opposed to a tracking device as demonstrated in reference 10.

When the sensing structure is stretched or heated, its spectral profile is linearly shifted. This results in a fraction of the light from the sensing grating falling outside of the reflection band of the grating and being transmitted to the photodiode. The quasi-square reflection profiles of these two chirped gratings permit a linear relationship between the change in strain/temperature encoded in the Bragg wavelength and the intensity of the light transmitted by the reference grating. The strain/temperature sensing range of the system is determined by the grating bandwidth. For example, a sensor grating with a bandwidth of 20 nm would permit a maximum sensing range of over ±10 mε (± 1%) or ± 770°C.

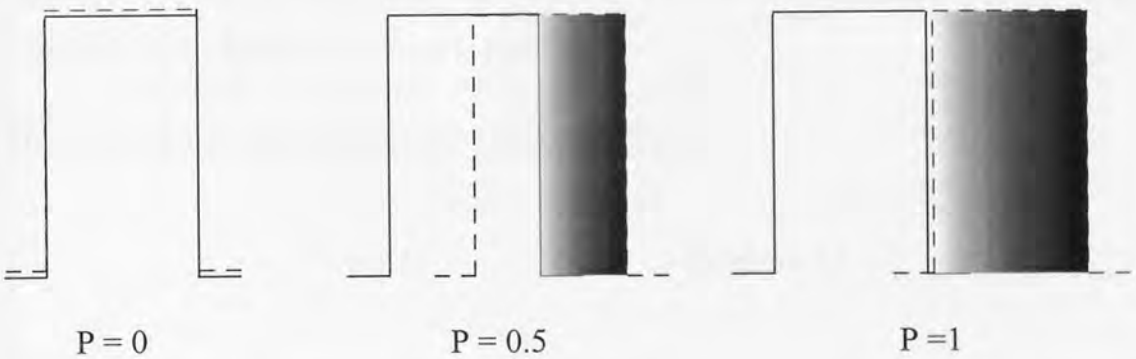

Figure 5.2: Pictorial representation of the basic IBCI principle. The solid line indicates the reference structure. The dotted line represents the sensing structure.

The overlap principle that forms the basis of the IBCI is demonstrated in figure 5.2. The figures indicate the fraction of power reflected by the sensor grating which is emergent from the interrogation system. In the first instance both of the identical structures are under the same strain and hence no power is transmitted, i.e. P=0. The second case shows the sensor being strained causing a linear shift in the spectral profile of the grating. The two gratings no longer overlap and half of the power reflected by

the sensing structure is transmitted to the photodiode, i.e. P=0.5. The final case shows the sensor being stretched beyond its measurement range, hence there is no overlap and all the power reflected by the sensing structure is transmitted, i.e. P=1. Therefore, the greater the strain on the grating the larger the induced shift, the less the overlap and the greater the transmitted power. The quasi-square profile of the two gratings permits this relationship to be linear. The gratings employed in the system have to be identical and have to have sufficient bandwidth to facilitate the desired measurement range.

The linear relationship afforded by the IBCI system can be demonstrated simply by assuming the following:

(i) The spectral profiles of the sensor and reference grating are perfect top-hat functions;

(ii) Both of the gratings have 100% reflectivity and no transmission loss;

(iii) The spectral profile of the source spectrum is perfectly flat;

(iv) The sensor and reference gratings are identical;

(v) The reference grating is kept unstrained at a constant temperature, i.e. the spectral profile of the reference grating is fixed.

The power reflected by the source (Ps) is given by:

$$Ps = \int_{a}^{b} A dx \qquad \textit{Equation 5.1}$$

where A is the amplitude of the source and a and b are the upper and lower wavelengths of the grating respectively.

Therefore,

$$Ps = A(b-a) = A\Delta\lambda \qquad \textit{Equation 5.2}$$

where $\Delta\lambda$ is the bandwidth of the structure.

The transmission of the reference of the grating, from assumption (ii), is zero between the lower and upper wavelengths of the structure and zero otherwise.

Consider the central wavelengths of the reference and sensor grating, λr and λs respectively. The difference between these two wavelengths determines the relative overlap of the gratings. Therefore, the power transmitted by the reference structure (Pt) which is the measured output of the system can be expressed as:

$$Pt = Ps(\lambda s - \lambda r)/\Delta\lambda \qquad \textit{Equation 5.3}$$

However, as the two gratings are identical, λs can be expressed as:

$$\lambda s = \lambda r + S.z \qquad \textit{Equation 5.4}$$

where S is the strain sensitivity of the grating and z is the applied strain. Therefore, substituting 5.4 into 5.3:

$$Pt = Ps(\lambda r + S.z - \lambda r) = Ps(S.z) \propto z \qquad \textit{Equation 5.5}$$

Therefore, the output of the system is directly proportional to the applied strain as required. This system was implemented and further developed experimentally.

All of the structures discussed in this chapter, unless indicated otherwise, were inscribed by two-beam transverse holographic exposure[11]. The required UV light (244 nm) was derived from a frequency doubled Argon ion laser. The chirp was introduced by controlled wavefront curvature[12] as described previously. The two identical gratings, in this first experiment, were fabricated in boron/germania co-doped fibre that had been kept in a hydrogen-loaded tube at 150 atm. for a week. The gratings were written at 1540 nm with a bandwidth of 10 nm and were approximately 5 mm long. Both were written to saturation. The spectral profiles of these two structures are shown in figure 5.3.

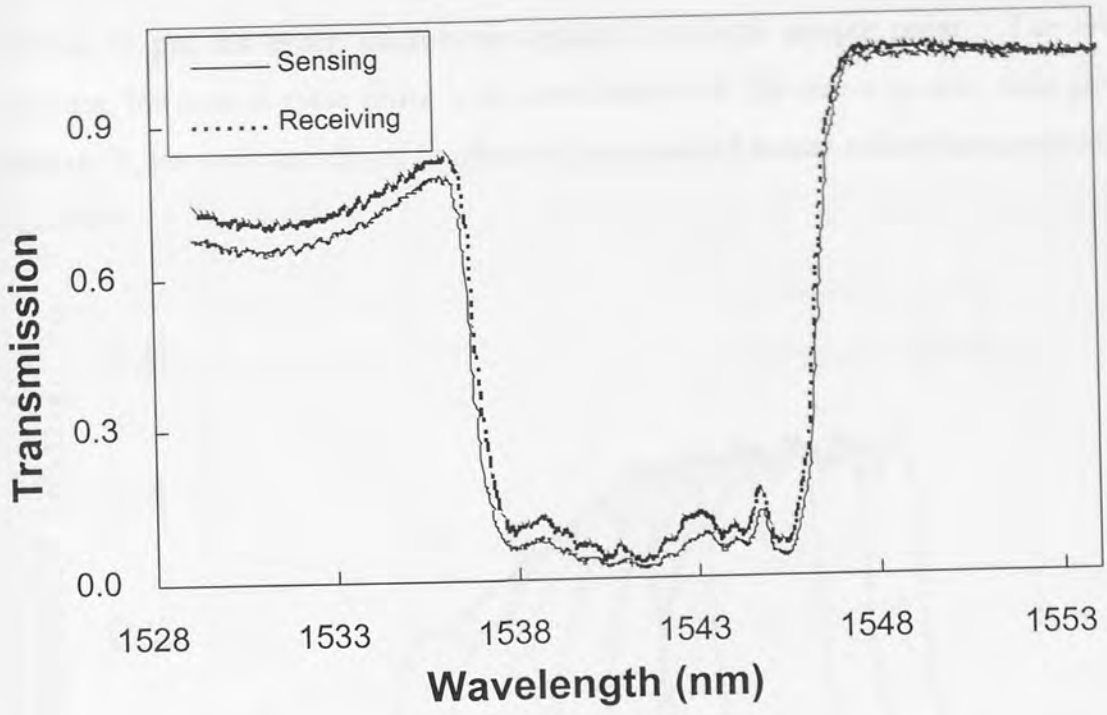

Figure 5.3: Transmission spectra of 10 nm chirped sensor and reference gratings.

The above spectra indicate the gratings' near identical responses. This is vital criterion if the system is to operate to its full potential.

The previous calculations simply demonstrated that the modelled output from such a system is directly proportional to the induced shift in the sensor grating. However, these calculations were based on impractical assumptions, e.g. both gratings having a perfect top hat function. It was decided to model the expected response from the system using actual data.

The spectral response of the erbium fluorescence was measured with a Hewlett-Packard Optical Spectrum Analyser (OSA). This data was captured by an in-house program (JWScope) and downloaded into Excel. The spectral profile of both gratings, in transmission and reflection, were then consecutively measured by the OSA and downloaded into Excel. The downloaded information was in the form of a two dimensional array, consisting of 800 points (wavelength vs. power).

The modelled erbium fluorescence response was convoluted with the reflection spectral profile of the sensor grating; thus giving the reflection from the sensing device (R_s). The profile of the sensor grating was then wavelength shifted by the appropriate

amount (1 pm for every microstrain applied) for each sample point. The erbium response, for each of these shifts, was convoluted with the sensor profile; thus giving a separate R_e for each stretch. A number of the modelled sensor reflections are plotted in figure 5.4.

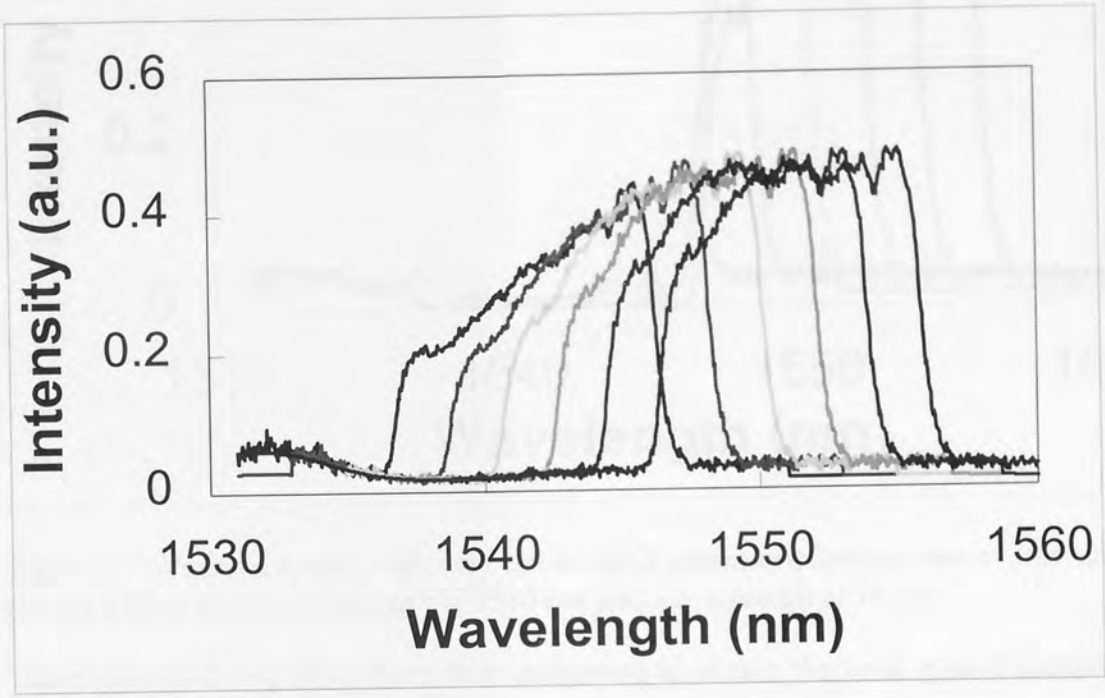

Figure 5.4: Modelled sensor reflection from a 10 nm chirped grating for varying strains.

The various R_e spectra clearly show the effect of the non-uniform erbium on the sensor's reasonably "top hat" profile. This non-uniform profile demonstrates itself in the reflection profile, which slopes up to the right. This slope is particularly noticeable in the first profile. As the grating is stretched its profile is linearly shifted. This shift moves the grating into a flatter region of the erbium fluorescence profile, hence the top of the grating response flattens out.

These shifted profiles were then convoluted with the transmission response of the reference grating. This gives the output from the IBCI sensor system for all the modelled strains. Some of the modelled output profiles are shown in figure 5.5.

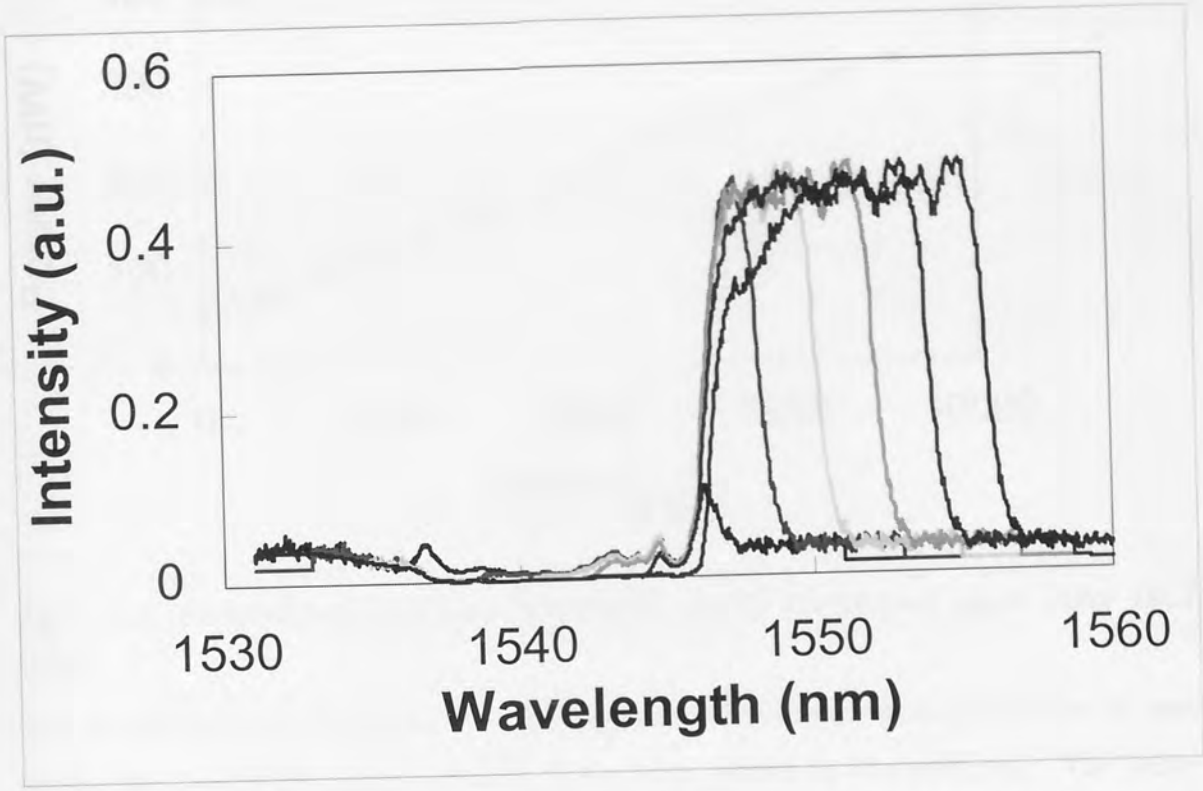

Figure 5.5: Modelled output response from an IBCI system employing a sensor and reference grating with a central wavelength of 1540 nm and a bandwidth of 10 nm.

These modelled responses were then integrated to obtain the total power output from the system for each applied strain. The modelled results are shown in figure 5.6. It is noted here that the measured power may be converted to an equivalent wavelength, i.e. the graph may be plotted as equivalent wavelength vs. strain. It is also noted that the photodiode measures the total output power from the system. Accurately the system is measuring power over a defined wavelength range. Therefore, a more accurate description would be that the photodiode is measuring power spectral density. However, a number of the results contained in this thesis have been published in international journals. The results presented here have been kept in their published format to maintain continuity and avoid ambiguity.

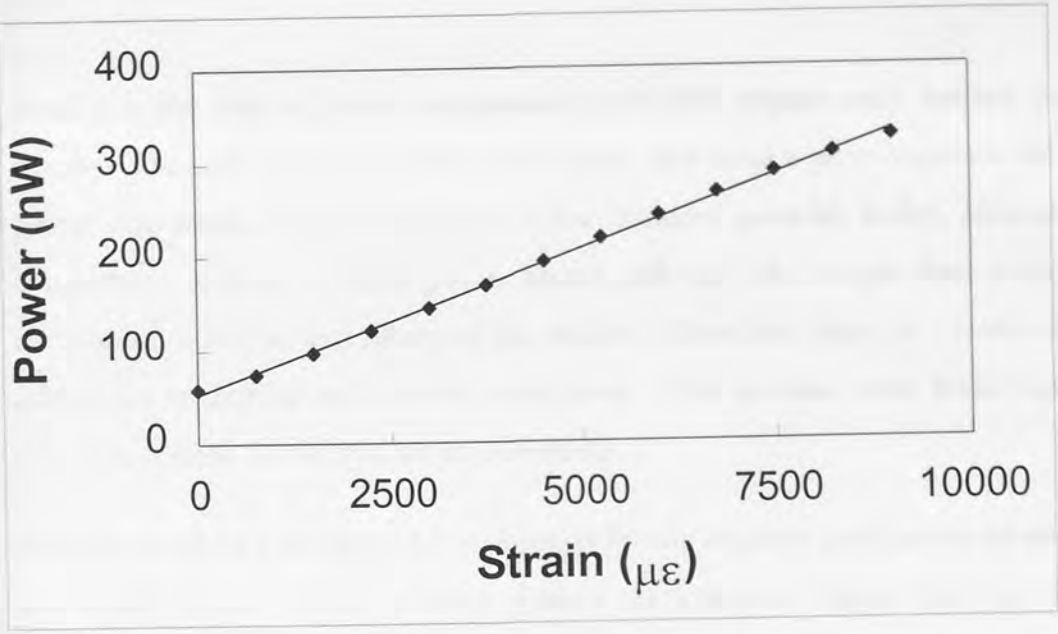

Figure 5.6: Modelled strain-to-power response for the 10 nm chirped single sensor IBCI system.

The model indicates a reasonably linear response. The small variations are due in part to the spectral profile of the erbium florescence, which is non-uniform. The other contributory factor is the non-ideal spectral profile of the grating; this would ideally be a top-hat function. However, a real grating has steep sloped edges rather than vertical ones. This results in reduced sensitivities at the points where the gratings nearly completely overlap and just before they are completely separate. Therefore, giving the curve a slightly S-shaped characteristic. The intensity offset is due to the non-100% reflectivity of the broadband reference grating and the slight difference between the two structures. The modelled linear fit has a gradient of 31 pW/με and an offset of 53 pW.

However, a cubic curve gives a better fit. The curve was determined to be:

$$PSD = -2 \times 10^{-10} \times S^3 + 2 \times 10^{-06} \times S^2 + 0.0234 \times S + 56.785 \qquad \textit{Equation 5.6}$$

where PSD is power spectral density and S is applied strain.

It is noted here that there is a trade off between the use of a cubic or linear strain extraction. The cubic equation gives a better fit and, hence, more accurate readings at the expense of adding complexity to the system. The linear fit results are within reasonable limits but not as accurate. However, if linear strain extraction is adopted, the system output is easily converted into strain by an electronic dividing circuit. Such a circuit is cheap (costing only a few pounds), fast (it can easily operate at 10 kHz),

small (i.e. the size of a few components parts that require only battery power) and simple. The cubic system, on the other hand, may need a pc to translate the measured power into strain. A pc is expensive (a few hundred pounds), bulky, adds unnecessary complexity, requires a mains power source and will take longer than a simple set of electronics to collect and interpret the results. Therefore, there is a trade off between achievable resolution and system complexity. The decision over which approach to take will depend on the system requirements.

The system shown in figure 5.1 was tested by the separate application of tensile strain and temperature. Both of these parameters induce a linear shift in the central wavelength of the spectral profile of the sensor grating. The sensor was prepared by stripping the fibre jacket over a 5 mm length at two points 20 cm apart with the grating centred in between the two. These two stripped sections were then glued to two steel grooved blocks and mounted onto the strain system described in the previous chapter. The reference grating was placed on the laboratory bench to ensure it was under no tension or compression. The sensor was then stretched in steps of 150 μm, up to 1 800 μm which corresponds to a strain of 9 mε (0.9%). The experiment was repeated several times. However, for clarity only the first set of results obtained are displayed in figure 5.7. A complete set of results obtained for a single experiment are shown in the next section.

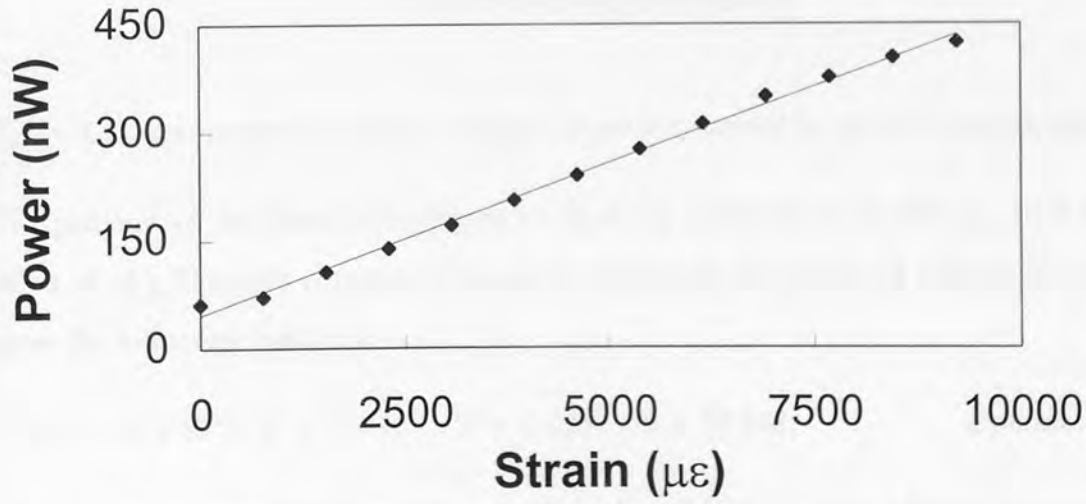

Figure 5.7: Measured strain-to-power response for the 10 nm chirped single sensor IBCI system.

(Errors in figure 5.7: ± 8 με for strain and ± 3 nW for power)

The above plot is reasonably linear with small variations as predicted by the model. These variations were investigated further by exchanging the photodiode for an optical spectrum analyser. Several plots were taken for different strains placed on the sensor, shown in figure 5.8. The unstrained sensor plots shows a small fraction of the light reflected from the grating being transmitted by the reference structure. The first strained result indicates the effect of the non-ideal profiles of the two gratings, i.e. the peak in this first plot is significantly smaller than the remainder. After these two results the rest demonstrate a linear increase in the transmitted light as registered by the photodiode. These spectra are similar to the modelled system output profiles shown in figure 5.6.

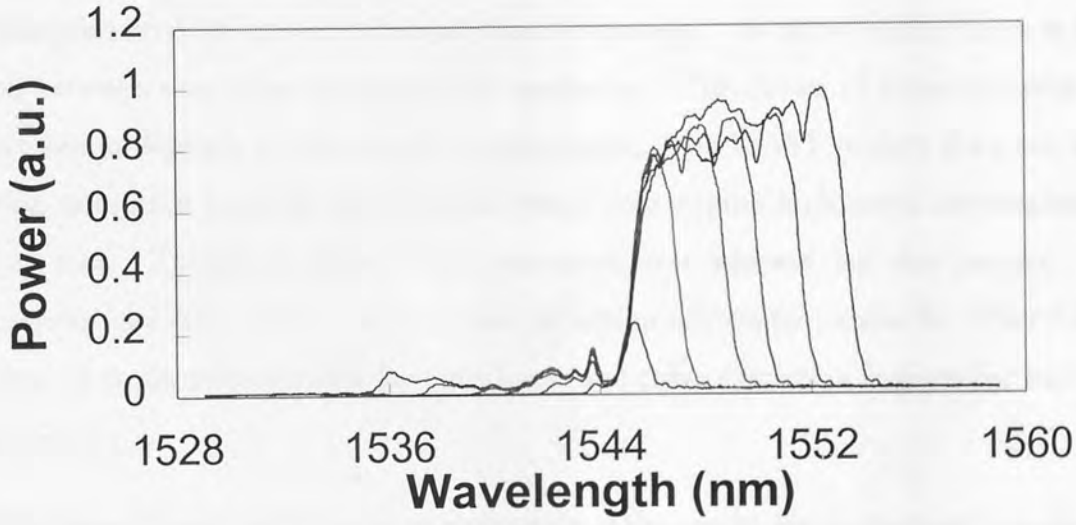

Figure 5.8: Light transmitted by the reference grating measured by optical spectrum analyser.

The gradient of the linear fit in figure 5.7 is of the order (42 ± 2) pW/με and it has an offset of 46 pW which compares reasonably well with the predicted values. A cubic fit gives the following function:

$$PSD = -4 \times 10^{-10} \times S^3 + 5 \times 10^{-6} \times S^2 + 0.0238 \times S + 57.548. \qquad \textit{Equation 5.7}$$

A comparison may be drawn between the achievable resolution offered by the cubic and linear fits by calculating the standard error between the value predicted by the fit

(x_f) and the actual measured value (x_m). This shall be taken as the standard error of the two values defined by:

$$\text{Error} = ((\text{SUM}((x_f - x_m)^2))^{1/2})/n \qquad \textit{Equation 5.8}$$

where n is the number of data points and sum indicates the summation of all the values in the range.

A linear fit for these results gives an error in strain measurement of 48 με, compared to 18 με for the cubic fit. As noted in the modelling section, the cubic fit gives considerable better results than the linear one. The adoption of a linear or cubic interpretation of the received power depends on the system requirements. The IBCI technique was originally developed for low resolution (~50 με), low cost (a few thousand pounds), high speed (>1 kHz) and simplicity. A system, which linearly interprets received power, offers all these advantages. As noted earlier there is a trade off between simplicity and achievable resolution. The choice of linear or cubic strain extraction depends on the system requirements. The MAST project does not require high resolution from the IBCI system, but it does require high speed interrogation at a low cost. Therefore, linear strain extraction was adopted for this project. Some projects may require the superior strain extraction offered by a cubic fit. Therefore, the error in strain measurement for both linear and cubic extraction is given for each set of results.

The linear fit may offer better interpretation if the results are normalised. As discussed earlier, part of the observed S shaped curve is contributable to the non-uniform profile of the erbium florescence light source. This can be minimised by normalising the results, i.e. dividing the system output by the sensor reflection.

The modelled results were normalised by dividing the output spectra by the appropriate sensor reflection profile. The resultant profile was then integrated to give the total system output power.

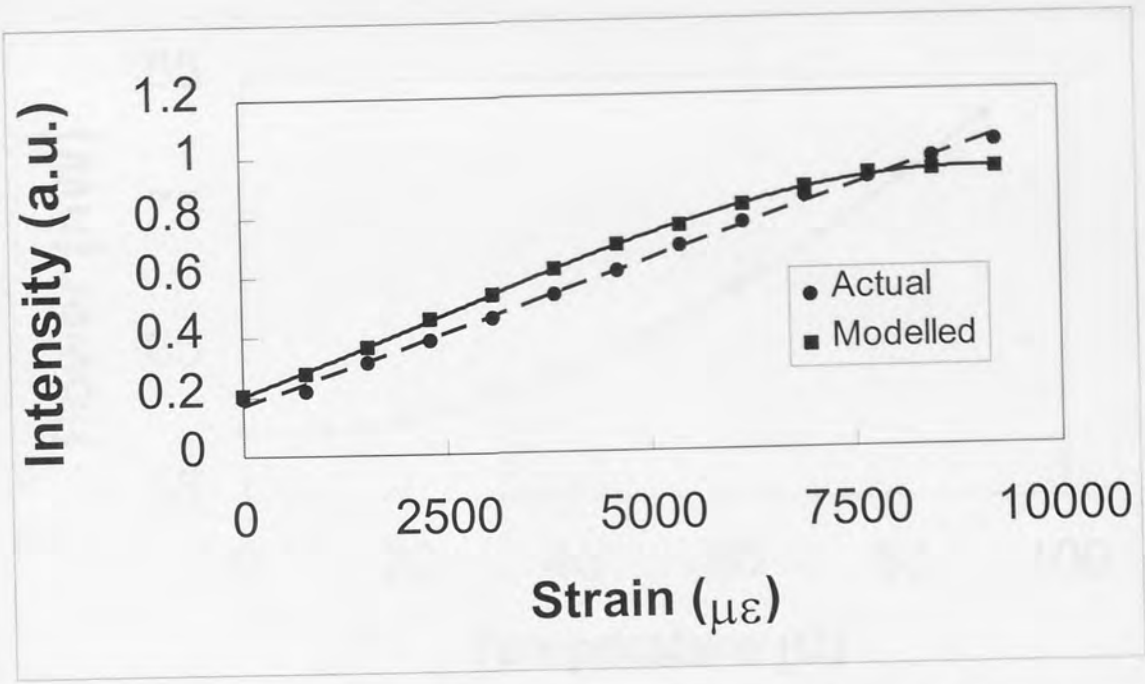

Figure 5.9: Normalised results for the 10 nm chirped single strain sensor IBCI system.

(Errors in figure 5.9: ± 8 με for strain and ± 0.007 for intensity).

The linear fit for the measured results had a gradient of $(95 \pm 5) \times 10^{-6}$ a.u./με, compared to a modelled response of 84×10^{-6} a.u./με. These results show a marked improvement in linearity; the linear error in strain measurement was determined to be 38 με. The cubic fit ($PSD = 6\times10^{-13}S^3 + 7\times10^{-9}S^2 + 7\times10^{-5}S + 0.1836$) is less appropriate with the normalised results; the cubic error in strain measurement for the normalised results was 24 με.

As discussed earlier, temperature also induces a linear shift in the spectral profile of a Bragg grating. The application of temperature, from 0 to 90°C, was modelled for the same experimental set up using the 10 nm bandwidth gratings. The modelling was done in the same way as that for the strain experiment, with the sensor profile being wavelength shifted by the appropriate amount (i.e. 13 pm for every degree Centigrade applied) for each sample point. The results from the modelling are shown in figure 5.10.

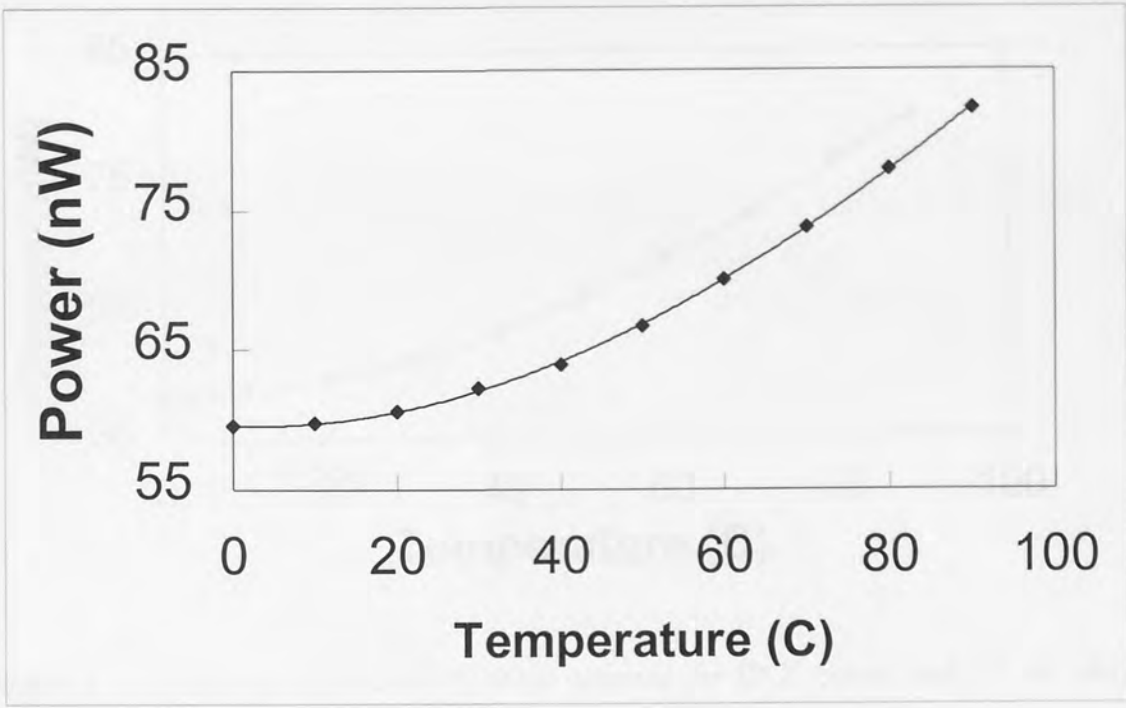

Figure 5.10: Modelled temperature-to-power response for IBCI system with 10 nm chirped gratings.

In this case the results clearly do not lend themselves to a linear fit. This is due to the fact that the overall sensor shift in Bragg wavelength is ~1/10 of that of the strain experiment. Therefore, the sloped, as opposed to the ideally vertical, edges of the grating's spectral response have a greater effect than in the strain experiment. A cubic fit gives the following function:

$$PSD = -7\times10^{-6}T^3 + 0.0036T^2 - 0.0209T + 59.584 \qquad \textit{Equation 5.9}$$

where T is the applied temperature.

To demonstrate the actual temperature resolution of this technique, the sensor was placed on a Peltier heat pump and, to ensure good thermal contact, covered with heat sink compound. The same heating arrangement discussed in the previous chapter was employed. The grating was then cooled to 0°C and heated, in steps of 10°C, up to 90°C. The heat pump was allowed to stabilise at its new temperature before data collection commenced. The results are shown in figure 5.11.

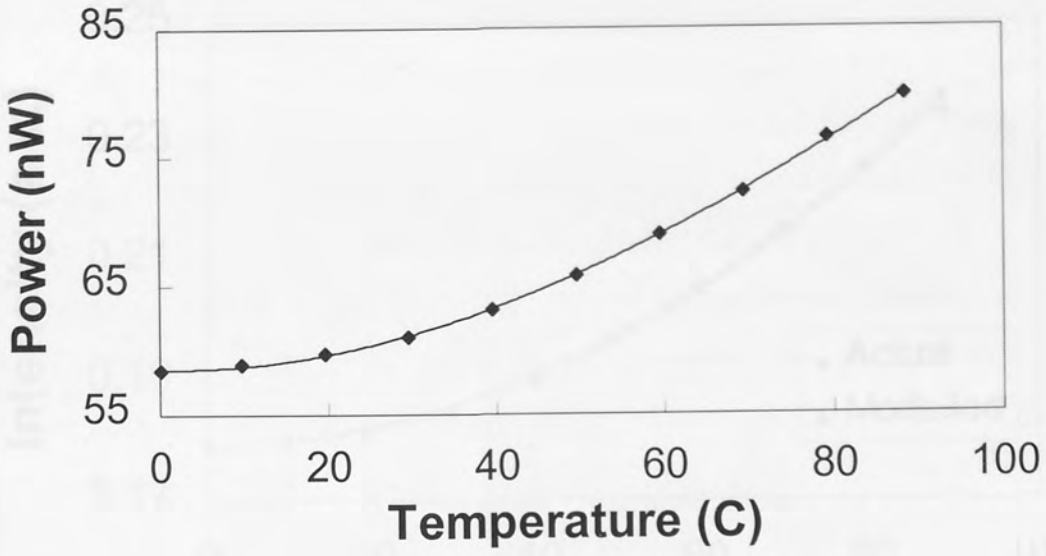

Figure 5.11: Measured temperature-to-power response for IBCI system with 10 nm chirped gratings.

(Errors in figure 5.11: ± 0.2°C for temperature and ± 0.3 nW for power).

The graph exhibits the predicted cubic response over the sensing range. A cubic fit gives the following function:

$$PSD = -9\times10^{-6}T^3 + 0.0037T^2 - 0.0153T + 58.571 \qquad \textit{Equation 5.10}$$

This result compares particularly well with the modelled response.

The error in temperature measurement for this fit was determined to be 0.45°C. This is achievable provided the photodiode employed has a resolution of at least 0.1 nW. Once again the results were normalised, using the same method as in the strain experiment. The normalised results are shown in figure 5.12.

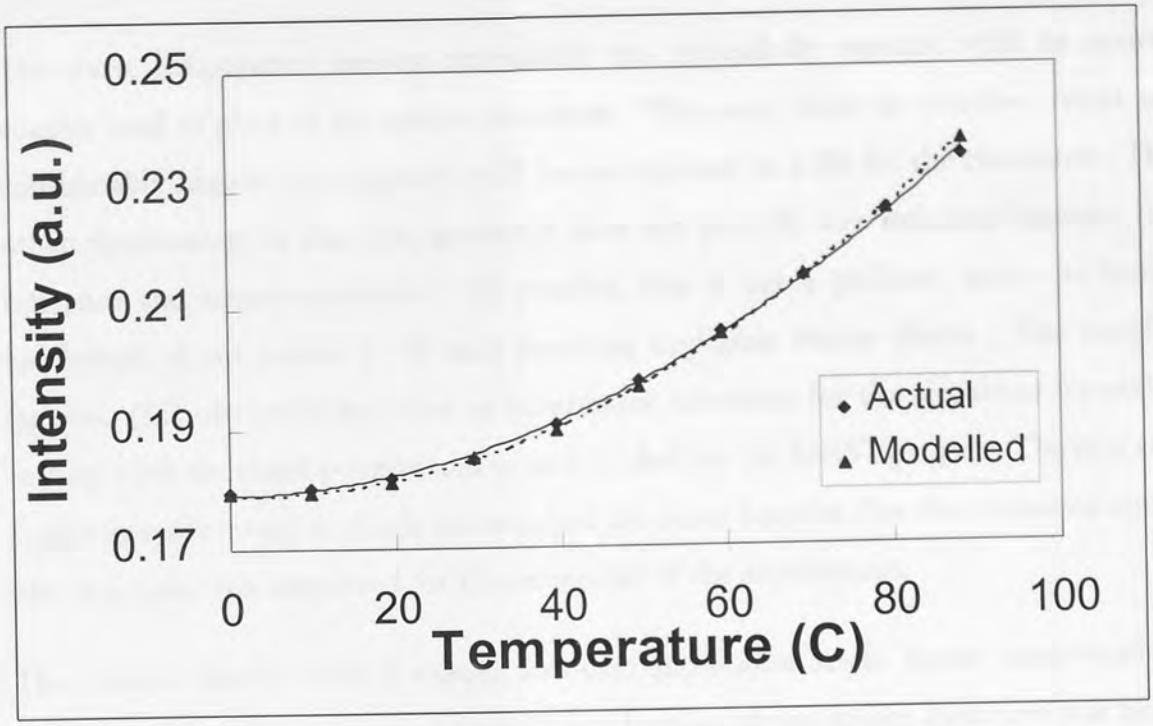

Figure 5.12: Normalised modelled and measured temperature-to-power response for IBCI system with 10 nm chirped gratings.

(Errors in figure 5.12: ± 0.2°C for temperature and ± 0.001 a.u. for intensity)

The modelled and the actual results are in good agreement with each other. The modelled response is:

$$PSD = -2\times10^{-8}T^3 + 1\times10^{-5}T^2 - 0.0001T + 0.1828 \qquad \textit{Equation 5.11}$$

which compares favourably with the determined experimental response of:

$$PSD = -3\times10^{-8}T^3 + 1\times10^{-5}T^2 - 0.0001T + 0.1798 \qquad \textit{Equation 5.12}$$

The error in temperature measurement for this normalised case was 0.25°C. It is noted here that this resolution is unlikely to be obtainable due to limits on the resolution of the photodiode. This resolution could be achieved if the photodiode had a resolution better than 0.04 nW. The resolution offered with this technique compares well with that achieved by Rao *et al*[13]. The group reported a resolution of ±0.2°C using a drift compensated Fabry-Perot filter to determine the Bragg wavelength of the grating sensor. A Fabry-Perot filter costs around five thousand pounds compared to few hundred pounds for two identical chirped gratings. The IBCI system is therefore an economical substitute for this system.

The above temperature sensing experiment was successfully repeated with an optical coupler used in place of the optical circulator. The losses from the coupler system are considerably higher. An effective 6 dB loss as opposed to 2 dB for the circulator. The other disadvantage is that this geometry does not provide any isolation between the reference and sensor structures. In practice, this is not a problem since the broad bandwidth of the source (~50 nm) produces negligible étalon effects. The coupler (approx. £60) obviously provides an economical substitute for the circulator (typically costing a few thousand pounds) and as such is ideal for the MAST project. The cost and availability advantage so much out-weighed the other benefits that the circulator could offer a coupler was employed for the remainder of the experiments.

This system clearly offers a simple, low-cost and robust strain sensor interrogation. However, it is uneconomical as a significant fraction of the source spectrum was being wasted. Therefore, the next stage in development was to wavelength division multiplex a number of sensors on a single line.

This system is intensity based, but due to its wavelength selective nature it does not suffer from the drawbacks of other intensity systems, i.e. it is the intensity over a specified wavelength range that is important not the overall intensity. Therefore, a multiplexed system is required to select the wavelength range of concern and reject all other wavelengths. This can be achieved with a Bragg grating. The schematic of a dual sensor interrogation scheme is shown in figure 5.13.

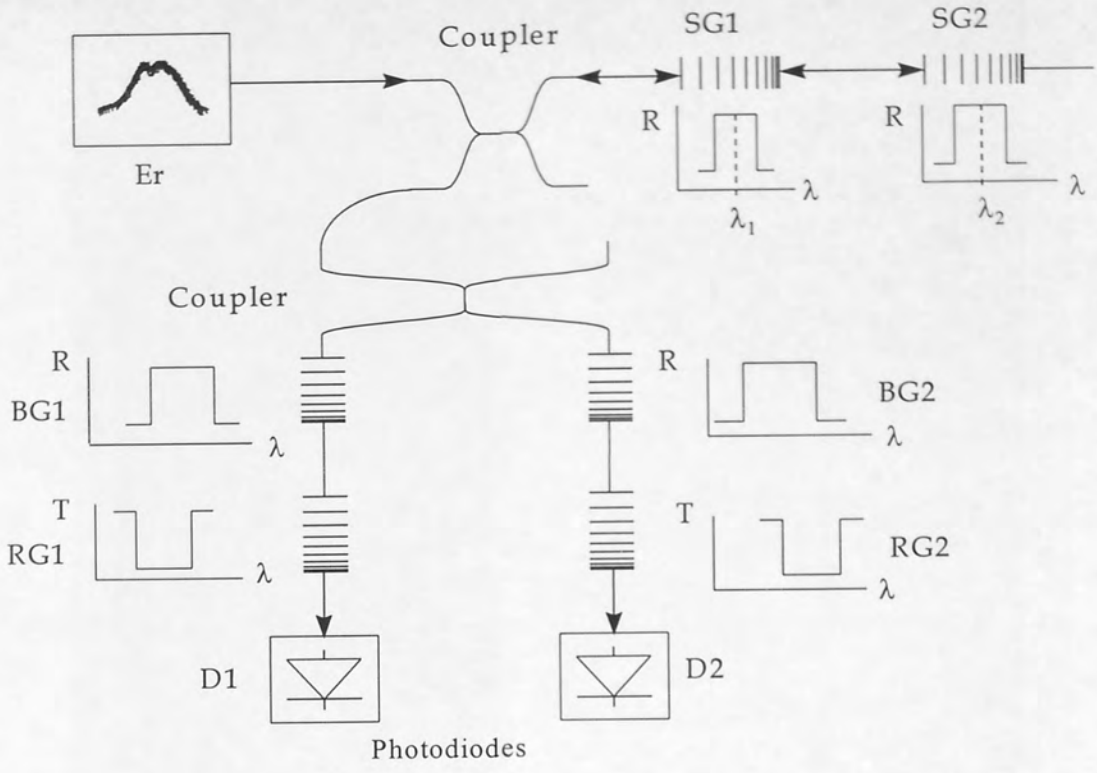

Figure 5.13: Schematic diagram of a twin sensor interrogation system.

This system is composed of two sets of identical gratings; the two sensors (SG1, SG2) and the two reference structures (RG1, RG2). Two broadband blocking structures (BG1, BG2) are used to reject the light from one of the sensors. This is achieved by writing the two blocking gratings with a sufficiently large bandwidth so as to cover the reflection spectrum of the sensor whether it is strained or not. The remainder of the system is made up from two 50:50 couplers, two photodiodes and an erbium fluorescence source.

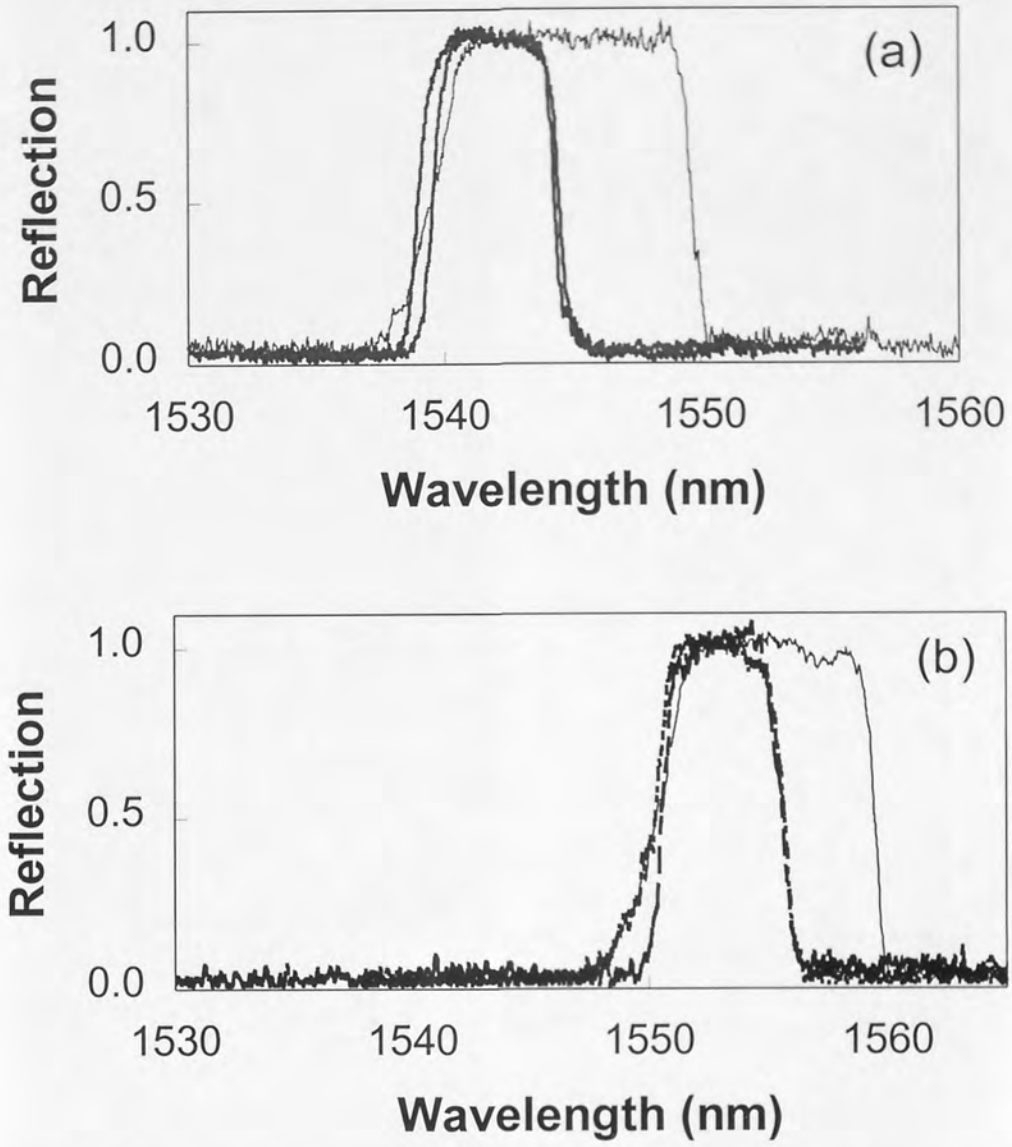

Figure 5.14. (a) Spectra of sensing, reference and blocking gratings SG1, RG1 and BG2. (b) Spectra of sensing, reference and blocking gratings SG2, RG2 and BG1.

The spectra of the gratings employed are shown in figure 5.14. All the gratings were written in hydrogenated, highly doped germanium and were 5 mm long. The two sensing gratings were written with central wavelengths of 1542.5 and 1552.5 nm and a 5 nm chirp. The strain sensitivity of a chirped FBG sensor inscribed in high doped germanium fibre is approximately 1 pm/με. These gratings will facilitate a sensing range of 4.5 mε. The application of 4.5 mε to sensor 1 will shift its spectral profile to 1544.5-1549.5 nm. If it is stretched any further its upper width half maximum (UWHM) will coincide with the lower width half maximum (LWHM) of the unstrained sensor 2.

The blocking or stopband gratings were required to have twice the bandwidth of the sensor and reference structures. For example, the shorter wavelength grating unstrained reflects light from 1550-1555 nm, whereas when strained 4.5 mε is applied to the structure its reflected range is 1545.5 -1559.5 nm. The two stopband gratings, BG1 and BG2 had a chirp of 10 nm and central wavelengths of 1545 and 1555 nm respectively. All gratings were written to saturation.

It is clear from the diagram that the interrogation system works exactly as it did in the single sensor case with the only difference being the stopband gratings. The stopband structures were written to limit the amount of cross-talk between the two sensors. Fibres contain insufficient photosensitivity to write 10 nm bandwidth gratings with 100% reflectivity. Hence, it is not possible to completely eliminate cross-talk between the two sensors.

As noted earlier, the side lobes of a grating's spectral response may also introduce cross-talk between the sensors. As with systems employing optical filtering, cross-talk, caused by side lobes, only occurs when the spectral response of the two sensors are in close proximity. In this case, cross-talk, caused by side lobes, will occur when the central wavelengths of the two gratings are less than 6.5 nm apart. It is therefore expected that the side lobes will contribute to the cross-talk in this experiment.

The modelling of this system was slightly more complicated than that of the single strain sensor. The reflection from SG1 was calculated and was then convoluted with the transmission profile of the reference grating RG1, i.e. in the same way the single strain sensor was modelled. This result was then convoluted with the transmission response of BG1. This final profile was integrated to give the total system output at D1. This process was repeated with the sensor profile being shifted, in steps of 250 με, up to 4.5 mε. Thus giving a complete set of power outputs corresponding to the various applied strains.

These modelled result, however, do not take into account the influence of SG2 on the output at D1. To determine this effect, the reflection profile from SG2 was calculated. This was then convoluted with the transmission profile of RG1 and BG1. This resultant profile was then integrated to give total power received at D1, due to the

reflection from sensor 2. As SG2 was not strained, this effect was constant and, therefore, the modelled power can just be added to the results determined for SG1. These results are shown with the experimental data in figure 5.15.

In this experiment, the fibre on either side of the first sensor (SG1) was stripped and then glued onto the two grooved blocks. These were mounted onto the displacement stage and the fixed stand mentioned earlier. The grating was then stretched in steps of 250 με, to 4.5 mε. The power at D1 was monitored and the results are shown in figure 5.15.

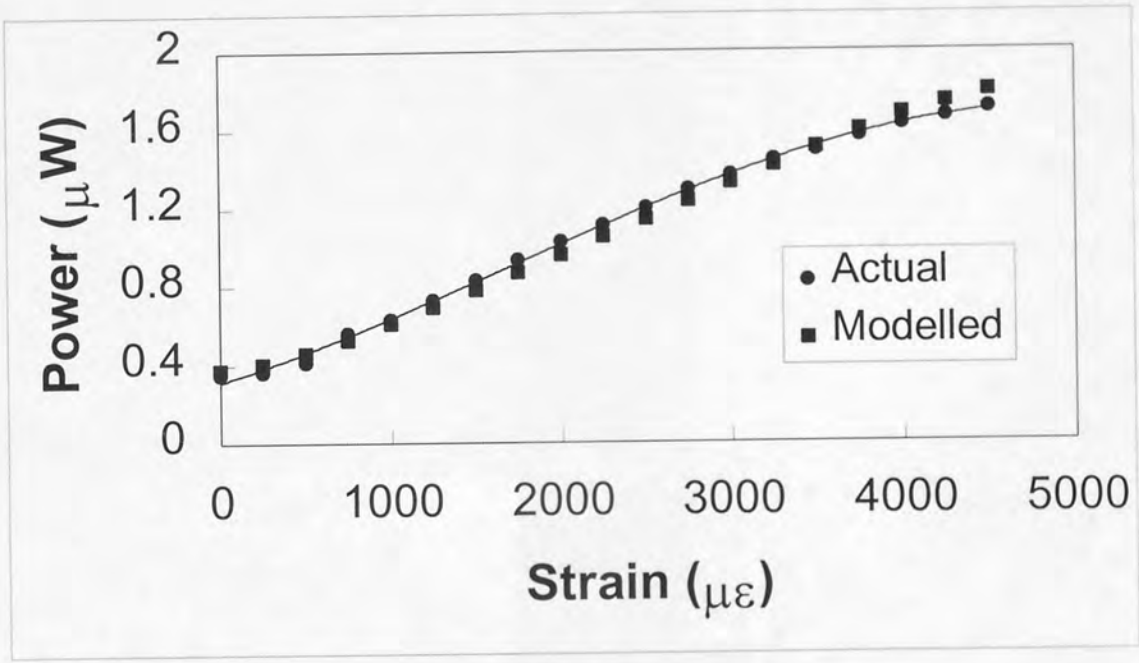

Figure 5.15: Modelled and measured strain-to-power response of sensing grating (SG1).

(Errors for experimental results in figure 5.15: ± 8 με for strain and ± 0.3 μW for power)

The familiar S shaped curve is still in evidence for the reasons discussed earlier. The strain response of the system with a linear fit was determined to be (0.336 ± 0.02) nW/με compared with a predicted response of 0.338 nW/με.

The response of this system is considerably higher than that of the single sensor. This is because a superior diode was employed to pump the erbium resulting in a more intense output. This difference presents a new problem as fluctuations in the source output power can result in erroneous strain measurements being recorded, e.g. an

increase in erbium fluorescence would incorrectly indicate that the sensors have been strained. This can be removed by normalising the results as they are taken.

A second arrangement, as shown in figure 5.16, was devised so that the results could be normalised as they were taken:

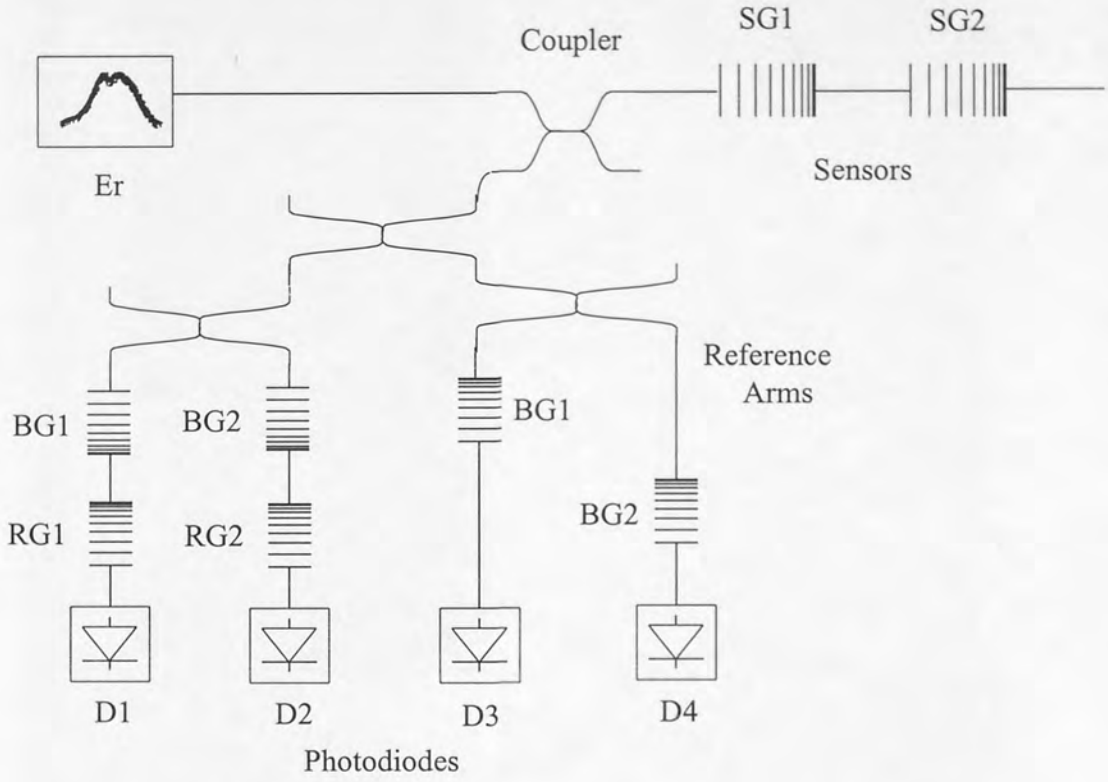

Figure 5.16: Experimental arrangement for normalised twin sensor interrogation.

This arrangement is identical to that in figure 5.13, except for the addition of two reference arms. These reference arms contain structures identical to the blocking gratings in the interrogation arms. The normalised output from such a system for sensor SG1 is D1/D3 and for SG2 is D2/D4. This output is insensitive to power and other such fluctuations as these are referenced out.

The normalised response from SG1 was modelled by dividing the system output, previously determined, by the power reflected by sensor 1. It was also decided to model the system output at D2, i.e. the response from the unstrained sensor, SG2. As previously mentioned, the blocking gratings do not have 100% reflectivity, hence there

will be some cross-talk. An indication of this cross-talk can be obtained by modelling the output at D2. The output at D2 was determined by:

1) Convoluting the various strain reflections from SG1 with the spectral profiles of RG2 and BG2;

2) Integrating the spectral profile determined in 1, to calculate the power received, due to sensor 1, at D2.

3) Convoluting the reflection profile from SG2 with the spectral profiles of RG2 and BG2;

4) Integrating the spectral profile determined in 3, to give the power received at D2, due to sensor 2;

5) By summing the powers calculated in 2 with the power modelled in 4 the total output at D2 is determined;

The modelling results are shown in figure 5.17.

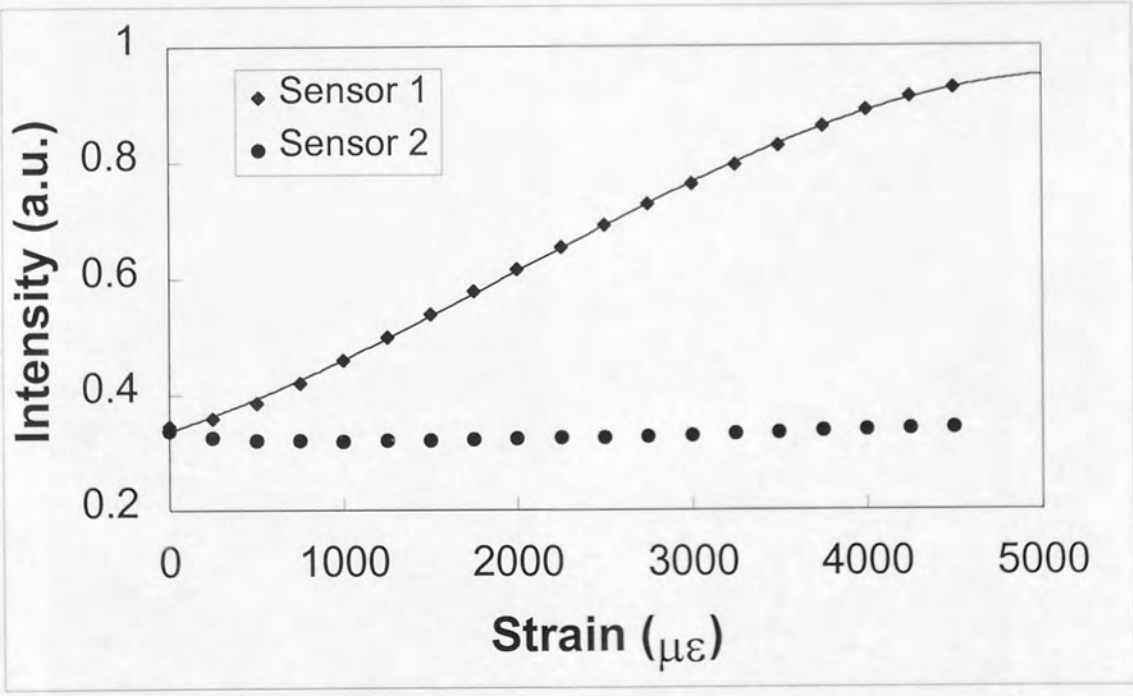

Figure 5.17: Modelled strain-to-power response for multiplexed strain sensor gratings, sensor 1and sensor 2.

The model predicts a cubic response for sensor one. It also predicts that sensor 2 will be effected by strain being placed on sensor one, i.e. there is some cross-talk between the two elements, as expected.

The experiment was set up, as shown in figure 5.16, with the same gratings used in the previous arrangement. All couplers were 50:50 and the photodiodes were connected to Anritsu power meters. The power meters were set to have a measurement wavelength of 1550 nm.

As in the previous experiment, the SG1 structure was glued onto the displacement and fixed stages. The sensor was then stretched in steps of 250 με up to 4 250 με. At each sample point readings were taken from D1 and D3 and put into Excel. These values were then divided and the result was plotted against strain, see figure 5.18.

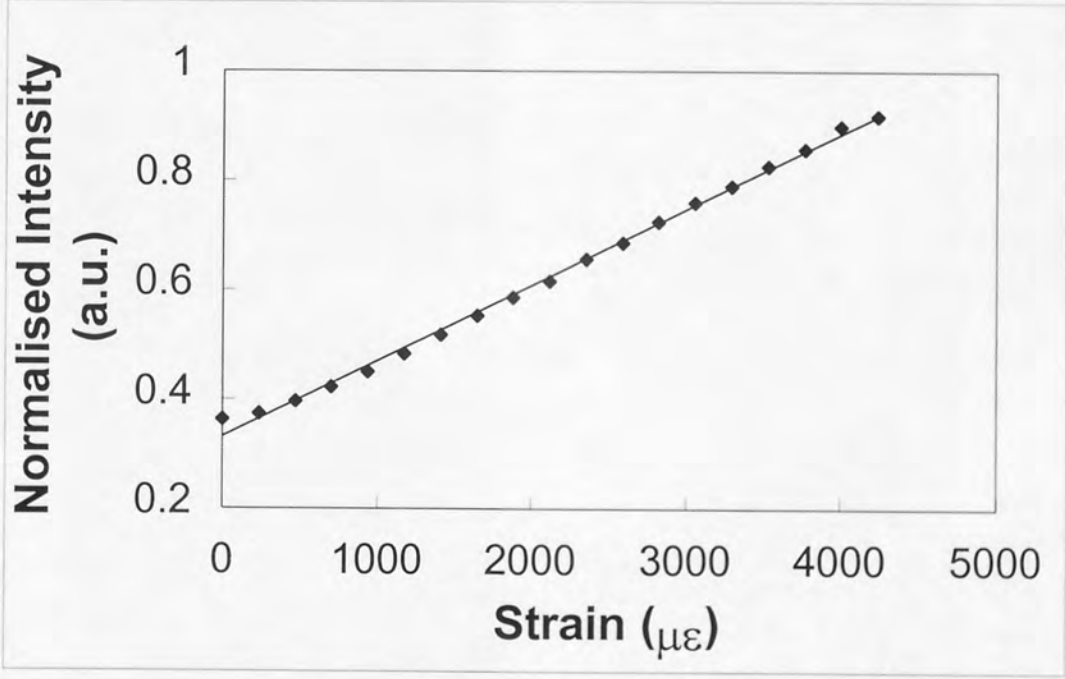

Figure 5.18: Normalise strain-to-power response for multiplexed strain sensor grating SG1.

(Errors in figure 5.18: ± 8 με for strain and 0.3 a.u. for normalised power)

A linear fit gives a sensitivity of (140 ± 8) × 10^{-6} a.u./με with an error in strain measurement of 20 με. Cubic strain extraction improves the error in strain measurement to 10 με.

A measurement of cross-talk is the difference between the readings at sensor 2 when (i) sensor 1 is unstrained and (ii) sensor 1 is strained to its measurement limit, i.e. 4 250 με. If no cross-talk occurs then sensor 2 would read 0 με in both cases. The cross-talk between the two sensors was determined, for this system, to be 19 με . Therefore, an error in strain measurement of 20 με indicated by the linear fit plus the determined cross-talk, gives a total system error of 28 με. This value is acceptable for the MAST project, which requires a maximum error in strain of 50 με.

This low-cost strain sensor interrogation system offers acceptable resolution. The presented system contains no active parts, except the light source, and is robust and rugged. The fact that the system is not scanned, as in the case of tuneable filters, results in a much faster interrogation system. The only limit placed on such a system is the speed that data can be collected from the photodiodes and processed. Hence, interrogation rates of a few kHz are easily achievable. This system is also capable of the truly simultaneous interrogation of multiple sensors. All these points make the IBCI system ideal for application in the MAST project. It is may also find application in strain monitoring in other SMART structures were high resolution is not required.

The MAST project's interrogation system was specified as operating in the 1.3 μm window. This window was chosen primarily due to the comparative cheapness of the components (e.g. a few hundred pounds for a 1300 nm diode compared to £5 000 for an erbium source). Therefore, the next step was to prove the reliability and workability of such a system at these shorter wavelengths.

5.3.2 1.3 μm applications

The first step was to prove that the single sensor system would operate with a 50:50 coupler in the 1.3 μm region. This experiment was also to give an indication of the achievable resolution with and without a reference arm. The reference arm gives, as has been demonstrated, improved results. However, more components, parts and processing are required. Therefore, it would be advantageous for a system to be developed in the 1.3 μm range that did not require a reference arm.

This possibility was examined by the implementation of the system in figure 5.19.

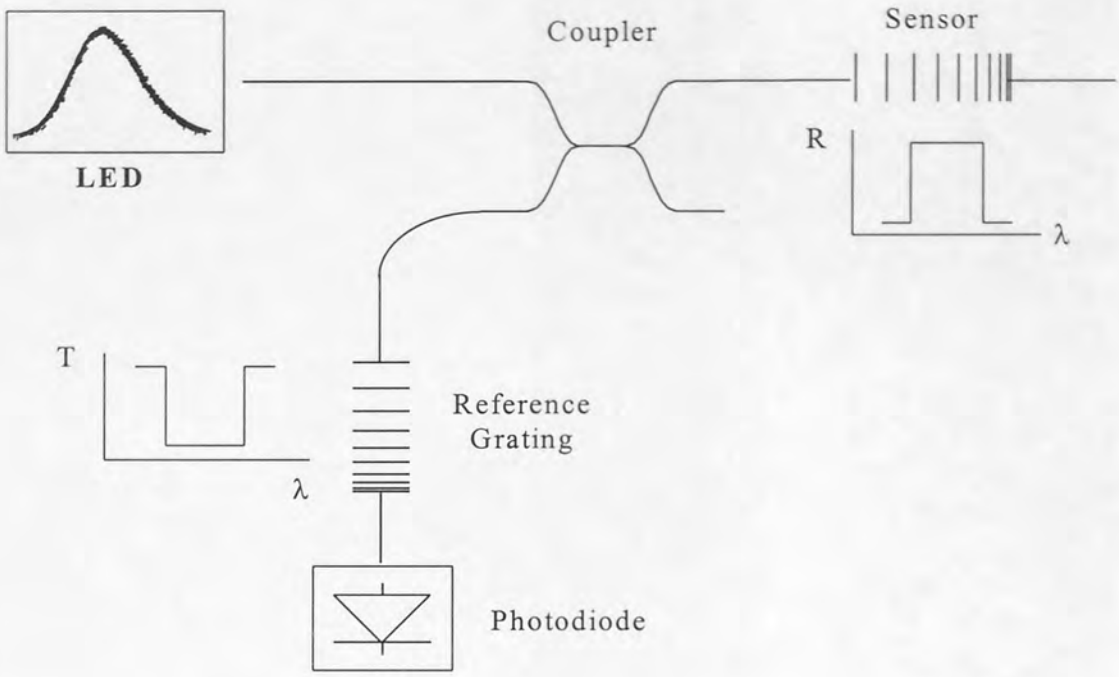

Figure 5.19: Basic experimental arrangement for IBCI system operating in the 1.3μm window.

The above system consists of a coupler, a photodiode and an LED. Two identical gratings were specifically written for application in this experiment. This system is cheaper than those investigated previously since a 1300 nm LED is significantly less expensive than an erbium fluorescence source. An erbium source requires a pump diode, which needs an expensive current driver and temperature controller. It also requires a length of expensive erbium and a WDM device. In comparison, an LED only requires a current driver and a temperature controller. It is also significantly cheaper while delivering more power. It has the advantage of a more regular spectral profile than erbium fluorescence, i.e. it is closer to the desirable top-hat function than the 1.5 μm source.

The reflection spectra of the two-near identical gratings are shown in figure 5.20. They both had a central wavelength of 1292 nm and a bandwidth of 8 nm. The structures were written into boron/germania co-doped fibre, which had been hydrogen-loaded at 150 atmospheres pressure at room temperature for one week prior to exposure.

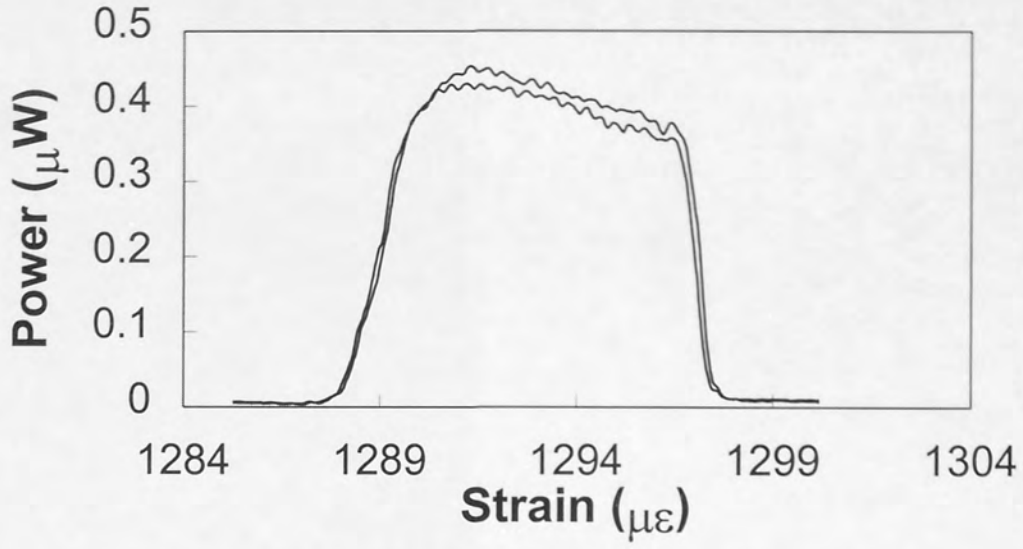

Figure 5.20: Reflection spectra of gratings employed in single sensor 1.3 μm IBCI system.

Once again the system response was modelled to observe how a change in source and wavelength window would affect the results. The LED response was modelled in Excel and convoluted with the reflection profile of the sensor grating to obtain the reflection from the sensing device (R_s). The profile of the sensor grating was wavelength shifted by the appropriate amount (1 pm for every microstrain applied) for each sample point. The profile, for each of these shifts, was convoluted with the LED spectral response; thus giving a separate R_s for each stretch. A number of the modelled reflections from the sensor are plotted in figure 5.21.

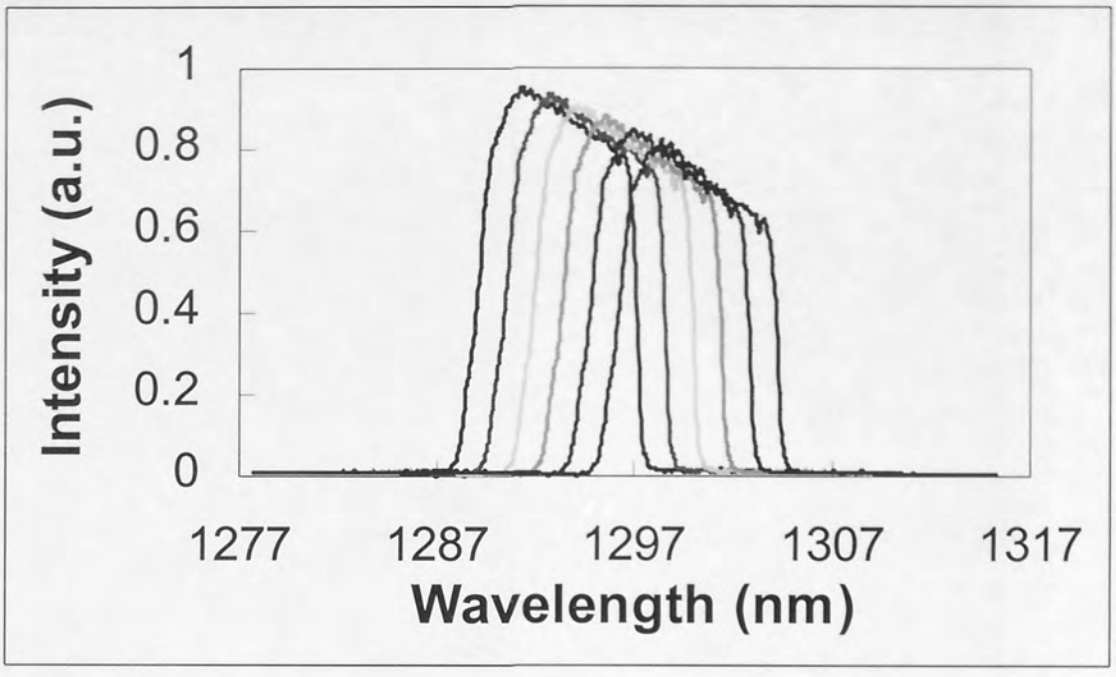

Figure 5.21: Modelled reflection from a 8 nm chirped grating for various applied strains.

These shifted profiles were then convoluted with the transmission response of the reference grating. This gives the output from the IBCI sensor system for all modelled strains, see figure 5.22.

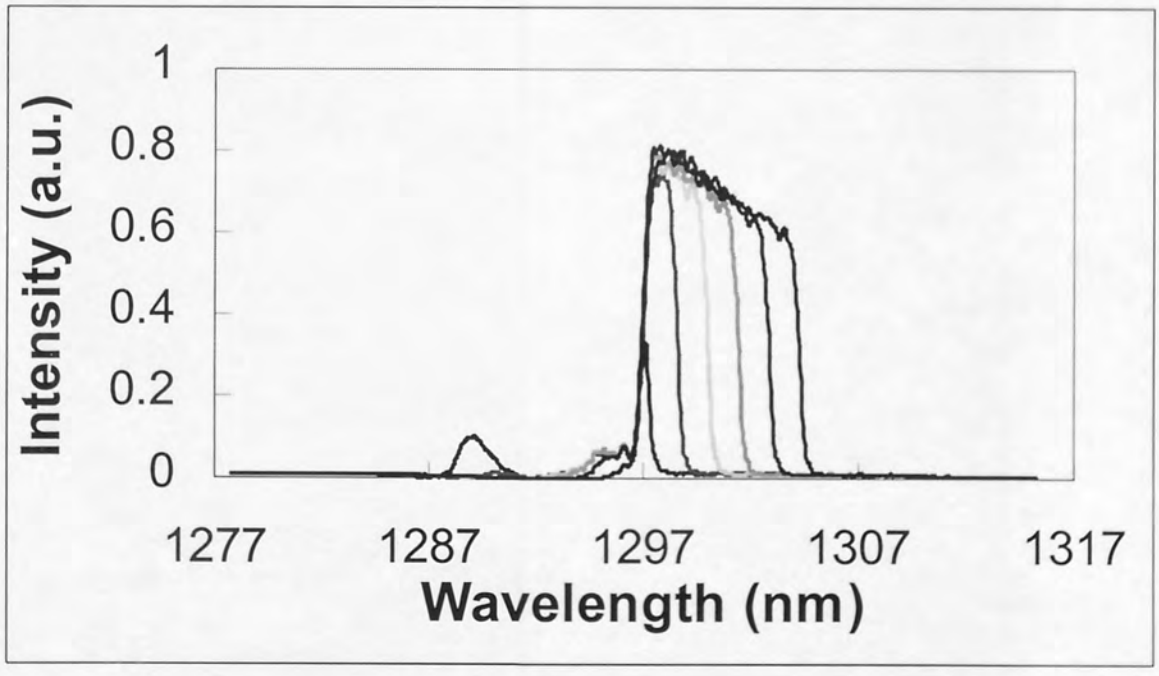

Figure 5.22: Modelled output response from an IBCI system employing a sensor and reference grating with a central wavelength of 1292 nm and a bandwidth of 8 nm.

These modelled responses were then integrated to obtain the total power output from the system for each applied strain. These results are shown in figure 5.23.

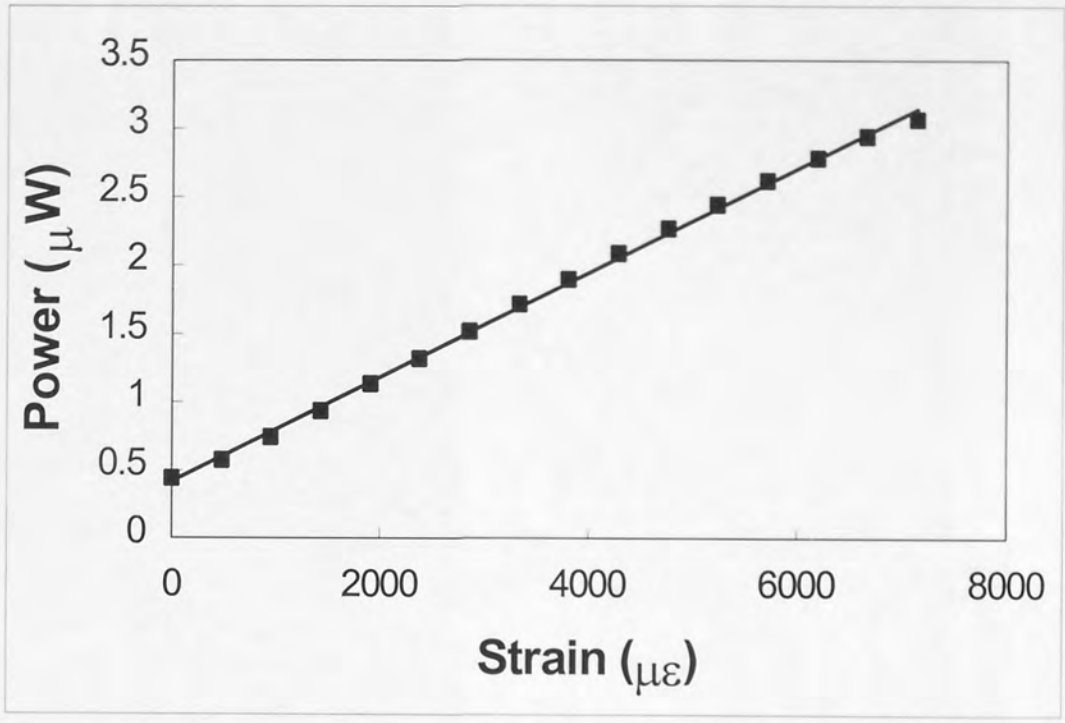

Figure 5.23: Modelled strain response for an ICBI system using two 8-nm chirped gratings in the 1.3 μm window.

The model predicts a linear response, with a gradient of 0.382 nW/με. A slight S curve is once again in evidence for the reasons discussed previously.

The sensor grating was prepared and bonded to the metal blocks before being attached to the displacement stage and load cell. The sensor was stretched in steps of 475 με up to 7 125 με. At each sample point the power was recorded from the Anritsu power meter which was connected to the photodiode. The power meter was set at a wavelength of 1300 nm. Three sets of results were then taken and are displayed in figure 5.24. The results from the load cell are also plotted. A near linear response from this indicates that no slippage occurred.

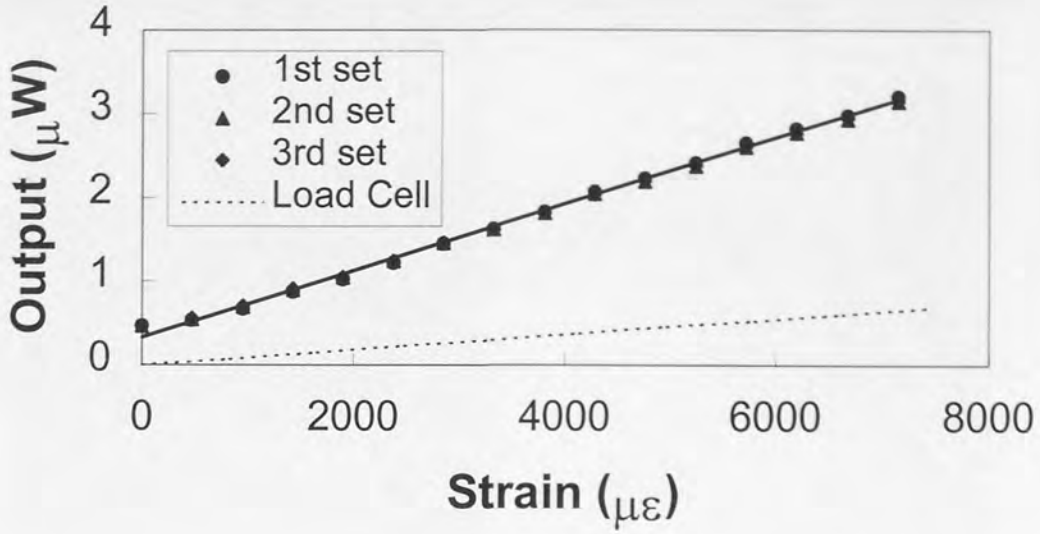

Figure 5.24:Strain encoded response measured from an ICBI system using two 8-nm chirped gratings in the 1.3 μm window.

(Errors in figure 5.24: ± 6 με for strain and ± 20 nW for power).

The sensor results, as predicted, exhibit a good linearity over the entire sensing range. The three sets of results shown are extremely close together. This indicates that the system gives excellent reproducibility, which is vital in its application in SMART structures. The initial intensity offset is due to the fact that the gratings do not have 100% reflectivity. The strain response achieved by this non-normalised system was (0.4±0.02) nW/με over a sensing range of 7.5 mε. The standard error for this system was calculated to be 0.05 nW. This corresponds to an error in strain of less than 1 με. However, the resolution of such a system could not exceed the resolution of the photodiode. Cubic strain extraction offers approximately the same error in strain measurement and gives no advantage over a linear interpretation of the results.

The resolution for this system is significantly better than that achieved at 1.5 μm. This is due to a number of reasons: (i) the LED spectral profile is closer to the ideal top hat function than the erbium fluorescence; (ii) the LED has a higher intensity output than the erbium hence increasing the signal-to-noise ratio of the system; and (iii) the photodiodes employed had a more linear response in the 1.3 μm region.

The accuracy of this method is reliant on the constant output of the LED and losses in the system. It is not possible to guarantee this especially on a yacht. This problem can

be reduced by normalising the output from the system. The normalised output from the system is shown in figure 5.25 along with the normalised modelled results.

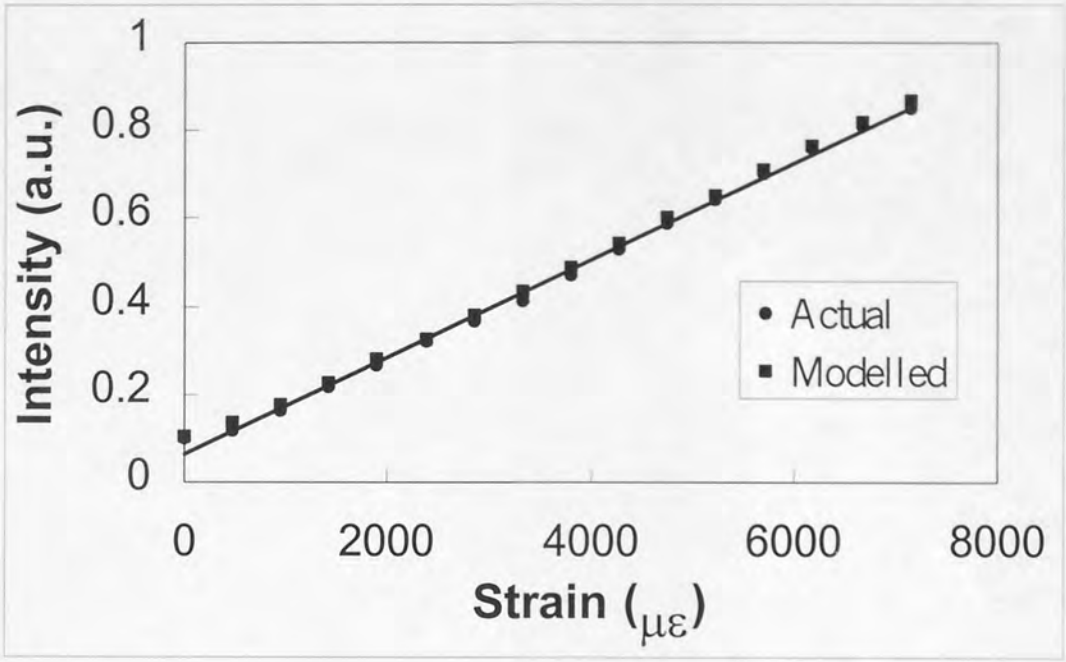

Figure 5.25: Normalised strain encoded response measured from an ICBI system using two 8-nm chirped gratings in the 1.3 μm window.

(Errors for experimental results in figure 5.25: ± 6 με for strain and ± 0.015 a.u. for intensity).

The modelled and actual results are in excellent agreement. The gradient of the linear fit for the experimental results was $(110 \pm 6) \times 10^{-6}$ a.u./με, which agrees with the modelled response of 110×10^{-6} a.u./με. The resolution, using linear strain extraction, was determined to be 40 με, as opposed to 11 με for a cubic fit.

The MAST project required very large range strain sensors from 1.5% compression to 1.5% tensile strain, i.e. a sensing range of 30 mε. This would require a sensor and reference grating with a bandwidth of 30 nm. These can be written using the holographic technique and 30 nm chirped phase masks are now commercially available. It is also possible to order such gratings from a number of commercial suppliers.

Two gratings 5 mm long were written, using the techniques mentioned earlier, into boron/germania co-doped fibre. Both gratings were written to saturation and had central wavelengths and bandwidths of 1283 nm and 30 nm respectively. The

transmission profile of one of these gratings and the emission spectra of the 1300 nm LED are shown in fig. 5.26.

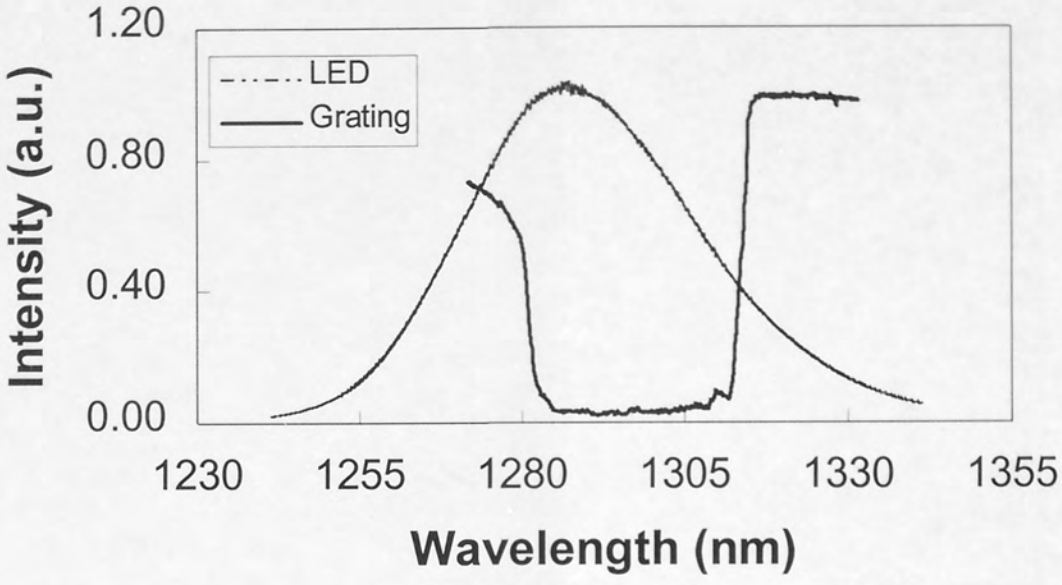

Figure 5.26: Transmission spectrum of a 30 nm grating and the spectral profile of a 1300 nm LED.

These gratings were employed in the sensor interrogation arrangement shown in figure 5.27.

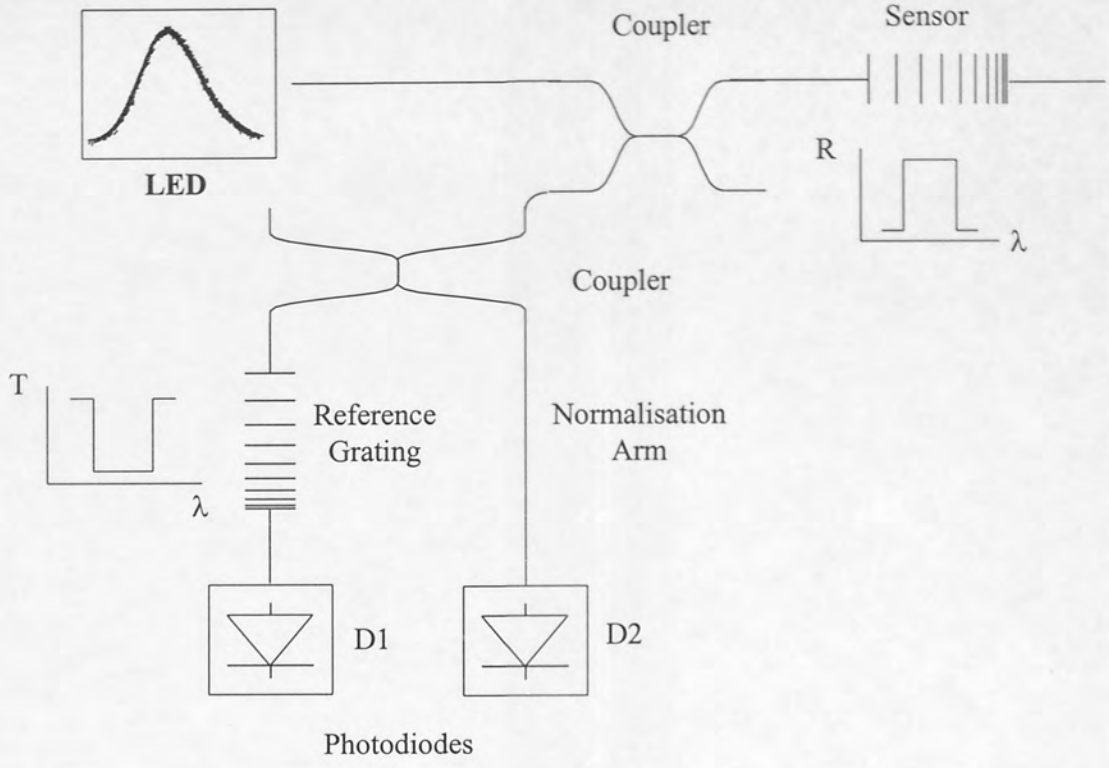

Figure 5.27: IBCI normalised arrangement for interrogation of a 30 nm sensor grating in the 1.3 μm window.

There was not an in-house capability to compress a grating. However, to demonstrate a large sensing range the sensor was to be stretched to 20 mε in steps of 1.1 mε. Unfortunately, the grating did not survive beyond ~12 mε. Such a large sensing range would be obtainable if the grating was suitably coated. The results obtained up to 11 mε are shown in fig 5.28.

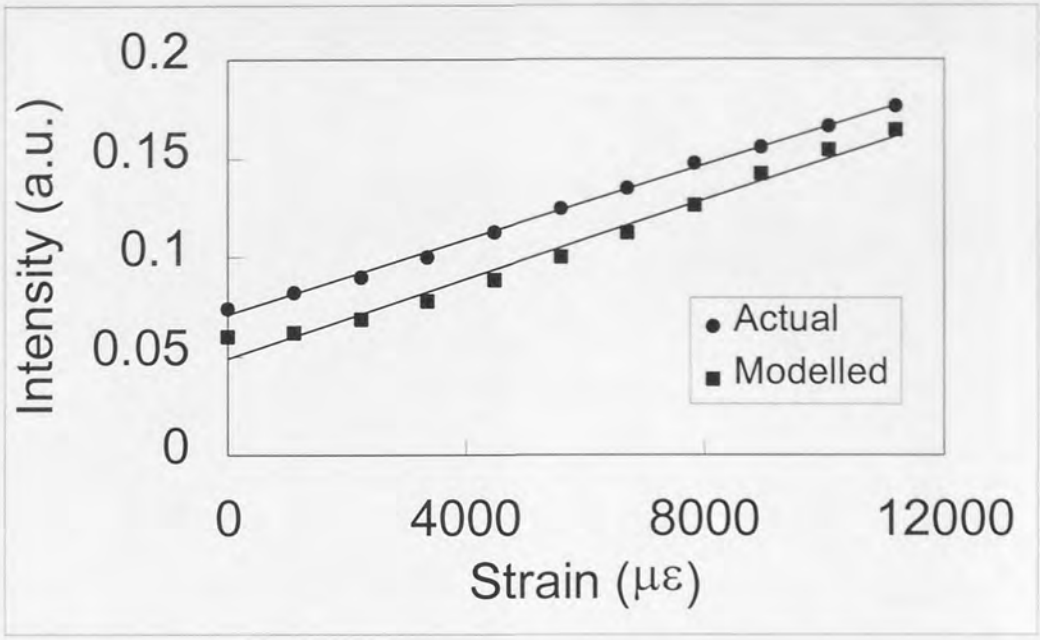

Figure 5.28: Modelled and measured strain encoded power response from an IBCI system employing a 30 nm FBG sensor.

(Errors for experimental results in figure 5.28: ± 30 με for strain and ± 0.002 a.u. for intensity)

The linear strain response of the system was determined to be $(9.5 \pm 0.5) \times 10^{-6}$ a.u./με (1.0×10^{-6} a.u/με modelled response). This response is less than that indicated by previous experiments because it has a much larger sensing range (this effect is discussed later on). The decreased response is also due, in part, to the spectral profile of the LED, shown in figure 5.15. The grating, as it is stretched, is shifted from the peak of the LED response, i.e. less light is reflected by the FBG sensor. Therefore, even when the profiles of the gratings are completely separate the normalised response will not be the expected one, but will be considerably less. This problem can be remedied by writing the identical gratings at a longer wavelength so the sensor grating is shifted towards the LEDs central wavelength rather than away from it. The next IBCI system to be discussed employs a sensor inscribed at a longer wavelength.

The standard error of the system was calculated to be 0.00049 a.u., which gives a strain resolution of 50 με (30 με using cubic strain extraction). This resolution can be improved by writing the gratings at a longer wavelength, hence, as discussed earlier, increasing the strain response of the system. However, the resolution offered by linear

strain extraction was deemed sufficient for the MAST project and this system was adopted and has been installed in the masts of several yachts.

The final step in this research was to demonstrate a multiplexed version of this system operating in the 1.3 μm window to see how it contrasts to the earlier system. A possible four sensor system which involves wavelength and spatial multiplexing is shown in figure 5.29. The dotted region shows a possible configuration that was not implemented in the experiment.

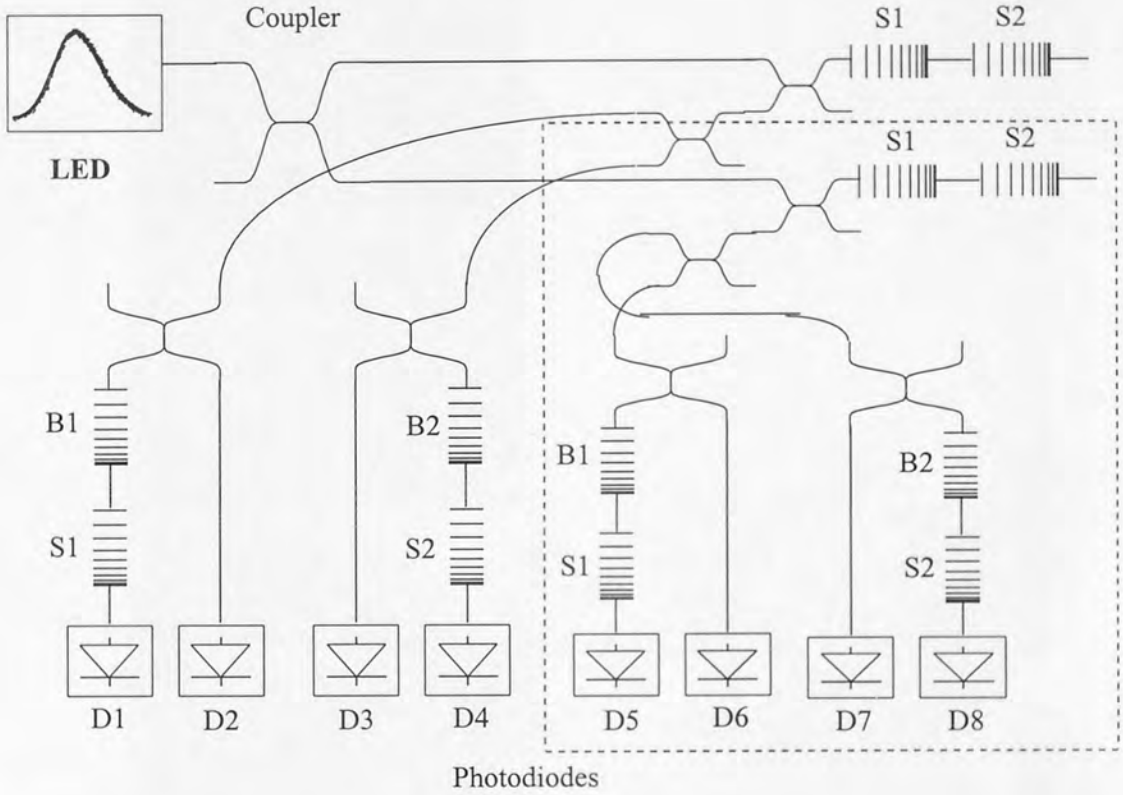

Figure 5.29: An IBCI wavelength and spatial multiplexing arrangement for the interrogation of four sensors.

The above system consists of the now familiar arrangement of light source, couplers, photodiodes and matching sets of gratings. The identical sensor and reference gratings pairs (S1, S2) were written with bandwidths of 6 nm and had central wavelengths of 1278 and 1296 nm respectively. The blocking gratings (B1, B2) both had bandwidths of 12 nm and had central wavelengths of 1300 and 1281 nm respectively. All the gratings were written to saturation in boron-germania co-doped fibre and were approximately 5 mm long. The profiles of the gratings employed are shown in figure 5.30.

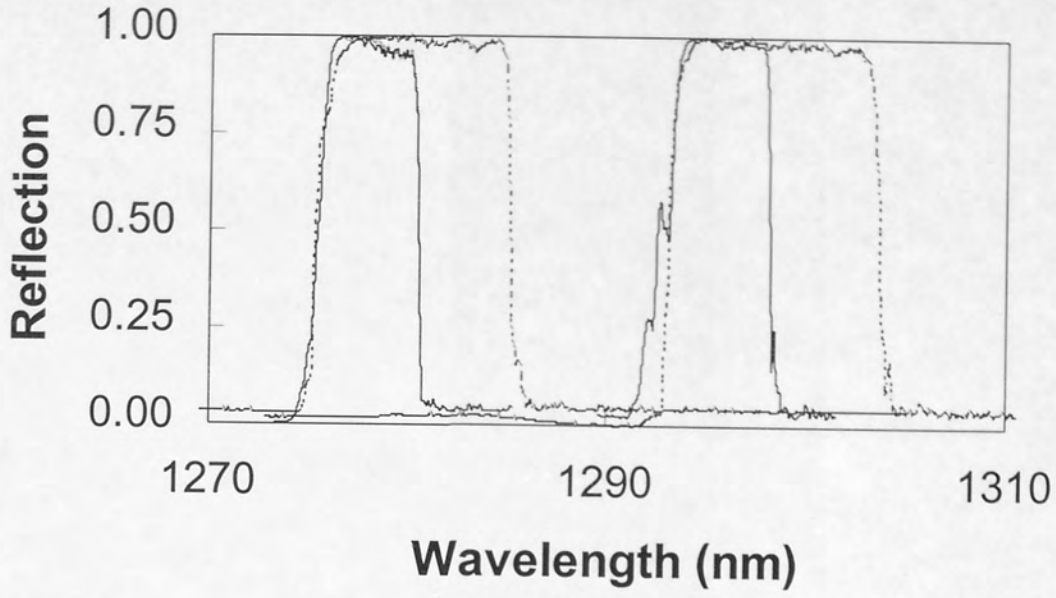

Figure 5.30: Blocking, reference and sensor grating spectra employed in twin sensor WDM IBCI system.

The system response was modelled, using the same method as in the previous 1550 nm dual sensor case. The output from both sensors was modelled with sensor 2 again remaining unstrained. The modelled results are shown in figure 5.31.

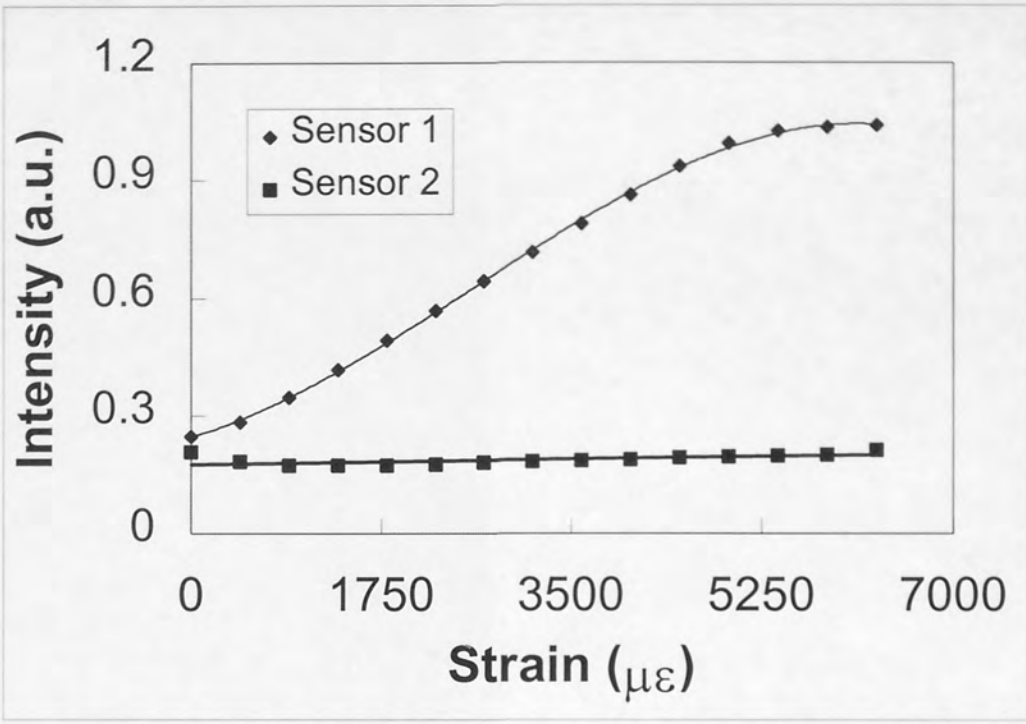

Figure 5.31: Modelled strain encoded light intensity for two sensors in a multiplexing ICBI system.

A linear fit to the modelled results gives a strain response of 140 × 10^{-6} a.u./με. However, a cubic fit, as shown in figure 5.31, is more appropriate to this set of modelled results.

The 1278 nm sensor grating was prepared and attached to the displacement stage and load cell. It was stretched in steps of 450 με up to 6.3 mε. The second sensor was left unstrained. At each sample point, a reading was taken from the two dual head Amartisu power meters for each of the four photodiodes. The results were recorded in Excel and the values of D1/D2 and D4/D3 were calculated and plotted against strain, see figure 5.32.

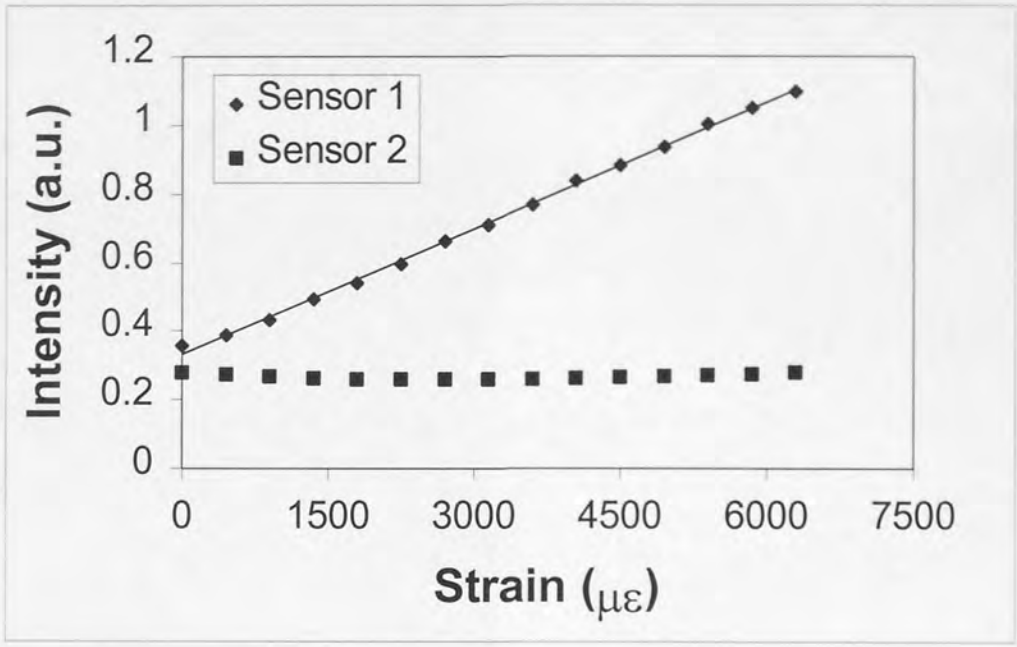

Figure 5.32: Experimentally measured strain encoded light intensity resulting from a multiplexing ICBI system.

(Errors in figure 5.32: ± 8 με for strain and ± 0.005 a.u. for intensity)

The dotted line showing the read-out voltage from the load cell indicates a linear increase in the tension on the sensor. The response from the strained sensor was highly linear and determined to be $(122 \pm 6) \times 10^{-6}$ a.u./με. The standard error in the predicted output was 0.0035 which corresponds to an error in the strain of about 18 με (11 με for a cubic fit). Therefore, the achievable resolution using linear strain extraction is about 20 με, i.e. the same as that for two sensors in the 1.5 μm window.

The normalised output is greater than the expected one as the strained sensor is moving towards the central wavelength of the LED output. Hence, the more the grating is strained the greater the intensity of light reflected which results in a better strain response than expected. The second line shows the response from the other unstrained structure. This is reasonably flat and demonstrates that there was little cross-talk between the two sensors. Some cross-talk is anticipated as the blocking gratings do not have reflectivities of 100%. The cross-talk for this system was determined to be 7 με. This is far less than the 1550 nm dual sensor system because of the spacing of the grating's spectral response. When sensor 1 is fully stretched its LWHM and UWHMs are shifted to 1281 and 1287 nm respectively. This compares with the spectral response

of the unstrained sensor 2 that has a LWHM and an UWHM of 1293 and 1299 nm respectively. Under these conditions the extremes of the spectral responses of the two structures are 6 nm apart. This is sufficiently far apart for the side lobes of the two gratings not to overlap. Hence, the cross-talk measured in this system is not due to the grating side lobes, but the non-100% reflectivity of the blocking gratings. Recall that the cross-talk in the 1550 nm case was 19 με. In that experiment, the spectral profile of the two gratings came within 0.5 nm of each other. Therefore, the cross-talk between multiplexed sensors can be reduced by writing their spectral profiles sufficiently far apart so that even when one sensor is fully exercised they are still more than 5 nm apart.

In theory, more than two sensors may be wavelength division multiplexed on a single fibre using the IBCI technique. However, the addition of more sensors would require more blocking gratings with larger bandwidths. Larger bandwidth gratings would have lower reflectivity due to the exhaustion of the fibre photosensitivity. Therefore, there would be more cross-talk between the sensors. Such a system would also require more couplers, hence reducing the system output and therefore the SNR. A superior solution is to WDM two sensors on one fibre and use spatial division multiplexing, as shown in figure 5.29, to facilitate the required number of sensors.

The normalised results for all the strain sensor systems are presented in table 5.1

Central Wavelength (nm)	BW (nm)	Sensing range (mε)	Single (S) or Dual (D) System	Linear response (a.u./με × 10^{-6})	Error in results (a.u./με × 10^{-6})	Linear strain error (με)	Cubic strain error (με)
1540	10	9	S	94	5	38	23
1542.5	5	4.45	D	140	8	20	10
1292	8	7.125	S	110	6	40	11
1283	30	11	S	9.5	0.5	50	30
1278	6	6.3	D	122	6	18	11

Table 5.1 Normalised results obtained for all IBCI strain experiments.

It is clear from the results that there is a correlation between sensing range (determined by the bandwidth of the sensor) and the linear response. This is to be expected as the maximum value obtainable from a normalised system is 1 a.u.. The minimum value obtainable from a normalised IBCI system is around 0.1 a.u.. This is due to the fact that the reference grating is not identical to the sensor and it does not have a reflectivity of 100%. Therefore, the normalised range of output for an IBCI system, regardless of sensing range is around 0.9 a.u.. Hence, the larger the sensing range the smaller the linear response. For example, a system with a sensing a range of 9 mε, is expected to have a linear response of 0.9/9 000, i.e. 100 × 10^{-6} a.u./με. This is in good agreement with the actual results obtained from such a system operating in the 1.5 μm window, see table 5.1.

There is also a correlation between the sensing range and error due to linear strain extraction. The greater the sensing range, the more inappropriate a linear, and the more appropriate a cubic, strain extraction is.

The achievable resolutions for the IBCI system do not compare favourably with those achieved by a number of interrogation methods discussed in chapter 3. A resolution of 1.5 nε/√Hz for a four sensor wavelength multiplexed system, employing a Mach-

Zender interferometer, was reported by Berkoff *et al.*[14]. This system demonstrated low crosstalk of –70 dB. However, it is only appropriate for measuring dynamic strains and interferometers are expensive, typically costing tens of thousands of pounds, and are difficult to set up.

The IBCI achievable resolutions are comparable to those achieved using an edge filter. Melles *et al.*[15] reported a resolution of tens of millistrain whereas Lobos Ribeiro *et al.*[16] achieved a resolution of 3.5 με with a biconical fibre filter.

An acousto-optic filter used as an interrogation instrument[17] in a multiplexed system[18] has been demonstrated to offer a resolution of 0.4 με at a scanning rate of 10 Hz. However, these systems require both feedback systems and complex components and are highly temperature sensitive. Also an acousto-optic filter is expensive in comparison to the IBCI system and offers a lower scanning rate. The resolution offered is excellent, but is far higher than that required for a number of applications. Most structural monitoring systems require resolutions in the region of 10s of με. Therefore the use of an acousto-optic filter, with its complexity and temperature sensitivity, would be inappropriate for such applications.

A resolution of 1 με has been reported for systems employing a Fabry-Perot filter[19]. Such a system can multiplex a number of sensors over a bandwidth of approximately 50 nm. This technique has been adopted as the main sensor system in the MAST project. Filters are moderately priced at approximately £5, 000 and in were used to wavelength division multiplex eight sensors with a measurement range of ± 3 500 με. It was determined that under certain extreme conditions parts of the mast would be stretched well beyond this limit. It was therefore decided that there should be a second sensor system that was capable of measuring ± 1.5% strain with a resolution of 50 με. The methods discussed here are either inappropriate, interferometer techniques are only used to measure dynamic strain, or more expensive than necessary e.g. £5 000 for a Fabry-Perot filter compared to a few hundred pound for a reference grating.

In summary, the IBCI system is capable of addressing either a number of sensors simultaneously or a single structure with a very large sensing range. This can be achieved at high speeds with acceptable resolution at a low cost. This method is also

robust and does not require any complex control electronics. These advantages make it an ideal solution for part of the requirements of the MAST project and has been incorporated into the final product. This system is also being developed further in collaboration with British Aerospace for shock detection in composite panels. The high speed interrogation makes it ideal for this application and it has already demonstrated as a workable technique.

5.4 Novel Edge Filter Technique

The IBCI technique has a number of advantages over other systems as previously discussed. However, it does have two main drawbacks. The first of these is that it employs chirped rather than uniform gratings. Uniform gratings are currently more easily available commercially than their chirped counterparts. Most gratings that are mass produced are done so with the phase mask technique. This method offers, amongst other things, excellent reproducibility, which is a requirement for the IBCI technique. However, chirped phase masks are currently more expensive than their uniform counterparts. It is likely though that with increasing demand the cost of chirped gratings will fall to that of uniform structures. The requirement of chirped gratings also precludes the use of this interrogation technique for systems that have already been installed with uniform gratings, i.e. the vast majority.

The main disadvantage of the IBCI system is the uneconomical use of the available bandwidth. For example, a uniform FBG sensor requires approximately 5 nm of 'free' spectral bandwidth if it is to measure up to 5 mε, i.e. a strain of 1 mε results in a wavelength shift of 1 nm. A sensor used in the IBCI configuration is shifted exactly the same amount however, it also has a FWHM equal to the maximum sensing range. In the above example, the sensor would shift 5 nm and it would have an equivalent bandwidth. Therefore, the IBCI sensor requires 10 nm of available source bandwidth to measure 5 mε, i.e. twice the bandwidth required by a uniform system. This limits the number of sensors it is possible to multiplex on a single line. A uniform FBG sensor system illuminated by a source of 40 nm bandwidth permits the multiplexing of four sensors each with a measurement range of 1% on a single line. An IBCI system

utilising the same source permits only two sensors with the same sensing range to be arranged on a single line.

A system that retained the advantages of the IBCI technique but addressed these two disadvantages would be ideal. A FBG interrogation system employing bulk optics to obtain an edge filter response was initially reported by Melles *et al.*[5]. This idea was later extended by Riberio *et al.*[20] who developed an all fibre edge filter. The edge filter method has the potential to fulfil these requirements. An interesting system based loosely on the edge filter technique was reported by Kersey *et al.*[21]. This approach involved the interrogation of a broadband sensor grating with a fixed wavelength narrowband source. The sensor had a ramp type of spectral profile. Hence, there is a linear change in reflectivity along one edge of the spectral response. This permits a linear relationship between the strain on the broadband sensor and the intensity of light reflected. This broadband sensor was fabricated using a phase mask with a curved fibre in the plane of the mask as described by Sugden *et al.*[22] and Zhang *et al.*[23]. The reporters suggested that such a device could find application as a pressure sensing probe.

However, such a grating has the potential to act as an edge filter in a system similar to that suggested by Melles *et al.*[5]. A grating with a ramped profile was manufactured using a novel technique[24], see figure 5.33. A 3 cm long phase mask with a 30 nm chirp was employed. A structure with an approximately symmetric spectral response, i.e. a normal, chirped grating would be produced by illuminating the photosensitive fibre with a UV beam through the phase mask. (A symmetric spectral response refers to the fact the profile between the LWHM and central wavelength is the mirror image of the response between the central wavelength and the UWHM. The spectral response of a normal, chirped grating approximates to this.) The beam would be translated along the fibre while keeping the phase mask and fibre static[25]. However, the spectral profile of a grating may be customised by dithering the phase mask during exposure. This is a variation on the method reported by Cole which involved the fibre being dithered[26]. If the phase mask is dithered during exposure, then the interference fringes are equally dithered. This has the same effect as exposing the fibre to fringe-less UV illumination and results in the saturation of the refractive index i.e. erasure of the grating. The percentage of erasure at a given point along the grating is determined by the period of

dithered exposure at that point, i.e. the longer the dithered exposure, the greater the erasure and therefore the lower the reflectivity of the grating at that wavelength. Therefore, by increasing the dithering time along the length of the fibre the reflectivity of the grating may be decreased giving the desired 'ramped' response.

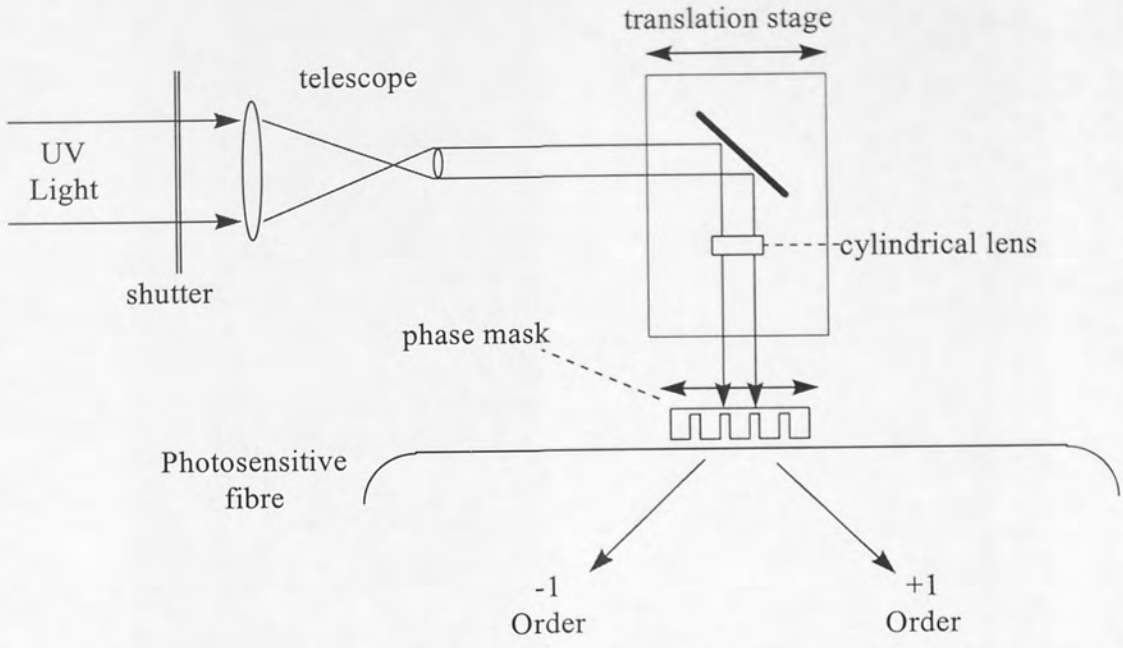

Figure 5.33: Schematic diagram of an asymmetric spectral response grating fabrication arrangement.

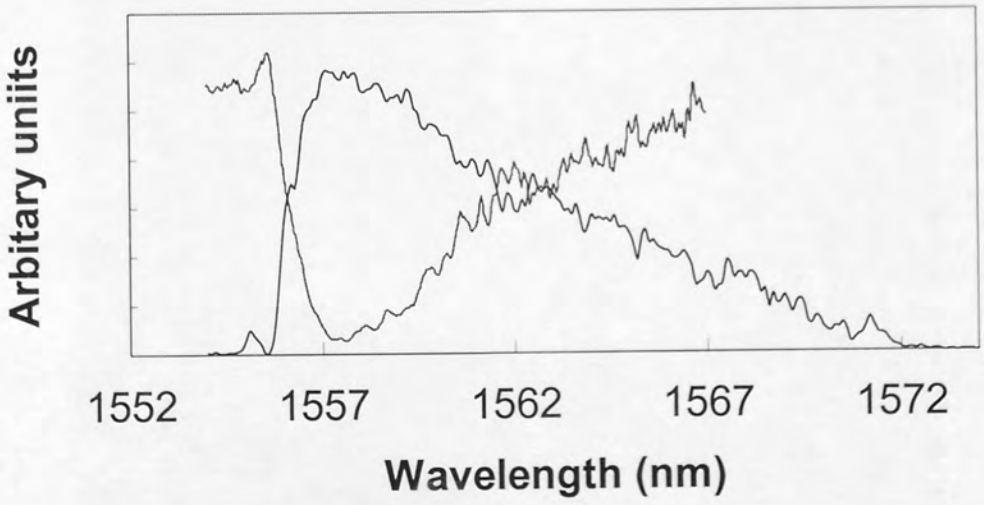

Figure 5.34: Reflection and transmission spectral profiles of the "ramped" grating employed.

The grating was fabricated using a frequency-doubled Argon ion laser operating at 244 nm. The diameter of the UV beam was reduced down to 0.5 mm and focused onto the optical fibre by a cylindrical lens. This lens was mounted onto a translation stage that permitted the beam to be scanned along the length of the phase mask. The phase mask was mounted onto a single piezoelectric displacement stage that was driven by a triangular waveform from a function generator. The magnitude of the dither was varied as the beam scanned along the phase mask giving the desired 'ramped' profile. This grating was inscribed into hydrogen loaded boron-germania co-doped fibre. The inscribed structure was 3 cm in length. The transmission and reflection spectral profiles are shown in figure 5.34. The required edge profile is considerably jagged, i.e. two or more wavelengths may have the same value of reflectivity. This jagged response is due to limitations in the writing method. The fibre cannot be exposed for exactly the correct amount of time through the dithered phase mask to produce an ideal linear response. However, even with this jagged profile, the edge response should be sufficient for low resolution sensing purposes.

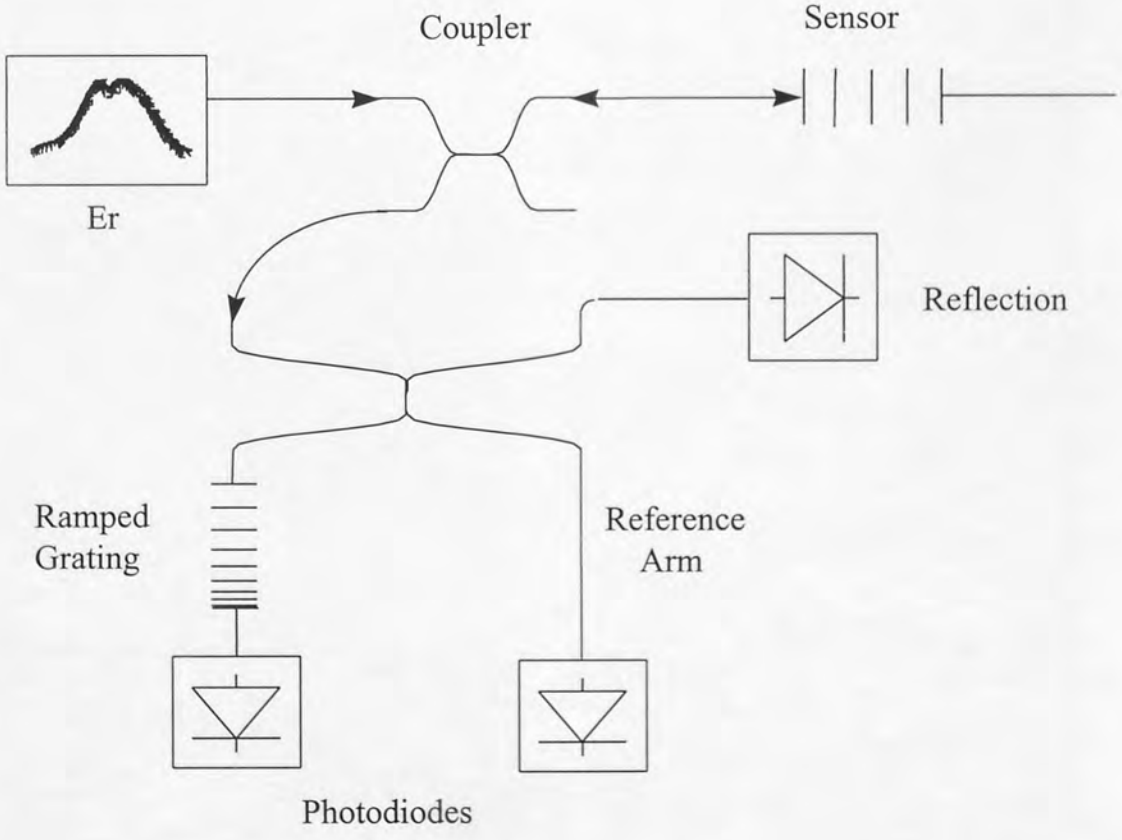

Figure 5.35: Experimental set-up for a single sensor interrogation system employing a grating with a ramped spectral profile.

The asymmetric spectral response grating was employed as an edge filter in the system above. A uniform fibre Bragg grating acts as a sensor and the asymmetric spectral response grating modulates its reflection intensity. The sensor was inscribed into boron-germania co-doped fibre by a frequency doubled Argon-ion laser. A linear phase mask was employed and a structure 1 cm in length with a central wavelength of 1556 nm was inscribed. The sensor was illuminated, via a coupler, by a broadband florescence source. The light reflected by the sensor is split by the 50:50 coupler with one half being incident on the grating with the asymmetric spectral response. The remaining half is transmitted to the reference arm.

There are two ways of interrogating the sensor; by examining the transmission or reflection from the 'ramped' spectral profile. The response of the sensor is normalised by dividing the transmitted or reflected intensity by the reference value. When the sensor is stretched its spectral profile is shifted to longer wavelengths; hence more light is transmitted and less is reflected by the 'ramped' structure. Both of these interrogation methods were investigated.

A 5 mm length of coating on either side of the sensing structure was stripped. The stripped sections were then placed onto steel groove blocks that were attached to the displacement stage and load cell. The fibre was held in place by rubber blocks that were screwed onto the top of these steel mounts. This mechanical method gave the same grip between the fibre and mount as the glue. However, it was easier to remove the fibre after characterisation had been completed as no de-bonding compound was required. The sensor was stretched in steps of 400 με, up to 6 mε. Again the results were taken from an Anritsu dual head power meter that monitored the two photodiodes. These results were then entered into Excel and processed. The results for both transmission and reflection are shown in figure 5.36.

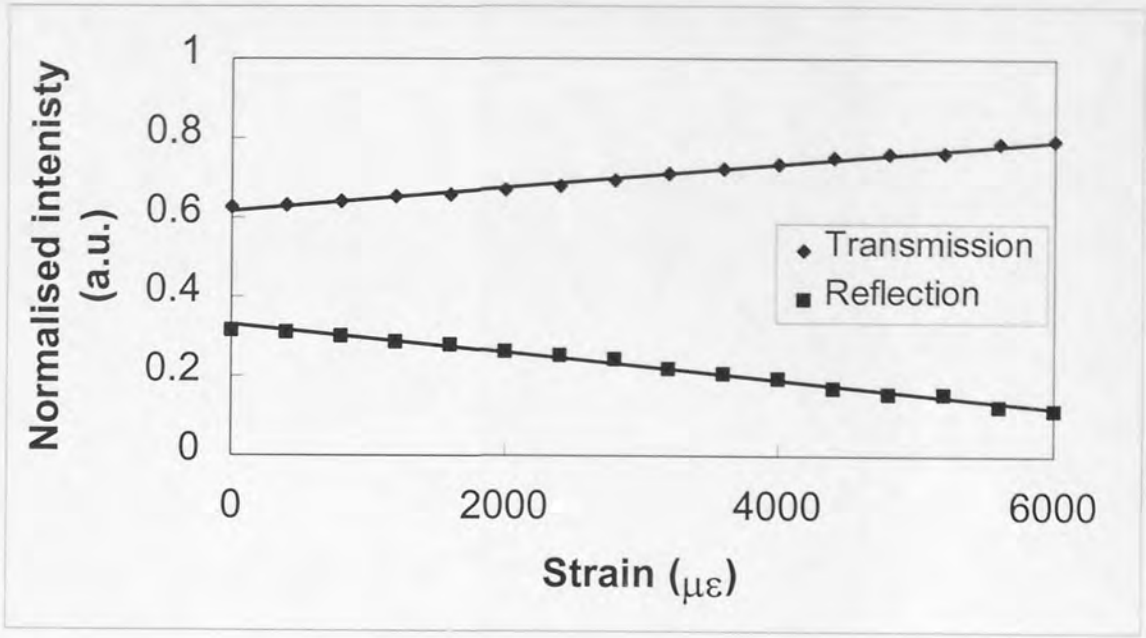

Figure 5.36: Strain to normalised power response for single sensor interrogation.

(Errors in figure 5.32: ± 8 με for strain and ± 0.08 a.u. for intensity)

The strain response for both reflection and transmission was linear and was determined to have a gradient of $-(34 \pm 8)\times10^{-6}$ a.u./με and $(29 \pm 8) \times 10^{-6}$ a.u./με respectively. These values are approximately in line with those obtained by the IBCI system. The spectral response of the ramped grating has a linear slope over approximately 15 nm. Assuming a strain sensitivity of 1 pm/με, an ideal normalised slope would have a gradient of $1/(15\times10^{3})$, i.e. 66×10^{-6}, a.u./με. The measured strain response is lower than this for two reasons. The grating with the asymmetric spectral response had a maximum reflectivity of 95%, i.e. it only covers from 0-0.95 a.u. The main reason is the spectral profile of the erbium fluorescence. The sensor grating is shifted along the trailing edge of the erbium spectral profile. Hence, as in the case of the 30 nm grating in the IBCI experiment, the sensitivity of the system is reduced.

The strain resolution of these two interrogation methods was determined to be 47 and 42 με respectively. These values are not as good as those achieved with the IBCI technique. This is mainly due to the jagged response of the edge filter. This response means that two or more values of applied strain may give the same received power, hence introducing ambiguity into the system. This problem is compensated to a certain

extent by the averaging effect of the grating which has a finite bandwidth. This effect can be observed and the action of the filter demonstrated more clearly by placing an OSA at the reflection output port. The results from a number of different strains on the grating are shown in figure 5.37.

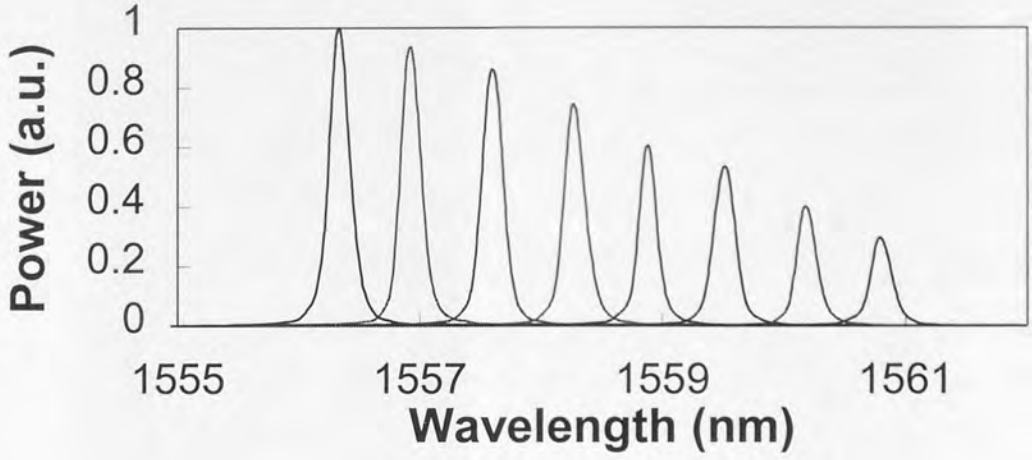

Figure 5.37: FBG sensor spectral profile reflected by the ramped structure at different wavelengths.

It would be possible to increase the resolution of this system if the response of the edge filter could be smoothed. However, such a device could still be employed in systems that required a resolution of 50 με, such as the MAST project. The measurement range of this system is determined by the spectral length of the linear slope of the asymmetric spectral response grating, which is approximately 15 nm in this case. Hence, this structure would permit the interrogation of a single sensor with a measurement range of 15 mε (1.5%). This measurement range is far greater than that required for the majority of sensor systems. Therefore, it is possible to utilise the redundant edge response to interrogate additional sensors.

A suitable arrangement for the simultaneous interrogation of twin sensors is shown in figure 5.38. The system consists of two uniform sensor gratings, the ramped grating previously discussed and two pairs of identical broadband gratings. In this scheme, the gratings may be interrogated in transmission only. Each sensor also requires its own reference arm as in the case of the IBCI system. The two broadband gratings (BG1, BG2) are required to prevent any cross-talk between the two sensors. The bandwidths

and central wavelengths of these gratings was determined by the measurement range of each sensor. The second sensor was also written into boron-germania co-doped fibre by UV illumination through a linear phase mask. It was approximately 1 cm in length and had a bandwidth of 0.5 nm. The stopband gratings were also written to saturation into hydrogenated boron-germania co-doped fibre.

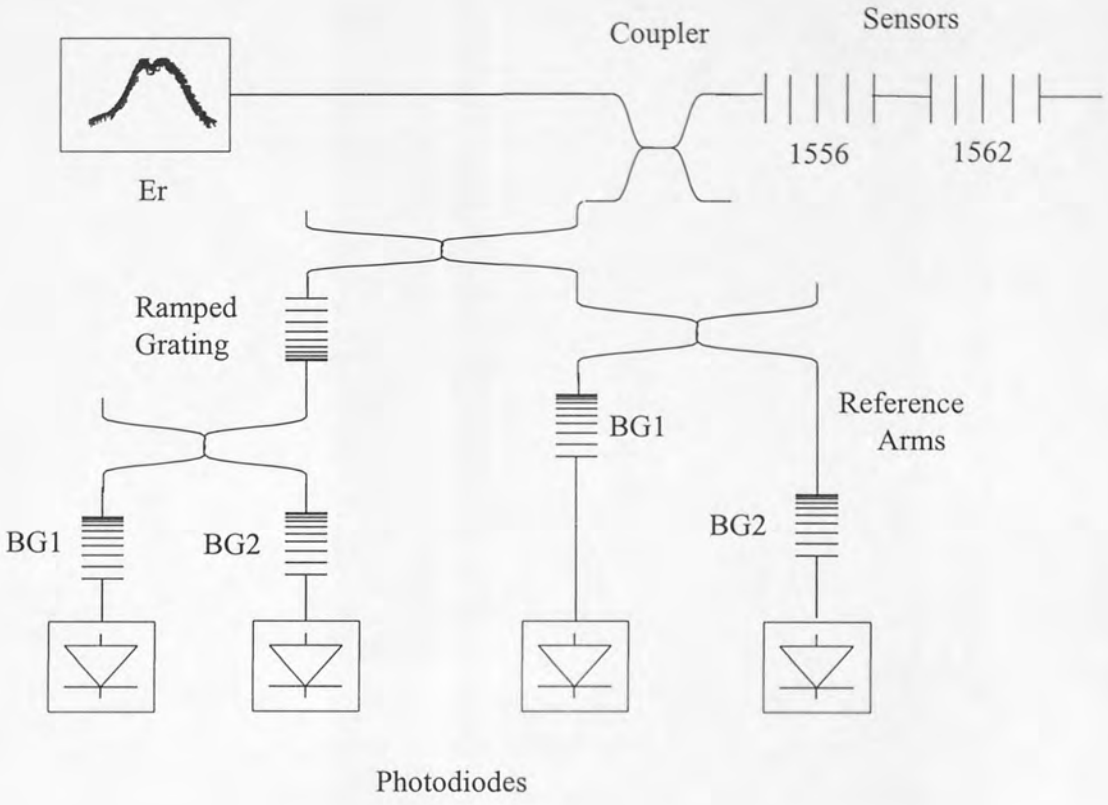

Figure 5.38: Schematic of the twin sensor interrogation system employing a grating with an asymmetric spectral response.

In this experiment the two uniform gratings had central wavelengths of 1556 and 1562 nm. Both sensors were required to measure up to 5 mε. Each grating has a sensitivity of 1 pm/με. This gives a maximum strain induced shift of 5 nm for the sensor gratings. Therefore, to reduce cross-talk, the stopband gratings were chosen to have a bandwidth of 6 nm with central wavelengths of 1558 (BG2) and 1564 nm (BG1).

The second sensor was prepared and mechanically attached to the two mounts. It was stretched in steps of 550 με up to 4.5 mε. The results obtained from it and the unstrained sensor are shown in figure 5.39.

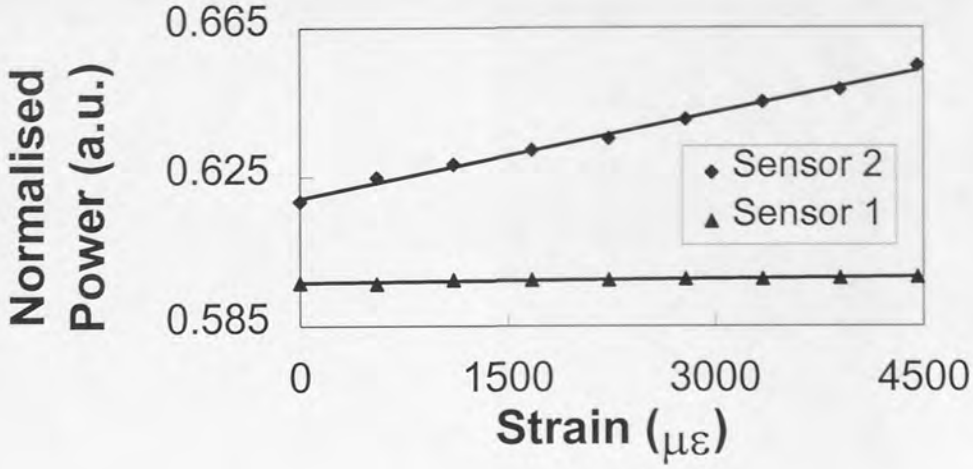

Figure 5.39: Strain to normalised power results for dual sensor system employing a grating with an asymmetrical spectral response.

(Errors in figure 5.39 are: ± 6 με for strain and ± 5 × 10^{-3} a.u. for intensity)

The results for the strained sensor are again fairly linear and have a gradient of (7.7±0.9)×10^{-6} a.u./με. This response is less than that previously obtained as sensor 2 operates along a shallower part of the edge filter than the 1556 nm structure. However, a closer linear fit was obtained giving an achievable resolution of 38 με which is an improvement on that of the other sensor. The cross-talk for this system was determined to be 44 με.

This level of cross-talk is quite high and may only be acceptable for systems that merely require an indication, rather than a precise measurement, of strain. It is hoped that a cheaper version of the full MAST sensor system could be installed in a number of commercially available dinghies. It is envisioned that such a system would give a colour coded, rather than a numerical, strain readout where red denotes extreme strain, green medium strain and blue little or no strain. This technique could provide an inexpensive basis for such a system.

There are a number of other limitations and trade-offs associated with this technique. The first is that the measurement range and multiplexing capability is limited by the spectral length of the edge response of the 'ramped' profile grating. This is more limiting than the bandwidth of the erbium source which limits the range of the IBCI system. For example, the total bandwidth available to the sensor system was 40 nm in

the IBCI case and 15 nm in the asymmetric case. It is possible to write an asymmetric spectral response grating with a larger bandwidth. However, this would result in a shallower edge filter response, hence reducing the sensitivity and resolution of the system. The IBCI technique suffers from no such trade-off. The IBCI system also offers considerably better achievable resolution and does not need a specialist grating.

The choice of which system to employ depends on a number of factors which include:

(i) Required resolution,

(ii) Measurement range and number of sensors in the system,

(iii) Compatibility with uniform gratings/existing systems,

(iv) Acceptable amount of cross-talk between sensors.

5.5 Conclusions

Two novel interrogation techniques have been demonstrated and discussed. Both systems have the potential to interrogate strain sensors in SMART structures and offer a number of advantages over other interrogation techniques, such as the tuneable filter[7] and interferometer methods[3]. These include extremely fast and, for multiple sensors, truly simultaneous interrogation. The suggested systems are also robust, passive, thereby requiring no control electronics and are simple to implement. Hence, the overall cost of the two suggested systems is considerably lower than that of previous techniques.

The first system, which employs the IBCI technique interrogates chirped grating sensors. This technique is particularly suitable for large strain sensing applications involving load measurement and damage detection in the maritime[27], aerospace[2] and civil engineering[1] industries. It offers the advantages of very high speed and simultaneous interrogation of sensors. It is also robust, passive, easy to install and inexpensive. It has two drawbacks which are (i) it is bandwidth intensive and (ii) it can only interrogate chirped gratings. It has been shown to offer a resolution of about 20 με for linear strain extraction and 10 με if cubic extraction is employed. It is expected

that chirped gratings will become readily available in the future, making this interrogation system a more commercially viable option. It can be suggested that this technique has the potential to be incorporated with a sensing scheme recently demonstrated by Davis *et al.*[28] which can interrogate 60 fibre grating sensors. Such a sensing architecture would be capable of large strain measurement, as well as de-multiplexing a large number of distributed sensors.

The second system has the potential to interrogate medium to large strain uniform FBG sensors. It is also robust, easy to install and cheap. It offers high speed and simultaneous interrogation of multiple sensors. While, it is less bandwidth intensive than the IBCI system it does not have the same multiplexing capability and requires a specialist grating. The resolution of the system was determined to be about 50 με.

---

[1] V. Dewynter-Marty, S. Rougeault, P. Ferdinand, D. Chauvel, E. Toppani, M. Leygonie, B. Jarret and P. Fenaux, "Concrete strain measurements and crack detection with surface-mounted and embedded Bragg grating extensometers", *Conf. Optical Fibre Sensors (OFS '97)*, Williamsburg, Virginia, Tech. Dig, 1997, OFA2-1.

[2] P.D. Foote "Fiber Bragg grating strain sensors for aerospace SMART structures", *2nd European Conf. SMART Structures and Materials*, Glasgow, Scotland, 2361, 1995, p 162.

[3] Y.J. Rao, D.J. Webb, D.A. Jackson, L. Zhang and I. Bennion, "High-resolution, wavelength-division-multiplexed in-fibre Bragg grating sensor system", *Electron. Lett.*, **32**, 1996, pp 924-926.

[4] A.D. Kersey, T.A. Berkoff and W.W. Morey, "High-resolution fibre-grating based strain sensor with interferometric wavelength-shift detection", *Electron. Lett.*, **28**, 1992, pp 236-238.

[5] S.M. Melle, K. Liu, and R.M. Measures, "A passive wavelength demodulation system for guided-wave Bragg grating sensors", *Photon. Technol. Lett.*, **4**, 1992, pp 515-518.

[6] A.B. Lobos Riberio, L.A. Ferreira, M. Tsvetkov and J.L. Santos, "All-fibre interrogation technique for fibre Bragg sensors using a biconical filter", *Electron. Lett.*, **32**, pp 382-383.

[7] A.D. Kersy, T.A. Berkoff and W.W. Morey, "Multiplexed fibre Bragg grating strain-sensor system with a fibre Fabry-Perot wavelength filter", *Opt. Lett.*, **18**, 1993, pp 1370-1372.

[8] T. Coroy, P.J. Ellerbrock, R.M. Measures and J.H. Belk, "Active wavelength demodulation of Bragg fibre-optic strain sensor using acousto-optic tunable filter", *Electron. Lett.*, **31**, 1995, pp 1602-1603.

[9] H. Gieger, M.G. Xu, N.C. Eaton and J.P. Dakin, "Electronic tracking system for multiplexed fibre grating sensors", *Electron. Lett.*, **31**, 1995, pp 1006-1007.

[10] M.A. Davies and A.D. Kersey, "Matched-filter interrogation technique for fibre Bragg grating arrays", *Electron. Lett.*, **31**, 1995, pp 822-823.

[11] G. Meltz, W.W. Morey and W.H. Glenn, "Formation of Bragg gratings in optical fibres by a transverse holographic method", *Opt. Lett.*, **14**, 1989, pp 823-825.

[12] K. Sugden, L. Zhang, J.A.R. Williams and I. Bennion, "Dissimilar wavefront technique for linear and quadratic chirps", *Photosensitivity and quadratic non-linearity in glass waveguides: Fundamentals and applications*, U.S., 1995, Tech. Dig., pp. 136-139

[13] Y.J. Rao et al. "In-situ temperature monitoring in NMR machines with a prototype in-fibre Bragg grating sensor system", ", *Conf. Optical Fibre Sensors (OFS '97)*, Williamsburg, Virginia, Tech. Dig, 1997, pp 354-357.

[14] T.A. Berkoff and A.D. Kersey, "Fiber Bragg grating array sensor system using a bandpass wavelength division multiplexer and interferometric detection", *Photon. Techno. Lett.*, **8**, 1996, pp 1522-1524.

[15] S.M. Melle, K. Liu, and R.M. Measures, "A passive wavelength demodulation system for guided-wave Bragg grating sensors", *Photon. Technol. Lett.*, **4**, 1992, pp 515-518.

[16] A.B. Lobos Riberio, L.A. Ferreira, M. Tsvetkov and J.L. Santos, "All-fibre interrogation technique for fibre Bragg sensors using a biconical filter", *Electron. Lett.*, **32**, 1996, pp 382-383.

[17] T. Coroy, P.J. Ellerbrock, R.M. Measures and J.H. Belk, "Active wavelength demodulation of Bragg fibre-optic strain sensor using acousto-optic tunable filter", *Electron. Lett.*, **31**, 1995, pp 1602-1603.

[18] H. Gieger, M.G. Xu, N.C. Eaton and J.P. Dakin, "Electronic tracking system for multiplexed fibre grating sensors", *Electron. Lett.*, **31**, 1995, pp 1006-1007.

[19] M.A. Davis, D.G. Bellemore, M.A. Putnam and A.D. Kersey, "Interrogation of 60 fibre Bragg grating sensors with microstrain resolution capability", *Electron. Lett.*, **32**, 1996, pp 1393-1394.

[20] A.B. Lobos Riberio, L.A. Ferreira, M. Tsvetkov and J.L. Santos, "All-fibre interrogation technique for fibre Bragg sensors using a biconical filter", *Electron. Lett.*, **32**, pp 382-383.

[21] A.D. Kersey, M.A. Davies and T. Tsai, "Fiber optic Bragg grating strain sensor with direct reflectometric interrogation", *Optical Fibre Sensors (OFS'96)*, **Tech. Dig.**, Sapporo, Japan, 1996, pp 634-637.

[22] K. Sugden, I. Bennion, A. Molony and N.J. Copner, "Chirped gratings produced in photosensitive optical fibres by fibre deformation during exposure", *Electron. Lett.*, 30, 1994, pp 440-442.

[23] Q. Zhang, D.A. Brown, L.J. Reinhart and T.F. Morse, "Linearly and nonlinearly chirped Bragg gratings fabricated on curved fibers", *Opt. Lett.*, 20, 1995, pp 1122-1124.

[24] L.A. Everall, K.E. Chisholm, J.A.R. Williams, X. Liu, R.M. De La Rue and J.S. Aitchison, "Optimisation of length-constrained apodised in-fibre Bragg grating filters," *Submitted to Opt. Comms.*, Sept 98.

[25] H.N. Rouke, S.R. Baker, K.C. Byron, R.S. Baulcomb, S.M. Ojha and S. Clements, "Fabrication and charcterisation of long, narrowband fibre gratings by phase mask scanning", *Electron. Lett.*, 30, 1994, pp 1341-1342.

[26] M.I. Cole "Moving fibre/phase mask-scanning beam technique for enhanced flexibility in producing fibre gratings with a uniform phase mask", *Electron. Lett.*, 31, 1995, pp 92-94.

[27] D. Roberts and P. Foote, "Carbon spars for superyachts and SMART mast technology", *International Conference on The Modern Yacht*, Portsmouth, 1998, paper 13.

[28] M.A. Davies, D.G. Bellmore, M.A. Putnam and A.D. Kersey, "Interrogation of 60 fibre Bragg grating sensors with microstrain resolution capability", *Electron. Lett.*, 32, 1996, pp. 1393-1394.

Chapter Six: Long Period Gratings

6.1 Chapter Overview.

This chapter examines the recent conception and development of long period gratings. A review of the work completed on these devices and their applications is given. Original temperature and strain characterisation results for a number of different period structures written into the same type of fibre are presented and discussed. The chapter ends with the implementation and development of a novel FBG sensor interrogation technique that utilises a long period device as an edge filter.

6.2 Long Period Gratings

Long period gratings (LPGs) have had a recent upsurge in interest, which coincided with a publication outlining their applications by Vengsarkar *et al.*[1] in 1996. LPG are structures which are, like their Bragg counterparts, based on the periodic modulation of the core refractive index. This modulation is brought about by the same mechanism as that for Bragg gratings. LPGs are essentially periodic structures that couple the guided fundamental mode in a single mode fibre to a forward-propagating cladding modes; the back reflection from such a grating is negligible. It is noted at this point that long period fibre gratings with periodicities in the hundreds of microns have been employed in the past for coupling from either one guided mode to another in multimode fibre or from one polarisation mode to another in single mode fibre. These structures have included a blazed grating in a two-mode fibre that has been employed to induce a $LP_{01} \leftrightarrow LP_{11}$ mode conversion[2], $LP_{01} \leftrightarrow LP_{02}$ mode converters have been demonstrated[3] and rocking filters have been written in single-mode fibres for polarisation mode conversion[4].

Long period structures are written fundamentally by the same process as Bragg gratings. The induced refractive index change for such structures is typically of the order 10^{-4}, which is considerably smaller than that for Bragg gratings. This is because a large refractive index modulation is not required and the smaller change has been demonstrated to give the structure a longer time of stabilisation[5]. In the case of fibre

Bragg gratings the forward propagating guided mode is coupled in to backward propagating guided (or radiative) modes. This coupling requires a structure with a short-period grating. However, LPGs couple the forward guided light at specific wavelengths out of the core and into one of a number of co-propagating cladding modes[6]. Coupling from the guided to the unguided modes is wavelength dependent, therefore the grating acts as a spectrally selective loss device. The exact refractive index periodicity required to scatter the desired wavelength(s) is dictated by the phase matching condition, which dictates the coupling of energy from one mode to another.

Fibre gratings satisfy the Bragg phase-matching condition between the guided and cladding or radiation modes, or another guided mode. This phase-matching condition is given by equation 6.1:

$$\beta_{01} - \beta = \Delta\beta = 2\pi/\Lambda \qquad \textit{Equation 6.1}$$

where β_{01} and β are the propagation constant of the fundamental guided mode and the mode to which coupling occurs respectively and Λ is the period of the grating.

As discussed previously, for conventional fibre Bragg gratings the coupling of the forward LP_{01} mode occurs to the reverse propagating mode ($\beta = -\beta_{01}$). In this case $\Delta\beta$ is large, hence the grating periodicity is small, typically of the order of 1 μm. Unblazed long period gratings couple the fundamental mode to the discrete and circularly symmetric forward propagating cladding modes, i.e. ($\beta = \beta_{clad}^{(i)}$) where $\beta_{clad}^{(i)}$ is the propagation constant of the ith cladding mode.

Considering $\beta = 2\pi n/\lambda$, equation 6.1 can be re-arranged to:

$$\lambda_i = [n_{01} - n_{clad}^{(i)}]\Lambda \qquad \textit{Equation 6.2}$$

where λ_i is the i^{th} coupled wavelength, n_{01} is the effective index of the core, $n_{clad}^{(i)}$ is the effective index of the i^{th} axially symmetric cladding mode. This equation has as many solutions as there are axially symmetric cladding modes. Since $\Delta\beta$ is discrete and a function of wavelength, this coupling to the cladding modes is highly selective leading to a wavelength-dependent loss. As a result, any modulation of the core and cladding guiding properties modifies the spectral response of long period gratings. Also these

cladding modes interact with the fibre jacket or any other material surrounding the cladding. Therefore, a change in the environment surrounding the grating (e.g. a change in temperature) leads to a change in the spectral response (see later).

Light coupled into the cladding quickly decays due to losses at the cladding/air interface, leaving a series of loss bands or resonances in the guided modes, see figure 6.1. These resonance peaks, from equation 6.2, are dependent on both the period of the structure and $n_{clad}^{(i)}$ which in itself depends on the index of the medium surrounding the cladding.

A typical LPG has a period in the hundreds of microns, a length of about 1-3 cm and an index modulation depth of 10^{-4} or greater. Its spectral response will exhibit a number of resonance peaks due to light being coupled into different cladding modes, see figure 6.1.

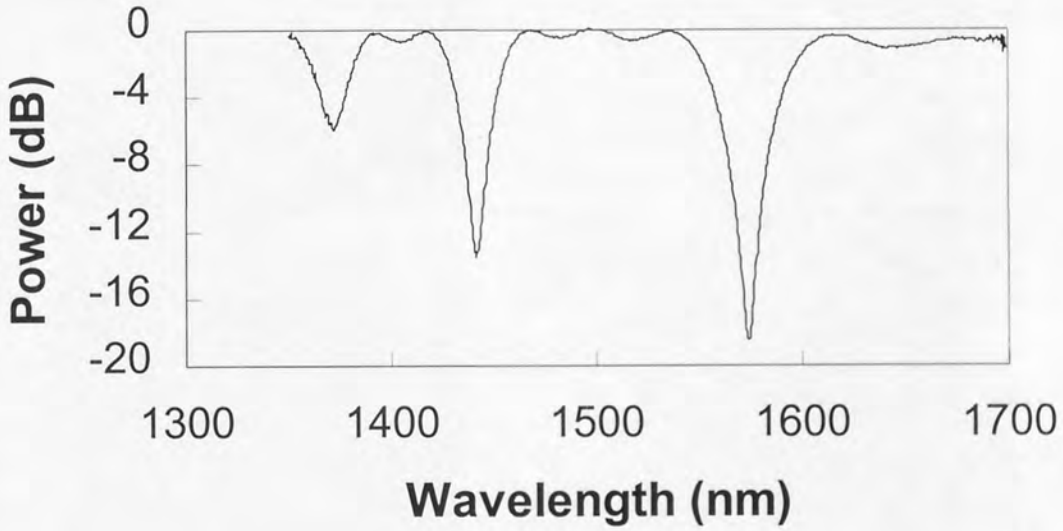

Figure 6.1: Spectral profile of a long period grating with a period of 500 μm and 1.1 cm in length.

Long period structures can be written in a number of ways and are generally simpler and cheaper to write than their Bragg grating counterparts. The three main inscription methods are:

(i) Point-by point writing technique. This was first reported by Hill *et al.*[2] and involves exposing the optical fibre to UV light through a slit. The unfocussed pulsed UV

light was derived from an excimer laser operating at 249 nm. The slit was slanted with respect to the fibre axis for a proper grating blaze. The fibre was translated in front of the UV beam by a motorised translation stage. Two methods were employed to fabricate gratings. In the first method, the motor stopped at each point and a single laser pulse impinged on the fibre through the slit. The second technique involved the continuous running of the motor with the laser flashing at regular intervals. Although this technique was used to fabricate blazed gratings it is applicable to the fabrication of long period gratings. This application is developed and discussed in the next section. A variation on this technique was recently reported by Davis *et al.*[7]. In this method a CO_2 laser was employed instead of UV exposure. The grating was inscribed with a writing wavelength of 10.6 mm. The authors concluded that the grating was written through stress relief and/or densification of the fibre rather than through photoexcitation or material removal. Structures were written into both hydrogenated and non-hydrogenated fibres. Hydrogen loading was found to enhance the writing sensitivity. This method has the advantage of employing a cheaper, safer source and optics.

(ii) The second method involves exposing the photosensitive fibre to UV light through an amplitude mask[1,4]. Hydrogenated loaded germanosilicate were exposed to UV light derived from a KrF laser operating at 248 nm through an amplitude mask made of chrome-plated silica, see figure 6.2. Each grating imprint on the mask was one inch long and structures with periods ranging from 60 μm to 1 mm were inscribed. The spectra of the structures were observed during the writing and the authors reported the measured peak loss and peak wavelength increased as a function of time.

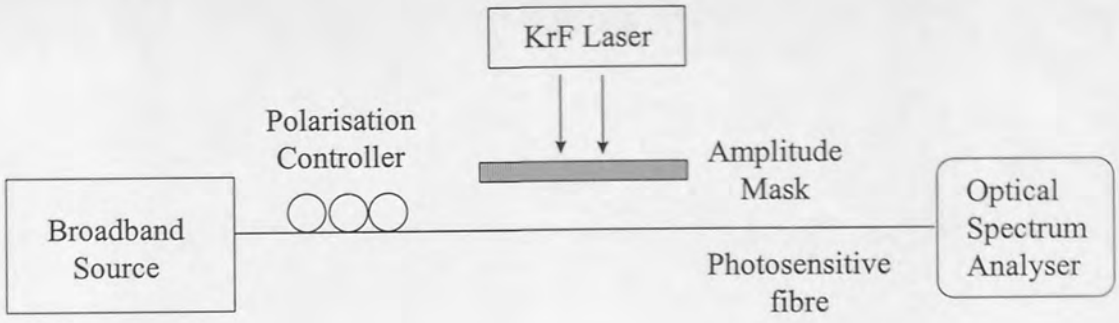

Figure 6.2 Experimental set up for long period grating fabrication by application of an amplitude mask.

(iii) The third method also involves exposure through an amplitude mask but in this technique the mask is "printed" onto the fibre. This photomask consists of a number of opaque lines on the outside of the fibre which are inscribed by a process known as microcontact printing. The printed fibre is exposed to UV light and a grating is inscribed in the core of the fibre, see figure 6.3. With this method the performance characteristics of the grating depend only weakly on the temporal or spatial coherence properties of the UV light and the mechanical vibrations of the bulk optics. This has the advantage of writing high quality gratings even when a long exposure time is required.

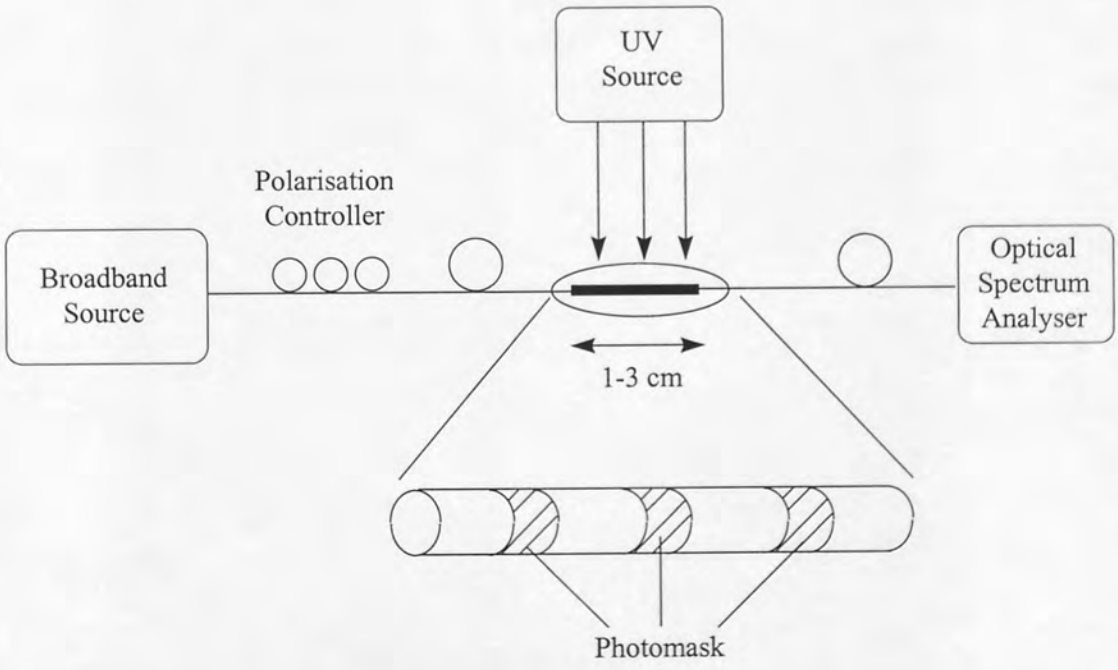

Figure 6.3: Apparatus for fabricating in-fibre long period gratings with a printed photomask.

Long period gratings are also, like their Bragg grating counterparts, sensitive to external perturbations. They can be extremely temperature sensitive with values of up to 0.154 nm/°C being quoted[8], which is over 10 times greater than that achieved by a Bragg grating at the same wavelength. The dependence of the peak wavelength on temperature can be determined by differentiating equation (6.2), viz:

$$\frac{\delta\lambda_p}{\delta T} = \frac{\Lambda.(\Delta n)^2}{\Delta n_g}.\left(\frac{1}{(\Delta n)}.\frac{\delta(\Delta n)}{\delta T} + \alpha\right) \qquad \textit{Equation 6.3}$$

where a is the thermal expansion co-efficient of the glass, Δn is the difference in refractive indices ($\Delta n = n_{01} - n_{lm}$), and Δn_g is the difference in group indices of the modes ($\Delta n_g = \Delta n - \lambda\delta(\Delta n)/\delta\lambda$).

The core and cladding modes occupy different regions and are governed by dissimilar wave-guiding conditions. Therefore, the effective indices of these two modes change differently with temperature. This leads to a range of temperature sensitivities for different fibres; in communications fibre, peak wavelength shifts range from 0.05 to 0.1 nm/°C. However, it is possible to manufacture a grating that is temperature insensitive by reducing the bracket in the right hand side of equation 6.3 to zero, i.e.:

$$\frac{\delta(\Delta n)}{\delta T} = -(\Delta n)\alpha \qquad \textit{Equation 6.4}$$

This is achievable by designing novel refractive index profiles[9]. Long period fibre gratings written into such multi-layer fibres have demonstrated greatly lowered temperature sensitivities of between -4pm to 1pm/°C. This type of grating is ideal for non-sensor applications that require a stable wavelength over a large temperature range. Therefore, such structures are more suited to certain applications than Bragg gratings.

A similar analysis results in the strain sensitivity of a mode being determined by the cladding strain-optic co-efficient which is given by[8]:

$$\xi_{ck} = \left(\frac{1}{n_{cl}}\right)\frac{\delta n_{cl}}{\delta\varepsilon} \qquad \textit{Equation 6.5}$$

where n_{cl} is the cladding index and ε is the applied strain. The authors analysed the guided mode by use of weakly guiding approximations and the cladding modes by considering the fibre as a multimode structure with no core. This analysis revealed that the strain sensitivity of long period gratings is also a strong function of the optical fibre parameters. The authors went on to communicate experimental results for a number of optical fibres in which strain sensitivities obtained varied from -7 to 15 nm/%ε.

In the same paper, the authors reported the effects of the surrounding medium on the grating. The effective index of the cladding modes is dependent on the refractive index of the medium surrounding the cladding. Any change in the effective index of the cladding mode, from equation 6.2, results in a shift in the peak transmission loss. Therefore the transmission peak of an inscribed structure is sensitive to the medium surrounding the fibre. Experimental results were communicated for a number of different fibres were the index of the surrounding medium was altered from 1.404 to 1.452. This action led to a shift in the peak transmission loss of the gratings ranging from -22.5 to -62.4 nm. They can also, be designed to be insensitive to refractive index changes. This was recently demonstrated by L. Dong *et al.*[10] and involves writing a structure into a depressed cladding fibre. This has the effect of transforming the LP_{11} mode in a single mode fibre into a leaky mode. A long period structure or Bragg grating permits coupling from the guided fundamental LP_{01} to the leaky LP_{11}. The LP_{11} is a core mode and has virtually no power distribution at the glass-air interface of the fibre. Hence, the transmission loss peak associated with coupling into this mode is insensitive to changes in the refractive index of the surrounding medium.

Long period gratings, unless deliberately designed, are sensitive to refractive index changes in the surrounding medium and may be used to detect such. Bragg gratings require etching of the cladding if they are to be employed as refractive index sensors. This is necessary to gain access to the evanescent field of the guided mode. This reduces the strength and durability of the sensor and makes it susceptible to damage. However, long period structures retain their endurance as the integrity of the fibre is not violated.

The strain, temperature and refractive index sensitivities of long period gratings indicate that may be employed to measure these external parameters. They are small, compact,

immune to electromagnetic interference and have larger temperature, strain and refractive index coefficients than Bragg gratings. However, they have two main disadvantages which are (i) they are highly bend sensitive and (ii) their large bandwidths limit their multiplexing capabilities.

Despite this they have been employed as temperature, strain[8] and chemical refractive index sensors[11]. One of their main applications is in combined FBG/LPG systems to separate strain and temperature[12]. The long period grating employed had a much larger temperature response than the FBG and a smaller strain response, which gives the potential for very accurate strain/temperature characterisation. The system interrogates a LPG using the reflection of two FBGs. This method gave excellent results with a rms deviation of ± 9 με and ± 1.5°C for strain and temperature respectively. This compares favourably with a similar experiment by Kanellopoulos *et al.*[13] that employed an FBG and a long period rocking filter. Another method which employed two fibre Bragg gratings and a long period grating was suggested by Zhang *et al.*[14]. However, in this method one FBG acted as a wavelength reference and the other as a temperature sensor. The information supplied by these two structures permitted the removal of any temperature effects from the long period grating which acted as a chemical sensor. The authors concluded that this temperature insensitive long period grating chemical sensor can be designed to be selective to certain specific chemical agents.

More recently, a novel system for simultaneously measuring strain and temperature with one long period grating only was reported by Bhatia *et al.*[15]. In the second chapter, a technique for separating strain and temperature utilising two fibre Bragg gratings reported by Xu *et al.*[16] was discussed. In this example, two Bragg gratings at different wavelengths were written into the same section of fibre. The two gratings had different temperature and strain sensitivities that permitted the writing and solution of two simultaneous solutions. The long period method works on the same principle of differing sensitivities and different wavelengths. However, as a long period grating has a number of transmission loss peaks only one such structure needs to be inscribed. The interrogation system employed is shown in figure 6.4:

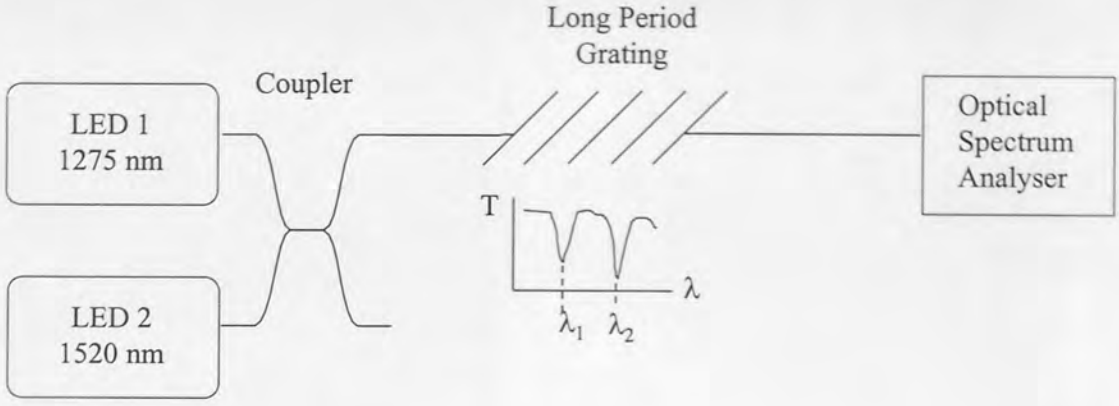

Figure 6.4: Experimental set-up for simultaneous temperature and strain measurement with a single long period structure.

The long period grating had a period of 280 μm and transmission loss peaks at 1607.9 nm and 1332.9 nm. The strain and temperature sensitivities of these two peaks were determined and, following from 6.2, found to be different. Hence, permitting the solving of the two simultaneous equations. Temperature and strain of up to 60°C and 2 mε respectively were simultaneously applied to the structure. The errors in measured strain and temperature were 42 με and 0.7°C respectively. This method permits the separation of strain and temperature with a single sensor.

Long period gratings also have a number of applications outside of the sensor field. One of their main applications is as band rejection filters[1,17]. Their inherently broad bandwidth makes them ideal for gain flattening in erbium-doped fibre amplifiers[18]. They have also found application in the wavelength stabilisation of erbium doped superfluorescent sources[19].

Long period structures have also found application in the optical switching field[20]. Optical devices are of great importance in ultra-high speed data processing and fibre gratings, which exploit the non-linearity of glass, are of particular interest[21]. The authors observed all-optical switching in a long period fibre structure at much lower intensities than those required for a Bragg grating. Such a device is compact, easy to fabricate and polarisation insensitive and could be a valuable component in all-optical networks.

These properties offered by long period structures ensure that they will have a place in both future communication networks[22,23] and sensor systems[8].

6.3 Novel Fabrication Technique for Long Period Gratings

As previously mentioned long period gratings may be written by point-by-point exposure[1], but are more usually written with an amplitude mask[4]. Although amplitude masks are not as expensive as phase masks, they are equally inflexible. A key issue for the integration of gratings into commercial systems is repeatability and compatibility with commercial production at minimal cost. A simple, flexible system to fabricate long period gratings has been developed and employed for the work described herein, and the principle is illustrated in figure 6.5. This technique extends the point-by-point fabrication technique, removing the need for an amplitude mask and permits the manufacture of a long period device with almost any design.

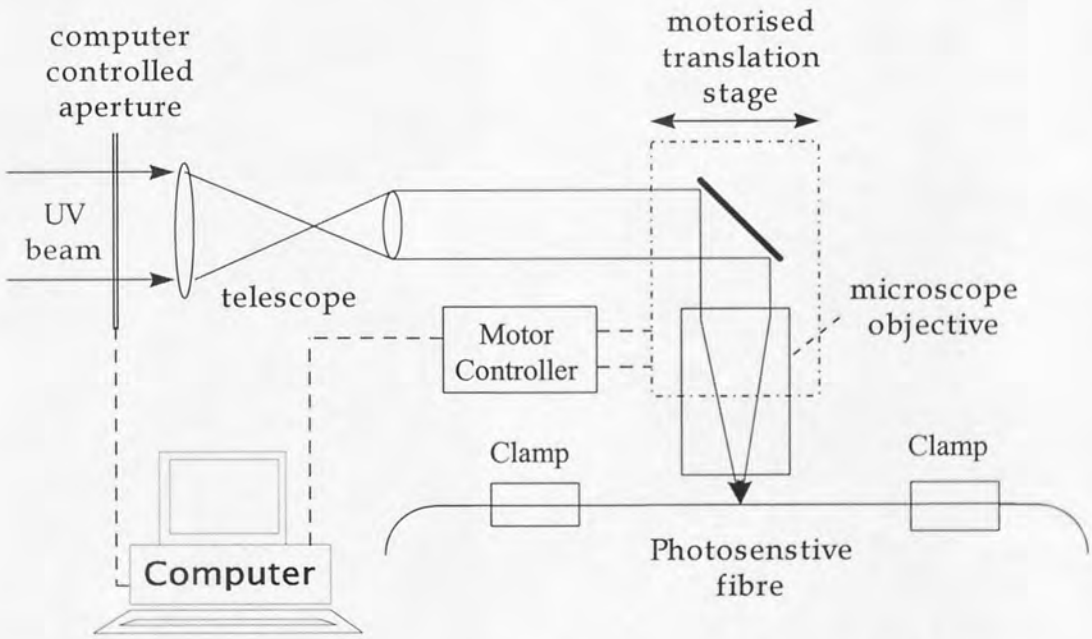

Figure 6.5: Experimental arrangement for the fabrication of long period gratings.

The system utilises a cw UV beam, derived from a frequency doubled Argon ion laser, which is reduced, to a diameter of less than 30 μm, and focused onto the fibre by a microscope objective. The ultraviolet beam is scanned along the fibre by a motorised translation stage; whilst the computer controlled aperture enables the fibre to be exposed at periodical distances. It is the switching of the ultraviolet beam that writes

the grating. The accuracy of the inscribed structure is dependent on the positional accuracy of the motor, but it is typically less than 0.1 μm per grating period. Numerical simulation of grating growth permitted the fabrication parameters to be adapted to facilitate the writing of a specified device. Figure 6.6 shows the typical transmission spectrum of a long-period grating fabricated by this method, with a period of 580 μm and 1.8 cm in non-hydrogenated boron-germania co-doped fibre. Three broad transmission loss peaks around 1360 nm, 1430 nm and 1520 nm were measured with an 18 dB transmission loss being achieved for the 1520 nm peak. This technique has been used to produce a number of other gratings with transmission peaks accurately located in the 1.3 μm and 1.5 μm broadband light source regions for optical sensing applications.

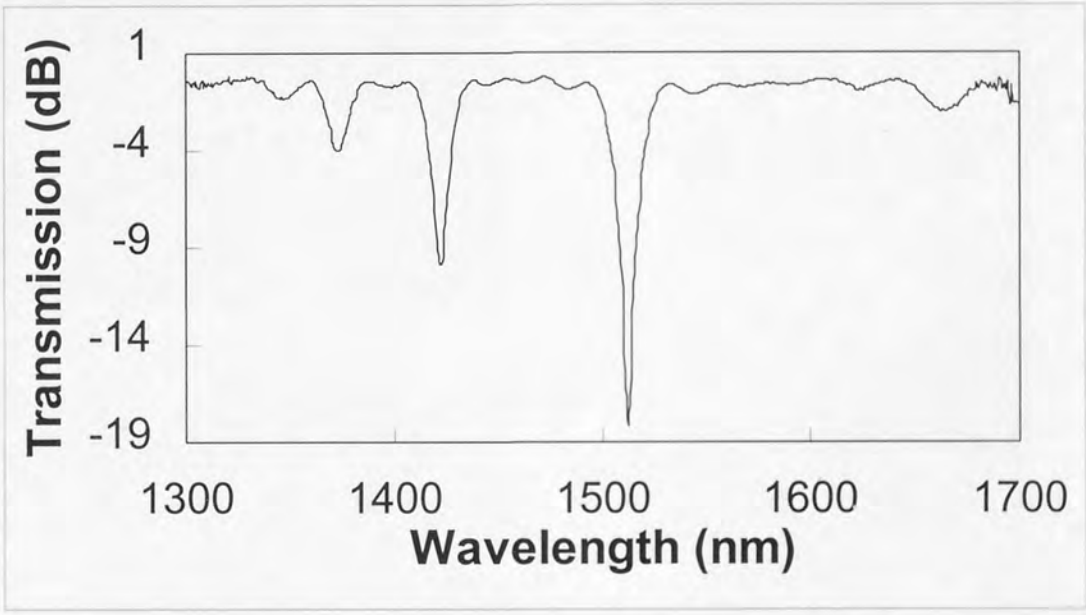

Figure 6.6: A typical transmission spectrum of a long period grating with an 18 dB loss peak around 1520 nm.

6.4 Strain and Temperature Characterisation

As previously discussed long period devices, like their Bragg gratings counterparts, may also be employed as sensors[1]. A number of results have been presented for long period gratings written into different host fibres[8]. This communication concluded that the fibre type has a significant effect on the strain, temperature and refractive index

sensitivities of the structure. However, to date no results have been presented for different period structures inscribed into the same fibre. This knowledge is important if a long period structure is to be employed in any environment were the temperature is likely to change or were the grating may be placed under tension/compression. It could also indicate the optimum grating period for a sensing structure, i.e. highly sensitive to the desired measurand and reduced sensitivity to other external parameters.

The temperature and strain properties of three gratings written into non-hydrogenated boron/germania co-doped fibre were examined. They were inscribed using the flexible point-by-point technique discussed in the previous section. The gratings were written with periods of 400, 500 and 600 μm resulting in transmission loss peaks at 1523 nm, 1565.7 nm and 1560.8 nm respectively, see figure 6.7. All of the structures were 1.1 cm in length.

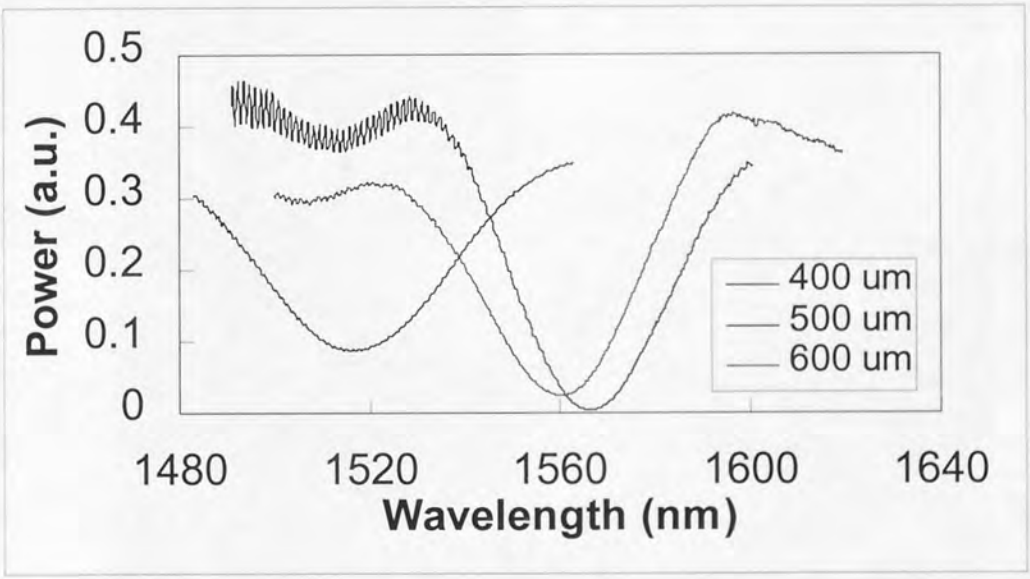

Figure 6.7: Spectral profiles of the three long period structures characterised.

The gratings were illuminated by a semiconductor laser amplifier (SLA), see figure 6.8. The amplifier was fabricated from InGaAs and was suitably coated with gold to suppress reflections and, hence, lasing. The amplifier is biased such that holes and electrons are swept into the active region where they recombine via spontaneous emission. This results in a low power output over a large bandwidth, typically 400 nm. The source output was rippled with a period of 1.5 nm, which is equal to the length of

the active region of the SLA. This was normalised out by dividing the transmission of the grating by the reference output.

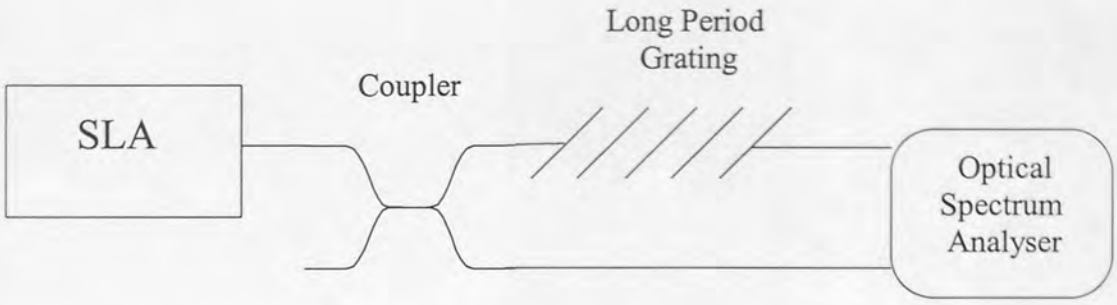

Figure 6.8: Schematic of characterisation system for long period structures.

The structure to be analysed was initially placed and bonded to the Peltier heat pump with thermal sink compound. The grating was kept as straight as possible during the process as long period structures suffer from severe bend loss. The Peltier was cooled by the ILX temperature controller to 0°C then heated in steps of 10°C, up to 80°C. At each sample point, two traces were taken from the OSA. The first of these covered the lower half of the grating; the second half the upper spectral end. This method was adopted to increase the resolution of the system. The OSA employed collected 800 data points for any scan size. Hence, the greater the scan bandwidth the greater the distance between the data points and, thus, the lower the resolution. This effect is negligible for uniform Bragg gratings as a scan over the complete reflection spectra would have a bandwidth of about 2 nm. However, long period structures have very broad bandwidths and one scan over its entire range gives low resolution. This resolution can be doubled, however, by halving the complete scan range and taking two sets of results; one at either half maxima. Each trace was an average of 50 scans. The traces were collected by an in-house program, JWScope, and were normalised and analysed in Excel. The transmission loss peak was defined to be the mid-point of the upper and lower half maximums.

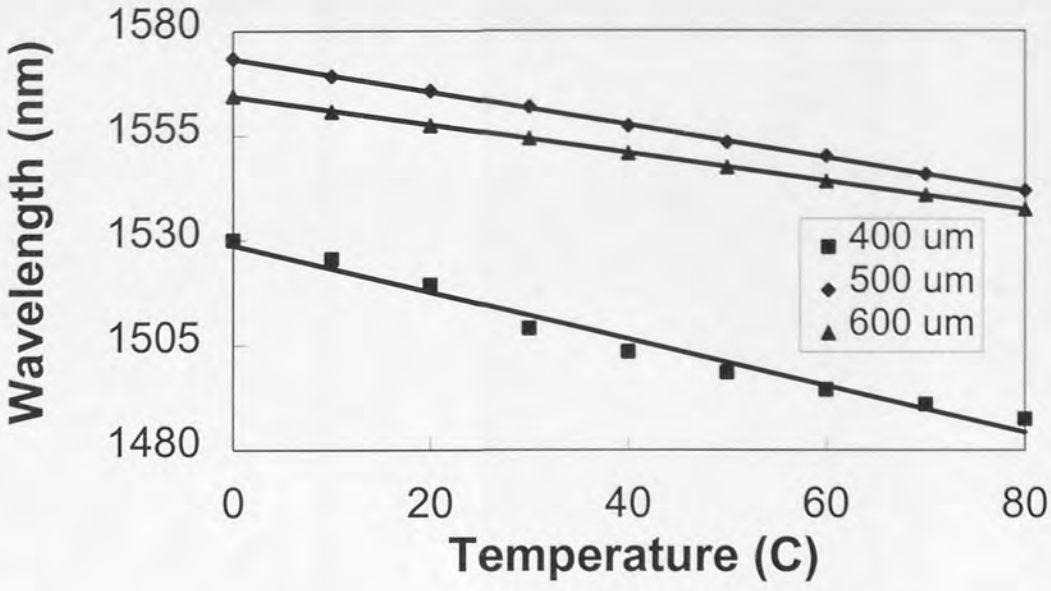

Figure 6.9: Temperature characterisation results obtained from the three long period structures.

(Error in figure 6.9 for temperature is ± 0.2°C and 0.06 nm for wavelength).

The above results demonstrate that all the long period structures examined had an approximately linear temperature response. This is important if they are to be employed as sensors or if temperature effects are to be taken into account. The sensitivity of each grating was found to be dependent on the period of the perturbation. The temperature sensitivities of the 400 μm, 500 μm and 600 μm were determined to be 0.557 nm/°C, 0.3939 nm/°C and 0.3374 nm/°C respectively (see table 6.1 for results summary and errors). There is a marked decrease in sensitivity with increasing period. This would at first appear contrary to equation 6.3. However, all of these gratings had a number of transmission loss peaks as given by equation 6.2. For the purposes of this experiment only the transmission loss peaks in the 1.5 μm window were considered. Hence, the three structures are coupling into different cladding modes resulting in a different value of n_{lm} and hence Δn, i.e. from equation 6.2 as the period is increased to keep the wavelength the same the value of Δn must be reduced.

These values are also much higher than those obtained for Bragg gratings, which are of the order of 0.013 nm/°C and have periods of around 1 μm. This indicates that long period gratings would make better temperature sensors. However, their broad

bandwidth and lack of reflection makes them more difficult to interrogate. This high temperature sensitivity leads to problems when they are involved in applications other than sensing. This sensitivity as previously discussed can be reduced drastically however this leads to complications in manufacture.

The structures were then mounted onto the translation stage/load cell strain system outlined previously. The gratings were stretched in steps of 370 με, up to 2 220 με. The results were gathered in the same way as those for temperature characterisation and are shown in figure 6.10.

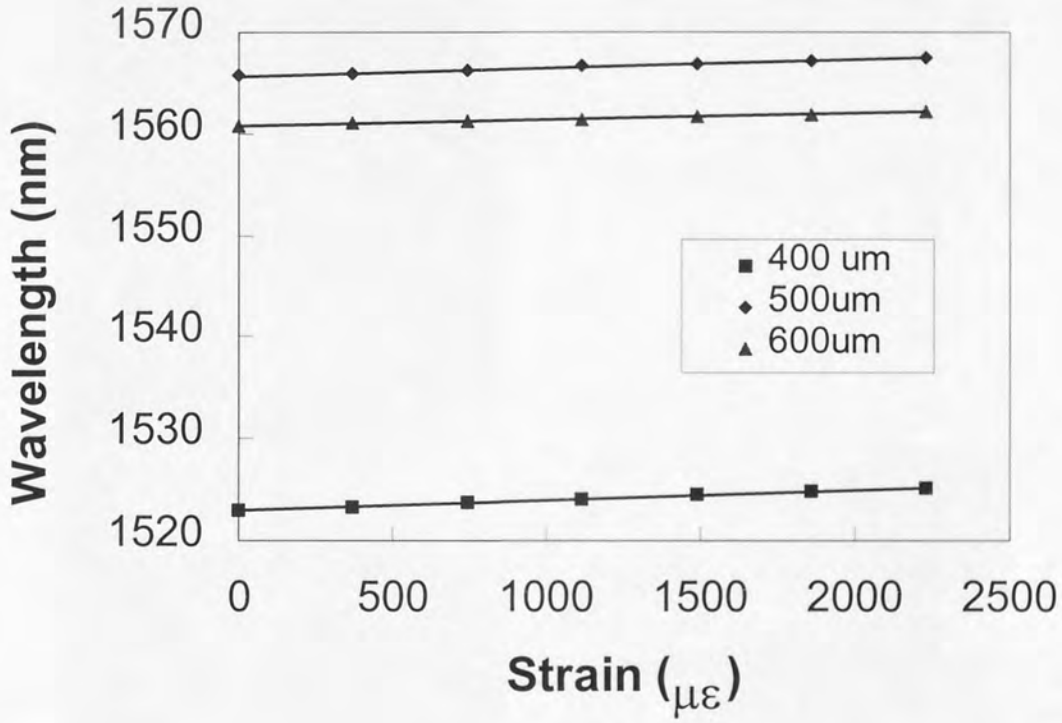

Figure 6.10: Strain characterisation results obtained from three different long period structures.

(Errors for figure 6.10 are ± 8 με for strain and ± 0.06 nm for wavelength).

The strain characteristics of all three gratings are also linear. The strain sensitivities of the 400 μm, 500 μm and 600 μm structures were determined to be 1 pm/με, 0.8 pm/με and 0.6 pm/με (see table 6.1 for results summary and errors). Once again there is a decrease in sensitivity with increasing period length. However, in this case the results are comparable to those achieved by Bragg gratings. This indicates that long period

structures are not as suitable for application as strain sensors as they are for temperature sensors. The temperature and strain sensitivities obtained and the errors on these results are shown in table 6.1.

Period of Structure (μm)	Peak loss (nm)	Temperature Sensitivity (nm/°C)	Error on Temperature (nm/°C)	Strain Sensitivity (pm/με)	Error on strain (pm/με)
400	1523	0.557	0.075	1	0.02
500	1565.7	0.394	0.079	0.8	0.03
600	1560.8	0.337	0.035	0.6	0.011

Table 6.1: Strain and temperature sensitivities of the three examined long period structures.

In conclusion, the sensitivity of the transmission loss peak of a long period grating at a certain wavelength to temperature and sensitivity is dependent on its period. These sensitivities are reduced with increasing period. Long period structures are more sensitive to temperature and have approximately the same strain sensitivity as fibre Bragg gratings.

6.5 FBG Strain Sensor Interrogation

In the previous chapter, an interrogation system based on the edge filter technique was demonstrated. The edge filter response was obtained from a specially written asymmetric spectral response fibre Bragg grating. This grating, as discussed, was difficult to write and the jagged edge response resulted in low resolution. A long period grating, while acting only as a loss mechanism, is considerably easier and cheaper to write. The novel fabrication technique mentioned in the previous section permits the writing of any long period grating. Hence, a grating can be written with both a controlled transmission peak wavelength and loss. A long-period grating has a broad transmission peak with shallow sides as compared to FBGs that have very steep, almost vertical sides. The transmission profile of a long period grating can be approximated to being linear over a fairly wide range. Hence, it is possible to replace the asymmetric spectral response grating in the previous experiment with a long period structure.

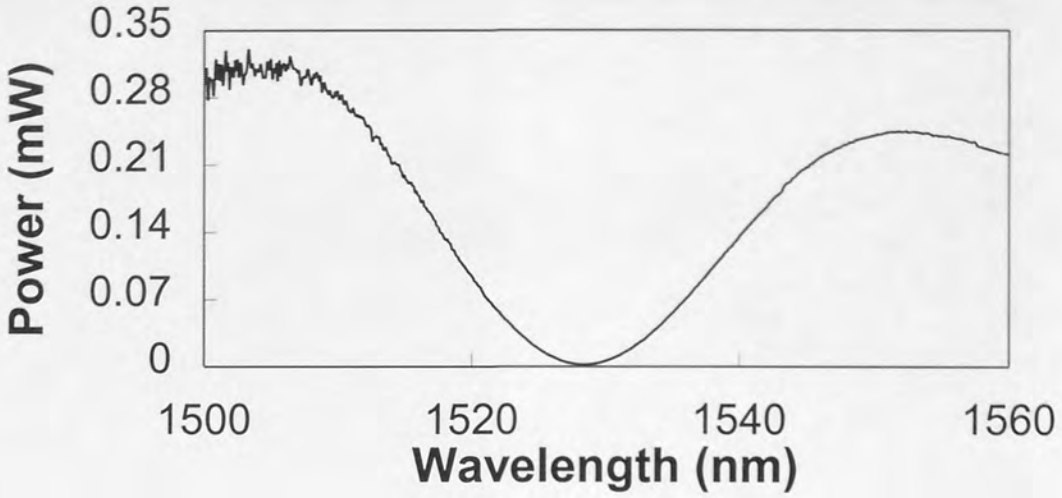

Figure 6.11: Spectral profile of the long period grating employed to interrogate an FBG sensor.

The above grating was written using the flexible point-by-point technique for the purpose of interrogating a uniform FBG sensor. The grating had a period of 580 μm and was 1.45 cm in length. It was inscribed in boron-germania co-doped that had been soaked in hydrogen at 150 atm. for a week. The grating had a 20 nm transmission peak centred at 1529 nm with a peak rejection ratio of 22 dB. This grating exhibits a near linear response of ~1.8 dB/nm between 1515 and 1525 nm. This near linear response over ~10 nm allows the device to be employed as an edge filter acting as a wavelength-to-amplitude converter, as in the case of the previous experiment.

The initial sensor system was set up as shown in figure 6.12 and consists of a FBG sensor, long period grating (see figure 6.11), an erbium fluorescence source, two couplers and two photodiodes. The reference arm is required to linearise the power-strain response with respect to the non-uniform erbium spectral response and fluctuations of the optical light source.

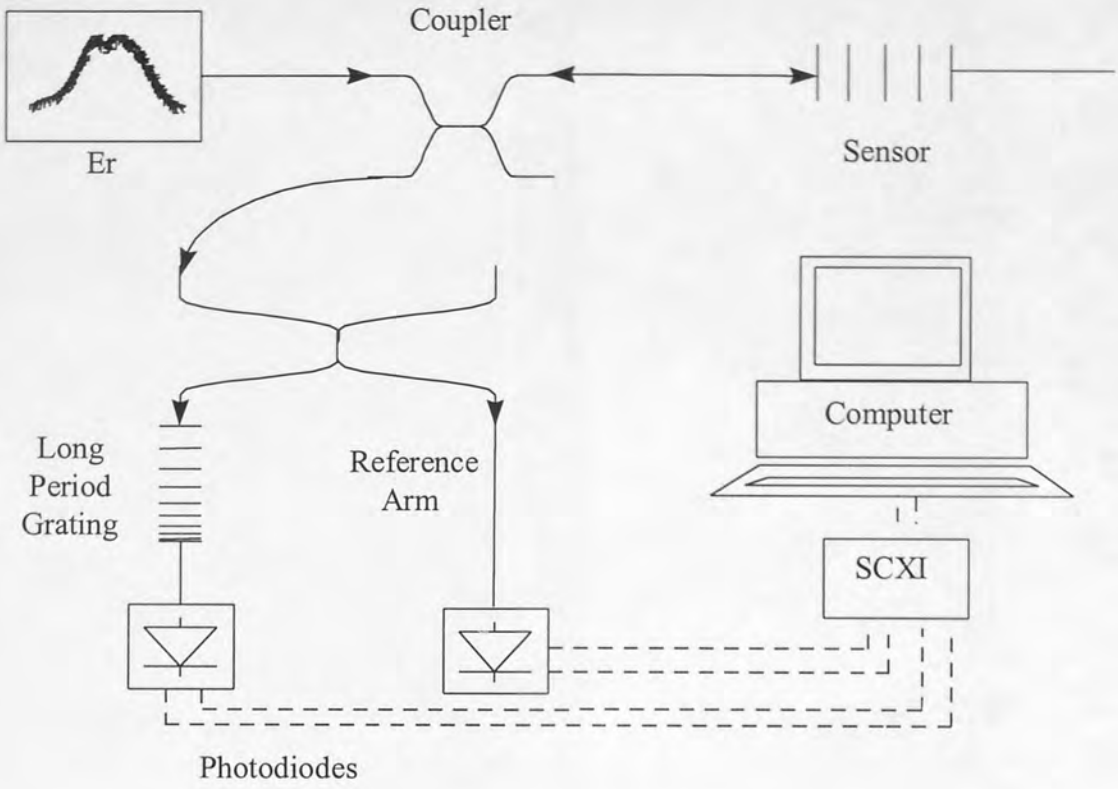

Figure 6.12: Schematic of initial sensor interrogation technique utilising a long period structure as an edge filter.

The FBG sensor grating was written into boron germania co-doped fibre using the two beam interferometric holographic technique. It was 5 mm in length and had a central wavelength and bandwidth of 1519 nm and 0.5 nm respectively. The linear slope of the long period grating terminated at about 1525 nm permitting an unambiguous sensing range of about 6 nm equivalent to ~6 mε. The sensing grating was secured onto two steel mounts, using two rubber blocks, which were then attached to the translation stage and load cell. The sensor was then stretched in steps of 550 με, up to 4 950 με. Two New Focus diodes that offered low-noise and in built amplification were employed to measure the resultant light levels. The output of both the two diodes was in the form of an analogue voltage, which was directly proportional to the input light intensity. These voltages were presented to a National Instruments signal conditioning (SCXI) system which amplified and conditioned the imputed voltage. A program was written in LabView to collect and measure these amplified signals which were written into two arrays. After data collection these stored arrays where moved into Excel were

they were processed and normalised. The normalised response of the system was then obtained by dividing the two signals. The results are shown in figure 6.13.

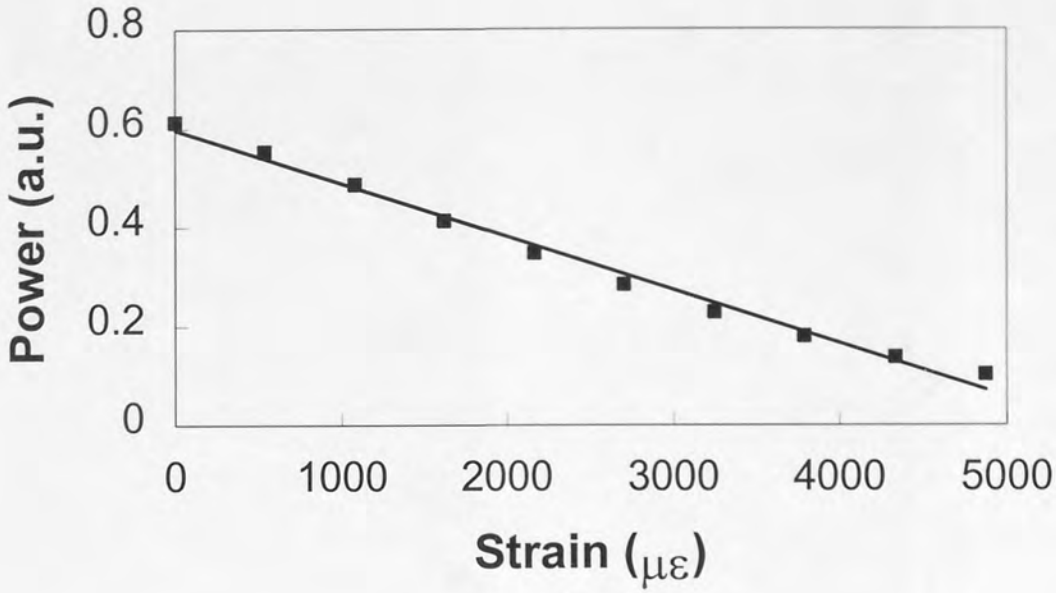

Figure 6.13: Results of normalised power against strain for initial long period interrogation system.

(Errors in figure 6.13 are ± 15 με for strain and ± 0.03 a.u. for power)

The results exhibit fair linearity over the complete sensing range. The strain response achieved by this system was $-(110 \pm 6) \times 10^{-6}$ a.u./με. The standard error of the system was calculated to be 0.005 a.u. which corresponds to an error in the measured strain of 47.6 με. This would be sufficient for the MAST project.

As in the case of the IBCI technique a cubic, rather than linear fit, is occasionally more appropriate. The cubic fit here is appropriate as the edge of a long period grating is itself curved rather than linear. In this case, a cubic fit an error in measured strain of 15 με, i.e. a third of that achievable with the linear fit.

A number of other projects may require better resolution over a smaller sensing range. This was further investigated by repeating the experiment with the sensor being stretched in steps of 11 με up to 110 με. The results were processed in Excel and are shown in figure 6.14.

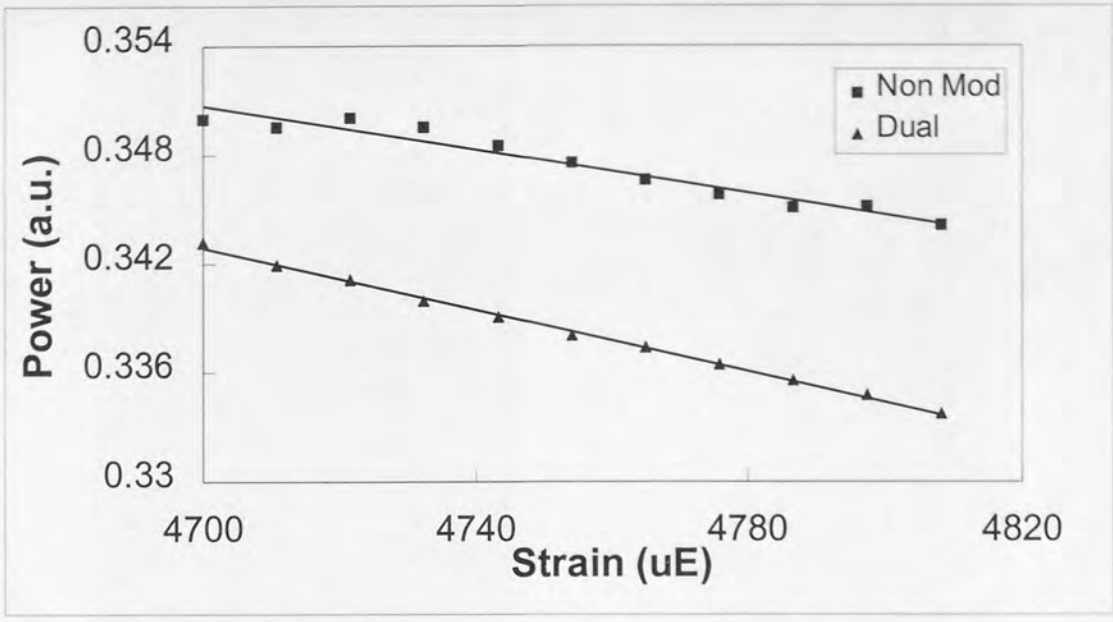

Figure 6.14: Normalised power-strain responses for unmodulated and modulated with dual lock-in detection methods

(Errors in figure 6.14 are ± 0.6 με for strain and 0.008 a.u. for power).

The results exhibit an improved linear relationship, as expected, over this smaller sensing range. The strain resolution of this system over this range was determined to be 2.4 με. The resolution of this range is not improved with a cubic fit. The edge of the long period grating is curved over 10 nm. This slope is evident in the previous set of results which were taken over a range of 5 mε, i.e. 5 nm. However, over a range of 110 με, i.e. 0.11 nm, this slope approximates more to a straight line. Hence, the linear fit is more appropriate over smaller ranges. The deviations in the linear fit are primarily due to electromagnetic interference. Noise is induced in the wires connecting the photodiodes with the lock-in amplifier and those between the lock-in amplifier and the SCXI system, hence the signal to noise ratio is reduced. This interference is less prominent in the previous experiment as the difference in received power between the different applied strains is 50 times larger than that in this case.

Both the large and small strain results can be improved by increasing the signal to noise ratio.

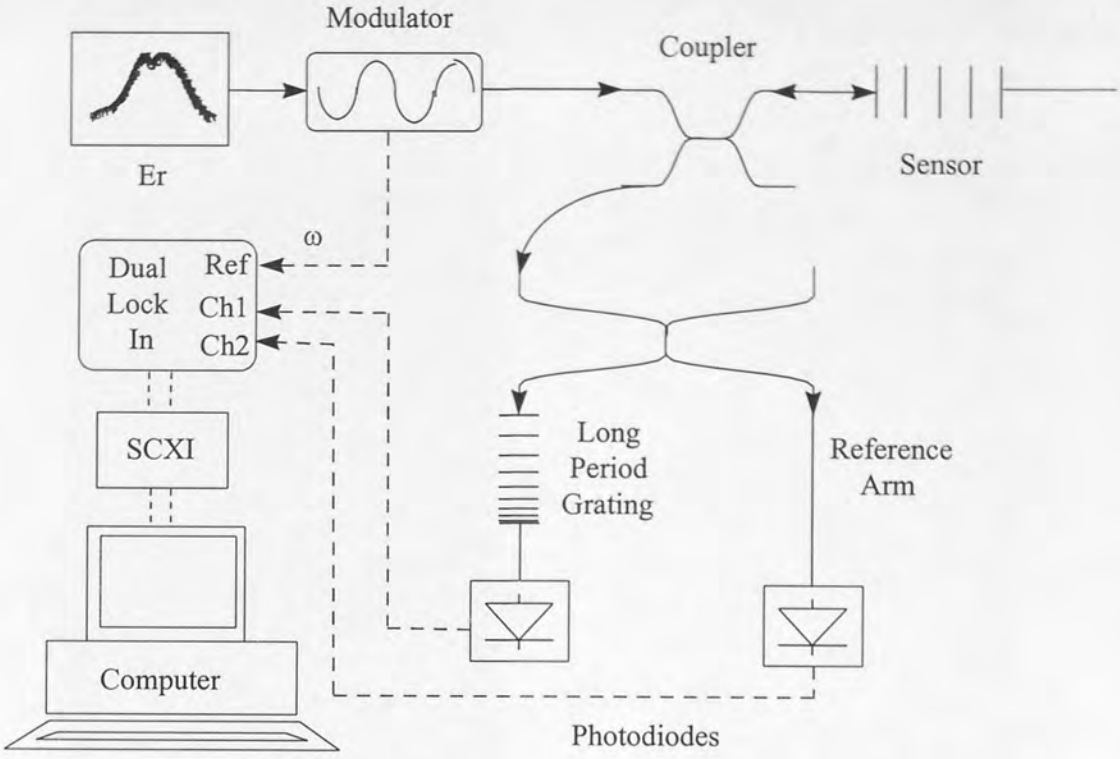

Figure 6.15: Experimental set-up for fibre grating interrogation system employing the dual lock-in technique.

It has long been demonstrated that the signal to noise ration in any given intensity based system can be increased by modulating the source, hence reducing extraneous 1/f noise. The required modulation was placed onto the source output by a lithium niobate modulator, inserted into the system as shown in figure 6.15. A function generator which emitted a sine wave with an amplitude of 10 volts was used to control the modulator. The output from the normalisation arm and transmission from the long period grating were measured using a Bentham dual lock-in amplifier. The amplifier was set to have a time constant of 300 ms. A synchronisation output from the function generator was connected to the amplifier permitting it to lock-in on and measure the two signals. These results could be either read on a digital output or by analysing the two analogue output signals. The two output voltage signals were again presented to and measured by the computer. These two signals were written into two arrays that could later be read and analysed by Excel.

The optimum modulation frequency was determined by repeating the same initial experiment, i.e. stretching the sensor in steps of 550 με, at frequencies of 330 Hz, 5

kHz, 20 kHz and 100 kHz. The sensor was stretched by the exact same amount and other than the addition of the modulation equipment the experiment remained the same. The greatest linear system response was obtained at 20 kHz; this frequency was adopted for all the modulation experiments. The results obtained were superior to those for the un-modulated case and demonstrate considerably improved linearity. The results are shown in figure 6.16.

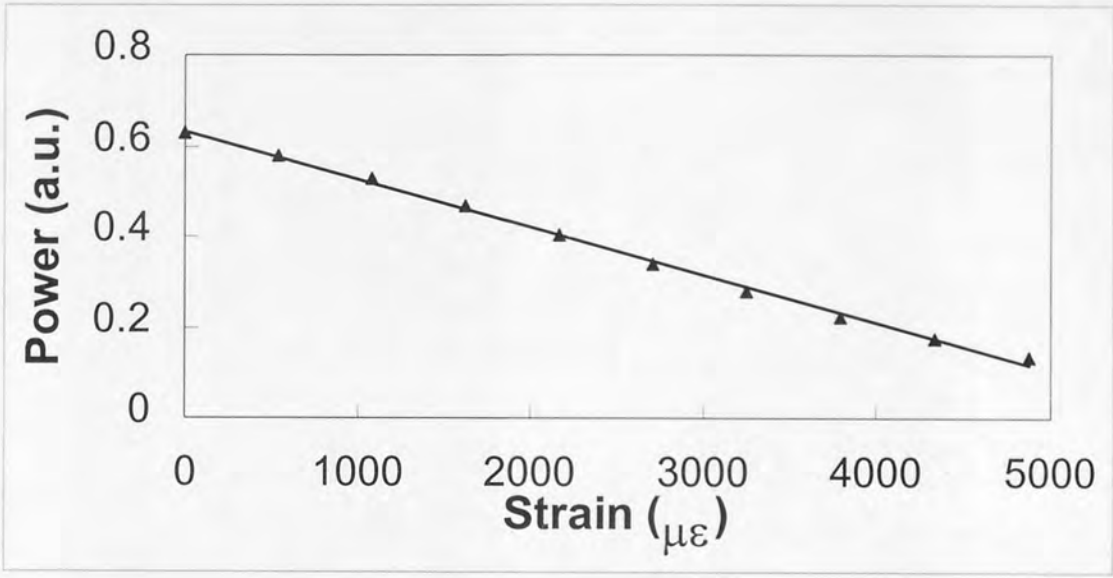

Figure 6.16: Results for normalised power against strain for the modulated interrogation system.

The linear strain response of the system was $-(100 \pm 6) \times 10^{-6}$ a.u/με and had an error in strain measurement of 31.6 με which is a third better than that obtainable without modulation. A cubic fit gives an error in strain measurement of 10 με. This response is comparable to that obtained with the IBCI technique for the same measurement range.

The resolution of the system over a smaller range can also be improved by increasing the signal to noise ratio. The experiment was repeated with modulation. Again, the sensor was stretched in steps of 11 με, up to 110 με. The normalised results are shown in figure 6.14(b). These results show considerable improvement on the un-modulated ones. The resolution of this system was determined to be 0.5 με over this range. This results is nearly five times better than that obtained by the un-modulated system and demonstrates that such a system can offer excellent sub-microstrain resolution.

This system therefore can be used to sense moderate ranges with a reasonable resolution or with excellent resolution over a small range. A very large sensing range, which is more applicable to the MAST project, may be obtainable with a more linear long period structure that has a wider bandwidth. A long period grating, with a period of 600 μm, was written into boron-germania co-doped fibre using the flexible point-by-point technique discussed in section 6.3. The grating had a transmission loss peak at 1560.2 nm and a bandwidth of 32 nm, see figure 6.17.

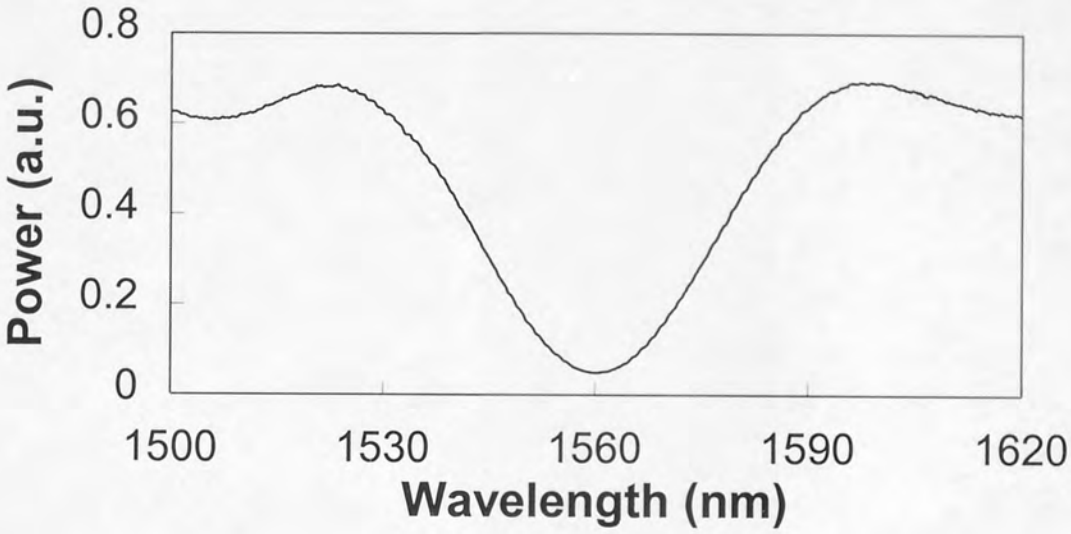

Figure 6.17: Transmission profile of 600 μm long period grating employed as an edge filter.

This grating had an appropriate linear slope between 1530 and 1555 nm, i.e. over a 25 nm range. A uniform sensor grating was written using the two beam holographic technique into boron-germania co-doped fibre with a central wavelength of 1532 nm. The sensor grating was mounted onto the strain application system and stretched in steps of 540 με up to 7.5 mε. Modulation was not employed in this technique. The results were collected by the computer and analysed in Excel and are shown in figure 6.18.

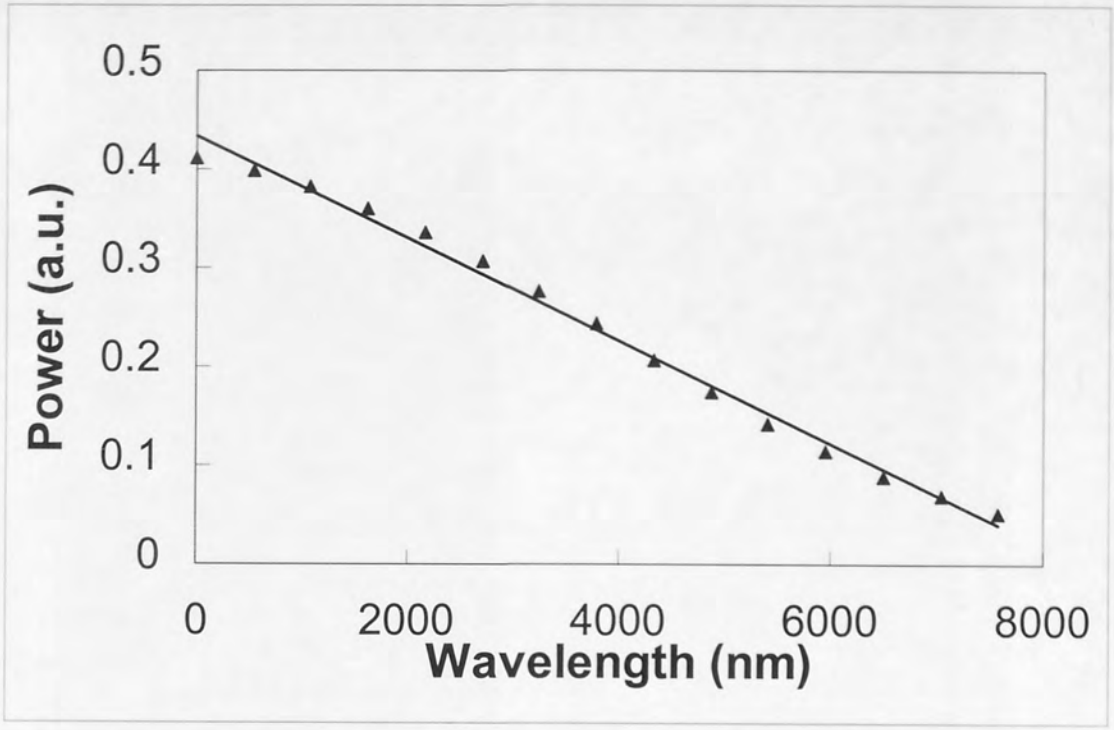

Figure 6.18: Results to show large obtainable dynamic range with alternative long period structure and sensing grating.

The results exhibit the expected linear response. The strain response of this system was determined to be $-(52 \pm 5)\times10^{-6}$ a.u./με. The calculated resolution using linear strain extraction was about 50 με. While this resolution is low it demonstrates that such a system can be used for measuring large strain. It also further highlights the trade off between system measuring range and achievable resolution. A superior resolution of 11 με is obtained by employing a cubic, rather than a linear, approximation.

All the results obtained from the strain sensor systems employing a long period grating are presented in table 6.3.

Central Wavelength (nm) of sensor	Long period grating period (μm)	Sensing range (με)	Modulated (M) or unmodualted (U) System	Linear response (a.u./με × 10^{-6})	Error in results (a.u./με × 10^{-6})	Linear strain error (με)	Cubic strain error (με)
1519	580	5 000	U	-110	6	48	15
1519	580	110	U	-64	5	2.4	-
1519	580	5 000	M	-100	4	32	10
1519	580	110	M	-41	3	0.5	-
1532	600	7 500	U	-52	5	50	11

Table 6.3 Normalised results obtained for all strain experiments employing a long period grating as an edge filter.

The linear response obtained using the 600 μm period grating is less than that achieved with the 580 μm structure. This is because the spectral profile of the 580 μm structure had an approximately linear response over 10 nm compared with over 25 nm for the 600 μm grating.

This interrogation technique is the same as the one employing the grating with the asymmetrical spectral response, i.e. an spectral edge profile is used to convert an applied strain into received power. These results are similar to those obtained with the asymmetrical spectral response (ASR) grating. The linear response obtained with the 580 μm period grating are greater than those obtained with the ASR structure because the long period conversion device had a linear response over 10 nm compared to 15 nm for the ASR grating. The linear response is also greater as the 1519 nm grating is on the "leading edge" of the erbium fluorsence whereas the 1556 nm sensor employed in the ASR system is on the "trailing edge".

The error in measurement due to linear strain extraction is approximately the same in both the long period edge filer (LPEF) and ASR systems. However, cubic strain extraction improves the results obtained from the long period system typically by a factor of three. Cubic strain extraction does not apply to the ASR system. The ASR

grating was written to have a linear spectral response; the deviation from the linear fit is due to the jaggedness of this response. However, cubic strain extraction applies to the LPEF system as these structures have a curved, as opposed to linear, spectral profile. This system is therefore more appropriate to measure strain provided the long period grating is temperature compensated, for the reasons discussed earlier, and cubic strain extraction is employed. As discussed in section 5.3.1, cubic strain extraction is more complex and requires a pc to determine the applied strain.

Assuming cubic strain extraction, the error in strain measurement is approximately the same for the IBCI and LPEF systems. This long period system, in this situation, is superior as it can interrogate uniform gratings as opposed to chirped structures. This offers a more economical use of the available source bandwidth. In addition to this uniform gratings are more commercially available than chirped structures.

However, the length of the edge of the grating's spectral profile limits the measurement range of the LPEF system. The IBCI system is limited by the grating's bandwidth, which is easier to tailor than the spectral response of a long period structure. The IBCI system is, therefore, more appropriate for extreme strain sensing applications. In addition, the chirped reference grating is not as temperature sensitive as the long period structure and, therefore, does not require the same level of temperature compensation. Indeed, the MAST project does not require temperature compensation for the reference grating; this is expected to be the case in most structural monitoring systems. Finally the IBCI system offers superior resolution for linear strain extraction. Therefore, this approach is preferable for systems that use linear strain extraction, which is cheaper, quicker and simpler than using a cubic extraction, i.e. the MAST project.

The results obtained from the LPEF system compare well with those achieved by other systems using edge filters. Melles *et al.*[24] reported a resolution of tens of millistrain using an edge filter response obtained using bulk optics. Lobos Ribeiro *et al.*[25] achieved a resolution of 3.5 με with a biconical fibre filter.

In summary, this interrogation method can be employed to interrogate uniform FBG strain sensors over a large range and requires no specialist grating. Its main disadvantage lies in the temperature sensitivity of the long period grating, i.e. any

change would result in an incorrect output. These experiments were performed in the laboratory were the temperature remained fairly constant, this is unlikely to be the case in "real" sensing environments. This problem can be overcome by either (i) actively compensating the grating e.g. placing it on a temperature regulated Peltier or (ii) employing a temperature insensitive long period grating[9] discussed earlier.

6.6 Conclusions

This chapter has examined the inscription and the properties of long period gratings and discussed how they have been employed in sensor[8] and telecommunication systems[22]. It is clear that such structures will continue to find application and they are expected to evolve with Bragg gratings. Temperature and strain characterisation results for three different period structures with transmission peaks in the 1.5 μm window were presented and discussed. It was concluded that the devices examined had a greater temperature sensitivity than Bragg gratings written at the same wavelength, e.g. 557 pm/°C compared to 13 pm/°C. The strain response of the long period structures is approximately the same as that obtained from Bragg gratings. It was also noted that the sensitivities of the three structures were reduced as the period was increased. This was due to the light being coupled into the different cladding modes in each case.

A novel technique for the interrogation of a uniform FBG strain sensor with a long period structure was presented and discussed. This method utilises the approximately linear slope of one edge of a long period structure. The system was demonstrated to be capable of interrogating over a range of 7 500 με with a resolution of 50 με. This result was improved by the application of the lock-in technique to a resolution of 31.6 με. These resolutions can be improved if a cubic, rather than a linear, interpretation is employed. The resolutions achieved, with a cubic interpretation, were 11 με and 10 με respectively.

The resolution of the interrogation system over a small range (110 με) was also investigated with resolutions of 2.4 and 0.5 με being obtained for the un-modulated and modulated cases respectively. A cubic fit is not suitable for this for such small sensing ranges.

This system is likely to find application in SMART structures as it offers a simple, cheap and high speed interrogation method for uniform period gratings.

---

[1] A.M. Vengsarkar, P.J. Lemaire, J.B. Judkins, V. Bhatia, T. Erdogan and J.E. Sipe, "Long period fibre gratings as band-rejection filters", *J. Lightwave. Technol.*, **14**, 1996, pp 58-65.

[2] K.O. Hill, B. Malo, K,A. Vineberg, F. Bilodeau and I. Skinner, "Efficient more conversion in telecommunications fibre using externally written gratings", *Electron. Lett.*, **26**, 1990, pp 1270-1272.

[3] F. Bilodeau, K.O. Hill, B. Malo, D. Johnson and I. Skinner, "Efficient narrowband LP01↔LP02 mode converters fabricated in photosensitive fibre: Spectral response", *Electron. Lett.*, **27**, 1991, pp 682-684.

[4] K.O. Hill, F. Bilodeau, B. Malo and D.C. Johnson, "Birefringent photosensitivity in monomode optical fibre: Application to external writing of rocking filters", *Electron. Lett.*, **27**, 1991, pp 1548-1550.

[5] F. Bakhti, J. Larrey and P. Sansonetti, "Annealing of long period gratings in standard hydrogen-loaded fibre", *Conf.: Bragg gratings, photosensitivity and poling in glass fibres and waveguides,* Williamsburg, U.S., **Tech. Dig.**, 1997, BSuD2-1.

[6] T. Erdogan "Cladding-mode resonances in short- and long-period fibre grating filters", *J. Opt. Soc. Am. A*, **14**, 1997, pp 1760-1773.

[7] D.D. Davis, T.K. Gaylord, E.N. Glytsis, S.G. Kosinski, S.C. Mettler and A.M. Vengsarkar "Long-period fibre grating fabrication with focused CO_2 laser pulses", *Electron. Lett.*, **34**, 1998, pp 302-303.

[8] V. Bhatia and A.M. Vengarsarkar, "Optical fibre long-period grating sensors", *Opt. Lett.*, **21**, 1996, pp 692-694.

[9] J.B. Judkins, J.R. Pedrazzani, D.J. DiGiovanni and A.M. Vengsarkar, "Temperature insensitive long period gratings", *Conf. on Optical Fibre Communication (OFC '96)*, **PD1**, San Jose, California, 1996.

[10] L. Dong, L. Reekie and J.L. Cruz, "Long period gratings formed in depressed cladding fibres", *Conf.: Bragg gratings, photosensitivity and poling in glass fibres and waveguides,* Williamsburg, U.S., **Tech. Dig.**, 1997, BMG 17-1.

[11] H.J. Patrick, A.D. Kersey, F.Bucholtz, K.J. Ewing, J.B. Judkins and A.M. Vengsarkar, "Chemical sensor based on long period fibre grating response to index of refraction", *Conf. on Lasers and Electro-Optics (CLEO '97)*, **Tech. Dig.**, 1997, CThQ5.

[12] H.J. Patrick, G.M. Williams, A.D. Kersey, J.R. Pedrazzini and A.M. Vengsarkar, "Hybrid fibre Bragg grating/Long period fibre grating sensor for strain/temperature discrimination", Photon. Technol. Lett., 8, 1996, pp 1223-1225.

[13] S.E. Kanellopoulos, V.A. Handerek and A.J. Rogers, "Simultaneous strain and temperature sensing with photogenerated in-fiber gratings", *Opt. Lett.*, 20, 1995, pp 333-335.

[14] Z. Zhang and J.S. Sirkis, "Temperature-compensated long period grating chemical sensor", *Optical Fibre Sensors (OFS '97)*, Williamsburg, Viriginia, **Tech. Dig.**, 1997, OWC39.

[15] V. Bhatia, D. Campbell, R. O. Claus and A.M. Vengsarkar, "Simultaneous strain and temperature measurement with long-period gratings", *Opt. Lett.*, **22**, 1997, pp 648-650.

[16]M.G. Xu, J.L. Archambault, L. Reekie and J.P. Dakin, "Discrimination between strain and temperature effects using dual-wavelength fibre grating sensors", *Electron. Lett.*, 30, 1994, pp 1085-1087.

[17] D.B. Stegall and T. Erdogan, "Long-period fiber-grating devices based on leaky cladding mode coupling", *Conf.: Bragg gratings, photosensitivity and poling in glass fibres and waveguides,* Williamsburg, U.S., **Tech. Dig.**, 1997, BSuB2-1.

[18] A.M. Vegsarkar, J.R. Pedrazzini, J.B. Judkins, P.J. Lemaire, N.S. Bergano and C.R. Davidson, "Long-period fibre-gratin-based gain equalisers", *Opt. Lett.*, 21, 1996, pp 336-338.

[19] H.J. Patrick, A.D. Kersey, W.K. Burns and R.P. Moeller, "An erbium-doped superfluorescent fibre source with long period fibre grating wavelength stabilisation", *Optical Fibre Sensors (OFS '97)*, Williamsburg, Viriginia, **Tech. Dig.**, 1997, OWB6-1.

[20] B.J. Eggleton, R.E. Slusher, J.B. Judkins, J.B. Stark and A.M. Vengsarkar, "All-optical switching in long-period fibre gratings", *Opt. Lett.*, **22**, 1997, pp 883-885.

[21] D. Taverner, N.G.R. Broderick, D.J. Richardson, R.I. Laming and M. Ibsen, "Nonlinear self-switching and multiple gap-soliton formation in a fibre Bragg grating", *Opt. Lett.*, **23**, 1998, pp 328-330.

[22] P. Sansonetti, "Fibre grating devices for telecommunications applications", *Conf.: Bragg gratings, photosensitivity and poling in glass fibres and waveguides,* Williamsburg, U.S., **Tech. Dig.**, 1997, JSuA3-1.

[23] T.A. Strasser "Fibre grating devices for WDM communication systems", *Conf.: Bragg gratings, photosensitivity and poling in glass fibres and waveguides,* Williamsburg, U.S., **Tech. Dig.**, 1997, BTuA1-1.

[24] S.M. Melle, K. Liu, and R.M. Measures, "A passive wavelength demodulation system for guided-wave Bragg grating sensors", *Photon. Technol. Lett.*, 4, 1992, pp 515-518.

[25] A.B. Lobos Riberio, L.A. Ferreira, M. Tsvetkov and J.L. Santos, "All-fibre interrogation technique for fibre Bragg sensors using a biconical filter", *Electron. Lett.*, **32**, 1996, pp 382-383.

Chapter 7: Conclusions

This thesis has addressed the fabrication of uniform period and chirped in-fibre Bragg gratings (FBGs). The main thrust of the work completed has been towards their application as strain sensors in SMART structures. A number of experiments have been completed and their results discussed. These have included:

(i) temperature and strain characterisation of uniform period and chirped gratings in different host fibres;

(ii) the temperature characteristics of a commercially available temperature compensated grating;

(iii) the implementation of a wavelength division multiplexed strain sensor system interrogated by a tuneable Fabry-Perot filter;

(iv) the development and implementation of a novel, chirped FBG sensor interrogation system in the 1.3. and 1.5 μm windows;

(v) the conception and realisation of a novel uniform FBG strain sensor interrogation technique. The interrogation of the sensors was facilitated by a specially written grating with an asymmetric spectral response;

(vi) the temperature and strain characterisation of long period structures with different periods written into the same fibre; and

(vii) the development and implementation of a system for interrogating uniform FBG strain sensors, utilising the edge response of part of a specifically written long period structure.

The initial work on the temperature and strain characterisation of uniform and chirped fibre Bragg gratings in three different germanosilicate host fibres provided some interesting results. It was concluded that the temperature sensitivity of a FBG is fibre dependent. Structures inscribed in standard telecommunications and high doped germania fibre exhibited temperature sensitivities of 17 pm/°C as compared to the

lower response of 13 pm/°C in boron-germania co-doped fibre. The strain response of an inscribed grating is approximately fibre independent with values of 1pm/με being obtained. Hydrogenation of the host fibre prior to ultraviolet exposure has no effect on the temperature or strain sensitivities of the structures. It was also concluded that the magnitude of a grating's bandwidth is insensitive to the application of strain and temperature.

The temperature sensitivity of a FBG is not desirable in a number of applications. Several commercial companies have produced specially packaged gratings to reduce this effect. Such a packaged grating was supplied by Melles Griot for temperature characterisation. The packaged grating had a temperature sensitivity of an order of magnitude less than that of an un-packaged structure. The dynamic response of the grating was also tested. It was concluded that the grating offered good temperature compensation for static and slowly varying temperatures. If the grating was cooled or heated rapidly, it took time for the grating to reach a final stable wavelength. This "settling time" was dependent on both the magnitude and rate of temperature change. However, in the majority of applications, the temperature of the environment is unlikely to change rapidly. This packaged grating would be of considerable use in such instances.

The application of FBGs as strain sensors was demonstrated by the implementation of a wavelength division multiplexed strain sensor system. The system demonstrated had five FBG sensors placed, spatially separate, on one fibre. The interrogation of the sensors was facilitated by the application of a tuneable Fabry-Perot filter. The system was controlled and the data gathered by a computer operating under a specially written LabView program. The LabView application was capable of interrogating the array of five sensors at a rate of 25 Hz. It was also capable of simultaneously calculating the central wavelength of each of the structures and, by assuming a strain sensitivity of 1pm/με, calculate the strain at that point. It is also possible to store a number of these calculated strains, hence creating a "black box" history of the structure. The system had a resolution of ± 10 με which is more than sufficient for most SMART structure applications.

The first novel interrogation method to be developed and implemented was the Identical Broadband Chirped Interrogation (IBCI) technique. This system is capable of interrogating chirped FBG sensors, where the chirp rate determines the measurement range of the sensor, e.g. a chirp of 5 nm facilitates a sensing range of 5 mε. This method is simple and low cost operating on the principle of employing identical broadband chirped sensors and rejection filter gratings in both single and multiple systems. It is robust, passive, easy to implement and offers high speed and, in the case of multiple sensors, truly simultaneous interrogation. This system finds particular application in the measurement of large strain. A linear fit between received power and applied strain is the simplest approach and offers all of the above advantages. However, a cubic fit can offer better resolution at the expense of system simplicity which may impact the speed and cost of the system.

All resolutions quoted are for linear fits, while those obtainable with a cubic function are in shown brackets.

It has been proved to give a resolution of 20 με (10 με) for dual sensor interrogation in the 1.5 and 1.3 μm telecommunication windows. Each sensor had a measurement range of approximately 5 mε. The cross-talk between the two sensors in the 1.5 and 1.3 mm systems was determined to be 19 με and 7 με respectively.

The IBIC technique was also demonstrated to offer a resolution of approximately 50 με (30 με) for a single sensor with a measurement range of 12 mε. Work has been completed on the development of an IBCI single sensor system capable of measuring ± 15 mε (1.5%). Four sets of these systems have been installed in the masts of four superyachts to complement a tuneable Fabry-Perot (TFP) interrogation system. The TFP system is capable of interrogating 60 sensors, each with a measurement range of ± 3 500 με and a resolution of ± 10 με at 500 Hz. At present, an IBCI system is being developed in collaboration with British Aerospace to detect and measure acoustic waves in carbon composite panels. The combination of low-cost and exceptional high speed interrogation offered by this technique makes it ideal for this application. The IBCI technique is also likely to find application involving load measurement and damage detection in the maritime and civil engineering industries.

The second novel interrogation method developed involved the application of a specially written grating, which had an asymmetrical spectral response, as an interrogation device. This grating was written to have an edge filter response which acts as a wavelength to amplitude converter. This system is capable of interrogating uniform devices, and hence it is less bandwidth intensive than the IBCI technique. At present, uniform structures are more commercially available and cheaper than their chirped counterparts. Therefore, it can be argued that this system is more cost effective than the IBCI method. However this is likely to change in the future if the demand for chirped gratings increases. The asymmetric spectral response (ASR) grating is a specialised structure and can be difficult to write. The ramped profile of the structure is inherently jagged which leads to lowered resolution and inaccuracy. The achievable resolution of this method for interrogating a single sensor over 6 mε was 42 με (28 με) and for a dual sensor system with a measurement range of 4.5 mε it was 38 με (25 με). This system does not have the large measurement range or the degree of multiplexing capability that the IBCI technique offers. The length of the ramped edge dictates the measurement range of the system. For example, the ramped edge of the grating written for the purpose of the experiment was 15 nm. This permits a measurement range of 15 mε and 7.5 mε for single and dual sensor systems respectively. A grating may be inscribed to have a longer edge profile, hence increasing the measurement range of the system. However, the resolution of the system is inversely proportional to the spectral length of the ramp, thus placing a limit on this length. This system will find application in the SMART structure field, where high resolution is not required.

There has recently been a resurgence in long period gratings as sensors and rejection filters. A novel fabrication technique based on the point-by-point method has been discussed. This flexible method may be employed to write a long period grating of any given specification with an accuracy of about 0.1 μm per grating period.

The temperature and strain characteristics of long period structures written by this process were also investigated. The work commenced with the temperature and strain characterisation of a number of different period structures inscribed into non-hydrogenated boron-germania co-doped fibre. The three gratings examined had a

transmission loss peak in the 1.5 μm window which was characterised. The three gratings had periods of 400, 500 and 600 μm. They had temperature sensitivities of 0.557 nm/°C, 0.3939 nm/°C and 0.3374 nm/°C respectively. Their strain sensitivities were determined to be 1 pm/με, 0.8 pm/με and 0.6 pm/με respectively. It was concluded that the temperature and strain sensitivities of a long period grating at a given wavelength are period dependent. This is due to the fact that the different periods are coupling the guided mode into different cladding modes. These cladding modes have different refractive indices, hence different temperature and strain sensitivities. It was further concluded that long period gratings can be inscribed to be far more sensitive to temperature than their Bragg counterparts. Also that long period structures have approximately the same strain response as Bragg gratings.

The final novel interrogation technique to be implemented utilised the linear slope afforded by a specially written long period structure. Long period gratings (LPGs) intrinsically have broad bandwidths and shallow "sides". The transmission profile of a LPG may be approximated to linear over a fairly wide range. A LPG is easier to fabricate and has a much smoother spectral profile than the ASR Bragg grating previously mentioned. A grating was specifically written which had an appropriate linear slope over a 25 nm range. The application of this grating in place of the ASR Bragg grating previously mentioned permitted a sensing range of 7.5 mε with a resolution of about 48 με (15 με). These results were improved by the application of a different long period grating and intensity modulation of the source. This single sensor system was demonstrated to give a resolution of 32 με (10 με) and 0.5 με over measurement ranges of 5 mε and 110 με respectively. This method offers several advantages over the ASR Bragg grating system. These include ease of fabrication of the interrogation structure, resolution and the available interrogation bandwidth. However, the long period structure will suffer from temperature induced inaccuracies unless it is either actively compensated or inscribed to be temperature insensitive. This method is likely to find application in SMART structures where expense is more important than resolution.

Future work includes the solution the temperature/strain cross-sensitivity problem. It is likely that the IBCI system will be capable of solving the problem. If the sensor and

reference grating are placed sufficiently close together they may be assumed to be at the same temperature. The IBCI system fundamentally measures the difference in central wavelength of two identical gratings. If the gratings are at the same temperature regardless of environmental temperature changes they will still have equal central wavelengths. Therefore, the only differential in central wavelengths will be strain induced. This may be demonstrated experimentally using the set-up shown in figure 7.1

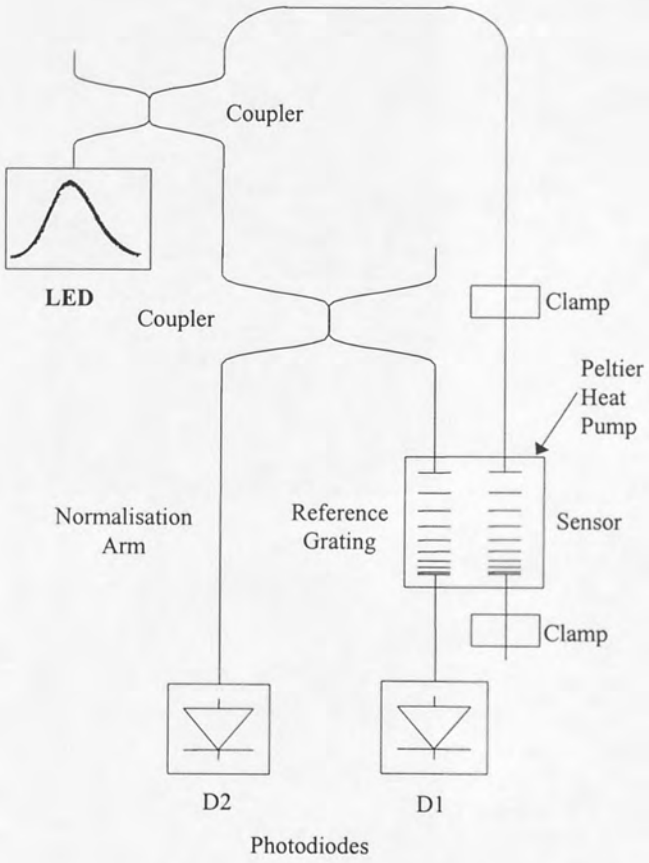

Figure 7.1: Schematic of a possible system set up to solve the temperature-strain cross-sensitivity problem via the IBCI technique.

This idea could be tested by setting a temperature on the Peltier heat pump (e.g. 0°C) then stretching the grating in steps of 500 με up to 5 mε. The stretching could then be repeated for different temperatures, 10°C, 20°C etc. If the theory is correct then the results obtained should be approximately the same for different applied temperatures.

This system to operate at maximum potential would require a flat source. If the source is not flat, then, as the sensor grating is moved by temperature the amount of light it reflects will alter. This changes the output intensity of the system, thus giving the impression that strain has been applied to the sensor. A flat source avoids this as the sensor grating will always reflect the same intensity regardless of its spectral position. A flat source would also permit the multiplexing of gratings in the system without the need for rejection gratings. In the systems explored blocking gratings have been required to prevent cross-talk. However, if a flat source is employed the reflection from other gratings in the system is constant, i.e. an offset which may be factored out. Suitable high power, flat spectral profile, erbium fluorescence sources are commercially available, but, at present, are expensive. However, the cost of these is also likely to fall in the future. A non-flat source may be used if a normalisation arm is employed as shown in figure 7.1. Ideally though the source would be flat and, therefore, the second arm would not be required.

Other future work would include the further characterisation of long period gratings particularly with reference to different host fibres. If they are to be employed as sensors, interrogation methods that are comparable to those used for Bragg gratings are required. The main problem with the application of such structures is their broad bandwidth which reduces their multiplexing capability. It would be beneficial if future work would address minimising their bandwidths.

The final interrogation system, which employs a long period grating, has the capability to address a number of sensors. The multiplexed system would be identical to that used in the ASR grating system, i.e. the long period structure would replace the ramped device. A long period grating with a linear response over 25 nm has been demonstrated. The symmetric nature of these structures gives an identical linear response on the other edge of the grating. Therefore, such a grating affords a combined edge response of 50 nm, which is approximately the bandwidth of an erbium fluorescence source. This grating could, therefore, interrogate up to 10 sensors with a measurement range of 5 mε.

There is still a substantial amount of work to be completed in the relatively new field of FBG sensors. This includes the development of cheaper and superior interrogation systems and solutions to the temperature/strain cross-sensitivity problem. There is a considerable amount of work being performed in the fabrication of both long period and Bragg gratings. This may lead to the development of superior sensing structures and will certainly reduce the cost and increase the availability of such devices. There has also recently been a considerable reduction in the cost and improvements in erbium fluorescent and broadband LED sources that are vital for the illumination of grating based systems. It is predicted that, with the cost of both sources and gratings being reduced, FBG sensor systems will continue to find a growing number of applications as well as increasing penetration into the areas already mentioned.

8. Publications arising from this work

1 R.W. Fallon, L. Zhang, I. Bennion, "Temperature and strain characterisation of uniform, chirped and bandpass in-fibre Bragg gratings", *Institute of Physics Meeting on In-Fibre Bragg Gratings and Special Fibres,* London, May 1996.

2 L. Zhang, R. W. Fallon, K. Sugden, I. Bennion, "Thermal stability of uniform-period, chirped and bandpass fibre grating structures fabricated in hydrogenated optical fibres" *CLEO Europe*, Hamburg, Germany, September 1996, CThB5.

3 R. W. Fallon, L. Zhang, A. Gloag and I. Bennion, "Identical broadband chirped grating interrogation technique for temperature and strain sensing", *Electron Lett*, **33**(8), April 1997, pp 705-707.

4 R. W. Fallon, L. Zhang, A. Gloag and I. Bennion, "Multibroadband chirped fibre grating system for large-strain sensing interrogation", *Institute of Physics Meeting on In-Fibre Bragg Gratings and Special Fibres,* London, May 1997.

5 R. W. Fallon, L. Zhang, A. Gloag and I. Bennion, "Multibroadband chirped fibre grating system for large-strain sensing interrogation", *Conf on Lasers and Electro-Optics (CLEO'97),* Baltimore, Maryland, May 1997, CTuN2.

6 K Sugden, L Zhang, J A R Williams, R W Fallon, L A Everall, K E Chisholm and I Bennion, "Fabrication and characterisation of bandpass filters based on concatenated chirped fibre gratings", *Journal of Lightwave Technology,* **15**(8), August 1997, pp 1424-1432

7 R W Fallon, L Zhang and I Bennion, "Multi-identical-broadband-chirped-grating interrogation technique for large-strain sensing applications", *IOP Sensors and their Applications VIII*, September 1997, Glasgow, pp 233-238.

8 L Zhang, R W Fallon, A Gloag, I Bennion, F M Haran and P Foote, "Spatial and wavelength multiplexing architectures for extreme strain monitoring system using identical-chirped-grating-interrogation technique", *Conf. on Optical Fiber Sensors (OFS'97)*, Williamsburg, Virginia, October 1997, OThC12.

9 R W Fallon, L Zhang, A Gloag and I Bennion, "Multiplexed identical-broadband-chirped-grating interrogation system for large-strain sensing applications", *IEEE Photonics Technology Letters*, **9**(12), December 1997, pp 1616-1618

10 L.A. Everall, R.W. Fallon, J.A.R. Williams, L. Zhang and I. Bennion, "Flexible Fabrication of Long Period In-Fibre Gratings", *Conf. on Lasers and Electro-Optics (CLEO'98)*, San Francisco, California, May 1998, CThO53.

11 R.W. Fallon, L.A. Everall, L. Zhang and I Bennion, "Multiple Strain Sensor Interrogation with an Asymmetric Grating", *Conf. on Lasers and Electro-Optics (CLEO'98)*, San Francisco, California, May 1998, CFE2.

12 R.W. Fallon, L. Zhang and I Bennion, "Long-period grating interrogating FBG strain sensor achieving combination of large dynamic range and high resolution" *Conf. on Lasers and Electro-Optics (CLEO Eurpoe '98)*, Glasgow, Scotland, September 1998, CWP3.

13 L. Zhang, R.W. Fallon, L.A. Everall, J.A.R. Williams and I. Bennion, "Large-dynamic range and high-resolution from a strain-sensing system using a long-period grating interrogating a FBG strain sensor", *ECOC '98*, Madrid, Spain, September 1998, WdD22.

14 R.W. Fallon, L. Zhang, L.A. Everall, J.A.R. Williams and I. Bennion, "All-fibre optical sensing system: Bragg grating interrogated by a long period grating", Submitted to *Meas. Sci. Technol.*, June 1998.